Technical Report

TR-10-67

An update of the state-of-the-art report on the corrosion of copper under expected conditions in a deep geologic repository

Fraser King
Integrity Corrosion Consulting Limited

Christina Lilja
Svensk Kärnbränslehantering AB

Karsten Pedersen
Microbial Analytics Sweden AB

Petteri Pitkänen, Marjut Vähänen
Posiva Oy

December 2010

Svensk Kärnbränslehantering AB
Swedish Nuclear Fuel
and Waste Management Co

Box 250, SE-101 24 Stockholm
Phone +46 8 459 84 00

ISSN 1404-0344
SKB TR-10-67

An update of the state-of-the-art report on the corrosion of copper under expected conditions in a deep geologic repository

Fraser King
Integrity Corrosion Consulting Limited

Christina Lilja
Svensk Kärnbränslehantering AB

Karsten Pedersen
Microbial Analytics Sweden AB

Petteri Pitkänen, Marjut Vähänen
Posiva Oy

December 2010

Keywords: SKBdoc 1246936, Posiva 2011-01, Copper, Corrosion, Canister, Nuclear waste, Lifetime prediction, Modelling, Thermodynamics, Kinetics, General corrosion, Localized corrosion, Stress corrosion cracking, Gamma radiation, Repository environment, Microbially influenced corrosion.

A pdf version of this document can be downloaded from www.skb.se 2011-10.

The following figures are reproduced with permission of the copyright holder:

Figures 2-1, 2-2, 2-3, and 5-12 with permission of Posiva Oy, Olkiluoto, Finland.

Figures 2-8, 2-9, 2-10, 2-11, 2-12, 2-13, 5-16, 5-17, 5-18, 5-19, 5-27, 6-8, and 6-9 with permission of the Nuclear Waste Management Organisation, Toronto, Canada.

Figure 4-2 with permission of Lawrence Livermore National Laboraotry, Livermore, CA, USA.

Figure 4-3 with permission of The Electrochemcial Society, Pennington, NJ, USA.

Figures 5-4, 5 7, and 5-20 with permission of Atomic Energy of Canada Limited, Chalk River, ON, Canada.

Figures 5-5, 6-3, and AII-1 with permission of Elsevier B.V., Amsterdam, Netherlands.

Figure 5-8 with permission of the Institute of Physics, Bristol, UK.

Figures 5-13 and 6-6(b) with permission of NACE International, Houston, TX, USA.

Figure 6-2 with permission of Maney Publishing, Leeds, UK.

Figure 6-5(a) with permission of The Minerals, Metals, and Materials Society, Warrendale, PA, USA.

Abstract

Copper has been the corrosion barrier of choice for the canister in the Swedish and Finnish, nuclear waste disposal programmes for over 30 years. During that time many studies have been carried out on the corrosion behaviour of copper under conditions likely to exist in an underground nuclear waste repository located in the Fenno-Scandian bedrock. This review is a summary of what has been learnt about the long-term behaviour of the corrosion barrier during this period and what the implications of this knowledge are for the predicted service life of the canisters.

The review is based on the existing knowledge from various nuclear waste management programs around the world and from the open literature. Various areas are considered: the expected evolution of the geochemical and microbiological conditions in the groundwater and of the repository environment, the thermodynamics of copper corrosion, corrosion during the operational phase and in the bentonite prior to saturation of the buffer by groundwater, general and localised corrosion following saturation of the compacted bentonite buffer, stress corrosion cracking, radiation effects, the implications of corrosion on the service life of the canister, and areas for further study.

This report is an updated version of that originally published in 2001/2002. The original material has been supplemented by information from studies carried out over the last decade.

The conclusion drawn from this review is that the original prediction made in 1978 of canister lifetimes exceeding 100,000 years remains valid.

Foreword

This report is an update of the report "Copper corrosion under expected conditions in a deep geologic repository" published as Posiva 2002-01 and SKB TR-01-23. The report has been selectively updated, but much of the original text has been retained in this revised version in order that it provide a resource in a single document. The authors are grateful to those who contributed to both the original and revised versions. A number of people contributed to the updated discussion of environmental conditions (Section 2), including Arto Muurinen, Ignasi Puigdomonech, and Lotta Hallbeck. The authors would also like to thank Margit Snellman and Barbara Pastina (Saanio & Riekkola) and Lars Werme (formerly of SKB) for their comments on various drafts of the report.

Among the major changes and additions to the report are:

- extensive updates and additional material in Section 2 "Geochemical and microbiological conditions at the repository depth"
  - new site hydrogeochemical data for Olkiluoto in Finland and the Laxemar and Forsmark sites in Sweden (Section 2.1)
  - an expanded discussion of the evolution of bentonite pore-water chemistry (Section 2.2)
  - a re-written section on microbial activity and modelling (Section 2.3)
  - the inclusion of a short section on the magnitude of the external gamma radiation field (Section 2.4)
  - an updated description of the evolution of the environment (Section 2.5)
- the previous sections on corrosion prior to and during water saturation have been combined into a new section that describes the corrosion of the canister in the repository atmosphere and in unsaturated buffer (Section 4)
- various additions to the new Section 5 titled "General and localized corrosion" including:
  - copper corrosion in highly saline groundwaters
  - the effect of an alkaline plume on canister corrosion
  - corrosion in the presence of sulphide
  - the effect of surface defects on localized corrosion
  - recent results from *in situ* corrosion tests
  - grain boundary corrosion
  - galvanic coupling to C-steel
- an updated discussion on stress corrosion cracking (Section 6) including:
  - recent experimental data
  - assessment of the various mechanisms proposed to account for SCC of copper
  - modelling developments
- an updated list of lifetime assessments for copper canisters performed for various international deep geologic disposal programs (Section 8)
- a review of those areas of future research identified in the original report that have been addressed and a revised list of areas of continuing study (Section 9)
- for each section that has undergone major changes, a summary section describing the changes made has been added at the beginning.

Contents

1 Introduction

The proposed repository in Sweden and Finland is based on the Swedish KBS-3 design. The basic concept for the disposal of spent fuel is based on its encapsulation and emplacement in crystalline rock at a depth of about 500 m. The spent nuclear fuel will be encapsulated in spheroidal graphite cast iron canisters that have an outer 50-mm-thick corrosion barrier of copper. Once filled and sealed, the copper-iron canisters will be emplaced individually in vertical boreholes in the floors of deposition tunnels excavated off central tunnels (the KBS-3V design). The space between the canisters and the wall of the borehole will be filled with compacted bentonite. The tunnels and shafts will be backfilled with a low grade bentonite (compacted blocks and pellets), and sealing plugs will be emplaced to block specific transport pathways for groundwater. An alternative approach, the so-called KBS-3H design, involves the horizontal placement of "supercontainers" in a deposition drift. The supercontainer comprises a copper canister surrounded by pre-compacted bentonite blocks in an outer metallic shell. The function of the canister in both designs is to isolate the spent fuel from the surrounding environment. The design lifetime of the canister is at least 100,000 years. In addition to the required chemical resistance, the canister must also have sufficient mechanical strength to withstand the loads caused by disposal at a depth of 400 to 700 m, i.e. an evenly distributed load of up to 7 MPa hydrostatic pressure from groundwater and 15 MPa pressure from swelling of the bentonite. Additional design requirements concern limitations on heat and radiation dose to the near field and choice of materials that do not adversely affect the performance of the near field buffer. Therefore, the maximum allowed surface temperature has been set to 100°C and the maximum allowed surface dose rate to 1 Gy/h. The fuel in the canister should also remain subcritical even if water enters the canister.

In order to meet these requirements, the canister has been designed with an insert that provides mechanical strength and keeps the fuel assemblies in fixed positions. The outer copper shell provides corrosion protection for the canister. This outer shell is made of oxygen free copper (Cu-OF). To improve the creep strength and the creep ductility of Cu-OF, 30 to 100 ppm phosphorus is added to oxygen free high conductivity copper. Figure 1-1 shows an expanded view of the copper – cast iron canister in the version designed for BWR fuel, with an alternative insert design for four PWR fuel assemblies (not shown).

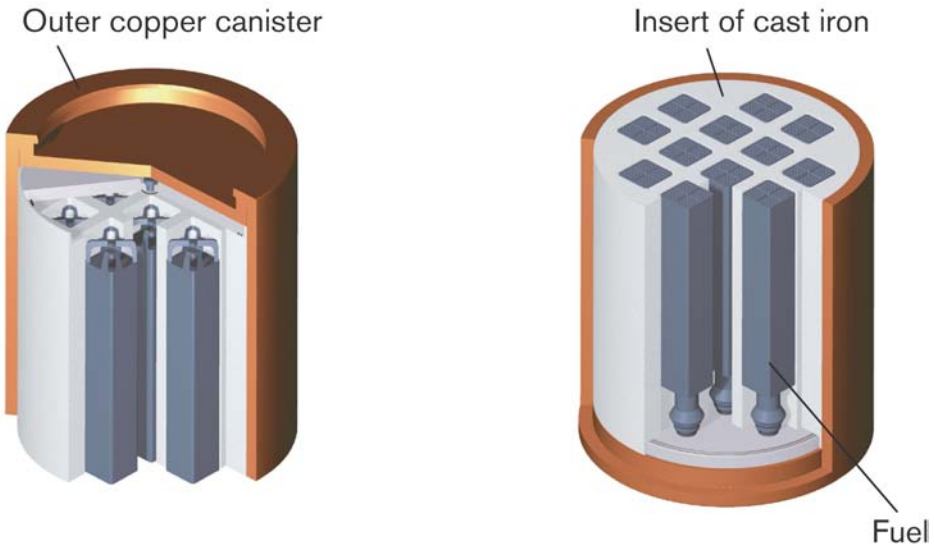

Figure 1-1. *Expanded view of spent BWR fuel disposal canister.*

Figure 1-2 illustrates the emplacement of the copper canister in compacted bentonite buffer material and sealing of the tunnels with bentonite backfill for the KBS-3 design repository.

The purpose of this report is to present the state-of-the-art of the knowledge of the corrosion of copper under the conditions expected in deep geological repositories in Sweden and Finland and to identify areas for further research. The report discusses the following topics:

- the chemical evolution of the repository and its surroundings;
- thermodynamic data relevant for copper corrosion;
- the corrosion modes and the extent of corrosion of the copper canister before emplacement and prior to water saturation of the compacted bentonite buffer after emplacement;
- general and localized corrosion of the canister after water saturation of the compacted bentonite buffer;
- the potential for stress corrosion cracking;
- corrosion induced by radiation;
- the implications for the canister service life; and
- areas for further research.

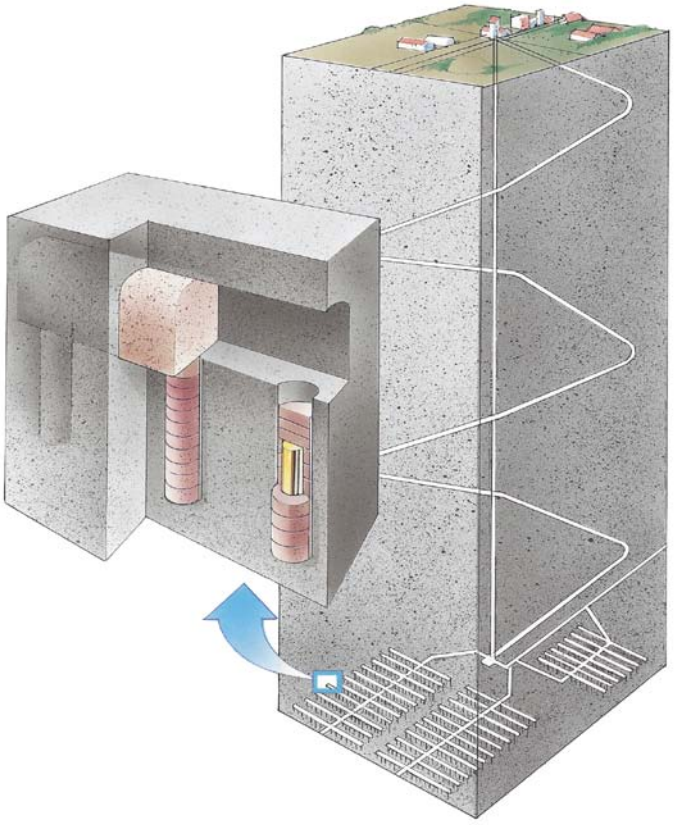

Figure 1-2. *Illustration of the emplacement of a copper canister in compacted bentonite buffer and sealing of the tunnels with bentonite rock backfill in an KBS-3 design repository.*

2 Geochemical and microbiological conditions at repository depth

This section provides a detailed discussion of the expected evolution of the composition of the groundwater and of the bentonite pore-water. Microbial processes involved in the groundwater environment and the bentonite buffer are discussed in detail and their assumed effect has been taken into account in assessing the values presented for groundwater and bentonite pore-water.

Summary of changes from the original report

Section 2 has been extensively updated since the original report. The most significant changes and updates include:

- revised groundwater compositions for the Laxemar and Forsmark sites in Sweden and the Olkiluoto site in Finland based on recent hydrogeochemical studies (Section 2.1),
- discussion of the effect of climate change scenarios considered in SR-Can (SKB 2006a) on the groundwater composition at repository depth (Section 2.1),
- an expanded discussion of the evolution of bentonite pore-water chemistry (Section 2.2),
- a re-written section on microbial activity and modelling (Section 2.3),
- the inclusion of a short section on the magnitude of the external gamma radiation field (Section 2.4), and
- an updated description of the evolution of the environment (Section 2.5).

2.1 Groundwater chemistry in the bedrock at repository depth in Finland and Sweden

2.1.1 Hydrogeochemical conditions at Forsmark and Laxemar

The current groundwater chemistry at the possible repository sites in Sweden is well established. The data in Tables 2-1 and 2-2 were used in SR-Can (SKB 2006a) and relate to the Laxemar and Forsmark areas, respectively.

Various factors may affect the groundwater conditions at repository depth. The effects of the excavation/operational phase and of future climate change were considered in the SR-Can safety assessment (SKB 2006a, b). For the base climate change variant, three stages or domains have been defined: the temperate, permafrost, and glacial domains. Because they correspond to the period during which the most rapid environmental changes will be occurring, the expected environmental changes during the first 1,000 years of the initial temperate domain were considered in detail. In addition, a greenhouse climate variant was considered to account for possible changes due to the anthropogenic production of greenhouse gases. The glacial cycle comprising the temperate, permafrost, and glacial domains is assumed to last for some 120,000 years, so that seven or eight such cycles can be expected during the one-million-year assessment period (SKB 2006a).

Excavation/operation phase: For both the Laxemar and Forsmark sites, the effects on salinity from upconing deep groundwater or draw-down of shallower groundwater are assessed to be unimportant for the safety of the repository (SKB 2006a, b) A short alkaline pulse in the groundwater from low-pH cement, shotcrete, and concrete is likely to occur, but its effects on canister corrosion will be negligible (King 2002).

Initial period of temperate climate after repository closure: At repository depth, the maximum salinity (12 g/L at Forsmark and lower at Laxemar, SKB 2006a, b) is expected during operation and immediately after closure. The salt content is expected to decrease slightly during the first 1,000 years due to the progressive inflow of waters of meteoric origin. For both sites, reducing conditions are expected to be re-established shortly after closure.

Table 2-1. Chemical composition of the groundwater at repository depth in the Laxemar area in Oskarshamn estimated within the SR-Can project. The concentrations are given both in mg/L and mol/L (M). Those parameters considered important for corrosion of the canister are highlighted in bold font. Nitrogen compounds (ammonium and nitrite) were not evaluated as part of the SR-Can project.

Constituent		At closure	After resaturation (< 100y after closure)	10,000 years into the future
pH		**6–9**	**7–8**	**7–8**
Eh	**mV**	**0 to –250**	**–180 to –250**	**–180 to –250**
Na^+	mg/L	15–990	15–990	15–294
	M	$(0.7–43)\cdot10^{-3}$	$(0.7–43)\cdot10^{-3}$	$(0.7–1.2)\cdot10^{-3}$
K^+	mg/L	2.6–29	2.6–29	2.6 –5
	M	$(0.7–7)\cdot10^{-4}$	$(0.7–7)\cdot10^{-4}$	$(0.7–1)\cdot10^{-4}$
Ca^{2+}	mg/L	40–960	40–960	40–600
	M	$(1–24)\cdot10^{-3}$	$(1–24)\cdot10^{-3}$	$(1–15)\cdot10^{-3}$
Mg^{2+}	mg/L	4–90	4–90	4 –10
	M	$(0.2–4)\cdot10^{-3}$	$(0.2–4)\cdot10^{-3}$	$(0.2–0.4)\cdot10^{-3}$
Alkalinity	mg/L	60–150	60–150	106–148
	M	$(1.0–2.4)\cdot10^{-3}$	$(1.0–2.4)\cdot10^{-3}$	$(1.8–2.4)\cdot10^{-3}$
Cl^-	**mg/L**	**11–2,910**	**11–2,910**	**11 –1,450**
	M	**$(0.3–82)\cdot10^{-3}$**	**$(0.3–82)\cdot10^{-3}$**	**$(0.3–41)\cdot10^{-3}$**
SO_4^{2-}	mg/L	7.5 –210	7.5 –210	7.5–40
	M	$(08–22)\cdot10^{-4}$	$(08–22)\cdot10^{-4}$	$(0.8–4)\cdot10^{-4}$
HS^-	**mg/L**	**0.03 –0.1**	**0.03–0.1**	**0.03–0.06**
	M	**$(0.9–3)\cdot10^{-6}$**	**$(0.9–3)\cdot10^{-6}$**	**$(1–2)\cdot10^{-6}$**

Table 2-2. Chemical composition of the groundwater at repository depth in the Forsmark-North Uppland area estimated within the SR-Can project. The concentrations are given both in mg/L and mol/L (M). Those parameters considered important for corrosion of the canister are highlighted in bold font. Nitrogen compounds (ammonium and nitrite) were not evaluated as part of the SR-Can project.

Constituent		At closure	After resaturation (< 100y after closure)	10,000 years into the future
pH		**6–9**	**7.1–8.7**	**6.7–8.3**
Eh	**mV**	**0 to –280**	**–190 to –280**	**–150 to –260**
Na^+	mg/L	90–3,750	90–3,750	65–2,860
	M	$(4–163)\cdot10^{-3}$	$(4–163)\cdot10^{-3}$	$(3–124)\cdot10^{-3}$
K^+	mg/L	1–136	1 –136	6–104
	M	$(0.3–35)\cdot10^{-4}$	$(0.3–35)\cdot10^{-4}$	$(2–27)\cdot10^{-4}$
Ca^{2+}	mg/L	58–1,900	58–1,900	56–1,580
	M	$(1.4–47)\cdot10^{-3}$	$(1.4–47)\cdot10^{-3}$	$(1.4–39)\cdot10^{-3}$
Mg^{2+}	mg/L	0.1–460	0.1–460	12–345
	M	$(0.01–19)\cdot10^{-3}$	$(0.01–19)\cdot10^{-3}$	$(0.5–14)\cdot10^{-3}$
HCO^{3-}	mg/L	5–290	5–290	19–290
	M	$(0.1–4.8)\cdot10^{-3}$	$(0.1–4.8)\cdot10^{-3}$	$(0.3–5)\cdot10^{-3}$
Cl^-	**mg/L**	**95–6,900**	**95–6,900**	**16–5,500**
	M	**$(2.7–194)\cdot10^{-3}$**	**$(2.7–194)\cdot10^{-3}$**	**$(0.3–154)\cdot10^{-3}$**
SO_4^{2-}	mg/L	19–900	19–900	19–690
	M	$(0.2–9.4)\cdot10^{-3}$	$(0.2–9.4)\cdot10^{-3}$	$(0.2–7.2)\cdot10^{-3}$
HS^-	**mg/L**	**0–0.3**	**0–0.30**	**0–0.23**
	M	**$0–10^{-5}$**	**$0–10^{-5}$**	**$0–10^{-5}$**

Permafrost domain: It is estimated that at Forsmark the ground will be frozen to a depth of 50 m or more for around 30% of the time of the glacial cycle (SKB 2006a, b). During this process, salts present in the surface waters and groundwaters will tend to accumulate at the advancing freeze-out front. The freezing process can give rise to an accumulation of saline water at the depth to which the perennially frozen front has reached. The saline waters formed in this manner within fractures and fracture zones might sink rapidly due to density gradients. Upconing of deep saline groundwaters is not considered to be of concern. The concentrations of major groundwater components such as chloride, sodium, calcium

and sulphate are expected to follow the same trends as the overall salinity described above. Other groundwater constituents, such as bicarbonate, potassium, iron, sulphide, and pH, are controlled by fast chemical reactions and are expected to remain largely unaffected by permafrost.

Glacial domain, stationary warm-based ice sheet: Modelling studies have suggested that during the glacial domain when the surface is covered by a static ice sheet, dilute melt waters (salinity < 0.1 g/L) may reach repository depth (SKB 2006a, b, c).

Glacial domain, advancing or retreating ice sheet: Higher salinities (~50 g/L) are predicted for advancing ice sheets because of upconing of deep saline groundwaters, but are predicted to occur for only a few centuries because of the relatively rapid advancement of the ice sheet. For retreating ice sheets, the salinities are similar to that for the stationary warm-based ice sheet described above because the rock volume has been "washed out" by dilute groundwaters prior to the retreat of the ice.

Glacial domain, immediately after retreat of the ice sheet: Infiltration of brackish or saline waters overlying the repository will result in an increase in groundwater salinity at repository depth.

Subsequent glacial cycles: The various geohydrological processes controlling the deep geochemical conditions are expected to be reversible so that the variations in groundwater composition described above will be repeated during each subsequent glacial cycle (SKB 2006a, b, c).

Greenhouse variant: The greenhouse variant considered in SR-Can assumes that the temperate period extends for the next 50,000 years due to warming of the atmosphere, thus delaying the onset of glaciation (SKB 2006a). However, no significant differences in groundwater salinity from the base variant are predicted to occur. Because of the land uplift, the greenhouse variant implies a greater decrease of the salinity for a longer time frame.

2.1.2 Hydrogeochemical conditions at Olkiluoto

2.1.2.1 Baseline conditions

The current groundwater chemistry at the possible repository site in Finland is well established but its future evolution is somewhat uncertain. Future evolution and the ensuing groundwater types at repository level at Olkiluoto are based on numerical simulations of site scale groundwater flow and salinity (Pastina and Hellä 2006). The model is calibrated based on past evolution calculations from the start of the Littorina stage 8,500 years ago to the present (Andersson et al. 2007, Posiva 2009). The data for Olkiluoto in Tables 2-3 and 2-4 present the predicted values at closure of the repository, after resaturation, and 10,000 years into the future (Pitkänen et al. (2004), Posiva (2009), Luukkonen and Nordman (2007), and Pastina and Hellä (2006)).

Table 2-3. The vertical variation of the main hydrochemical parameters and microbes at Olkiluoto shown against indicative depth ranges (Posiva 2009). The variation in pH is caused by calcite equilibrium in deep groundwaters and follows the variation in carbonate (alkalinity) and increasing contents of Ca (not shown in the Table). Vertical lines in the redox column depict steady conditions. Variation in dominant microbe populations are shown. MOB, MRB, IRB, SRB are methane oxidizing and manganese, iron, and sulphate reducing bacteria, respectively.

Depth (~m)	Used classification	Water type	Cl (mg/l)	pH	Alkalinity (meq/l)	Redox	Microbes
0	Fresh HCO_3	Ca-Na-Mg-HCO_3-SO_4	<10	5,5	<0,5	Post-oxic	MOB,Acetogens, MRB, SRB
10		Ca-Na-Mg-HCO_3-(SO_4-Cl)	10	7	3	Sulphidic	Acetogens, IRB, MRB, SRB
100	Brackish HCO_3	Na-(Ca)-Cl-(HCO_3-SO_4)	2000	7,8	4		
200	Brackish SO_4	Na-(Ca)-Cl-(SO_4)	4500	7,5	1,0		Acetogens, MRB, IRB
300	Brackish Cl	Na-Cl	5000	8,2	0,4	Methanic	Acetogens, SRB, IRB, MRB
400	Saline	Na-Ca-Cl	6000	8	0,2		Acetogens, Methanogens
600			14000	7,8			
		Ca-Na-Cl					
1000			50000	7,5	<0,2		Methanogens, Acetogens

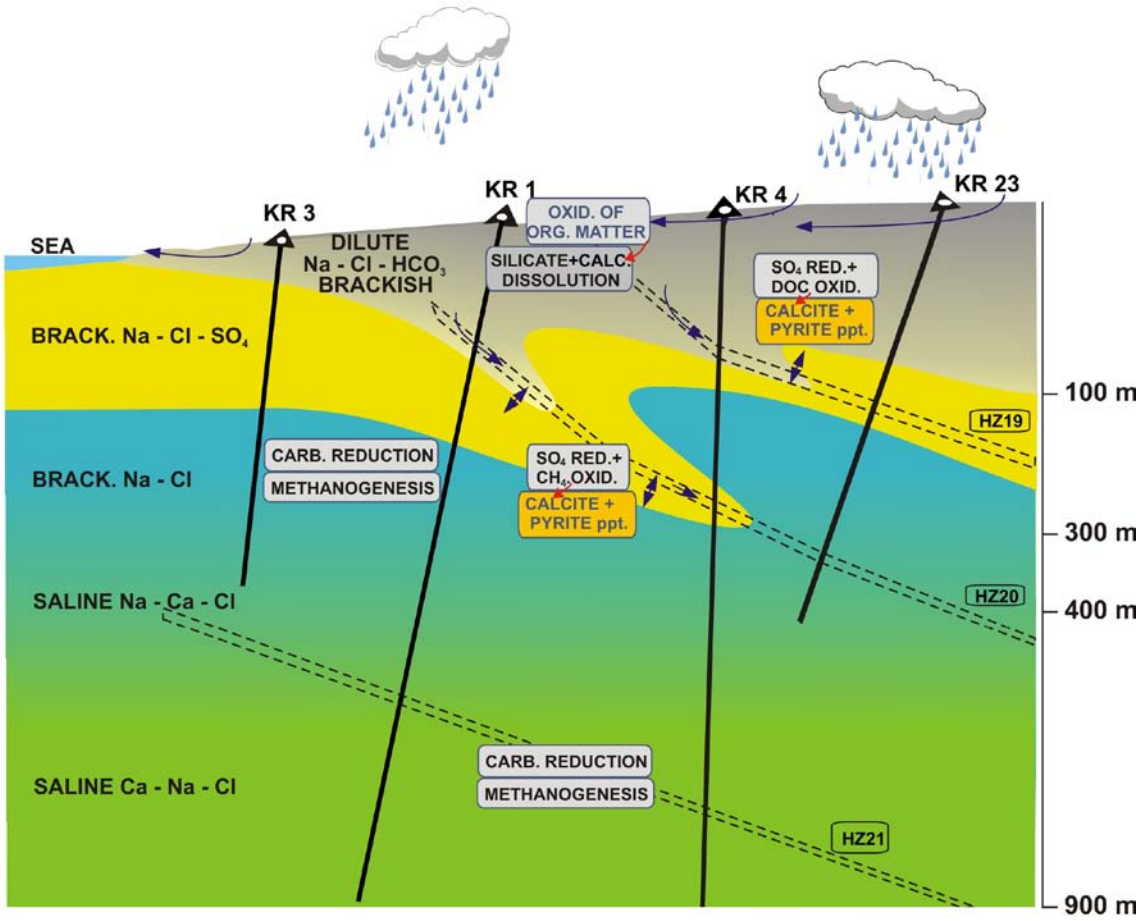

Figure 2-1. *Illustrated hydrogeochemical site model of the baseline groundwater conditions with main water-rock interactions at Olkiluoto (Posiva 2009). Changes in colour describe alteration in the water type. The most-dominant hydrogeological zones HZ19, HZ20, HZ21 are also presented with indications of groundwater flow (→) and mixing (↔). Rounded rectangles contain the main source and sink reactions controlling pH and redox conditions. Enhanced chemical reactions dominate in the infiltration zone at shallow depths, and at the interface between the Na-Cl-SO_4 and Na-Cl groundwater types. Note that the illustration depicts hydrogeochemical conditions in the variably conductive fracture system, not in the diffusion-dominated pore space inside the rock blocks.*

Changes in climate and the geological environment have had a significant effect on local palaeohydrogeological conditions, and have left clear imprints on chemical and isotopic signatures (Table 2-3, Figure 2-1). Interpretation of data indicates that there are at least six end-member water types influencing current groundwater compositions at the Olkiluoto site (Pitkänen et al. 2004, Posiva 2009). They originate from different periods, ranging from modern times, through former Baltic stages, to pre-glacial times:

Modern:

- meteoric water that infiltrated during terrestrial recharge (during the last 0–2,500 a),
- water infiltrated from a local freshwater reservoir.

Baltic stages:

- sea water from the Gulf of Bothnia (0–2,500 a),
- Littorina sea water (2,500–8,500 a, major infiltration during the early stage),
- colder climate meteoric water probably glacial melt water (more than 10,000 a ago).

Pre-glacial times:

- saline water (brine) which intruded and/or was formed under the influence of hydrothermal activity (pre-Quaternary, probably early Phanerozoic to Precambrian in age).

A detailed description of the hydrochemical characteristics and history of the groundwaters occurring presently at different depths in Olkiluoto is given by Pitkänen et al. (2004) and Posiva (2009).

Shallow groundwaters from overburden and bedrock ("fresh HCO_3" classification in Table 2-3) are the most representative of modern meteoric infiltration, but clear imprints of early meteoric infiltration, mixed with former groundwaters can be observed down to depths of 100 m to 150 m ("brackish HCO_3" classification). Brackish SO_4-type groundwater is the dominant result of Littorina infiltration. The influence of glacial melt is observed both in brackish SO_4- and brackish Cl-type groundwaters. The original brine end-member has been diluted with meteoric water to form saline – brackish groundwater from 300 m depth downwards. Brackish Cl-type groundwater represents the end-product of this dilution.

2.1.2.2 Assessment of temporal hydrogeochemical evolution

The following assessment of future hydrogeochemical estimates of potential groundwater infiltrating the repository (Table 2-4) is based on groundwater data from Olkiluoto (Pitkänen et al. 2007), interpreted hydrogeochemical evolution in the past (Andersson et al. 2007, Posiva 2009, Pitkänen et al. 1999, 2004), numerical groundwater flow predictions for the future (Pastina and Hellä 2006), and observations done for other sites in Finland. The ranges of constituents in the

Table 2-4. Potential hydrogeochemical conditions at repository depth (400–600 m) at the Olkiluoto site. The concentrations are given both in mg/L and M. Those parameters considered important for corrosion of the canister are highlighted in bold font.

Constituent		Baseline	At closure, infiltration into unsaturated bentonite	After closure and saturation (i.e. up to 100 years)	After closure up to 10,000 years
pH		**7.6–8.1**	**6.8–8**	**6.8–8**	**6.9–7.8**
Eh	**mV**	**–200 to –300**	**Oxic to –250**	**–150 to –250**	**–170 to –220**
Dissolved inorganic carbon	M	$(< 0.30)\cdot10^{-3}$	$(0.1–3)\cdot10^{-3}$	$(0.1–3.5)\cdot10^{-3}$	$(1–5)\cdot10^{-3}$
Cl^-	**mg/L** **M**	**6,000–16,000** **$(1.7–4.5)\cdot10^{-1}$**	**2,500–16,000** **$(0.7–4.5)\cdot10^{-1}$**	**2,000–9,000** **$(0.5–2.5)\cdot10^{-1}$**	**300–3,500** **$(0.08–0.1)\cdot10^{-1}$**
Na^+	mg/L M	2,400–4,800 $(1.0–2.0)\cdot10^{-1}$	1,000–4,800 $(0.4–2.0)\cdot10^{-1}$	1,000–3,300 $(0.4–1.4)\cdot10^{-1}$	250–1,500 $(0.1–0.6)\cdot10^{-1}$
Ca^{2+}	mg/L M	800–4,800 $(0.2–1.2)\cdot10^{-1}$	250–4,800 $(0.06–1.2)\cdot10^{-1}$	100–2,300 $(0.03–0.6)\cdot10^{-1}$	60–600 $(0.02–0.15)\cdot10^{-1}$
Mg^{2+}	mg/L M	25–70 $(1.0–2.9)\cdot10^{-3}$	40–150 $(0.2–0.6)\cdot10^{-2}$	70–150 $(0.3–0.6)\cdot10^{-2}$	20–200 $(0.4–0.8)\cdot10^{-2}$
K^+	mg/L M	10–20 $(2.6–5.1)\cdot10^{-4}$	5–20 $(1.3–5.1)\cdot10^{-4}$	5–20 $(1.3–5.1)\cdot10^{-4}$	5–20 $(1.3–5.1)\cdot10^{-4}$
SO_4^{2-}	mg/L M	< 40 $< 0.4\cdot10^{-3}$	0–400 $0–4.2\cdot10^{-3}$	0–400 $0–4.2\cdot10^{-3}$	80–400 $(0.8–4.1)\cdot10^{-3}$
HS^-	**mg/L** **M**	**< 0.5** **$< 0.3\cdot10^{-4}$**	**0–25** **$0–8\cdot10^{-4}$**	**0–42** **$0–13\cdot10^{-4}$**	**0–37** **$0–11\cdot10^{-4}$**
NH_4^+	**mg/L** **M**	**< 0.05** **$< 0.03\cdot10^{-4}$**	**< 1** **$< 5\cdot10^{-5}$**	**< 1** **$< 5\cdot10^{-5}$**	**< 0.6** **$< 3.3\cdot10^{-5}$**
NO_2^-	**mg/L** **M**	**< 0.02** **$< 4\cdot10^{-7}$**	**< 0.02** **$< 4\cdot10^{-7}$**	**< 0.02** **$< 4\cdot10^{-7}$**	**< 0.02** **$< 4\cdot10^{-7}$**
$CH_4(g)$	mL/L M	130–400 $(0.6–1.8)\cdot10^{-2}$	< 400 $< 1.8\cdot10^{-2}$	< 250 $< 1.1\cdot10^{-2}$	0.1–30 $(0.004–1.3)\cdot10^{-3}$
$H_2(g)$	mL/L M	< 0.4 $< 1.8\cdot10^{-5}$	< 0.4 $< 1.8\cdot10^{-5}$	< 0.05 $< 2.2\cdot10^{-6}$	< 0.01 $< 4\cdot10^{-7}$
*DOC**	*mgC/L* *M of C*	*< 2* *$< 1.7\cdot10^{-4}$*	*< 2* *$< 1.7\cdot10^{-4}$*	*< 2* *$< 1.7\cdot10^{-4}$*	*< 2* *$< 1.7\cdot10^{-4}$*
Microbes		**acetogens, methanogens**	**aerobic bacteria, SRB, IRB, methanogens**	**SRB, IRB, methanogens**	**IRB, SRB,**

* Current dissolved organic carbon (DOC) data are unreliable. Deep samples with high pump rate generally have only a few mg/L DOC.

initial condition are selected from current database and geochemical modelling results, representing water analyses at the potential repository depth of about 420 m. Particularly important information compared to the earlier report (King et al. 2001, 2002a) has been taken from the safety case evolution report and its background reports (Luukkonen and Nordman 2007, Pastina and Hellä 2006) in which site-scale total dissolved solids (TDS) predictions are simulated with flow modelling for the next 100,000 years and beyond. The report presents detailed predictions of average salinities for the first repository tunnel and of maximum salinities in the whole repository based on the hydraulic properties of rock and water as they are described in the 2004 Olkiluoto site description (Posiva 2005). The flow and salinity simulations were updated by Löfman and Poteri (2008) with the hydrogeological model in the 2006 Olkiluoto site description (Andersson et al. 2007). The calculations did not indicate significant differences compared to previous results. However, they predicted some stronger dilution in groundwater entering the disposal tunnels in the long term than the earlier calculations. Therefore, the reader should be careful with the values presented in Table 2-4, because it is clear that the hydrogeological model will change during the site investigations associated with ONKALO construction (cf. Posiva 2009) and, therefore, predictions on salinity distributions will be updated after a few years. Salinity predictions also depend significantly on selected climatic scenarios. The presented ranges in Table 2-4 cover the TDS variations predicted in both simulation rounds.

Salinity and chloride

The current salinity of groundwater at repository depth ranges from 10 to 20 g/L TDS (Andersson et al. 2007). During the repository operation, non-saline meteoric water and Baltic seawater are expected to be drawn towards the repository from above, and saline water from below. According to flow simulations (Pastina and Hellä 2006) however, infiltration of meteoric water is limited to above the repository level and SO_4-rich brackish groundwater will mix and dilute originally saline groundwater around the repository. Seawater intrusion may also dominate the drawdown from the surface as results from Äspö suggest (e.g. Luukkonen 2001). Therefore, the salinity of the groundwater is expected to remain at least brackish around the repository. If the repository crosses hydraulic features extending deeper down into the highly saline groundwater environment, upconing of saline water will locally increase the salinity level at repository depth. During the operational phase (100 years) the TDS may rise from 4-12 g/L at the time of emplacement of the first canister to 10-25 g/L in the vicinity of the excavations at repository level and up to 50 g/L at 550 m depth, based on groundwater flow simulations and depending on the extent of fracture grouting (Löfman 2005, Pastina and Hellä 2006, Löfman and Poteri 2008).

As a result of postglacial land uplift, the hydraulic gradient will increase at Olkiluoto and dilute meteoric infiltration will penetrate deeper in the bedrock in such a way that the groundwater at repository level may become fresh (TDS about 0.5 g/L) after several tens of thousands of years. This is possible according to calculations if glaciation does not develop during this time period. It is quite evident according to the compositions of current shallow groundwaters that normal water-rock interaction prevents the salinity from decreasing to any lower level in such a climate scenario.

In the far future, however, Olkiluoto and possible sites in Sweden will endure glacial cycles with a permafrost stage, glaciation, deglaciation and another temperate climate interglacial period, with a marine stage at current coastal areas. Hydrogeochemical interpretations concerning the past cycle (Pitkänen et al. 1999, Posiva 2009) indicate that during glaciation the salinity at Olkiluoto has not been significantly higher than currently found at repository depth. The results of geochemical modelling suggest that the Cl^- concentration may not have been more than currently observed at 600 to 700 m depth, approximately 22 g/L, corresponding to 35 g/L TDS. The flow simulations (Pastina and Hellä 2006) predict salinity increases of about 25 g/L under permafrost and ice sheets over several tens of thousands of years.

During the past deglaciation the salinity probably decreased. However, dilution caused by glacial melt infiltration has been less than 10% at the repository level and the groundwater has remained saline (Posiva 2009). The remnants of glacial water deep in the bedrock at Olkiluoto are not necessarily melted from the Weichselian ice sheet and observed indications of glacial water at these depths may have resulted from gradual infiltration and mixing of earlier colder climate waters (Pitkänen et al. 2004, Posiva 2009). Dilution has instead been more effective in the upper part of the bedrock

just after glaciation, so that roughly half of the groundwater has had glacial origin at the depths where SO_4-rich groundwater dominates at present. According to flow predictions, the effect of deglaciation at repository level is not significant if the duration of the ice retreat across the Olkiluoto site is about ten years, as was the average melting rate for the Weichselian case (Pastina and Hellä 2006). However, if the retreat is halted (cf. the Salpausselkä stage during the Weichselian deglaciation) and the ice margin stays at Olkiluoto for several hundreds of years, melt water might reach the repository along transmissive fracture zones.

A marine stage is probable during the next temperate domain. It is also possible that the Baltic basin will be filled with oceanic water. The Cl^- content of current Atlantic seawater is about 20,000 mg/L, but marine input is not considered to reach repository depth without any dilution according to the results from the Olkiluoto and Hästholmen sites. Potassium is generally high in marine water (up to 400 mg/L). However, in current groundwater conditions, K^+ has been depleted strongly in marine-derived groundwater (brackish SO_4 type) mostly by cation exchange, to as little as 10–30% of the level of the original content in Littorina Sea water. However, this marine-derived groundwater has not yet reached the repository level, so the concentration will further decrease before the groundwater has descended to the 400–500 m level.

pH and redox conditions

In the long term the pH and the redox conditions will be buffered by the same processes as in the initial state resulting in similar pH and redox values. The stage just after closure is an exception when the pH values can be slightly acidic and the redox potential positive. Oxygen initially trapped in the repository will be consumed by corrosion of the canister, by reaction with oxidisable minerals, and by reaction with organic matter (SKB 2006a). The anaerobic oxidation of organic matter coupled to the reduction of iron (III) compounds (oxidised during the operational phase) and/or SO_4^{2-} ions will subsequently reduce the redox potential to negative values. Aerobic oxidation of organic matter and CH_4 will produce CO_2, which tends to decrease the pH of the infiltrating groundwater. Fracture calcites are strong pH-buffers and equilibrium with calcite is considered to increase the pH above 7 soon after closure.

After the initial oxygen consumption by the processes described above, it is not expected that oxygen will intrude into the repository level. Below about 300 m depth, studies of methane and of isotopic composition at Olkiluoto indicate that the deep stable groundwater system has not been disturbed by glacial and post-glacial transients and that neither oxidising glacial melt water nor marine water have mixed in this deeper system (e.g. Posiva 2009). As a result, non-oxidising conditions have been maintained at repository depth over geological timescales.

Changes in pH conditions will be dependent on the mixing of infiltrating groundwaters, assuming calcite buffers the pH. Simulations with PHREEQC (Parkhurst and Appelo 1999) indicate that mixing of CH_4-rich and SO_4-rich groundwaters decreases the pH to just below 7 when the salinity of the final waters vary from 9 g/L to 5 g/L which is the predicted average salinity of infiltrating water in the repository during the first 10,000 years (Luukkonen and Nordman 2007, Pastina and Hellä 2006). If the salinity is higher than 9 g/L or lower than 5 g/L, the pH is probably higher corresponding to values in the current initial stage groundwaters.

Sulphide

In general, the sulphide concentration is initially fairly low (< 1 mg/L), although single higher values (up to 12 mg/L) have been measured in the mixing zone of SO_4-rich and CH_4 groundwaters, i.e. brackish SO_4^{2-}- and brackish Cl^-- type groundwaters (Figure 2-1). Dissolved CH_4 and SO_4 are together thermodynamically unstable, but they are not able to react spontaneously in low-temperature environments (Appelo and Postma 2005). However, consortia of certain microbes can reduce SO_4^{2-} with energy gained from anaerobic CH_4 oxidation producing HS^- which is unstable in the presence of reactive iron/iron compounds (Pedersen 2008). Increased concentrations of dissolved sulphide are probably the result of the lack of reactive iron and precipitation, as iron sulphide formation is kinetically limited by the slow release of iron from silicates (Pitkänen et al. 2004, Pitkänen and Partamies 2007).

The upper ends in the range of dissolved sulphide in the Table 2-4 for the operational phase and after closure of the repository are based on geochemical simulations presented in the safety case evolution report (Pastina and Hellä 2006). Reactive iron does not occur initially at repository depth at Olkiluoto, but disturbed conditions during construction and operation will produce ferric oxyhydroxides in the excavation damaged zone (EDZ). Reactive iron may also be introduced in the backfill. Consequently, the sulphide concentration will probably be lower than simulations suggest. Sulphide is consumed in the simulations by pyrite precipitation in bentonite backfill (which contains iron oxyhydroxide) in the repository deposition tunnels (Luukkonen and Nordman 2007). Similarly sulphide may be precipitated by ferric hydroxides. The model results suggest that groundwater sulphide will not reach the deposition holes and the bentonite around the canister.

The alternative way that sulphide could approach the canister is through a fracture intersecting the deposition hole. Arbitrarily assuming a sustained concentration of 1 mmol/L HS^- in the fracture for 100,000 years, the amount of sulphide that could react with the topmost surface of the canister is predicted to be 59 mol, or 49 mol/m^2 (for diffusion limited transport). This amount would correspond to about the reaction of 100 mol/m^2 of copper, equivalent to a depth of corrosion of about 0.7 mm after 100,000 years by general corrosion. With the present observed maximum concentration of sulphide in Olkiluoto (12 mg/L or 0.36 mmol/L), it would thus take some 20 million years to corrode the canister uniformly (Pastina and Hellä 2006).

There are a number of uncertainties affecting the sulphide behaviour, such as the kinetics of the geomicrobial CH_4–SO_4 redox reaction and the kinetics of pyrite or FeS precipitation.

Ammonium

Ammonium is produced by the decomposition of organic debris in seabed sediments. It is easily removed from groundwater by irreversible cation exchange processes. Therefore, the concentration of ammonium will probably be below the detection limit, except if seawater intrusion reaches the repository level fairly quickly. Slight enrichment of ammonium has been observed in groundwaters collected from the vicinity of the ONKALO tunnel, which may indicate contamination due to blasting (Pitkänen et al. 2008). The enrichment of ammonium either by seawater intrusion or excavation is possible only during the operational phase. However, ammonium concentrations will not likely reach concentrations higher than a few mg/L according to the monitoring results during ONKALO construction (Pitkänen et al. 2008).

Methane

Methane is associated with non-marine groundwater deep in the bedrock. The content of methane increases with salinity so that the current saline groundwater types between 400–600 m depth contain 200–500 mL_{NTP}/L, while the sulphate-poor brackish groundwater above contains about 50 to 150 mL_{NTP}/L. These values suggest that there is a possibility of SO_4 reduction by CH_4 if marine-derived groundwater is mixed in the system. At greater depths, near the 1,000 m level, CH_4 is near saturation in the saline groundwater (Paloneva 2009) and there is the possibility of gas phase formation if the temperature increases or the pressure decreases, e.g. if the groundwater migrates towards the repository. Bacterial methane formation, which is evident at Olkiluoto (Pitkänen and Partamies 2007), could also cause oversaturation and gas phase separation at great depths. The behaviour and accumulation of methane is also currently under investigation at Olkiluoto.

Hydrogen

Hydrogen concentrations also increase with depth and are in the range 10^{-6} to 10^{-5} mol/L dissolved H_2, equivalent to a H_2 partial pressure of 10^{-3} to 10^{-2} bar (Table 2-4 and Auqué et al. 2006). Hydrogen will not accumulate significantly to reach mL_{NTP}/L levels in groundwater, since it will be actively used by microbes which use it as an energy source in anaerobic processes. A slight enrichment in saline groundwater may be controlled by the decreased activity of methanogens to produce CH_4 with very low DIC contents (Posiva 2009). Following failure of the outer copper shell, however, significant amounts of H_2 will accumulate in the near field because of anaerobic corrosion of the cast iron insert.

Dissolved Organic Carbon (DOC)

The DOC concentrations are generally low in groundwaters with long residence times because it is used as an energy source in anaerobic microbial processes. However, in groundwaters with short residence times, DOC contents may be relatively high, because biological degradation of large organic molecules, such as humic acids, is a slow process (Appelo and Postma 2005). If fresh HCO_3-rich groundwater is drawn down to repository depths, DOC concentrations would occasionally increase. The infiltration seems to be a relatively slow process according to the flow simulations (Löfman and Poteri 2008). Thus it is believed that the DOC content will remain low in deep groundwater.

2.2 Bentonite pore-water chemistry in the repository

2.2.1 Processes determining bentonite pore-water chemistry

The water in bentonite can be divided between that in the interlamellar space and that in the larger external pores. Because of the negative charge on the surface of the clay particles, an electrical double layer (EDL) exists with a higher concentration of cations than anions near the clay surface. Some of the external water is trapped within the EDL from which chloride is largely excluded because of its negative charge. The remainder of the external water where chloride can exist is considered to be free water. Figure 2-2 presents different porosity types in compacted bentonite in equilibrium with 0.1 M NaCl solution as a function of the clay density. The curves are based on measured data for chloride porosity and modelling with the Donnan model (Muurinen 2006a). Both the porosity associated with the external water and that corresponding to the free water outside the EDL decrease with increasing density. In this discussion, bentonite pore water is considered to be the free water in the pores of the bentonite, where the double layer effects can be ignored. If there is equilibrium between the bentonite and the solution outside of the bentonite, the chemical composition in that space of the pores should be equal to the external solution.

Bentonite normally consists of the clay mineral montmorillonite and of accessory minerals, e.g. feldspars, quartz, calcite, dolomite, siderite and pyrite. The desired physical properties are mainly governed by the montmorillonite, which therefore normally dominates the bentonite material in commercial products. The type and amount of accessory minerals vary quite substantially between the different commercial products depending on the mining site. Montmorillonite has a relatively low solubility, and the actual accessory mineral composition in combination with added water solution

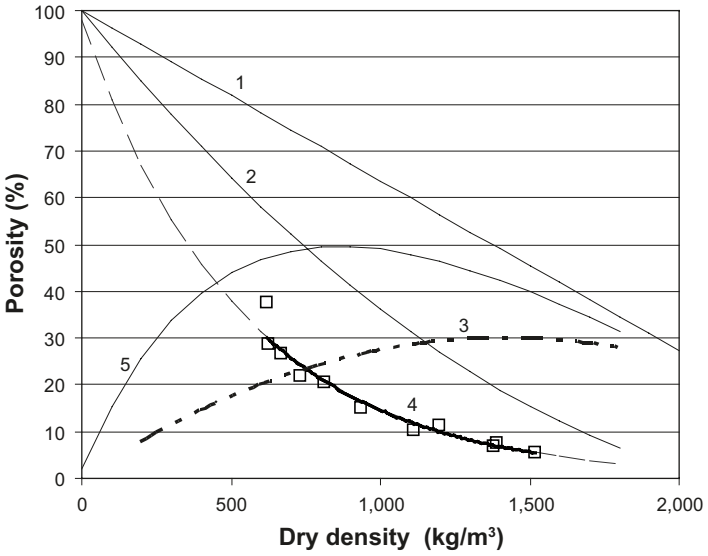

Figure 2-2. *Different pore types in bentonite based on measured data with 0.1 M NaCl and modelling with the Donnan model (Muurinen 2006a). 1) total porosity, 2) external porosity, 3) interlamellar porosity, 4) chloride porosity and 5) porosity not accessible for chloride.*

and the interactions with the surrounding groundwater therefore determine the pore-water composition. Figure 2-3 gives a schematic illustration of the geochemical equilibrium processes considered most important in the modelling by Luukkonen (2004). The montmorillonite layering and interlayer sites seen on the left participate by cation exchange. The important mineral equilibria are presented on the right and the entrapped gases on the top.

The main clay mineral in Wyoming MX-80 bentonite is Na-montmorillonite. The second reference bentonite, Deponit CA-N, mentioned in Pastina and Hellä (2006) has Ca- and Mg-montmorillonites as the dominant clay minerals and is relatively rich in carbonate minerals (up to 13% of calcite + siderite + dolomite). The presence of carbonates is of special relevance due to their pH buffering capacity. Similarly, its pyrite content is higher than that of MX-80, which is beneficial for the redox buffering capacity. However, the presence of pyrite in MX-80 and Deponit CA-N may be detrimental for corrosion of the canister on the assumption that the dissolution of pyrite, a polysulphide, results in the release of sulphide.

According to the current concept, the compacted bentonite blocks placed in the deposition hole are designed to produce a density after saturation and homogenization of 1,950–2,050 kg/m^3 (dry density 1,484 – 1,640 kg/m^3). The initial degree of saturation is planned to be 75–81% (Pastina and Hellä 2006). Following closure, the repository host rock and EDZ are expected to return to saturated conditions over a few years. The mechanism of bentonite saturation and the time needed for it are still unclear. According to Hökmark (2004), the buffer will be fully water-saturated within about 3 or 4 years, provided there is sufficient supply of water at the buffer/rock interface. Furthermore, Hökmark (2004) concluded that the saturation time might depend more on hydrological conditions around individual deposition holes, the hydrological buffer/rock interaction, and restoration of the groundwater pressure after repository closure, than on the properties of the bentonite. Lempinen (2006) also modelled the resaturation period and found that, depending on the hydrological boundary condition, the duration of the resaturation period could be longer than previously anticipated, extending from about 30 to 40 years up to hundreds of years. At full saturation, the planned value of the bentonite density is about 2,000 kg/m^3 and the hydraulic conductivity is very low, less than 10^{-12} m/s (SKB 1999a).

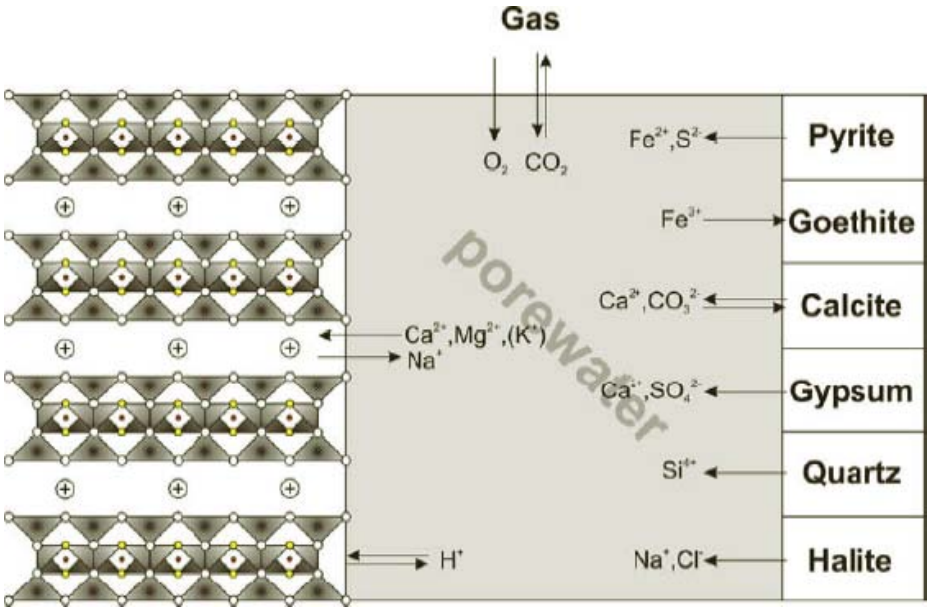

Figure 2-3. *Schematic illustration of geochemical equilibrium processes used in modelling by Luukkonen (2004). The montmorillonite layering and interlayer sites are seen on the left, the mineral equilibria on the right and the entrapped gases on the top.*

When the spent fuel canister and bentonite have been placed in the deposition hole, heating starts to dry the inner parts of the bentonite. All near-field materials will experience a period of heating and a subsequent period of cooling. Elevated temperatures will continue to persist for thousands of years, but the maximum temperature will be reached between 10 and 30 years after disposal. The maximum temperature of 100°C is calculated assuming dry bentonite, but saturation of the bentonite is likely to reduce this by up to 15°C (Raiko 1996, Ageskog and Jansson 1999). The temperature rise in the near field will not adversely affect the performance of the bentonite buffer. Current data suggest that the mineralogical and chemical properties of the bentonite in the deposition hole will not be affected by temperatures below 130°C (SKB 1995, Wersin et al. 2007). Support for the stability of bentonite at higher temperatures is given by various natural analogues, such as for example for bentonite occurring at a depth of 500 m at Hamra, Gotland in Sweden (SKB 1992), which has been heated to temperatures of 110–120°C for at least 10 Ma during its geological history without any signs of cementation or significant deterioration (Crawford and Wilmot 1998). According to Karnland and Birgesson (2006), some reservations have to be made in the case of illitisation for the conditions which are not covered in the earlier studies. The conditions mentioned are high pH, low liquid-to-solid ratio, diffusive silica transport and divergent bentonite composition compared to that examined. The temperature conditions in the repository system will approach the natural situation after 10,000 years when the decay heat has declined to less than one per cent of its original value (SKB 1999b).

The general trends of temperature effects on the near-field chemical processes are known (Table 2-5), and some experimental and modelling studies are available. Some laboratory experiments have shown a redistribution of the easily dissolving accessory minerals (e.g. gypsum and calcite) during water saturation of bentonite under a thermal gradient. Calcium sulphate (gypsum, anhydrite) and calcium carbonate (calcite) have a decreasing solubility with increasing temperature, which was proposed as a possible cause for their precipitation. Another possible cause may be evaporation of water from the hot area of the bentonite followed by vapour transport to the cold area and simultaneous flow of the condensed water towards the hot area. The latter process has been observed to also transport other easily dissolved substances derived from groundwater, e.g. sodium chloride (halite). The precipitation of gypsum has been confirmed in the LOT field experiments at Äspö (Karnland et al. 2000, Muurinen 2006b). In Muurinen (2006b), chloride was also analyzed at different distances from the heater, but no precipitation or concentration peak of chloride close to the heater was found in the fully saturated clay during the five-year experiment. The evaluated chloride porosity (15%) at the dry density of 1.5 g/cm^3 is quite high compared to the values normally obtained at about the same salinity and density (Figure 2-2). This may indicate pumping of chloride from the groundwater to the bentonite during saturation.

The bentonite porewater constituents potentially important for the corrosion of the copper canister are given in Table 2-5; also included are the processes that have an effect on the constituents. Some of the processes have fast kinetics, some are reversible, some irreversible, and for some reactions to occur microbial activity is a prerequisite. The processes given in bold italics are the most-significant processes in causing notable changes in the corresponding constituents.

The assessment of long-term porewater evolution here is based on modelling exercises (Arcos et al. 2006, Bruno et al. 1999, Domènech et al. 2004, Luukkonen 2004, Luukkonen et al. 2005, Wanner et al. 1992, Wersin et al. 1994a, Wersin 2002, Wieland et al. 1994). Experimental results on the interaction of aqueous solutions with bentonite are available from short-term batch experiments (e.g. Snellman et al. 1987, and others), from interaction experiments with compacted bentonite and external solutions (Muurinen and Lehikoinen 1999), and from the LOT experiment in the Äspö HRL after the five-year experiment (Muurinen 2003, 2006b).

Table 2-5. Constituents important in determining the influence of bentonite porewater on the corrosion of copper and the associated processes affecting the values. Constituents and processes which are dominant are given in bold italics.

Constituent	Cause of possible changes in the constituent values	direction of change
pH	***– calcite dissolution***	⇨ increase
	precipitation	⇨ decrease
	– surface protonation	⇨ increase
	– deprotonation	⇨ decrease
	– pyrite dissolution	⇨ decrease
	– temperature increase	⇨ decrease
	– decrease in redox potential (Eh)	⇨ increase
	– decrease of partial pressure of CO_2	⇨ increase
Alkalinity	– calcite dissolution	⇨ increase
	precipitation	⇨ decrease
Redox potential (Eh), O_2	***– corrosion of the canister***	⇨ decrease
	– active microbial processes	⇨ decrease
	– oxidation of pyrite	⇨ decrease
	– oxidation of other Fe(II) minerals	⇨ decrease
	– oxidation of HS	⇨ decrease
	– O_2 from groundwater	⇨ increase
Cl^-	– halite dissolution	⇨ increase
	– diffusion in/out	⇨ increase/decrease
Ca^{2+}	– $CaSO_4$ (anhydrite or gypsum) dissolution	⇨ increase
	– calcite dissolution	⇨ increase
	precipitation	⇨ decrease
	– ion exchange with Na^+	⇨ decrease
	– diffusion in/out	⇨ increase/decrease
SO_4^{2-}	– oxidation of pyrite	⇨ increase
	– $CaSO_4$ (anhydrite or gypsum) dissolution	⇨ increase
	– diffusion in/out	⇨ increase/decrease
HS^-	***– microbially mediated sulphate reduction***	⇨ increase
	– pyrite precipitation	⇨ decrease
	– oxidation	⇨ decrease
	– diffusion in	⇨ increase
NH_4^+	– ion exchange with Na^+	⇨ decrease
	– diffusion in	⇨ increase
CH_4(g)	– temperature increase	⇨ decrease CH_4(aq)
	– pressure increase	⇨ increase CH_4(aq)
	– diffusion in	⇨ increase
Microbes	– water activities comparable to saturated compacted bentonite = > microbes not viable	⇨ no effect

The interaction of the porewater with the accessory minerals as well as montmorillonite surface reactions will be the processes controlling the geochemical evolution of the system. These reactions are summarised below (Bruno et al. 1999, Arcos et al. 2006):

Dissolution-precipitation of carbonates. The minerals of importance are calcite, dolomite and siderite which can dissolve/precipitate according to the following reactions:

$CaCO_3(s) + H^+ \leftrightarrow Ca^{2+} + HCO_3^-$

$CaMg(CO_3)_2(s) + 2H^+ \leftrightarrow Ca^{2+} + Mg^{2+} + 2HCO_3^-$

$FeCO_3(s) + H^+ \leftrightarrow Fe^{2+} + HCO_3^-$.

The reactions are important pH determinants and the last one also has an effect on the redox potential.

Protonation-deprotonation of the surfaces. This process contributes to the pH buffering according to the following reactions on the smectite surfaces:

$\equiv SOH + H^+ \leftrightarrow \equiv SOH_2^+$

$\equiv SOH \leftrightarrow \equiv SO^- + H^+$.

Cation-exchange reactions. The main cation-exchange reactions are the following:

$NaX + K^+ \leftrightarrow KX + Na^+$

$2NaX + Ca^{2+} \leftrightarrow CaX_2 + 2Na^+$

$2NaX + Mg^{2+} \leftrightarrow MgX_2 + 2Na^+$.

The control exerted by this process on the calcium and magnesium concentrations in the porewater also directly affects the dissolution-precipitation of the Mg and Ca minerals in the porewater.

Sulphate dissolution/precipitation. This dissolution of gypsum is a source of sulphate and calcium ions, the latter also participating in the dissolution/precipitation of calcite.

$CaSO_4 \leftrightarrow Ca^{2+} + SO_4^{2-}$.

The precipitation of gypsum and anhydrite is dependent on the temperature, so that this process strongly depends on the thermal gradient during the non-isothermal period of the repository.

Equilibrium with pCO_2 in an open system. Equilibrium between calcite, dissolved CO_2, HCO_3^-, and CO_3^{2-} determines the pH:

$CaCO_3(s) + CO_2(aq) + H_2O \leftrightarrow Ca^{2+} + 2HCO_3^-$.

This reaction is important especially in an open system.

Oxidation-reduction processes in bentonite. The redox potential will be controlled by the redox active components in the bentonite. If pyrite is present, the oxidation of the polysulphide can occur (initially when O_2 is present) through the following reaction:

$FeS_2(s) + 3.75O_2(aq) + 3.5H_2O \rightarrow Fe(OH)_3(s) + 2SO_4^{2-} + 4H^+$

The reaction is irreversible under repository conditions if reducing microbes are not present. Siderite oxidation is another potential redox-controlling reaction:

$FeCO_3(s) + 2.5H_2O + 0.25O_2(aq) \leftrightarrow Fe(OH)_3(s) + H^+ + HCO_3^-$.

Other processes include the dissolution of silicates and aluminosilicates, but these reactions are less important for copper corrosion.

2.2.2 Predicted bentonite pore-water composition

The chemical conditions in the bentonite porewater are determined by a combination of the reactions above and the diffusion of the chemical components from the groundwater to the porewater and vice versa. The direction of the diffusion can change since the groundwater concentration is expected to vary as a function of time.

Table 2-6 gives the estimated values for the constituents of interest in bentonite porewater at Olkiluoto. These conditions are also considered representative for the Swedish sites (except for the chloride and methane contents, which are lower at the Swedish sites). The assessment is based on the assumption that bentonite becomes fully saturated within the first 100 years, by which time the infiltrating groundwater becomes anoxic again.

The composition of Äspö groundwater is closest to that of Olkiluoto groundwater. Accordingly, the evaluated values for Olkiluoto given in Table 2-6 are based on the modelling results for Äspö, but the values in saturated bentonite are also based on experimental results (Snellman et al. 1987, Muurinen and Lehikoinen 1999, Muurinen 2006b). The major differences between Äspö and Olkiluoto groundwater are the pH and salinity (Na^+, Ca^{2+}, Cl^-), but the ranges considered at different time periods are large.

Table 2-6. Estimated constituent values in bentonite porewater at Olkiluoto during the evolutionary periods considered. Those parameters considered important for corrosion of the canister are highlighted in bold font.

Constituent		Infiltrating groundwater at closure	Porewater in saturated bentonite (up to 100 years)	Porewater after closure up to 10,000 years
pH		**6–8**	**7–9**	**7–9**
Redox potential (Eh)	**mV**	**Oxic to –250**	**–150 to –250**	**–170 to –220**
DIC	M	$(0.1–3.5)\cdot10^{-3}$	$(0.3–3)\cdot10^{-3}$	$(0.3–3)\cdot10^{-3}$
Cl^-	M	**$(0.3–4.5)\cdot10^{-1}$**	**$(0.5–4.5)\cdot10^{-1}$**	**$(0.08–0.1)\cdot10^{-1}$**
Na^+	M	$(0.4–2.0)\cdot10^{-1}$	$(3–5)\cdot10^{-1}$	$(3–4)\cdot10^{-1}$
Ca^{2+}	M	$(0.3–1.2)\cdot10^{-1}$	$(4–40)\cdot10^{-3}$	$(4–40)\cdot10^{-3}$
SO_4^{2-}	M	$(0–4.2)\cdot10^{-3}$	$0.4\cdot10^{-1}$	$0.4\cdot10^{-1}$
HS^-	**M**	**$(0–1)\cdot10^{-3}$**	**$(0–1.3)\cdot10^{-3}$**	**$(0–1.1)\cdot10^{-3}$**
NH_4^+	**M**	**$< 3.3\cdot10^{-5}$**	**$< 3.3\cdot10^{-5}$**	**$< 3.3\cdot10^{-5}$**
$CH_4(g)$	M	$1.8\cdot10^{-2}$	$1.1\cdot10^{-2}$	$(0.004–1.3)\cdot10^{-3}$

Bruno et al. (1999) have modelled the interaction of bentonite and groundwater applying first an instantaneous equilibrium followed by a number of exchange cycles with new incoming groundwater. In the modelling exercise for the repository, the expected porewater/bentonite ratio (0.41cm^3 water/cm^3 bentonite) was used, and the amounts of accessory minerals (calcite and pyrite) were included, as well as the ion-exchange processes. The interaction with three Swedish groundwaters (Äspö, Finnsjön, and Gideå) was modelled.

Based on a hydraulic conductivity of 10^{-11} m/s and a hydraulic gradient of 0.1 in the bentonite (thickness of 0.35 m), Wanner et al. (1992) and Wieland et al. (1994) estimated a period of 13,800 years for the total porewater replacement. According to this estimation, the bentonite porewater would not be fully replaced after 10,000 years, i.e. by the end of the second evolutionary period considered here. Another estimation based on a hypothetical water flow leaving the near field (SITE-94 1996) implies total replacement of the bentonite porewater after 10,000 years.

Arcos et al. (2006) modelled the near-field evolution according to the pathway used by the groundwater to contact the near field. In the first case, a fracture in the host rock was assumed to intersect the deposition hole. In the second case, the groundwater was in contact with the bentonite buffer through the tunnel backfilling material. The water types used in the modelling were Forsmark groundwater, Laxemar saline water to simulate the higher salinity water, and Grimsel ice-melt water to simulate intrusion of ice-melt derived groundwater. The bentonite types were MX-80 and Deponit Ca-N.

pH

Wieland et al. (1994) modelled (using a mixing tank approach) the evolution of pH in the near field contacting bentonite with simplified Allard and Äspö groundwaters. In the case of Allard groundwater, the pH remained fixed at 8.4 while calcite was present in the system (up to about 90 exchange cycles), but after complete removal of calcite the pH gradually decreased to about 6.8. The pH value of 8.4 is comparable to the experimentally obtained value of 8.6 (Muurinen and Lehikoinen 1999). However, the modelling results (Wieland et al. 1994) in the case of Äspö groundwater and the experimental results with simplified Olkiluoto groundwater (Muurinen and Lehikoinen 1999) are not correspondingly comparable. The modelling results indicated a lower pH (about pH 6) than the experimental measurement gave (pH 8.1). It has to be noted that the tested saline solutions differed in composition, especially in the initial pH values and alkalinity (five times higher in the modelling exercise).

According to the modelling of Bruno et al. (1999), the pH-buffering capacity is not significantly affected by the replacement of porewater with granitic groundwater, whether from Äspö, Gideå or Finnsjön. The large input of Ca^{2+} with the groundwater (e.g. Äspö and Olkiluoto) induces precipitation of calcite and buffers the alkalinity, keeping the pH levels above pH 8. This agrees well with the measured bentonite porewater of pH 8.1 obtained in short-term experiments (Muurinen and

Lehikoinen 1999) when the contacting solution was simulated Olkiluoto groundwater. In the direct measurements performed in bentonite samples from the LOT experiment (Muurinen 2006b), the pH values varied from pH 7.2 close to the rock to pH 8.2 close to the heater.

In the determination of the pH value of a system, there are limitations, both in experiments and modelling exercises. The major limitation is the lack of knowledge of the partial pressure of carbon dioxide (pCO_2) in the systems considered, and on the other hand, whether the systems should be treated as open or closed when modelled. In experiments, control of the gaseous phase is also difficult and often inadequate. Muurinen and Lehikoinen (1999) modelled the bentonite porewater chemistry of their experiments applying both a closed and open system approach. In the closed system the obtained pH value was 1 to 2 pH units higher than in the open system where log pCO_2 = –3.36 was assumed. The experimental values agreed with those of the open system.

The modelling results by Arcos et al. (2006) indicate that the interaction of present-day (Forsmark) groundwater with bentonite buffer has minor effects on the pH evolution of the system, regardless of the type of bentonite (MX-80 or Deponit CA-N) considered in the model. The pH buffering capacity is caused by carbonate minerals if they are present and surface hydroxyl sites on the clay. In the case where carbonate minerals are not present, the pH is set only by surface acidity reactions, and thus the buffering capacity is smaller. The intrusion of the high-salinity Laxemar water (close to the groundwater of present-day Olkiluoto) in the system has no significant effect on the pH evolution, which is predicted to stay close to pH 7.0. The most significant changes are predicted when the dilute and alkaline ice-melting derived water enters into the system. Then the dissolution of carbonate minerals is enhanced and increases the pH of the bentonite porewater to pH 8.3.

Oxygen and redox potential

There are several chemical and microbial processes that may contribute to the depletion of trapped oxygen within the repository, including microbially induced reactions near the bentonite/host rock interface, corrosion of the copper canister, and inorganic reactions with minerals (especially pyrite) in the bentonite.

The uptake of oxygen by microorganisms and geologic media has been demonstrated and the results summarized by Puigdomenech et al. (2001). In the conclusions it was stated that, once anoxic conditions have been reached, the return towards reducing conditions proceeds for several months via different reaction paths. The various paths are probably mediated by bacterial activity and controlled by equilibration of the solution with magnetite, pyrite and Fe(III) oxyhydroxides.

However, in saturated bentonite the microbial processes cease or proceed only at a very low level (see Section 2.3) leaving only solution-mineral processes. Wersin et al. (1994a) calculated the evolution of oxygen in the near field, taking into account oxygen diffusion and the oxidation of pyrite and dissolved Fe(II). The effect of increased temperature (60°C) and hydrostatic pressure was assumed to dissolve all available O_2 in the porewater. The time for the predicted O_2 concentration to decrease to 1% of the initial level ranged between 7 and 290 years and the elapsed time at which the transition to anoxic conditions occurred was estimated to be within the same time range. Thus, the redox potential of –100 to –400 mV_{SHE} was estimated to prevail after 10–300 years of emplacement.

The simulations by Bruno et al. (1999) indicated that the reduction capacity of the bentonite system would only be exhausted after 300,000 years if a continuous flow of Äspö groundwater equilibrated with the atmosphere were reacting with bentonite with the lowest pyrite content (0.01 wt.%). According to Arcos et al. (2006), the redox state of the system seems to be controlled by the regional groundwater, which was in equilibrium with pyrite and siderite.

These calculations do not include the effect of canister corrosion on O_2 consumption. Corrosion of the canister can account for much of the O_2 in the repository, especially that in the buffer in the deposition hole. Calculations for a Canadian repository design suggest that 30–50% of the initially trapped O_2 could be consumed by canister corrosion, rather than by reaction with dissolved Fe(II) or reaction with microbes (King and Kolář 2006a).

Large-scale tests to evaluate oxygen consumption in bentonite have been carried out in the framework of the LOT project (Muurinen 2006b). Although there are significant uncertainties and

variability between different locations within the repository, the numerical simulations and large-scale tests indicate that the timescale for oxygen depletion from individual KBS-3V deposition holes is no more than a few hundred years at most, and could be as little as a few years (Muurinen 2006b). In direct measurements of the LOT samples, the Eh values measured with a Pt electrode varied from –287 mV_{SHE} close to the rock to –366 mV_{SHE} close to the heater and with the gold electrode from –183 mV_{SHE} to –228 mV_{SHE}, respectively.

Chloride

The eventual chloride content in bentonite porewater is determined by the concentration of Cl^- in the saline groundwater. The small amount of halite present as an accessory mineral in bentonite did not have any noticeable effect in experiments when the contacting solution was saline (TDS = 24 g/L), but increased Cl^- was observed in the case of fresh solution (TDS = 0.25 g/L) (Muurinen and Lehikoinen 1999). If the concentration increases due to the pumping process during the non-isothermal saturation phase, diffusion will even out the differences in bentonite porewater and the contacting groundwater in the long term.

Sulphate and sulphide

The sulphate concentration is substantially increased in bentonite porewater when compared to the content in the contacting solutions, both saline and fresh. This has been observed in experiments (Muurinen and Lehikoinen 1999) and in modelling (Bruno et al. 1999), and results from the dissolution of gypsum (or anhydrite). Microbes are not expected to be significantly active in saturated bentonite and consequently sulphate is not expected to be extensively converted to sulphide by microbial processes (see discussions in the following section). The sulphide content in bentonite porewater is foreseen to remain at the levels of the diffusing groundwater. Sulphide, which is diffusing from the groundwater into bentonite, may be precipitated by iron compounds in the clay, as proposed by Luukkonen et al. (2005). This is supported by the experiments by Muurinen (2001), who noticed that MX-80 consumed about 6 mg of sulphide per gram of bentonite. Precipitation of sulphide would delay its transport to the surface of the copper canister.

Ammonium

Ammonium present in groundwater and diffusing into bentonite is likely to become removed by the cation-exchange process (Appelo and Postma 1993), but as no experimentally verified data are available, the estimated values given are those estimated for groundwater.

Methane

The concentration of methane in bentonite porewater will reflect the contents in the contacting groundwater.

Hydrogen

The concentration of hydrogen will reflect the contents in the contacting groundwater. Studies of the impact of hydrogen gas on porewater chemistry (pH) are ongoing within the studies on the horizontal deposition variant, KBS-3H. The study is related to the impact of the supercontainer shell material surrounding the bentonite. Significant amounts of H_2 will also be produced following failure of the outer copper shell due to anaerobic corrosion of the cast iron insert.

2.3 Microorganisms

2.3.1 Groundwater microbiology at repository depth in Finland and Sweden

Microorganisms are generally a fully integrated part of any geochemical system on our planet within the temperature range of liquid water at atmospheric pressure. Research over the past 20 years has clearly shown that this is true for deep groundwater systems as well (Pedersen 2001, 2005c, Reitner et al. 2005). Modelling of deep groundwater geochemistry should, therefore, include biological processes. The biogeochemistry of deep groundwater is expected to influence a radioactive waste

repository in many different ways (Pedersen 2002). Two microbial processes are of particular importance for the understanding of copper corrosion processes in a repository. They are biological reduction of oxygen to water and the microbial reduction of sulphate to sulphide. Oxygen reduction is advantageous because of the corrosive nature of oxygen to copper. Microorganisms will reduce any intruding or remaining oxygen in a repository by the metabolic oxidation of organic carbon, methane and hydrogen, to mention the most common electron donors in deep groundwater. Sulphide production, on the other hand, poses a threat to the integrity of the canister because of its corrosive effect on copper. The electrochemical part of a corrosive process must, of course, occur at the surface of the canister, but the oxidants that cause corrosion can originate from elsewhere. The microbial reduction of oxygen and production of sulphide can occur both in the groundwater outside the buffer and backfill material, i.e. in the so called far-field, as well as in the buffer and backfill, the so called near-field.

Established knowledge

The total numbers of unattached subsurface microorganisms (in groundwater) in specific boreholes have been published for several Fennoscandian Shield sites. The published data sets cover groundwater from the Stripa research mine (Pedersen and Ekendahl 1992a, Ekendahl et al. 1994, Ekendahl and Pedersen 1994), the Äspö HRL area (Pedersen and Ekendahl 1990, Pedersen et al. 1996, Kotelnikova and Pedersen 1998) and the Finnish sites investigated by Posiva (Haveman et al. 1999, Haveman and Pedersen 2002a, b, Pedersen et al. 2008). The variability was found to be rather small. Generally, the average total number of cells found in the Fennoscandian Shield igneous rock aquifers is within the range 10^4–10^5 cells mL^{-1}, although the range of single observations is from $1 \cdot 10^3$ to $5 \cdot 10^6$ cells mL^{-1}. This range is thought to be controlled by viruses that attack bacteria (Kyle et al. 2008). The generally modest variability in total numbers between boreholes and the non-variability in total numbers within specific boreholes is indicative of stable environments with little, or no, changes in the conditions for microbial life.

Microorganisms commonly attach and grow on available surfaces. Data on attached microorganisms on deep aquifer rock surfaces are not available. However, introduced surfaces have been used as proxies for aquifer surfaces. The number of attached cells on glass surfaces installed in flow-through devices under atmospheric pressure increased to about 10^5 cells cm^{-2} in less than 20 days (Pedersen and Ekendahl 1992b, Ekendahl and Pedersen 1994). After prolonged exposure up to six months, the numbers increased to about 10^7 cells cm^{-2}. A comparison of glass surfaces with rock surfaces showed no significant difference (Anderson et al. 2006b). Application of *in situ* pressure, relevant to a repository, resulted in numbers of attached bacteria that were in the range observed for atmospheric pressure (Anderson et al. 2006a, b, Nielsen et al. 2006). It seems safe to conclude that the published data on attached microorganisms in groundwater from repository depth are reliable and relevant. It is important to understand that although steady-state numbers of attached and unattached microbes in deep groundwater are observed, the microbial ecosystems can still be active, provided predation is ongoing. Recently, viruses that attack bacteria have been found in deep groundwater from Äspö HRL (Kyle et al. 2008). The importance of these observations will be discussed in the ongoing research section.

As mentioned above, sulphide production and oxygen reduction are the two most important processes that influence the rate of corrosion of the copper canisters. There are several metabolic routes that may eventually lead to oxygen reduction and sulphide production. Oxygen can be reduced by microorganisms during their concomitant oxidation of organic material as shown in reactions 2-1 and 2-2 below. A special group of microorganisms, the methanotrophs, reduces oxygen with methane as the electron donor and a representative species from the Äspö HRL has been named and described as *Methylomonas scandinavica* (Kalyuzhnaya et al. 1999).

$$C_6H_{12}O_6 + 6O_2 \rightarrow 6CO_2 + 6H_2O \qquad 2\text{-}1$$

$$CH_4 + 2O_2 \rightarrow CO_2 + 2H_2O \qquad 2\text{-}2$$

During the construction of the Äspö HRL tunnel, the fate of oxygen during shallow groundwater intrusion was explored on a large scale at 70 m depth (Banwart et al. 1996). It was found that microorganisms reduced the intruding oxygen concomitant with organic carbon oxidation. These results were followed up with a small scale experiment denoted REX at 380 m depth (Puigdomenech et al. 2001). Again, it was found that microorganisms played a major role in the reduction of introduced

oxygen. Modelling of the REX data suggested that microorganisms will rapidly reduce oxygen in backfill and buffer, within weeks after water saturation (Yang et al. 2007). It is, consequently, established knowledge that oxygen reducing microorganisms will contribute significantly to the removal of oxygen from repository environments. However, microbial oxygen reduction on a large scale in buffer and backfill remains to be demonstrated. Ongoing research in the Äspö HRL addresses this task and is briefly presented in Section 2.3.2.

Sulphide is produced exclusively as depicted in reactions 2-3 to 2-5 below by coherent phylogenetic groups of bacteria called the sulphate reducing bacteria (SRB). The species *Desulfovibrio aespoeensis* was described by Motamedi and Pedersen (1998) and has since then been used as a model species for various purposes (e.g. Moll et al. 2004). It should be stressed that reactions 2-3 to 2-5 are only the overall reactions showing the starting and end products. The stepwise reduction of the sulphur and oxidation of the carbon source takes place inside the cells in many linked physiological steps that are too extensive to be presented here (cf. Pedersen 2008).

$$2CH_3CH_2COOH + 2H^+ + SO_4^{2-} \rightarrow 2CO_2 + 2CH_3COOH + H_2S + 2H_2 \quad 2\text{-}3$$

$$CH_3COOH + 2H^+ + SO_4^{2-} \rightarrow 2CO_2 + H_2S + 2\,H_2O \quad 2\text{-}4$$

$$4\,H_2 + 2\,CO_2 \rightarrow CH_3COOH + 2\,H_2O \quad 2\text{-}5$$

The presence of SRB in deep groundwater has been demonstrated with cultivation methods. The most commonly used method is based on dilution and cultivation followed by a statistical judgement of the most probable number of the cultivated organism. Sulphate reducers (reactions 2-3 and 2-4) have been found in numbers ranging from $10^0 – 10^4$ in groundwater from Olkiluoto and the Äspö HRL area (Pedersen 2001, Pedersen et al. 2008). Autotrophic acetogens (reaction 2-5) have been demonstrated to be abundant in Äspö HRL tunnel boreholes (Kotelnikova and Pedersen 1998). The organisms performing reactions 2-3 and 2-4 above were abundant in deep groundwater. Hydrogen is a key gas that is required for acetate production by autotrophic acetogenes (reaction 2-5). This gas has been found in almost every sample of deep groundwater analysed for gas in the range between 10^{-8} up to 10^{-3} M (Pedersen 2002).

Ongoing research

The established knowledge reviewed above comprises data mainly obtained between 1987 and 2002 from the Stripa research mine, the Äspö HRL, the four Finnish sites Hästholmen, Olkiluoto, Romuvaara, and Kivetty analysed during Posiva's site selection process, and the uranium analogue site in Palmottu.

The dataset analysed here comprises about 100 observations between 2003 and 2006, distributed over approximately 35 boreholes at four sites. The sites were Forsmark and Laxemar that were investigated as potential sites for a Swedish deep repository, the Äspö HRL tunnel, and the Finnish site in Olkiluoto. In Olkiluoto both deep and shallow groundwaters have been investigated (Pedersen 2008, Pedersen et al. 2008). The shallow Olkiluoto groundwater ranges from 3 to 25 m in depth and the deep groundwater ranges from 50 to 564 m in depth (Pedersen 2006). The shallow groundwater was sampled and analysed four times over a period of about 2 years, from 2004–2006. The observed total numbers of microorganisms is shown in Figure 2-4, and is consistent with earlier data (Pedersen 2001). The range of microorganisms was significantly larger for the shallow groundwater compared to the deep groundwater.

The two groups of microorganisms judged most important for the evaluation of possible sulphide corrosion processes are the autotrophic acetogens and the sulphate reducing bacteria. Autotrophic acetogens were observed in 91 of a total of 99 samples (Figure 2-5) and sulphate reducing bacteria could be cultivated from 78 out of 100 analysed samples (Figure 2-6). It can safely be concluded that these two groups of microorganisms frequently occurred at all investigated sites. It was deemed important to obtain reaction rates for the reactions 2-3 to 2-5. Such data must be obtained under *in situ* repository conditions. Therefore, the necessary equipment and tools for this purpose have been set up at the 450 m depth in the Äspö HRL tunnel. A specific site, denoted MICROBE (Pedersen 2000, 2005a, b), has been developed and this site is presently generating data within the so called MICORED project.

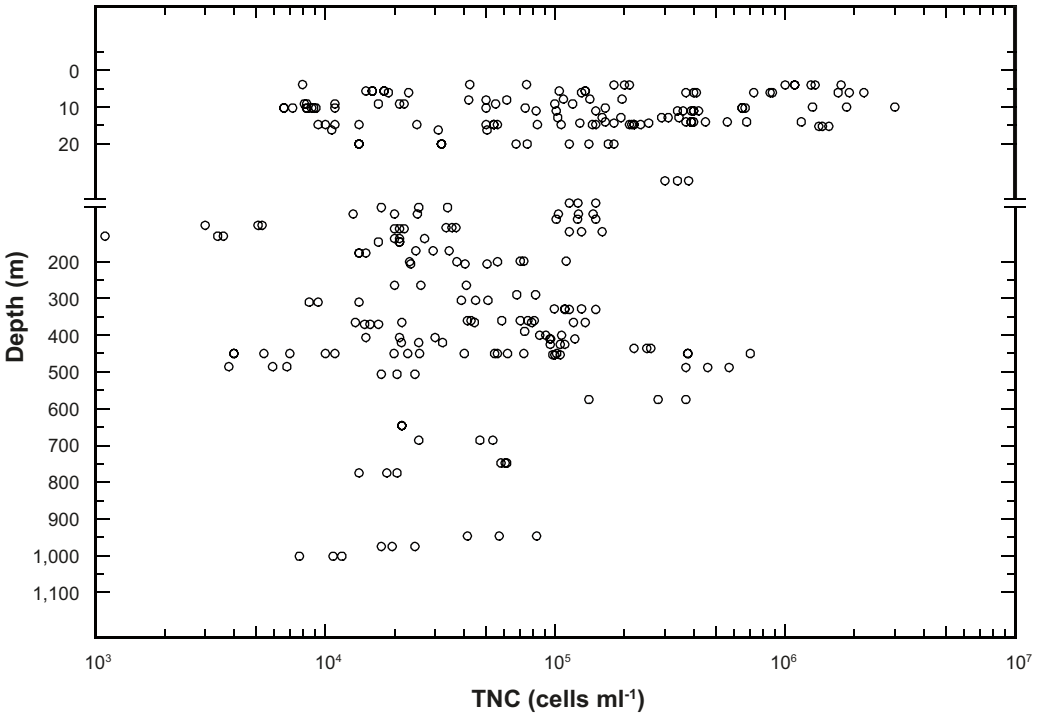

Figure 2-4. *Total number of cells (TNC) in ground water as a function of depth. The data set comprises triplicate analyses of the numbers in about 100 samples from shallow boreholes in Olkiluoto and deep boreholes in Olkiluoto, Forsmark, Laxemar, and Äspö HRL. The data were obtained between 2000 and 2006.*

It has been found that bacteriophages, viruses that attack bacteria, are common at the MICROBE site and in the Äspö HRL tunnel. If these phages are active, and much data are at hand that point in this direction (Kyle et al. 2008), data on bacterial numbers must be interpreted differently from the case where phages are absent. Active phages kill bacteria and cause cell lysis, which means that the attacked cell disappears and cannot be observed with enumeration methods. The total numbers of cells in deep groundwater are fairly constant within a range as depicted in Figure 2-4 and the number of phages showed an equal distribution at about ten times higher numbers than the microbe counts (Kyle et al. 2008). A cell-virus ecosystem can be very active and cell growth and division can be rapid. However, the observed number of bacteria will be constant because the death rate will be approximately equal to the growth rate. It may, therefore, appear as if the ecosystem is inactive and that growth is not ongoing, judged from numbers alone. The new data on phages shows that process rates must be determined with methods that do not depend on cell numbers. Instead, the microbial production and consumption of reactants should be analysed. Such data are presently being obtained at the MICROBE site at Äspö. However, it should be stressed that microbial numbers are still needed for purposes other than determination of process rates. Experimental results from the MICROBE site have now confirmed that hydrogen stimulates the microbial production of acetate and sulphide under *in situ* conditions. When hydrogen was added, the system responded with the growth of acetogens and SRB, and with acetate and sulphide production rates that significantly exceeded that of the control system.

In conclusion, microbial processes leading to the production of acetate and sulphide and the microorganisms executing those processes seem to be common in deep rock aquifers. These microorganisms are active and their activity is stimulated by hydrogen which, after failure of the outer copper shell, will be produced by anaerobic corrosion of the cast iron insert.

2.3.2 Microbiological processes in buffer and backfill

Established knowledge and ongoing research have shown that microbial processes of importance for the integrity of the canisters with respect to corrosion are present and ongoing in groundwater at repository depths. The most important microbial processes are the production of acetate and sulphide. It is generally anticipated that such processes will not be harmful or contribute to canister corrosion as long as they occur in the far field, outside the buffer and backfill. But, if these processes propagate in the backfill, and in particular, in the buffer close to the canisters, it is not possible to ignore them in the safety analysis.

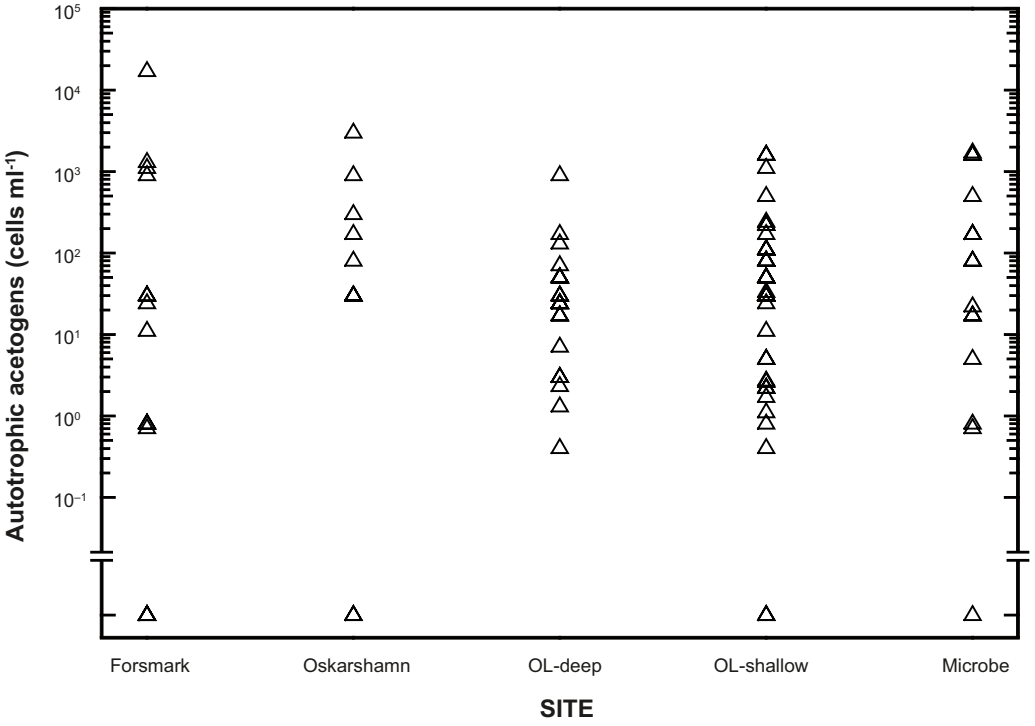

Figure 2-5. *The most probable numbers of autotrophic acetogens in 99 samples from shallow boreholes in Olkiluoto (OL-shallow) and deep boreholes in Olkiluoto (OL-deep), Forsmark, Laxemar (Oskarshamm), and Äspö HRL (Microbe). The data were obtained between 2003 and 2006.*

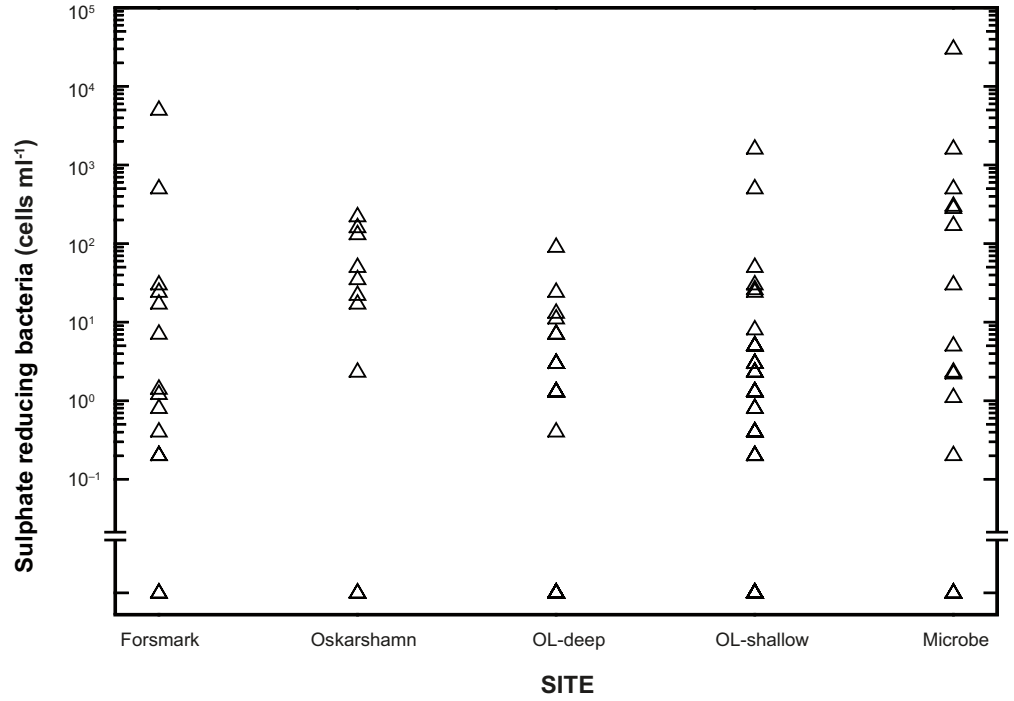

Figure 2-6. *The most probable numbers of sulphate reducing bacteria in 100 samples from shallow boreholes in Olkiluoto (OL-shallow) and deep boreholes in Olkiluoto (OL-deep), Forsmark, Laxemar (Oskarshamm), and Äspö HRL (Microbe). The data were obtained between 2003 and 2006.*

They must be explored with respect to constraining variables and possible rates. Established knowledge extends about 14 years back in time when the AECL Buffer Container Experiment (BCE) was analysed for microorganisms at the decommissioning of the test (Stroes-Gascoyne et al. 1997). Since then, several projects have continued to investigate the microbiology of various near-field environments.

Established knowledge

The Canadian Buffer Container Experiment

A full-scale test of the Canadian nuclear fuel waste disposal concept was carried out 240 m underground in the AECL underground research laboratory between 1991 and 1994 (Stroes-Gascoyne et al. 1997). This test comprised a heated container surrounded by a 5 cm layer of 100% sand closest to the canister and a 50/50% mixture of sand and Avonlea sodium bentonite as buffer. The heater in the container provided heat equivalent to that anticipated from a canister in a Canadian repository. During the experiment, the heat caused the mass transport of water, and moisture content gradients developed in the buffer ranging from 13% closest to the heater to 23% at the rock wall of the deposition hole. Upon decommissioning after 2.5 years, microorganisms could be cultured from all samples having a moisture content above 15% but not from samples with a moisture content below 15%. Heterotrophic aerobic and anaerobic bacteria were found in numbers ranging from 10^1 to 10^6 cells per gram dry weight) (gdw^{-1}) of buffer. Approximately 10^2 gdw^{-1}, or less, sulphate reducing bacteria and methanogens were also found.

Identification of buffer population members was performed using Analytical Profile Index (API) strips for isolated bacteria and 16S rDNA gene sequencing for *in situ* samples. Evidence for various types of beta, gamma, and delta groups of *Proteobacteria* and Gram-positive bacteria and a yeast were found.

The results suggested that a buffer of the Canadian type will be populated by active microorganisms when the moisture content is above a value where free water is available for active life. The area closest to the container will be devoid of life due to the observed redistribution of moisture. The water activity defines the availability of water for life and it appeared to be high enough in the 50/50% sand mixture to allow life as judged from the high numbers of cultivable microorganisms after 2.5 years exposure. Increasing the bentonite content to 100%, as is the case in the KBS-3 concept, will lower the water activity. The pore size in a compacted sand-bentonite mixture is larger than in compacted bentonite clay only. Taken together, the use of bentonite only as buffer will result in a higher swelling pressure, a lower average pore size, and a lower water activity than that obtained in the BCE test with a sand-bentonite mixture. These changes will constrain microbial life in a KBS-3 situation significantly more than in the BCE buffer design. A range of different experiments with 100% bentonite supports this conclusion, as shown below.

Survival of introduced bacteria

To study the physical properties of a bentonite buffer, several long-term tests (LOT) of buffer material have been performed in granitic rock 450 m underground at the Äspö HRL. The typical LOT was set up under conditions similar to those expected initially in a repository, except for the absence of radioactivity and a difference in scale. Therefore, LOT provided the opportunity for exposing strains of bacteria to conditions realistic for a repository buffer. The main focus with respect to microbial processes in the LOT parcel S1 was on sulphide-producing bacteria and their ability to survive (Pedersen et al. 2000a). Bacteria were chosen for different relevant characteristics. Sulphate-reducing bacteria (SRB) included *Desulfovibrio aespoeensis* isolated from deep Äspö HRL groundwater, the moderately halophilic bacterium *Desulfovibrio salexigens* and the thermophilic, spore-forming *Desulfotomaculum nigrificans*. Aerobic bacteria included *Deinococcus radiophilus*, a bacterium that can tolerate high doses of radiation and severe desiccation, the chemoheterotrophic bacterium *Pseudomonas aeruginosa* that frequently occurs in soil, the chemo-organotrophic and chemolithotrophic (hydrogen-utilizing) organism *Ralstonia eutropha*, the chemoheterotrophic, spore-forming bacterium *Bacillus subtilis* and the thermophilic spore-forming bacterium *Bacillus stearothermophilus*.

Suspensions of the SRB (anaerobic) and aerobic bacteria were mixed with bentonite clay to give a solution of approximately 100 million bacteria gdw^{-1} clay. The clay with bacteria was subsequently formed into cylindrical plugs with 20 mm length and diameter, and installed in bentonite blocks exposed to low (20–30°C) and high (50–70°C) temperatures. The blocks were installed in the LOT S1 parcel immediately after incorporation of the bacteria plugs. The experiment was terminated after 15 months. The major outcome was elimination below the detection limits for all except the spore-forming bacteria. All of the three spore formers survived at the low temperature. The numbers remaining were, however, much lower than the approximately 100 million spore-forming bacteria gdw^{-1} clay initially introduced, so that only between one-100th and one-10,000th of the original number were left. The death rate of cells and spores could therefore be interpreted as being higher than the growth rate, which may have been zero, or close to zero. At the high temperature, the sporeforming SRB *D. nigrificans* and some of the introduced *B. subtilis* were the only surviving bacteria. They most probably survived as spores, which are metabolically inactive and do not produce sulphide. A slow but significant death rate of viable cells and spores would eventually lead to the complete eradication of life in the buffer.

The LOT S1 experiment delivered results that were obtained under conditions very close to the conditions that will prevail in a repository. However, it was deemed important to follow up these survival data with data on activity. Laboratory experiments were designed in which the mixing of various bacterial species with swelling bentonite was studied at different temperatures in oedometers designed for laboratory investigations (Pedersen et al. 2000b). These experiments mimicked the LOT S1 experiment and most of the species used in the LOT were again used here. Suspensions of the bacteria were added on top of the bentonite at the start of the experiments and the survival and the transport of the respective species into the bentonite were followed. A clear trend of fewer cultivable bacteria at depth was seen in the clay. This trend was consistent as the incubation time was increased from 8 h to 28 weeks. The number of cultivable microorganisms decreased with increasing incubation time, except for *D. radiophilus* and *B. subtilis*, suggesting that most of the bacteria were sensitive to the harsh temperature and swelling pressure conditions in the compacted clay. The activity of SRB was investigated with radioactive $^{35}SO_4^{2-}$ two-dimensional autoradiography. The production of silver sulphide on silver foils in contact with the clay was studied. Sulphate-reducing bacteria were found to be active, reducing sulphate at the lowest density studied, 1.5 g cm^{-3}, but sulphate reduction activity ceased at higher densities up to 2 g cm^{-3}. The results suggest that the number of viable micro-organisms in a repository bentonite clay buffer will decrease rapidly during swelling and very few viable and active cells will be present at full compaction.

Presence, survival and activity of naturally occurring bacteria in bentonite

The experiments reported above with the LOT S1 parcel and subsequently with the oedometers were all performed with introduced bacteria grown in laboratory cultures. In the laboratory, and during field work, it became apparent that the bentonite being used, MX-80 contained viable bacteria. Therefore, bentonite (Wyoming MX-80) was used as inoculum for enrichment cultures with a medium selective for SRB (Masurat et al. 2010a). DNA was extracted from these enrichment cultures and phylogenetic analysis showed that 16S rDNA gene sequences in the enrichment cultures were identical to *Desulfovibrio africanus*. The conclusion was that *D. africanus* was present in the commercial bentonite. In samples with increasing salt concentrations inoculated from enrichment cultures, sulphide production was detected at salt concentrations up to 4%. Further, temperature-range experiments revealed that the SRB from the enrichment cultures grew at temperatures up to 40°C. These results, as well as the sigmoid morphology of cells in the enrichment cultures, supported the conclusion that *D. africanus* was present in the commercial bentonite MX-80 when delivered from the producer.

It is known that bentonite is heated during the processing after mining. Therefore, the heat resistance of the enriched SRB was investigated. The MX-80 bentonite was heated for 20 h in 100°C dry heat prior to incubation in growth medium. The results showed that the SRB in the bentonite survived the heat and were viable. This suggests that SRB survive the processing of commercial bentonite which, therefore, may act as a source of SRB to the buffer. It consequently became important to investigate if SRB can be active and produce sulphide under *in situ* repository conditions.

As sulphide is corrosive to copper, sulphide production by SRB in bentonite (MX-80 Wyoming) saturated with groundwater from 450 m underground was investigated (Masurat and Pedersen 2004, Masurat et al. 2010a). Copper coupons were placed in blocks of bentonite compacted to 1.5, 1.8 and 2.0 g cm^{-3} saturated density, corresponding to swelling pressures of approximately 0.1, 1.5 and 7.8 MPa, respectively. Lactate was added to the bentonite as a source of energy and organic carbon for SRB. Radioactive sulphur ($^{35}SO_4^{2-}$) was used as a tracer for sulphide production. Produced copper sulphide ($Cu_x{}^{35}S$) was localized and quantified by electronic two-dimensional autoradiography. The mean sulphide production rates observed were $1.5 \cdot 10^3$, $3.1 \cdot 10^2$ and $3.4 \cdot 10^1$ fmol ^{35}S mm^{-2} day^{-1} for swelling pressures of 0.1, 1.5 and 7.8 MPa, respectively. The use of sterile filtered (0.2 µm) groundwater resulted in $1.5 \cdot 10^2$ and $2.4 \cdot 10^1$ fmol^{35}S mm^{-2} day^{-1} for swelling pressures of 1.5 and 7.8 MPa, respectively. Additional *in situ* experiments at the MICROBE site were performed with sterile filtered (0.2 µm) groundwater and bentonite that was heated to 120°C for 15 h. Sulphide production rates in the heated bentonite were 1.3 to 16-times lower compared to controls treated at 25°C. These results again suggest that bentonite is a second source of SRB, in addition to the groundwater. Further, all experiments showed that increasing bentonite density correlated with decreasing sulphide production rates. The sulphide production rate was thus inversely coupled to the swelling pressure. The exact threshold swelling pressure or threshold density for microbial activity was not determined in these experiments.

Pedersen (2010) reports the results of a series of tests similar to those presented by Masurat et al. (2010a), except that experiments were performed with either no or different types of added nutrient. The control experiment contained no added energy or carbon source, a second experiment contained a H_2/CO_2 mixture, and a third contained lactate. In addition, copper coupons were located at different distances from the reservoir of bulk solution containing the sulphate and added nutrients, if any. Approximately 26 times and 7 times more sulphate reduction occurred in the lactate- and H_2/CO_2-amended tests than in the control, respectively. Furthermore, based on the derived value of the sulphide diffusion coefficient, all of the $Cu_x{}^{35}S$ on the copper coupons could be accounted for by sulphide produced in the bulk solution diffusing through the bentonite to the copper. The measurements were not sufficiently sensitive to determine whether there had been any *in situ* reduction of sulphate in the bentonite. Pedersen (2010) concluded that it is possible that corrosion of the canister by SRB may be limited to that due to microbial activity at the bentonite-rock interface and the subsequent diffusion of that sulphide to the canister. The concentration of sulphide will depend on the SRB growth conditions and the presence of Fe(II) which will control the solubility of sulphide.

In the bulk of the buffer, both the culturability and the viability of microbes are expected to decrease with time. Provided the swelling pressure remains above about 2 MPa, microbes will be barely metabolically active after buffer saturation, due to the low water activity in combination with the high density and a swelling pressure that is higher than the turgor pressure of the bacteria (i.e. the pressure inside the bacterial cells), which is reported to be around 2 MPa (Masurat 2006). Thus, although the issue of microbial activity in the buffer is still under investigation, it is unlikely that significant activity on the canister surface will occur.

Ongoing research

Three large-scale demonstration and research programmes at Äspö HRL include microbiological research. They are the long term tests (LOT) of bentonite performance, the canister retrieval test (CRT), and the prototype repository. The LOT A2 parcel and the CRT canister were decommissioned during 2006 and reporting is ongoing. The prototype has been analysed since 2004 (Eriksson, 2008).

Long term test of buffer material – Parcel A2

The "Long term test of buffer material" (LOT) is a series of experiments which was initiated at the Äspö Hard Rock Laboratory (HRL) in 2000, where hypotheses and models regarding the stability of bentonite buffer in a possible KBS-3 repository for spent fuel are tested. In the LOT experiments a number of copper canisters with heaters have been placed in blocks with bentonite and heated to a temperature of 90°C, the so-called S-tests. The LOT experiments also include so-called A-tests where the temperature in the copper canister heater has been elevated to 130°C to accelerate the

processes that are harmful to the bentonite buffer. The LOT parcels have previously been sampled after a little more than one year of exposure. The LOT parcel A2 that was sampled in 2006 had been exposed to the adverse conditions for more than 5 years.

Bacterial analyses were undertaken on samples from 20 positions in the bentonite of the LOT A2 parcel. They were taken from the top block number 38, denoted TOP LOT, and the double block 19–20 in the middle of the parcel denoted MID LOT. This parcel has been stored underground at 450 m depth in the Äspö tunnel with a 130°C heater in the centre since the start of the LOT experiments. Bacteria from the bentonite were cultivated in specific media for different purposes. The total amount of cultivable heterotrophic aerobic bacteria (CHAB), SRB, and autotrophic acetogens (AA) that produce acetate from hydrogen and carbon dioxide were examined. The content of adenosine-triphosphate (ATP) in the bentonite was also analysed. The density, water content, and temperature data from these tests are listed in Table 2-7. The results showed that 10^0–10^2 viable sulphate-reducing and acetogenic bacteria and 10^3–10^5 heterotrophic aerobic bacteria per gram bentonite were present in the TOP LOT (Table 2-8) after five years exposure, where the temperature and the density were below the values limiting life. This limit is believed to be somewhere between 1.8 and 2.0 g bentonite cm^{-3} as judged from previously published results (Pedersen 2002). The MID LOT showed some low numbers of CHAB at three positions, but otherwise all bacterial counts were below detection.

Table 2-7. Temperature, density, and water content in the sampled bentonite from LOT A2 parcel.

Measurement	Position	Distance from Cu (cm)									
		9	8	7	6	5	4	3	2	1	0
Temperature (°C)	TOP LOT	19	–	19	–	19	–	19	–	19	19
Density (kg m^{-3})	TOP LOT	1,847	–	1,862	–	1,859	–	1,879	–	1,864	–
Water content (%)	TOP LOT	33	–	30	–	29	–	29	–	29	–
Temperature (°C)	MID LOT	67	–	73	–	81	–	91	–	101	101
Density (kg m^{-3})	MID LOT	1,928	–	1,955	–	1,969	–	1,978	–	1,982	–
Water content (%)	MID LOT	39	–	41	–	37	–	38	–	38	–

Table 2-8. Enumeration of cultivable heterotrophic aerobic bacteria (CHAB), sulphate-reducing bacteria (SRB), autotrophic acetogens (AA) and determination of the ATP content in the TOP LOT and MID LOT bentonite from the LOT A2 parcel.

		Distance from Cu (cm)									
Analysis	Position	9	8	7	6	5	4	3	2	1	0
CHAB (CFU[a]·$10^3 g^{-1}$ ± stdev)	TOP LOT	8 ± 4	13 ± 9	9 ± 5	3 ± 2	13 ± 5	0.7 ± 0.3	22 ± 14	58 ± 7	0.6 ± 0.3	4 ± 0.4
MPN SRB (g^{-1} with 99% confidence limits)	TOP LOT	–	–	5 (2–30)	–	22 (3–53)	–	–	11 (2–39)	–	7 (3–41)
MPN AA (g^{-1} with 99% confidence limits)	TOP LOT	–	27 (3–64)	7 (3–42)	–	17 (4–64)	–	35 (2–54)	6 (3–37)	15 (3–54)	10 (2–36)
ATP (amol·10^5 g^{-1} ± stdev)	TOP LOT	–	–	–	–	–	–	–	–	–	–
CHAB (CFU[a]·10^3 g^{-1} ± stdev)	MID LOT	–	–	0.12 ± 0.08	–	–	49 ± 34	–	–	0.09 ± 0.08	–
MPN SRB (g^{-1} with 99% confidence limits)	MID LOT	–	–	–	–	–	–	–	–	–	–
MPN AA (g^{-1} with 99% confidence limits)	MID LOT	–	–	–	–	–	–	–	–	–	–
ATP (amol·10^5 g^{-1} ± stdev)	MID LOT	–	–	–	–	–	1 ± 0.2	–	–	–	–

[e] CFU – colony forming units

The most important results were that AA and SRB could be cultivated from the TOP LOT but not from the MID LOT. This shows that bacteria involved with sulphide production will be present in compacted bentonite when the density and the temperature falls below the expected values for a repository. Bacteria in the TOP LOT bentonite were viable and had the potential to produce both sulphide and organic carbon in the form of acetate from hydrogen and carbon dioxide. The elevated density, the high temperature and the low water content in the MID LOT bentonite compared to the TOP LOT bentonite obviously made it difficult for the bacteria to survive. However, in a few MID LOT samples bacteria were still viable. The threshold density for microbial activity in the compacted LOT bentonite appeared to be closer to 2.0 g cm^{-3} than to 1.8 g cm^{-3}. It was not possible to distinguish the effects of density, temperature, and water content on the survival of bacteria.

The Canister Retrieval Test

The Canister Retrieval Test (CRT) was an experiment that started at Äspö HRL in 2000. The primary aim was to determine whether it was possible to retrieve a copper canister after disposal under authentic KBS-3 conditions. However, the CRT also provided a unique opportunity to investigate if bacteria survived in the bentonite buffer during 5 years of exposure. Therefore, during the retrieval of the canister, microbiological samples were extracted from the bentonite buffer and the bacterial composition was studied, analogous to how the LOT A2 was investigated.

During the CRT retrieval, microbiological analyses of a total of 66 samples at the C2, R10, R9 and R6 levels in the bentonite from the CRT were obtained. Cultivation and analysis followed the procedures of LOT A2 as described above. The results showed that 10^0–10^2 viable sulphate-reducing and acetogenic bacteria and 10^2–10^4 heterotrophic aerobic bacteria per gram bentonite were present after five years in the borehole. Bacteria with several morphologies could be found in the cultures with bentonite. Most of the bacteria were detected in the bentonite buffer close to the rock but in a few samples viable bacteria were found in bentonite close to the copper canister. Results and conclusions generally agreed with the results and conclusions obtained during the LOT A2 project.

Prototype

The prototype repository project is an international full-scale model project of the planned deep repository for Swedish spent fuel. It is conducted at the Äspö HRL in crystalline rock at approximately 450 m depth. A monitoring programme investigates the evolution of chemistry, gas, redox conditions and the reduction of oxygen in different parts of the prototype repository. One of the specific aims is to monitor the microbial consumption of O_2.

The evolution of the gas composition and the numbers of oxygen consuming bacteria and sulphide producing bacteria have been followed since 2004 in three consecutive investigations (Eriksson, 2008). Analysis of the gas showed the presence of hydrogen, helium, nitrogen, oxygen, carbon monoxide, carbon dioxide, methane, ethane, and propane in samples from 16 points within the prototype repository. All sampling points in the prototype that delivered groundwater were analysed for the total number of bacteria, the amount of ATP (bio-volume), cultivable heterotrophic aerobic bacteria, sulphate reducing bacteria, and methane oxidizing bacteria. In addition, groundwater from about 6 boreholes in the surrounding rock has been analysed for the same bacteria analysed from sample points inside the prototype repository.

The gas data generally show that oxygen is disappearing, at least in proportion to other gases present. The microbiological results show that aerobic bacteria such as cultivable heterotrophic aerobic bacteria and methane oxidizing bacteria thrive in the aerobic prototype environment, but not in the anaerobic surroundings. In contrast, anaerobic sulphate reducing bacteria were more abundant in the anaerobic groundwater surrounding the prototype compared to inside the prototype (Figure 2-7). Overall, the observations support the present hypothesis (Yang et al. 2007) that oxygen will be consumed by bacteria within a short time span (i.e. weeks to years), as opposed to the long time span of many years predicted by abiotic processes (Wersin et al. 1994b).

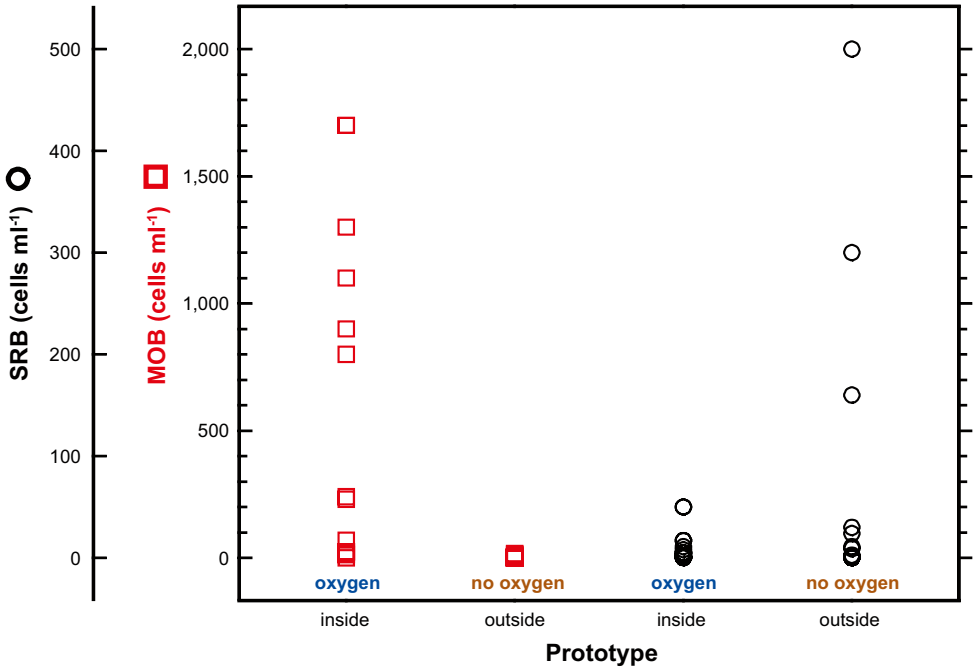

Figure 2-7. *The numbers of sulphate reducing bacteria (SRB) and methane oxidizing bacteria (MOB) observed in sample points inside and outside the prototype repository.*

2.3.3 Canadian studies of the effects of bentonite density and pore-water salinity on microbial activity

In addition to the large-scale tests described above, an extensive laboratory study has been conduced in the Canadian programme into the effects of bentonite density and pore-water salinity on microbial activity (Stroes-Gascoyne et al. 2006, 2007a, b). The focus of this work was to examine the effects of water activity (a_W) on microbial activity in simulated repository environments, based on the well-known effect that low water activity has on suppressing microbial activity in a wide range of systems (Brown 1990). In the Canadian studies, the pore-water a_W was adjusted by varying the bentonite density and/or the pore-water salinity. Ultimately, the information obtained from this study is to be used for designing repository sealing materials to preclude microbial activity in the near field and, in particular, microbiologically influenced corrosion (MIC) of the canister (Stroes-Gascoyne et al. 2007b).

Figure 2-8 shows the effect of the water activity on the natural aerobic microbial population in highly compacted bentonite with ~95% water saturation. There is strong evidence for a reduction in the number of culturable microbes for water activities < 0.96, regardless of whether that activity is achieved through adjusting the clay density or the salinity of the pore water. Culturability was measured by taking samples of the compacted bentonite after the test, dispersing them in a nutrient-rich growth medium, and then counting the number of colonies formed when plated on to an agar-containing growth medium. Thus, these numbers over-estimate the *in situ* microbial activity during the exposure, since other factors such as lack of water or nutrients or lack of space will limit activity within the pores of the bentonite.

The other feature of interest from Figure 2-8 is the rapid rise in post-test activity at $a_W > 0.96$. At these high water activities, achieved by only loosely compacting the bentonite with double-distilled water or a relatively low salinity simulated groundwater solution, not only is the initial microbial population (indicated in the figure by the dashed horizontal line at a population of ~200 CFU/g) not reduced as at lower a_W, but it in fact multiplies during the course of the exposure. This growth leads to a sharp increase in the culturable population by over four orders of magnitude over a narrow range of a_W. The water activity of 0.96, therefore, represents a threshold below which the population of culturable microbes is reduced. Whether these microbes are killed or simply dormant due to the low a_W is not currently known, but the important fact is that exposure to low a_W renders them inactive and unable to grow through normal metabolic activity.

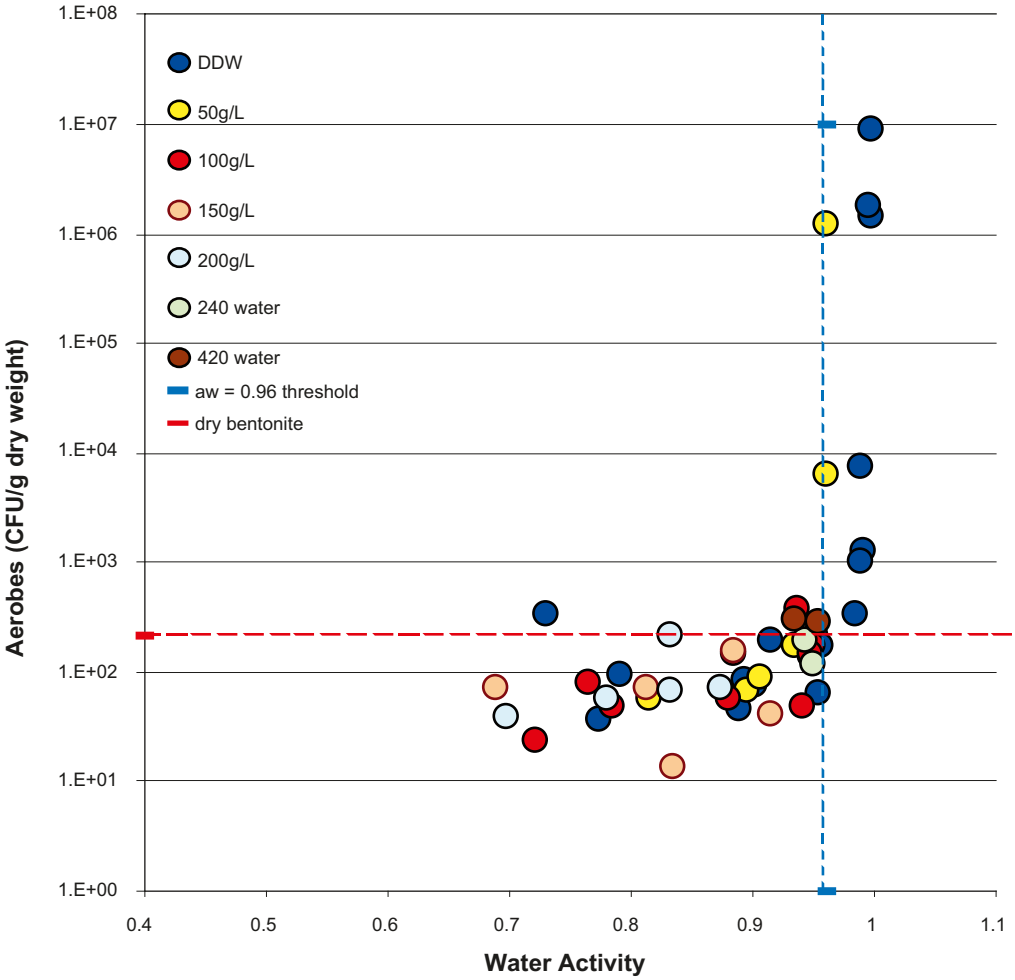

Figure 2-8. *Number of culturable heterotrophic aerobes as a function of measured water activity (a_w) following exposure to compacted bentonite for 40–90 days (Stroes-Gascoyne et al. 2006). The bentonite was compacted with various salinity waters, including double-distilled water (DDW), artificial groundwaters with salinities of 50–200 g/L, and two natural groundwaters from depths of 240 and 420 m (TDS 0.7 g/L and 89 g/L respectively).*

Salinity affects microbial activity through the effect on the osmotic potential and, hence, the water activity. As noted above, the reduction in a_W in compacted bentonite can be achieved through the presence of saline pore fluids. Figure 2-9 shows the effect of salinity on the post-test culturability of naturally occurring microbes in bentonite (Stroes-Gascoyne et al. 2006, 2007a, b). It can be seen that a pore-water salinity of 80–100 g/L is sufficient to prevent growth of the indigenous population.

In both Figures 2-8 and 2-9, the horizontal dashed line at ~200 CFU/g represents the background natural population in the as-received bentonite. It is interesting to note that there is evidence that progressively lower a_W and/or higher pore-water salinity reduces the culturable microbial population below that initially present. These data provide convincing evidence that microbial activity is suppressed by low water activity.

It is not possible to completely exclude some role of the bentonite swelling pressure on microbial activity. Figure 2-10 shows many of the same data from Figures 2-8 and 2-9 expressed in terms of the swelling pressure measured for the various bentonite densities and pore-water salinities used in the tests. Interestingly, the "threshold" swelling pressure above which microbial activity is suppressed is approximately 2 MPa, the same value reported from Swedish studies (Section 2.3.2). However, there are some conditions under which microbial activity is suppressed at swelling pressures < 2 MPa. These tests are invariably those with high pore-water salinity, in which the water activity is < 0.96. These latter tests seem to provide good evidence that the water activity alone can explain the observed suppression of microbial activity in highly compacted bentonite.

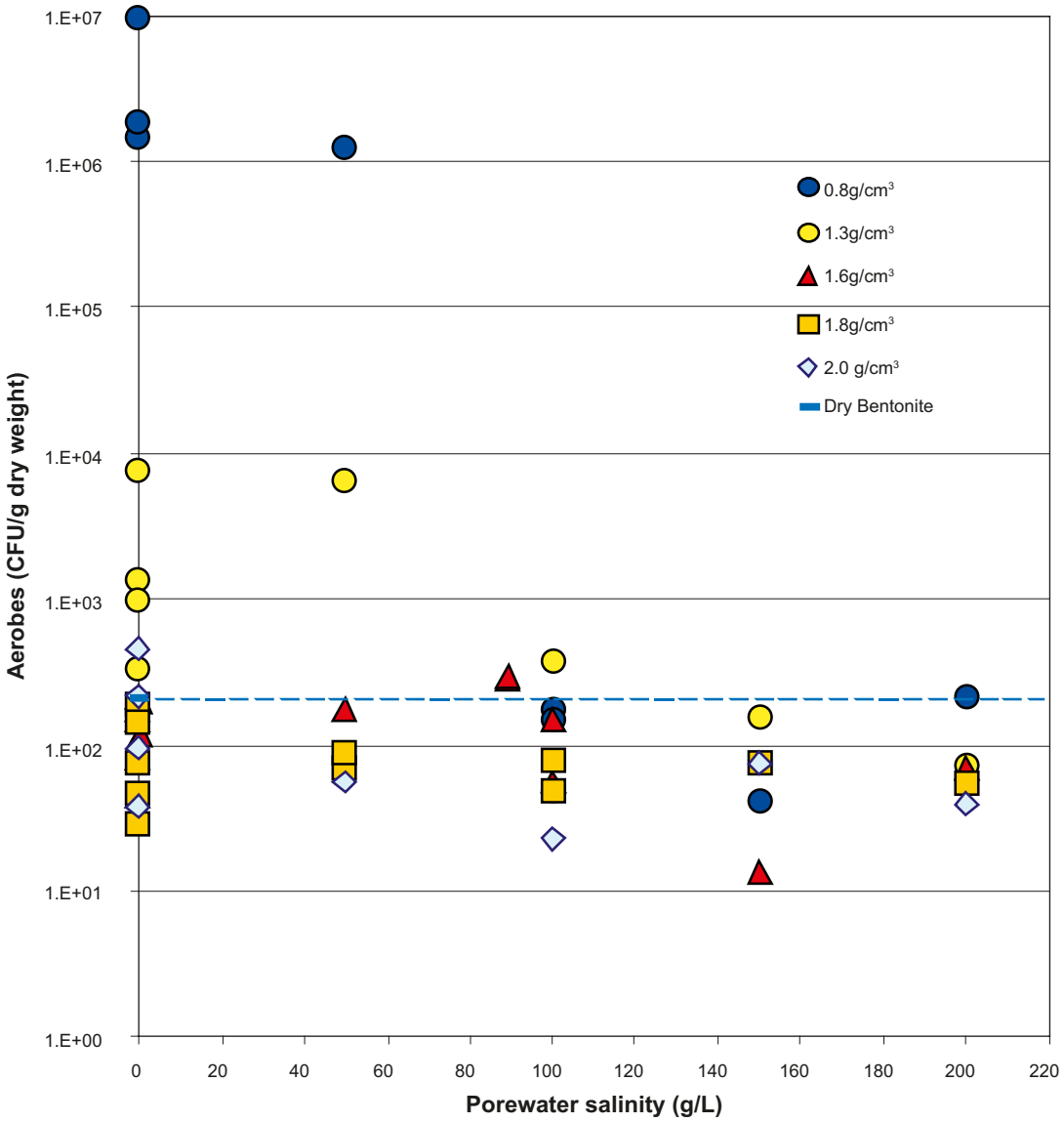

Figure 2-9. *Effect of pore-water salinity on the culturability of aerobes following exposure to compacted bentonite of various densities for periods of 40–90 days (Stroes-Gascoyne et al. 2006). Experiments were performed with compaction densities of 0.8–2.0 g/cm³.*

Regardless of the precise physiological cause of the suppression of microbial activity, the data in Figures 2-8 to 2-10 provide a practical engineering solution to controlling microbial activity in the near field. Figure 2-11 shows the data re-plotted in terms of the bentonite dry density. In fresh waters, a bentonite dry density of 1.6 g·cm^{-3} is sufficient to suppress microbial activity, with lower densities similarly effective in saline environments.

2.3.4 Modelling of microbial processes in the repository

Ultimately the long-term effects of microbial activity on the integrity of the canisters must be assessed, just as for any other corrosion process to which the canister may be susceptible. King and co-workers (King and Kolář 2006b, King et al. 2002b, 2003, 2004) have developed a model to predict the extent of microbial activity in a deep geological repository and the effect of that activity on the corrosion of copper canisters. The model is based on the same modelling principles used for the Copper Corrosion Model (CCM) for general corrosion of copper in compacted bentonite (see Section 5), and is termed the Copper Corrosion Model for Microbiologically Influenced Corrosion (CCM-MIC). The model does not predict the corrosion consequences of a biofilm on the canister surface because microbial activity is deemed not to occur in highly compacted bentonite, in line with the results of the experimental studies in Section 2.3.3.

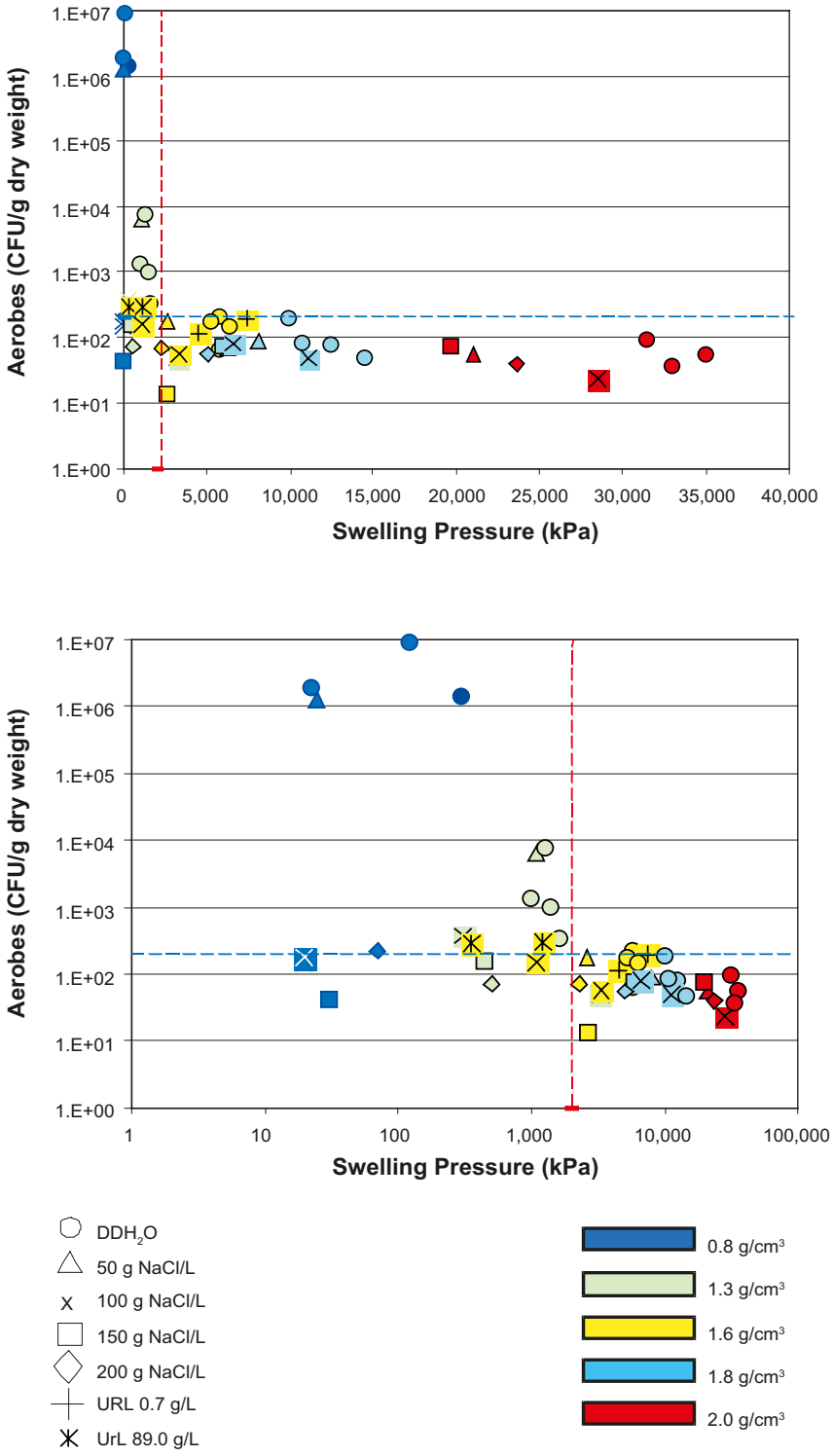

Figure 2-10. *Effect of bentonite swelling pressure on the culturability of aerobes following exposure to compacted bentonite of various densities for periods of 40–90 days (Stroes-Gascoyne et al. 2006). The two figures show the same data plotted on log and linear swelling pressure scales. The horizontal blue dashed line represents the background natural population of microbes in the as-received bentonite. The vertical red dashed line represents a swelling pressure of 2 MPa. Symbols relate to salinity of water added to bentonite prior to compaction to the density indicated by the colour of the symbol.*

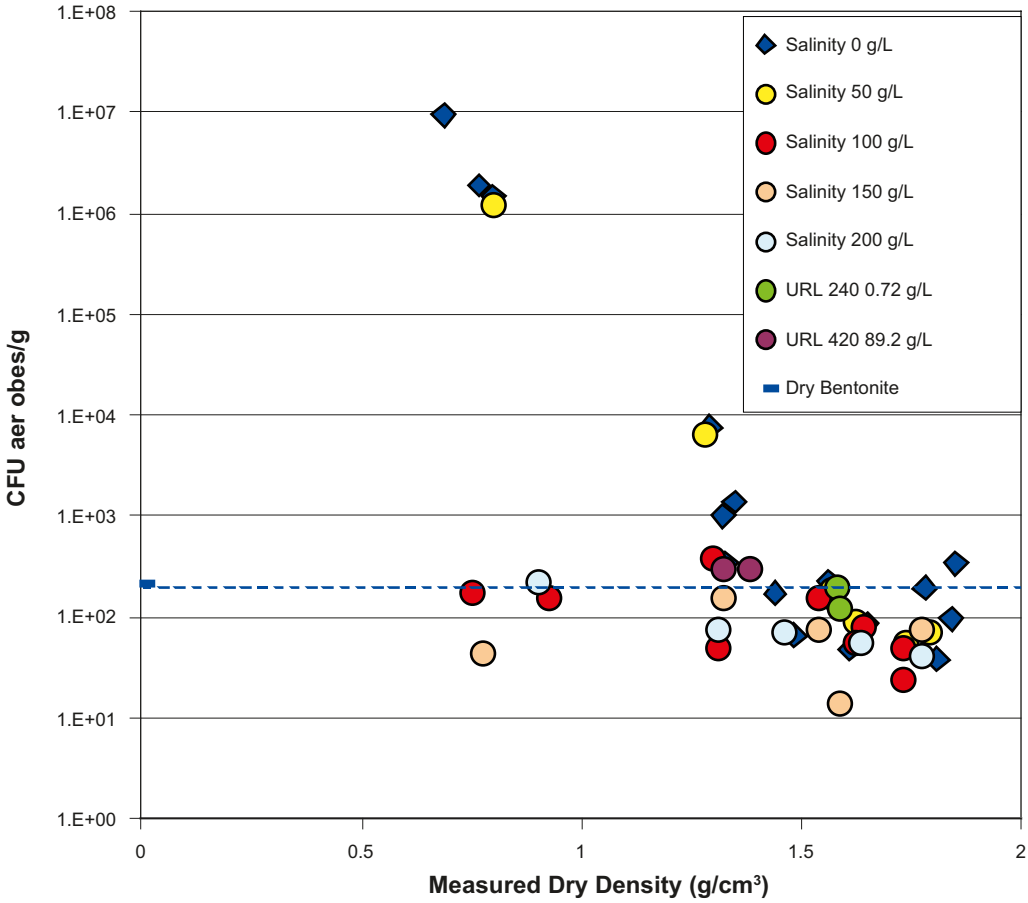

Figure 2-11. *Effect of bentonite dry density on the culturability of aerobes following exposure to compacted bentonite of various densities for periods of 40–90 days (Stroes-Gascoyne et al. 2006). The bentonite was compacted with various salinity waters, including artificial groundwaters with salinities of 0–200 g/L and two natural groundwaters from depths of 240 and 420 m.*

A series of fifteen microbial processes are included in the MIC model in addition to the "abiotic" corrosion mechanism considered in the CCM (see Figure 5-16). These fifteen processes represent a series of microbial reactions that occur in nature in sequence as environmental conditions evolve from aerobic to anaerobic, and include: aerobic respiration, denitrification, N_2 fixation, nitrosofication, nitrification, ammonia oxidation, fermentation, iron reduction, and sulphate reduction (Figure 2-12). This particular set of processes was chosen because of its relevance to the corrosion of copper, in particular the aerobic consumption of O_2, the generation of possible stress corrosion agents (ammonia, nitrite, and acetate), and the formation of sulphide by SRB. The fifteen microbial processes are assumed to involve 12 different types of microbe. Three forms of organic material are considered; peptide and glucose derived from the degradation of the naturally occurring organic material in the bentonite, and acetate derived from the fermentation of peptide and glucose. In addition to the ten inorganic species considered in the CCM, eight additional inorganic species are included in the CCM-MIC; namely: sulphide (HS^-), hydrogen produced by the fermentation of glucose, sulphate, ammonia, nitrogen, nitrite, nitrate, and $Cu(NH_3)_2^+$, which can be produced by the dissolution of copper in ammonia solutions.

A mass-balance equation is defined for each of the 18 abiotic species, the three types of organics, and the 12 types of microbe. These mass-balance equations represent the net effect of diffusive mass transport, adsorption/desorption, precipitation/dissolution, homogeneous chemical reactions, microbial reactions, and cell growth processes on the spatial and temporal distributions of the concentrations of each of the species in the model. An energy-generating and cell-generating equation is written for each microbial process, so that the increase in microbial population during active metabolism can be predicted. The rates of microbial processes are described using Monod or other types of rate expressions. Various factors that may limit microbial activity are considered, including:

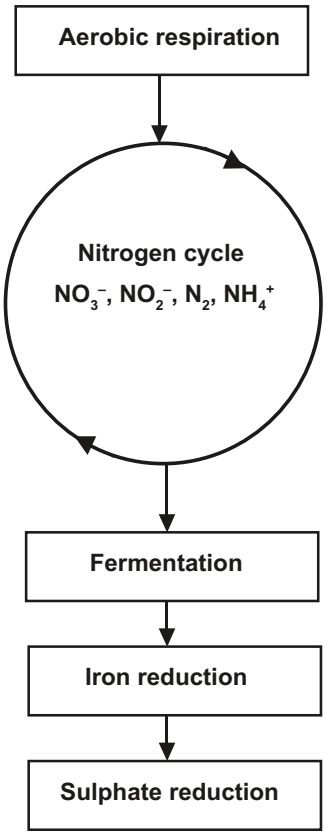

Figure 2-12. *Sequence of microbial reactions considered in the CCM-MIC (King et al. 2002b).*

1. Redox potential.
2. Temperature.
3. Water activity.
4. Availability of organic carbon.
5. Availability of terminal electron acceptors (e.g. SO_4^{2-}, NO_3^-, O_2, Fe(III)).

The microbial population is subject to a defined death rate, with a fraction of the organic carbon from dead cell material being recycled to support further cell growth. In addition, microbes cannot move through the bentonite because of their large size in relation to the pore size in compacted buffer.

Of these limiting factors, that of most interest here is the restriction of microbial activity below a threshold water activity. As described in Section 2.3.3, the absence of free water is one explanation for the absence of microbial activity in compacted bentonite. In the CCM-MIC, microbial activity is assumed not to occur in any of the repository sealing materials if the water activity is < 0.96, either as a consequence of high osmotic potentials due to saline pore fluids or because of a high suction potential due to desiccation of the sealing material or rock.

The CCM-MIC has been used to predict the extent of microbial activity in a Canadian repository (King and Kolář 2006b). Results suggest that the extent of such activity in the repository near field is limited and that the concentration of aggressive microbial metabolic by-products at the canister surface is minimal. The highest concentrations of any of the possible SCC agents at the canister surface is < 10^{-5} mol/L in the case of ammonia (Figure 2-13), which is only produced after the consumption of all oxidants in the system. The interfacial concentrations of other SCC agents (nitrite and acetate ions) are even lower (< 10^{-10} mol/L), partly because of the absence of microbial activity close to the canister and partly because ammonia, nitrite, and acetate are consumed in other microbial processes (King and Kolář 2006b). The flux of HS^- to the canister surface is also small, partly because of the

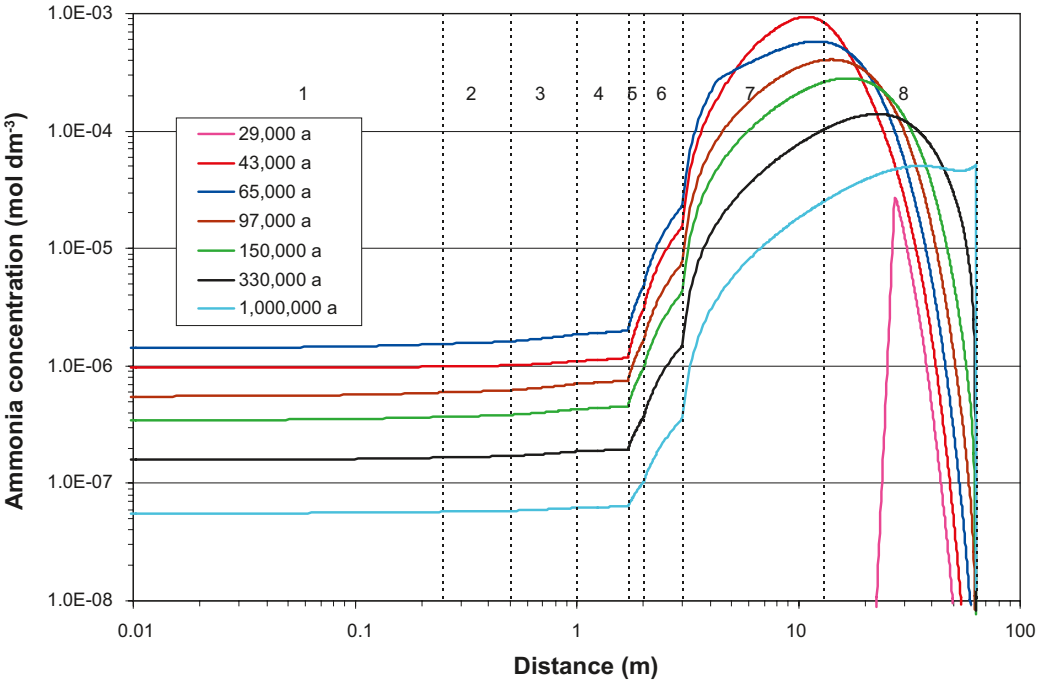

Figure 2-13. *Predicted concentration of ammonia at the canister surface due to microbial activity in a canadian-design repository (King and Kolář 2006b). Layers 1 through 8 refer to the inner and outer buffer, dense and light backfill, inner and outer EDZ, and near- and far-field rock, respectively.*

precipitation of sulphide as mackinawite (FeS) in the buffer and backfill. Approximately 8–30% of the initially trapped O_2 was predicted to be consumed by aerobic microbial activity, the remainder being consumed by the oxidation of Cu(I) to Cu(II), the reduction of which supports corrosion of the canister. Overall, the extent of microbial activity is limited because cells are predicted to die, and not re-activate, during the harsh initial period of several hundred years of elevated temperatures and desiccated sealing materials.

The main conclusion from the CCM-MIC, however, is that microbial processes in the repository can be quantified and predicted in the same manner as other forms of canister corrosion. Applications of such techniques in other areas include: sub-surface microgeochemistry (Hunter et al. 1998), groundwater remediation (Prommer et al. 2000), biodegradation (Kindred and Celia 1989, Prommer et al. 1999), denitrification of aquifers (Kinzelbach and Schäfer 1991), and the disposal of low- and intermediate-level waste (Humphreys et al. 1995).

2.3.5 State of the art conclusions

Published data suggest that microorganisms will not be viable in the buffer under repository conditions relevant for the KBS-3 concept. Data from ongoing research and published data suggest the following parameters are important in controlling microbial activity: 1) the amount of free water needed for active microbial life as reflected by water activity and moisture content measurements, 2) the temperature, where increasing temperature will decrease the viability of microorganisms present, and 3) the swelling pressure and pore size of the buffer which will exert an increasing constraint on the space for living cells with increasing buffer density.

Ongoing research has demonstrated that when hydrogen is present in bentonite, from groundwater or generated in the process of iron corrosion (if iron is present in the repository), sulphide will be produced by SRB, possibly via autotrophic acetate production. The data from the MICROBE site at Äspö HRL –450 m show that hydrogen triggers sulphide production in groundwater. A similar hydrogen effect on sulphide production seems to be present in bentonite, as judged from the long-term test (LOT) and canister retrieval test (CRT) microbe results.

The effect of moisture content and water activity has been reasonably well established. Research has been initiated to determine the effect of dry density at the threshold density for microbial activity of approximately 1.6 $g \cdot cm^{-3}$. The effect of temperature has not yet been investigated under controlled conditions.

The results of microbial modelling suggest that the overall consequences of microbial activity on canister corrosion are minor. The CCM-MIC allows the long-term effects of microbial activity on canister corrosion to be assessed, in exactly the same manner as for other corrosion processes.

2.4 Radiation effects

The radiation from a spent fuel canister could affect the chemical conditions in the near field. The ionizing radiation will produce both molecular and radical oxidants and reductants through radiolysis. The oxidants and reductants are produced in equivalent stoichiometric amounts, but the higher reactivity of some species compared to others may affect the redox conditions in the canister near field. The concentrations of the different species formed during radiolysis depend on the type of radiation, the dose rate, the composition of the aqueous solution, and material of fabrication and wall thickness of the canister.

The ionizing radiation of importance outside a spent fuel canister is gamma radiation. The absorbed dose rate outside a canister with 30-year-old fuel will be less than 1 Gy/h (SKB 2006b). At this low dose rate the effect of the production of oxidants is expected to be small to negligible (Shoesmith and King 1999). Caesium-137, with a half-life of about 30 years, dominates the gamma radiation outside the canister. This means that after a few hundred years the dose rate will have dropped to insignificant levels. Furthermore, the canister surface is expected to be dry during the period of highest dose rates, further limiting the production of deleterious radiolysis products.

2.5 Expected corrosion environment for the canisters

As will become clear from the information presented in this section, the nature of the repository environment and of the corrosive conditions at the canister surface will evolve with time. In general terms, this evolution will involve a transition from aggressive conditions initially to environments that are relatively benign. Initially, the environment will be warm and aerobic. However, as the canister cools and the trapped atmospheric oxygen is consumed by microbial processes, by reaction with Fe(II)-containing minerals, and by corrosion of the canister, the environment will become cool and anoxic. From a corrosion perspective, the corresponding corrosion processes will evolve from relatively rapid and possibly localized to slow and more uniform in nature in the long term.

In considering the evolution of the repository environment and its effect on the corrosion of the canister, it is important to distinguish between the groundwater environment in the host rock and the pore-water environment within the bentonite. The presence of the highly compacted bentonite will "buffer" the canister-surface environment from some of the processes and changes that may occur in the groundwater. For example, the dissolution of mineral impurities and ion-exchange processes in the bentonite, coupled with the slow rate of mass transport, will result in a pore-water environment that will only slowly equilibrate with the groundwater in the rock surrounding the deposition holes and tunnels. In addition, the extent of microbial activity in the bentonite surrounding the canisters will be suppressed, if not prevented entirely, compared with that possible in the groundwater. It is the near-surface environment within the bentonite that is important in determining the corrosion behaviour of the canister.

It is convenient to consider three phases in the evolution of the near-field environment: the initial condition (the first 0 to 30 years following repository closure), the transient period over the first 100 years or so following repository closure, and the long-term, including the effects of glacial and climate changes. The details of how the near-field environment will change will depend to some degree on the site conditions and the repository design. Here, a generic description of the evolution is given.

Initially, the near-field environment will be warm and aerobic. Air trapped in the pores of the buffer and backfill sealing materials will create aerobic conditions that can support corrosion of the canister. Partial desiccation of the bentonite may occur due to the heat generated from the canister. The bentonite pore water will become conditioned by the dissolution of mineral impurities and by ion-exchange processes and, depending upon the rate of influx, by the incoming groundwater.

During the first 100 years or so, the repository and near-field environments will evolve significantly. The temperature will attain a maximum 10–30 years after closure and then decay to ambient values over a period of several thousand years. At the same time, the trapped atmospheric O_2 will be consumed by microbial processes, reaction with Fe(II) and pyrite, and by corrosion of the canister itself. Various experimental and modelling studies indicate that the establishment of anoxic conditions will take from a few years to a few hundred years. Microbial processes are expected to consume much of this O_2, although the suppression of microbial activity in the bentonite buffer may result in a significant fraction of the O_2 being consumed by mineral oxidation and canister corrosion. During this period, the pore-water salinity will increase as the bentonite becomes saturated by the saline groundwater. The pore-water pH is expected to remain in the range pH 7–8 and to be buffered by the presence of calcite. Saturation of the bentonite will result in a swelling pressure of several MPa being applied to the canister. Once the repository has become anoxic, it is expected to remain so indefinitely. Sulphide, present naturally in the groundwater and present in the bentonite as pyrite impurities, will control the redox conditions. Microbial activity in the groundwater and, depending upon the bentonite density, within the repository could act as another source of sulphide.

Following the transient period, the repository environment will evolve only slowly. Over glacial timescales (of the order of 120,000 years for a complete glacial cycle), changes in the groundwater salinity are possible due to the infiltration of dilute glacial melt water and, possibly, the upconing of deep saline groundwaters. Modelling of glacial events suggests that the groundwater composition will change during the different stages of the glacial cycle. Although changes in salinity at repository depth are possible during the glacial cycle, there is no evidence that O_2-bearing melt water will reach the repository horizon (Section 2.1.2.2) (Posiva 2009). Anoxic conditions are expected to prevail in the repository at all times, with corrosion controlled by the rate of supply of HS^- to the canister surface.

3 Review of thermodynamic data for copper of relevance to copper corrosion

There have been no significant further publications on the thermodynamics of the corrosion of copper since the publication of the original report. The following is a summary of the current state of the art.

3.1 General

Thermodynamic data allow the stable states within a multi-component system to be predicted. With the approach used here, and in all the references cited, free energies of formation, and the enthalpies and entropies for aqueous species are given for the reference state of infinite dilution. Entropies and heat capacities allow equilibrium constants to be calculated for any temperature within the intended range (0–100°C). In order to give acceptable estimates of the stability of the aqueous species, the departure from infinite dilution should be recognised; activity coefficients should be estimated, particularly for charged species.

3.2 Thermodynamic parameters

Fundamental functions of thermodynamics of aqueous systems at constant pressure (P) and constant temperature (T) are defined by the Gibbs free energy (G), enthalpy (H) and entropy (S):

$$G = H - TS \qquad 3\text{-}1$$

The Gibbs free energy is the measure of the available energy in a system, if pressure and volume (V) of the system are constant (i.e. there is no 'PV' work). The term TS may be defined as unavailable energy, or bound energy. Entropy may be defined as a measure of the system disorder and randomness, while (at constant P) enthalpy describes the heat content. Absolute values of G and H cannot be determined, but the change in their values can be measured when a system shifts from one state to another (i.e. a chemical reaction takes place):

$$\Delta G = \Delta H - T\Delta S \qquad 3\text{-}2$$

In phases containing numerous components, as for example (natural) waters, the term chemical potential (μ) is used to define the partial Gibbs free energies of each component:

$$\mu_i = \left(\frac{\partial G}{\partial n_i} \right)_{P,T,n_i} \qquad 3\text{-}3$$

Differences in chemical potentials between species determine the thermodynamic driving force which allows reactions to take place. There is a logarithmic relationship between chemical potential and activity (a) of each species ($\mu_i = \mu_i^o + RT\ln a_i$). The activity scale is fixed by means of a standard state (denoted by superscript ^{o}) and by a reference state. The reference state for a dissolved component in water is infinite dilution, in which the activity of the component equals its molal concentration, and approaches zero. The standard state is the hypothetical ideal solution, in which the component has unit concentration and unit activity.

Compilations of thermodynamic data for copper have been published by Puigdomenech and Taxén (Puigdomenech and Taxén 2000, Puigdomenech and Taxén 2001) and by Ahonen (Ahonen 2001). The work by Puigdomenech and Taxén also contains thermodynamic data for a large number of auxiliary species in the system chlorine-fluorine-oxygen-sulphur-nitrogen-phosphorous-carbon-hydrogen-sodium-calcium. The basic data include the free energy of formation from the elements

(ΔG_f), entropy (S^o) and heat capacity (C_p) for each chemical compound. An alternative approach is used by Ahonen, who lists the free energies of reaction (ΔG^o_r), the reaction entropies (ΔS^o) and the change in heat capacity (ΔC_p).

3.3 Equilibrium constants

The most frequently used thermodynamic parameter in solution chemistry and in aqueous geochemistry is the thermodynamic stability constant, which is defined as the quotient of the activities of the reaction products and reactants.

Equilibrium constants are calculated from thermodynamic data according to

$$\ln K^\circ = -\frac{1}{RT}\sum_i \nu_i \, \Delta G^\circ_f(i) \qquad 3\text{-}4$$

where K° is the standard equilibrium constant, R is the gas constant, T is the absolute temperature, $\Delta G^\circ_f(i)$ is the Gibbs energy of formation for a reactant (or product) i, and ν_i is the corresponding stoichiometric coefficient.

For a general equilibrium reaction

$n\,A + m\,B = p\,C + q\,D$

the relationship between the standard equilibrium constant and the value for a given ionic medium is

$$\begin{aligned} K^\circ_{eq} &= a_C{}^p \, a_D{}^q \, a_A{}^{-n} \, a_B{}^{-m} \\ &= \gamma_C{}^p \, [C]^p \, \gamma_D{}^q \, [D]^q \, \gamma_A{}^{-n} \, [A]^{-n} \, \gamma_B{}^{-m} \, [B]^{-m} \\ &= \gamma_C{}^p \, \gamma_D{}^q \, \gamma_A{}^{-n} \, \gamma_B{}^{-m} \, K_{eq} \end{aligned} \qquad 3\text{-}5$$

where the square brackets [] indicate concentration, a_i and γ_i are the activity and the activity coefficient of species i, respectively, and K°_{eq} and K_{eq} are the equilibrium constant for standard and non-standard conditions, respectively. The two sets of thermodynamic data referenced here allow K°_{eq} to be calculated. The more useful conditional equilibrium constant (K_{eq}) can only be estimated through activity coefficients.

3.4 Effect of temperature

The effect of temperature on Gibbs energies for solids and gaseous compounds can been obtained from the integrals of the heat capacity temperature functions,

$$\Delta G^\circ(T) = \Delta G^\circ(T_0) - (T - T_0)\Delta S^\circ(T_0) + \int_{T_0}^{T} \Delta C^\circ_p \, \mathrm{d}T - T\int_{T_0}^{T} \frac{\Delta C^\circ_p}{T} \mathrm{d}T \qquad 3\text{-}6$$

This procedure is described in many references, for example in Kubaschewski et al. (1993) and Puigdomenech et al. (1997). The equilibrium constant at temperature T is then calculated from equation 3-4.

Using the listed ΔH_r compiled by Ahonen the expression for the equilibrium constant takes a slightly different form (Langmuir 1997):

$$\ln \frac{K(T)}{K(T_o)} = \frac{-\Delta H^o_r}{R}\left[\frac{1}{T} - \frac{1}{T_0}\right] + \frac{\Delta C^o_p}{R}\left[\frac{T_0}{T} - 1 - \ln\frac{T_0}{T}\right] \qquad 3\text{-}7$$

Equation 3-7 is valid for cases where ΔC_p (the change in heat capacity) is independent of temperature.

3.5 Effect of salinity

Available thermodynamic data are valid at infinite dilution. The effects of finite salt concentrations are in general large and some kind of estimate of this effect is required.

In principle, there are two methods. One can use conditional equilibrium constants and enter concentrations instead of activities in the equilibrium expressions or one can use activity coefficients and enter the product concentration times activity coefficient in the equilibrium expressions. In practice, the value of a conditional equilibrium constant can be estimated only through activity coefficients with application of equation 3-5.

3.5.1 Activity coefficients

Thermodynamic equilibrium constants give the relationship between the activities of species. Usually the concentration of a given species is of greater interest than the chemical activity. The chemical activity, a_i, of an aqueous species, i, is related to its concentration, C_i, through the activity coefficient, γ_i:

$$a_i = \gamma_i C_i \qquad 3\text{-}8$$

The standard state for the aqueous species is infinite dilution, at which point the activity coefficient is unity. At higher concentrations, the dependence of the activity coefficient on the concentration can be complicated. The deviations from unity are significant and some kind of estimate is usually required.

Single ion activity coefficients cannot be independently measured, only their total effect on the thermodynamic stability constants and on osmotic pressure. The mean activity coefficient ($\gamma_\pm$) of an electrolyte solution is the geometric mean of the individual activity coefficients (e.g. Langmuir 1997)

$$\gamma_\pm = \left[\left(\gamma_+^{n+}\right)\left(\gamma_-^{n-}\right)\right]^{1/n} \qquad 3\text{-}9$$

where $n+$ and $n-$ refer to the charges of the anionic and cationic components, respectively. At infinite dilution (i.e. in pure water), the mean activity coefficients and single-ion activity coefficients approach unity. With increasing salinity electrostatic interactions between dissolved ions decrease their chemical potentials (i.e. they become 'less active'). Formation of aqueous complexes or ion-pairing also have the effect of decreasing the value of the mean activity coefficient. The mean activity coefficients of various pure electrolytes can be measured experimentally, and are available in compilations of thermodynamic data (e.g. Lobo 1989, Robinson and Stokes 1959).

In dilute solutions, single ion activity coefficients may be estimated using either the Debye-Hückel or Davies approximations:

$$\log \gamma_i = \frac{-z_i^2 A\sqrt{I}}{1 + Bå\sqrt{I}} \qquad I < 0.1\ M \qquad 3\text{-}10$$

$$\log \gamma_i = -z_i^2\ A\left(\frac{\sqrt{I}}{1+\sqrt{I}} - b\,I\right) \qquad I < 0.5\ M \qquad 3\text{-}11$$

where z_i is the charge of species i, I is the ionic strength of the solution,[1] and A and B are temperature dependent constants (A ~0.509 and 0.328 at 25°C) that can be calculated from known parameters. A common value for b (an empirical correction for the effects of increasing ionic strength such as the decrease in the dielectric strength and ion pairing) in equation 3-11 is 0.2 although Davies originally proposed a value of 0.3. The ranges of applicability are those suggested by Stumm and Morgan (Stumm and Morgan 1996).

[1] The ionic strength I is given by $I = \frac{1}{2}\sum z_i^2 C_i$ where Z_i and C_i are the ionic charge and concentration of species i, respectively.

The experimental determination of thermodynamic data is frequently made in solutions of relatively high concentrations through addition of inert ions which influence the ionic strength I. The Specific Interaction Theory, or SIT-model (Brönsted-Guggenheim-Scatchard model) has been found suitable for the estimation of single-ion activity coefficients at relatively high concentrations. The SIT-model includes one electrostatic term and additional terms that describe the crosswise influence of each ion of the opposite charge.

$$\log \gamma_i = \frac{-A_z i^2 \sqrt{I_m}}{1 + B\mathring{a}\sqrt{I_m}} + \sum_k \varepsilon_{(i,k,I_m)} m_k \qquad 3\text{-}12$$

where ε is the interaction coefficient, i denotes the species considered, k and m_k denote the counter-ion and its concentration, respectively, and I_m is the ionic strength in molal units. The first term of the equation is the conventional extended Debye-Hückel equation describing the long-range electrostatic interactions between ions having opposite charges. The second term describes the short-range interactions of an ion with other ions of opposite charge. The SIT approach has been adopted as the standard procedure in the NEA Thermochemical data base review for the extrapolation from high ionic strengths to the reference state of infinite dilution (Grenthe et al. 2000). Examination of the SIT interaction coefficients of various ion pairs reveals some systematic dependence on the charge of the ions involved. Figure 3-1 shows a plot of SIT interaction coefficients versus the charge of the ion.

Pitzer has derived a system of equations that can describe the behaviour of mixed as well as single electrolytes with high accuracy (Pitzer 1991, Pitzer 1995). The Pitzer equations are useful as a framework for describing the properties of a chemical system. Single electrolyte parameters are determined from activity coefficients determined in solutions of one salt at a time. Mixing terms can be determined from osmotic effects in binary mixtures of salts using the previously determined single electrolyte parameters. In Pitzer's approach to solution chemistry, complex formation plays a very small role. Almost all solutions are treated as fully dissociated but with pairwise interaction coefficients for ions of opposite sign as well as for ions of the same sign. Even Pitzer is forced to recognise HSO_4^-, as an aqueous complex and treat sulphuric acid more as a 1:1 electrolyte than as a 2:1 electrolyte although it is fully dissociated at low concentrations.

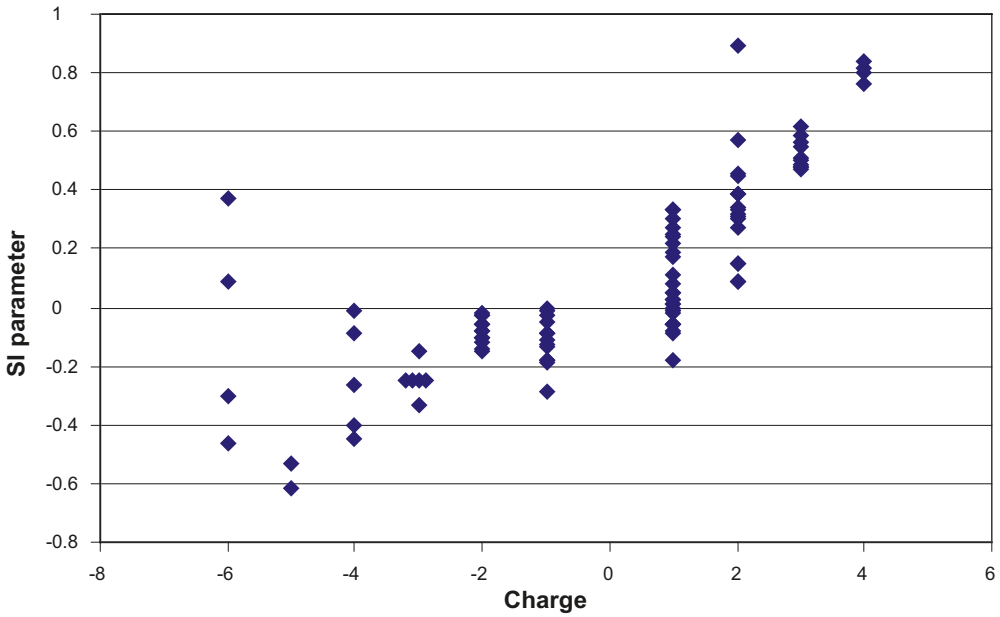

Figure 3-1. *Single-ion SIT-parameter data from Grenthe et al. (2000).*

Natural groundwaters are complicated in composition. The application of the SIT (and Pitzer) approaches requires specific data for the ions in various hydrogeochemical environments. Because this is not possible in most cases, simplifications must be used. The most useful of these simplifications, using the SIT approach, are those in which the coefficient in the second term in equation 3-12 is dependent only on the species under consideration or the coefficient is a constant. An example is the "b-dot" model (also known as the 'Truesdell-Jones' (T-J) model or the 'WATEQ Debye-Hückel' model) (Langmuir 1997):

$$\log \gamma_i = -z_i^2 A \frac{\sqrt{I}}{1 + B\text{å}\sqrt{I}} + b\,I \qquad 3\text{-}13$$

For this model, values of b are presented in the literature for some specific ions. Examples are shown in Tables 3-1 and 3-2. Another similar model, the "modified Helgeson model" (Puigdomenech and Taxén 2000), includes an additional logarithmic term intended to account for dilution of the solution in terms of the mole fraction of the salt:

$$\log \gamma_i = -z_i^2 A \frac{\sqrt{I}}{1 + B\text{å}\sqrt{I}} - \log(1 + 0.018015I) + b\,I \qquad 3\text{-}14$$

Parameter values for B, å and b in equation 3-14, at different temperatures, are given in Puigdomenech and Taxén (2000). It is suggested that, in the absence of sufficient data (i.e. ionic radii parameter å for all the species involved), the å values for NaCl can be used throughout.

Table 3-1. Non-zero 'b-dot' values in the Nagra/PSI thermodynamic database.

ion	Al^{3+}	Ba^{2+}	Ca^{2+}	Cl^-	F^-	Fe^{2+}	K^+	Li^+	Mg^{2+}	Mn^{2+}	Na^+	SO_4^{2-}	Sr^{2+}
b	0.19	0.09	0.15	0.01	0.08	0.16	0.01	0.2	0.22	0.22	0.06	–0.07	0.11

Table 3-2. Ion size (a_i=å) and b values for the Truesdell-Jones (b-dot) equation for individual ion activity coefficients (Langmuir 1997).

	a_i	b		a_i	b
H^+	4.78	0.24	Fe^{2+}	5.08	0.16
Li^+	4.76	0.20	Co^{2+}	6.17	0.22
Na^+	4.0	0.075	Ni^{2+}	5.51	0.22
	4.32	0.06	Zn^{2+}	4.87	0.24
K^+	3.5	0.015	Cd^{2+}	5.80	0.10
	3.71	0.01	Pb^{2+}	4.80	0.01
Cs^+	1.81	0.01	OH^-	10.65	0.21
Mg^{2+}	5.5	0.20	F^-	3.46	0.08
	5.46	0.22	$C1^-$	3.71	0.01
Ca^{2+}	5.0	0.165	ClO_4^-	5.30	0.08
	4.86	0.15	HCO_3^-	5.4	0
Sr^{2+}	5.48	0.11	SO_4^{2-}	5.0	–0.04
Ba^{2+}	4.55	0.09		5.31	–0.07
$A1^{3+}$	6.65	0.19			
Mn^{2+}	7.04	0.22			

Note: The equation, which applies to predominantly NaCl solutions, may be generally reliable up to an ionic strength of about 2 mol·dm^{-3}.

3.5.2 Choice of method for estimation of the effects of salinity

The departures of the activity coefficients for charged species from unity are, as a rule, large and some kind of estimate is required. Figure 3-2 shows approximate applicable ranges for the methods discussed here. The limits are those suggested by Langmuir (1997). The figure also shows the mean activity coefficient of NaCl as a function of concentration at 25°C. The different methods are applied with the parameter values suggested. Results can be compared to the experimentally determined values. It should be realised that, beyond the limiting form of the Debye-Hückel equation, none of the methods described here is based on an understanding of the nature of the interaction between ion-ion and ion-solvent.

The choice of method should be based on the following considerations:

- Available data.
- Consistency between complexation constants and interaction coefficients.
- Concentration and main components of the electrolyte, ground water or ionic medium.
- Temperature.
- Required/desired accuracy.

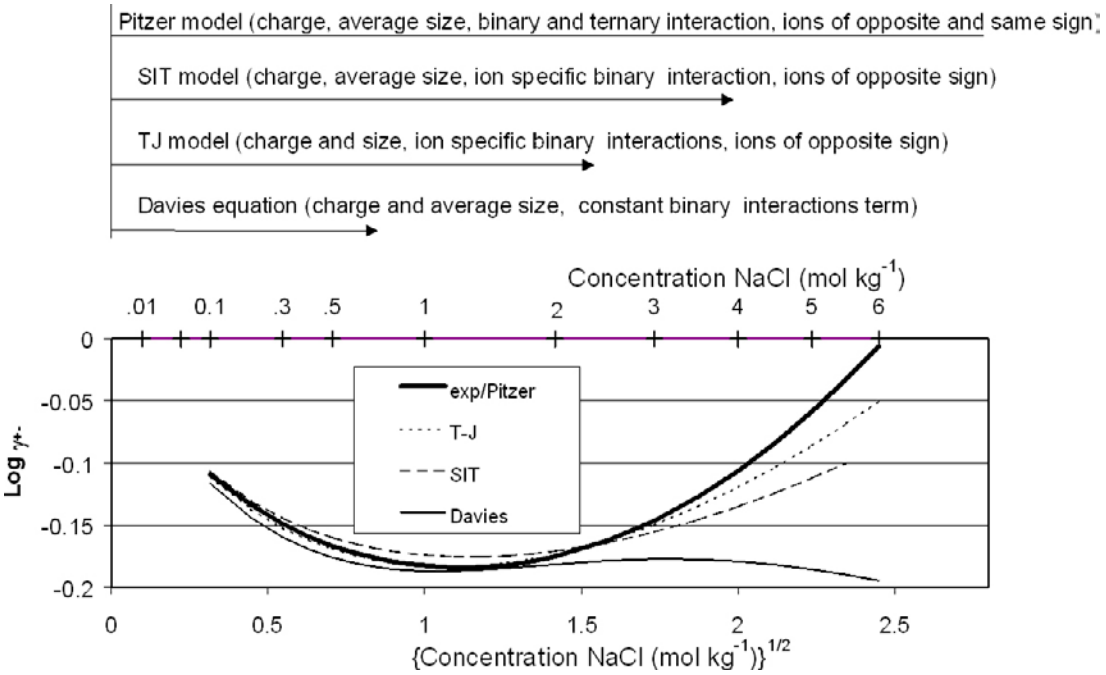

Figure 3-2. *Approximate applicable ranges for some different methods of estimating activity coefficients adapted from Langmuir (1997) using the mean activity coefficient for NaCl at 25°C as an example. Experimental data from Robinson and Stokes (1959). Pitzer equations using $\beta^{(0)} = 0.0765$, $\beta^{(1)} = 0.2664$, $C^{\Phi} = 0.00127$. Truesdell-Jones method using $B = 0.328$, å = 4.0, $b = 0.075$ for Na^+, å = 3.71, $b = 0.01$ for Cl^-. SIT equation using $\varepsilon(Na^+, Cl^-) = 0.03$. Davies equation using $b = 0.2$. (See Langmuir 1997 for definition of the symbols). The ionic strength expressed in mol kg^{-1} was used in all equations. [NaCl]aq was calculated using an equilibrium constant of log k = –0.78 for estimation of the ionic strength for the Davies equation. [NaCl]aq was not considered for other methods, for which the inclusion of [NaCl]aq would be detrimental to their performance. The "true" ionic strength was used for the Davies equation. For the other methods the "true" ionic strength is equal to the stoichiometric ionic strength since [NaCl]aq is considered to be non-existent. See Section 3.8*

3.6 Effect of pressure

The effect of pressure (p) on equilibrium constants may be estimated from (Langmuir (1997), Stumm and Morgan (1996)):

$$\log \frac{K^{o}_{p}}{K^{o}_{p^\circ}} = -\frac{\Delta V^{o}_{r}(p - p^\circ)}{\ln(10)\,R\,T} \qquad 3\text{-}15$$

where p° is the standard pressure (1 bar), and ΔV°_r is the standard molar volume change for the reaction. The expected hydrostatic pressure at the planned repository depth of 500 m is estimated to be of the order of 50 bars. Puigdomenech and Taxén (2000), with reference to Langmuir (1997), state that the experimentally determine value of ΔV°_r for dissociation reactions is ≥ –50 cm^3/mol. Molar volumes for many minerals may be found in Robie and Hemingway (1995). The "maximum" value of ΔV°_r = –50 cm^3/mol, corresponds to an increase of 0.26 log-units in the equilibrium constant at 300 bars.

3.7 Evaluation and selection of thermodynamic data

Appendix I contains the selection of thermodynamic data tabulated in SKB TR-00-13 (Puigdomenech and Taxén 2000). The sources of the values and a discussion of their selection can be found in this reference. Appendix II contains a previously unpublished selection of thermodynamic data and discussion by Ahonen. These values comprise two more-or-less independent selections of data. As will be shown in a discussion of their application in Section 5, the difference between the two sets, in terms of equilibrium concentrations of Cu(I), is not significant.

3.8 Consistency

There are a number of important questions of consistency of the data. The thermodynamic database should, of course, be internally consistent so that the stability of a compound can be calculated unambiguously. Additions of a chemical compound to the database should be made with a consideration of the thermodynamic parameters of the species already in the database and with regard to the thermodynamic parameters of the components used in the source. It must also be realised that old experimental data can be subject to re-evaluation (Baes and Mesmer 1976).

Consistency is also important in the selection of the method and parameters values for the estimation of activity coefficients. Lower values than predicted from the Debye-Huckel theory may be interpreted as due to the presence of a complex aqueous species or it may be interpreted as an interaction coefficient. For example, NEA TDB-2 (Grenthe et al. 2000) contains values for the interaction coefficient between CO_3^{2-} and Na^+ and between Cu^{2+} and Cl^-, whereas SKB TR-00-13 (Puigdomenech and Taxén 2000) contains equilibrium constants for $NaCO_3^-$ and $CuCl^+$.

Another example where care must be taken to maintain consistency is shown below. The success of a description using specific interaction coefficients may be determined by comparison with experimentally determined mean activity coefficients $\gamma_\pm$. Related, but not identical, is the single ion activity coefficient or specific ion activity coefficient γ_i. The difference between the concepts is shown below for a NaCl solution which is assumed to be partly associated.

$$\gamma_\pm = \frac{a_{Na+}}{[Na^+]_{tot}} = \frac{a_{Cl-}}{[Cl^-]_{tot}} \qquad 3\text{-}16$$

$$\gamma_{Cl^-} = \frac{a_{Cl-}}{[Cl^-]_{free}} \qquad \gamma_{Na^+} = \frac{a_{Na+}}{[Na^+]_{free}} \qquad 3\text{-}17$$

$$[Cl^-]_{free} = [Cl^-]_{tot} - [NaCl]_{aq}$$
$$[Na^+]_{free} = [Na^+]_{tot} - [NaCl]_{aq} \qquad 3\text{-}18$$

There is some confusion about these two definitions of activity coefficient. It is obvious that for electrolyte solutions where complex formation or ion-pairing is significant, ion specific activity coefficients cannot be determined from mean activity coefficients without considering the equilibrium constants for aqueous complex species. A related issue is the definition of ionic strength I. The ionic strength is in principle defined as:

$$I = \frac{1}{2}\sum z_i^2 C_i \qquad 3\text{-}19$$

where the sum is taken over all charged species in the solution. So what is the ionic strength of 1.0 mole NaCl per kg water? From the definition above it would be slightly less than 1.0 m because a fraction of the salt is bound in the neutral complex. Parallel to the definition above, which is sometimes referred to as the 'true' ionic strength (Helgesson et al. 1981), is the stoichiometric ionic strength. The stoichiometric ionic strength has the value of 1.0 m in a 1.0 m NaCl solution because it assumes full dissociation of the salt.

To minimise confusion, any estimate of ion specific activity coefficients should be accompanied by a list of the values of the equilibrium constants used and an explicit definition of the ionic strength, including the concentration scale used (molar or molal). For reactions where water occurs in the reaction formula, it is useful to know whether the activity of water was considered explicitly or included in the activity coefficients of the other reactants and products.

3.9 Uncertainties

Neither SKB TR-00-13 (Puigdomenech and Taxén 2000) nor the compilation by Ahonen (Ahonen 2001) contain systematic estimates of the uncertainties in the thermodynamic parameters. The assignment of uncertainties to thermodynamic parameters calls for a critical review of all the relevant literature (Wanner and Östhols 2000) and is beyond the scope of the present section. Some general remarks can nevertheless be made.

The thermodynamic parameters are generally determined at 25°C and estimates of the values at other temperatures are frequently associated with an extrapolation error. The extrapolation in terms of concentration of the electrolyte introduces further errors. The combination of elevated temperatures and high concentrations seems to give rise to the widest error limits. Grenthe et al. (2000) predict that, assuming that the relevant interaction coefficients for the SIT-method are known for 25°C, the uncertainty in $\log_{10} \gamma_j$ will be up to 0.13**Im* (*Im* is the ionic strength in moles kg^{-1}) within the temperature range 0 to 50°C. Worst case estimates of the uncertainties, from this source alone, for the reactions:

$Cu(s) + 2\ Cl^- + H_2O = CuCl_2^- + OH^- + ½\ H_2(aq)$

$Cu(s) + 3\ Cl^- + H_2O = CuCl_3^{2-} + OH^- + ½\ H_2(aq)$

at 50°C, suggest that the equilibrium concentrations of $CuCl_2^-$ and $CuCl_3^{2-}$ cannot be calculated to better precision than ±4*0.13 = ±0.52 and ±5*0.13 = ±0.65 logarithmic units respectively, at *Im*=1.0.

We do not know the value of the SIT-interaction coefficients for $CuCl_2^-$ and $CuCl_3^{2-}$, with the relevant cations in a groundwater, even at 25°C. SI-theory predicts an activity coefficient of unity for neutral species such as $H_2(aq)$. Other models and sources predict ($dlog\ \gamma/d\ I$) ≅ 0.1 for neutral species (Harned and Owen 1958). There is also uncertainty in the thermodynamic parameters at infinite dilution at 25°C. A tentative conclusion is that the equilibrium concentration of copper, arising from corrosion of metallic copper, during evolution of dissolved hydrogen, at 1.0 m ionic strength and 50°C, should not be quoted to better precision than ±1 logarithmic unit.

4 Corrosion under atmospheric conditions and in unsaturated bentonite

Before complete saturation of the repository, the canisters will be exposed to two distinct sets of unsaturated environmental conditions. First, the canisters will be exposed to the atmosphere in the encapsulation plant and underground facility and may undergo corrosion if the relative humidity is sufficiently high. Second, following emplacement of the canisters and of the compacted bentonite, there will be a period of unsaturated conditions until the near-field saturates with incoming groundwater. Corrosion during these two periods is considered in this section, along with an assessment of the initial state of the canister at the time of emplacement. Corrosion under fully saturated conditions is considered in Section 5.

Summary of changes to the original report

The new Section 4 "Corrosion under atmospheric conditions and in unsaturated bentonite" combines material from Section 4 "Corrosion prior to water saturation" and Section 5 "Corrosion during water saturation" of the original report.

The revised text contains additional information from atmospheric corrosion studies, including *in situ* measurements from the Äspö HRL. Since the original report, a more-complete mechanistic understanding of salt deliquescence and of the initial wetting behaviour of the canister surface has been developed, a description of which is included in the revised report. The "initial" condition of the canister at the moment of emplacement is described in Section 4.2.

4.1 Corrosion before emplacement

After the fuel has been encapsulated, the copper canisters will be transported without unnecessary delay to the geologic repository and deposited. The expected time between encapsulation and deposition will normally be several weeks. During that period, the canisters will be exposed to indoor air either at the encapsulation plant or at the repository site and to the atmosphere inside the vessel that will be used for transporting the canister to the repository site. The indoor air is expected to have a temperature of about 20°C. Due to the heat generated by the spent nuclear fuel, the canister itself will have a temperature higher than the surrounding air. The expected maximum surface temperature for a canister with a heat generation of 1.7 kW is somewhat less than 50°C when the canister is exposed to freely circulating air. When inside a radiation shield, the temperature may approach 100°C.

After sealing, the canisters are assumed to be stored in a facility with levels of air pollution comparable to those in an urban atmosphere. The environment at the repository site is rural, with no other additional sources of pollutants than created by repository operations. Also here, the pollutant levels are assumed to be equivalent to an urban atmosphere or better. Irrespective of the storage period, the canisters will be stored in well-ventilated areas and, in the case of a coastal site, protected from salt spay. The maximum levels of pollutants detrimental to copper are estimated to be (Leygraf and Graedel 2000, Shreir et al. 1994):

SO_2 100 $\mu g \cdot m^{-3}$
NO_2 75 $\mu g \cdot m^{-3}$
NH_3 < 20 $\mu g \cdot m^{-3}$
H_2S < 3 $\mu g \cdot m^{-3}$

4.1.1 Theoretical background

Leygraf and Graedel (2000) have reviewed the mechanisms and kinetics of atmospheric corrosion and King (2006), and King and Kolář (1997a) have considered the consequences of atmospheric corrosion of copper canisters for spent fuel disposal.

The formation of a water film on the metal surface is of fundamental importance to atmospheric corrosion. The thickness of this water film varies from a few monolayers at low relative humidity to thousands of monolayers at 100% relative humidity (King 2006, Leygraf and Graedel 2000). When a "critical relative humidity" is exceeded the corrosion rate increases markedly with increasing humidity. This critical relative humidity depends on the surface conditions of the metal but is generally in the range 50–70%. Below this level, the corrosion rate is for all practical purposes negligible.

When the thickness of the water film exceeds about three monolayers, its properties become similar to those of bulk water. This occurs approximately at the critical relative humidity. As this film thickens with further increases in humidity, water-soluble pollutants will dissolve in the moisture film in equilibrium with the gaseous phase. The SO_2 present in the air will dissolve forming HSO_3^- and can be oxidised to sulphate by oxidants in the air. The NO_2 is assumed to be absorbed in the moisture film as HNO_3.

The aqueous phase acts as an electrolyte for electrochemical reactions where the cathodic reaction is the reduction of an oxidant from the atmosphere. The corrosion products that are formed may precipitate and form a protective layer, resulting in a decrease in the corrosion rate with time. For copper, this layer generally has a duplex structure, with an inner layer of cuprous oxide (Cu_2O) and an outer layer of a precipitated basic Cu(II) salt such as atacamite/paratacamite ($Cu_2(OH)_3Cl$), brochantite ($Cu_4(OH)_6SO_4$), or malachite ($Cu_2(OH)_2CO_3$), with the nature of the Cu(II) solid dependent on the predominant anion in the aqueous layer.

4.1.2 Atmospheric corrosion in the encapsulation plant and repository

The indoor relative humidity in Scandinavia depends on geographic location. Coastal areas have higher relative humidity than inland locations. The relative humidity also has seasonal variations with higher relative humidity during the summer months. The actual indoor humidity will depend on the ventilation of the facility, but will be below the critical humidity at least during the winter months.

The elevated surface temperature (50°C) of the copper canister will ensure a relative humidity close to the canister surface considerably lower than the critical humidity. The corrosion rate can, therefore, be assumed to be very low. Rice et al. (1981) have reported corrosion rates for copper exposed at ambient temperature in different atmospheres and for periods of 12 to 18 months. For city atmospheres, they reported corrosion rates of 6 to 27 nm/year. These data are in agreement with the rates for corrosion of copper in dry air (Miley and Evans 1948). They found that a layer of predominantly copper oxide was formed on the surface and that this layer inhibited further corrosion when it had reached a thickness of 9–10 nm. These data refer to room temperature. There are, as far as we know, limited data available for the relevant canister temperature (see below). If the conclusion that the corrosion rate decreases to very low values after a layer of corrosion products of a certain thickness has been formed is correct, the corrosion rates at 50°C should not differ much from that measured at room temperature. Alternatively, if there is a temperature dependence, it is not unreasonable to assume a doubling of the corrosion rate for each 10°C increase. This would mean that the corrosion rate would be approximately 10 times higher at 50°C than at 20°C, i.e. the expected corrosion rates would be 60 to 270 nm per year.

Taxén (2004) describes an atmospheric corrosion study at the Äspö Hard Rock Laboratory (HRL). Copper coupons were exposed to the natural humid sulphide-containing atmosphere of the HRL with and without compacted bentonite present. Tests were performed at ambient temperature and, in the case of the test with bentonite, also at 75°C. Corrosion rates were estimated based on mass loss or from electrochemical stripping of the corrosion products under galvanostatic conditions. Corrosion rates were < 0.1 μm/yr, which is significantly lower than typical surface atmospheric corrosion rates in Sweden, suggesting that the HRL atmosphere is less corrosive than normal surface atmospheres. It is assumed that the Äspö HRL atmosphere would be typical of the atmosphere in the repository. The only corrosion product detected was γ-$Cu_2(OH)_3Cl$ (paratacamite), although the presence of Cu_2O is also likely and may not have been detected due to sampling artifacts (Taxén 2004).

King and Kolář (1997a) discuss two studies of atmospheric copper corrosion at elevated temperatures. Roy and Sircar (1981) report logarithmic oxidation kinetics in dry air at temperatures between 75°C and 150°C, while Pinnel et al. (1979) report parabolic kinetics. Both studies were performed

in dry air and, although the rate laws they propose give quite different kinetics for the growth of the oxide layer at 100°C, they predict a total oxide thickness after a few years exposure in the range 30 to 70 nm. Pinnel et al. (1979) found that pollutants in the air increased the oxidation rate by a factor of between 3 and 8.

In conclusion, storing the copper canisters for extended periods of time before disposal should have a negligible effect on their service life after disposal. Radiation effects are expected to be minimal (see Section 7). The total corrosion wall penetration even after two years storage will be less that 1 μm. The most likely corrosion product will be copper oxide.

4.1.3 Corrosion due to handling and operational factors

Damage of the canister surface caused by handling during emplacement is unlikely to significantly affect the corrosion behaviour. Unlike some passive materials, copper is not susceptible to galvanic corrosion due to embedded iron particles resulting from the use of steel handling equipment. In fact, iron particles would temporarily galvanically protect the canister surface. Scratches and other defects in the surface oxide caused by handling would rapidly oxidize when exposed to the repository environment until the protective oxide layer has been reformed. Also, handling would not introduce stress raising defects of sufficient size to cause cracking in the absence of a suitable environment for stress corrosion cracking (see Section 6). Plastically deformed material might preferentially dissolve, but this localized dissolution would stop once the deformed material had been corroded.

4.2 Initial condition of the canister

From the perspective of the subsequent corrosion behaviour, the important characteristics of the initial state of the canister include:

1. Nature and thickness of surface film (oxide).
2. Nature and concentration of surface contaminants.
3. Canister dimensions (corrosion allowance) and mechanical properties.
4. Maximum weld defect size.
5. Mechanical damage and cold work.
6. Level of residual stress.

As noted above, the emplaced canister will be covered by an air-formed oxide with a thickness of a few tens to a few hundreds of nanometres.

The encapsulation plant is expected to be a relatively clean industrial environment. Surface contamination by dust, lubricants, other organics, and salt particles, however, is possible. Further surface contamination by potentially deliquescent salts will occur upon emplacement as the canister contacts the bentonite clay. As discussed below, it is reasonable to expect that the canister surface will be contaminated leading to surface wetting prior to complete saturation of the buffer.

Although the nominal corrosion allowance of the copper is 50 mm, deformation during forming and hot rolling, post-weld machining, and other processes could lead to a reduction in wall thickness. SKB (2010) estimate the minimum copper wall thickness upon emplacement to be 47.5 mm. The mechanical properties of the canister material (tube, lid and base, and weld) are expected to meet or exceed the design requirements of a strain to failure of > 40% and a creep ductility of > 15% (SKB 2010). A maximum grain size of 360 μm has been specified (Andersson et al. 2004) and, although there is no specific requirement for the minimum yield strength, annealed copper typically has a value in excess of 60–100 MPa.

Based on the analysis of a series of trial friction-stir welds, SKB (2010) estimate the maximum size of an undetected weld defect in a population of 6,000 canisters to be 10 mm, for normal welding operations. The defect is most likely to take the form of joint line hooking.

Handling of the canister and impacts incurred during emplacement may lead to mechanical damage and the introduction of cold work. Raiko et al. (2010) summarize the results of a number of studies of the effect of impacts of various loads on the deformation of the copper shell. An applied load of 500 MPa results in a strain of 12% and a displacement (indentation) of 1.1 mm, which is considered to be the maximum tolerable. Higher loads of 600 and 700 MPa result in 23 and 53% strains and indentations of 2 and 3.9 mm, respectively. Cold work increases the susceptibility of copper to SCC in nitrite solution (Section 6.1.2.2), although samples with 20% cold work were only marginally more susceptible than annealed material.

Residual stress levels have been measured for both friction-stir welds (FSW) (Raiko et al. 2010) and electron-beam welds (EBW) (Gripenberg 2009). For FSW, the residual stresses on the outer surface tend to be compressive with values up to –60 MPa, with smaller compressive (and, in some cases, slightly tensile) stresses on the inside of the canister. Tensile stresses are found mid-wall. In contrast, EBW tend to exhibit tensile residual stresses up to 70 MPa, balanced by compressive stresses in the adjacent base metal. (Gripenberg 2009).

4.3 Corrosion in unsaturated bentonite after emplacement

4.3.1 Hydrogeochemical aspects of the saturation of bentonite

After emplacement in the deposition holes, it will no longer be possible to actively control the composition of the atmosphere to which the canister is exposed. The relative humidity in the repository is expected to be high. At the Äspö laboratory, the relative humidity is about 80% and the humidity in the repository should be similar.

In the KBS-3V repository design, the canisters will be deposited in 8-m-deep hol es surrounded by 0.35-m of highly compacted bentonite with low hydraulic permeability. The tunnels will be backfilled with compacted low-grade bentonite. The buffer and backfill are not saturated with water during the installation. About 40% of the total amount of water in the buffer must be provided by the host rock. This wetting process, leading to the final water saturated conditions around the waste canisters, the form of its progress, and its duration will influence the form and the extent of the corrosion during this phase in the canister service life.

The heat generated by the waste will lead to a redistribution of the moisture in the bentonite. The bentonite blocks will initially have a water content of 17%, corresponding to equilibrium with air with a relative humidity of 75% (70% water saturation for the bentonite blocks with the highest density). The canister wall is expected to reach a temperature of up to 100°C. The temperature gradient in the bentonite created by the elevated canister temperature redistributes the water and lowers the water content closest to the canister to about 10%. This corresponds to a relative humidity of about 50%. Even though this is considerably lower than the ambient repository relative humidity, it is still high enough to be above the critical relative humidity required to establish aqueous conditions. Corrosion is, therefore, expected to proceed via electrochemical reactions similar to those considered in aqueous solutions (see Section 5).

The progress of the wetting process is incompletely understood. Börgesson and Hernelind (1999) have modelled the wetting of the bentonite and found the overall wetting process to be sensitive to the rock properties and the boundary conditions. However, Börgesson and Hernelind (1999) give a typical example of the water saturation process. In their example, they assume that the water is supplied to the deposition hole at a rate of 0.044 L/h through two fractures and through the rock matrix with a permeability of 10^{-13} m/s. The water pressure reached its full value of 5 MPa a distance of 10 m from the deposition hole. In the model, there was no gap between the bentonite blocks and the canister surface. As a consequence, no definite conclusions can be made concerning how and when the bentonite contacts the canister. The calculations showed a quite uneven increase in the degree of water saturation around the canister during the first 5-8-years. Full water saturation was achieved after about 12 years.

This inhomogeneous increase in water content in the bentonite will also most probably result in an uneven swelling of the buffer. As a consequence of this, the gap may close in some areas while it remains open in others. Sites where the bentonite first contacts the copper canisters are possible

locations for the spatial separation of anodic and cathodic processes. It is to be expected that the electrochemical reduction of oxygen will be faster at sites where there is a good supply of oxygen, where there is an electrolyte present, and where there is only a small separation from a site where electrochemical corrosion of copper can take place. Locally increased corrosion rates may therefore be expected at the three phase boundary; copper/moist bentonite/air. However, since the gaps close gradually as the bentonite swells, the location of these sites will not be constant. Once the bentonite has reached full saturation, the whole canister surface will have been exposed to this condition. The fact that some sites have been exposed to conditions that enable electrochemical corrosion longer than others may cause slightly uneven corrosion. Apart from that, the gradual closing of the gaps is not likely to result in any significant localised effects.

The maximum possible corrosion attack can be estimated from mass balance considerations. As an example, the total volume of buffer and backfill in the deposition tunnel and the deposition hole is 150 m^3/canister. The porosity in the bentonite and the backfill material can be conservatively estimated to be 40%. If all of this porosity consisted of air, the amount of O_2 per canister would be 12.5 m^3, or approximately 560 mol. Assuming that Cu_2O is formed as the corrosion product, 2,240 mol of copper or 140 kg could be oxidised. This corresponds to a maximum depth of corrosion of 840 µm evenly distributed over the canister surface. In reality the corrosion will be considerably smaller since residual oxygen will also be consumed through reaction with accessory minerals in the buffer and backfill and through microbial activity. These processes, which have been found to be very rapid (Section 2.2.2), will also consume the oxygen in the groundwater that has been in contact with air during the construction and operation phase of the repository (Puigdomenech et al. 2001). Wersin et al. (1994a) have modelled the corrosion of copper in saturated bentonite taking into account transport by diffusion of oxygen in addition to flow, equilibrium reactions and kinetic processes at the bentonite-canister interface. The results indicate a conservative corrosion rate of 7 µm/year for oxic conditions. A sensitivity analysis indicates that the main uncertainties arise from the diffusion properties of the clay. King and Kolář (1997a, 2006a) performed bounding calculations of the corrosion during the unsaturated phase in the repository as a result of uniform attack. The assessments relate to a proposed Canadian repository concept with in-room emplacement rather than the in-floor emplacement that is one of the configurations being considered by SKB and Posiva. Predicted corrosion depths ranged from less than 90 nm in the case of oxidation (see Section 4.1.2) to about 90 µm in the case of thin-film corrosion. (Note: the estimation of the maximum amount of corrosion depends strongly on the amount of O_2 per canister, which in turn is dependent upon the assumed repository design).

The temperature gradient through the bentonite may affect the buffer function by different enrichment processes of dissolved substances. One such process is ion transport parallel to water uptake from the outer cooler parts of the bentonite, or from the surrounding groundwater, to the wetting front in the originally unsaturated bentonite. The transport is assumed to take place by a cyclic evaporation/condensation process in which water is sucked in from cooler parts, evaporates at the wetting front, and is partly redistributed in the form of steam. Dissolved salts will thereby be deposited at the wetting front.

A second possible process is precipitation of species which have lower solubility at higher temperature, such as calcium sulphate (gypsum) and calcium carbonate (calcite). Both these minerals may be present in the bentonite as impurities.

4.3.2 Corrosion considerations during the saturation of bentonite

Very few long-term experiments have been performed under conditions that realistically simulate the early stages of the development of the repository, with the exception of the results from the pilot phase of a “Long Term Test of Buffer Material” at Äspö Hard Rock Laboratory (Karnland and Sandén 2000, Karnland et al. 2000). In these experiments, heaters in copper tubes were buried in bentonite clay in deposition holes drilled into the rock. The clay also contained copper coupons for corrosion testing. The analyses of the clay at the copper-clay interface showed enrichment in both calcium sulphate and calcium carbonate. The mean corrosion attack on the copper was found to be 3 µm per year. This is in quite good agreement with the modelling results of Wersin et al. (1994a). The corrosion attack was somewhat uneven, but both optical microscopy and SEM revealed no signs of pitting. Several types of corrosion products were present, among them Cu_2O and $Cu_2CO_3(OH)_2$ (malachite). These corrosion products have obviously been formed under oxidising conditions.

King et al. (1992) have reported laboratory experiments of copper corrosion in compacted bentonite/sand mixtures using a saline synthetic groundwater (0.97 M Cl^-). A number of experiments were deliberately performed in unsaturated bentonite, and in others it is likely that the buffer was also unsaturated for part of the exposure time at least. Under those conditions, a basic cupric chloride ($CuCl_2 \cdot 3Cu(OH)_2$) was found as discrete crystals on top of an oxide layer that that they reported as possibly Cu_2O. The corrosion rates were in the range 30–50 µm/year. It is reasonable to assume that copper chlorides/hydroxy chlorides may also form as an initial corrosion product in saline groundwaters during the water saturation phase in compacted pure bentonite.

Recently, Pusch (2008) studied the effect of copper corrosion on the properties of MX-80 bentonite, a saponite clay from Milos, Greece, and an illite-smectite mixed layer clay from Friedland. The compacted clay was in contact with copper samples, the underside of which were heated. The other end of the clay column was wetted with a solution of 1 wt.% $CaCl_2$. The effects observed with MX-80 were similar to those reported by King and co-workers (King et al. 1992, Litke et al. 1992) for Avonlea bentonite and sand:bentonite mixtures. Precipitation of corroded copper was observed, as was the transport of copper some distance into the clay. High interfacial Cu concentrations were found. At the end of the relatively short 8-week exposure, the copper coupons were found to have undergone localised corrosion, with some areas corroded surrounded by areas in which the original polishing lines could still be seen. This form of corrosion is consistent with an early stage in the development of the roughened surfaces observed by King and co-workers (Section 5). As discussed in more detail below, the use of $CaCl_2$ to wet the clay would have enhanced the localised nature of the attack as this species deliquesces at very low relative humidity and would have resulted in non-uniform wetting of the surface. There were differences in the rate of corrosion for the different clays and the extent to which Cu diffused away from the corroding interface. However, any difference in corrosion rate is of little importance for copper canisters in the repository, as it is the inventory of trapped atmospheric O_2 that determines the amount of corrosion, with the corrosion rate only (partly) determining the time at which anoxic conditions are established in the repository.

Brennenstuhl et al. (2002) studied the effect of different rates of access of O_2 to the canister surface. Preliminary results suggested that although areas in contact with fully swollen bentonite may corrode faster than areas in contact with partially swollen material, the extent of localisation diminishes with time as the oxygen concentration falls. No discrete pitting was observed in any of the tests. Coupled with the gradual swelling of the bentonite over the entire canister surface, the degree of localisation of the attack due to this phenomenon is expected to be small.

King (2006) considered the evolution of the corrosive environment at the canister surface during the unsaturated phase in a Canadian repository. Corrosion during this period is determined by the time at which the canister first becomes wetted and the subsequent distribution of moisture on the surface. In turn, the wetting behaviour of the surface depends on the time dependence of the relative humidity in the pores of the bentonite (which is equivalent to the water activity in the clay) and the nature of surface contaminants on the canister. (Here it is assumed that saturation of the bentonite occurs uniformly, but if it does not then this is another mechanism by which, in this case large-scale, differences in the extent of surface wetting could arise).

Wetting of the surface is determined by the deliquescence point of surface contaminants (Figure 4-1). As the canister surface temperature cools and the relative humidity of the bentonite pore water increases, surface contaminants will progressively deliquesce, i.e. absorb moisture from the atmosphere and dissolve. At the deliquescence point, a saturated solution of the salt (or salt mixture) is formed, with the activity of water in the solution at equilibrium with that in the vapour phase. Different salts (and other contaminants, such as grease residues and other organics) deliquesce at different temperatures and relative humidities (Figure 4-2). The more soluble the salt the lower the deliquescence relative humidity and/or the higher the deliquescence temperature. Mixtures of salts, especially involving nitrates, deliquesce at lower relative humidities than single, less-soluble salts. Following deliquescence, increased relative humidity results in a progressive dilution of the solution.

Contamination of the canister surface may arise from a number of sources. Handling and exposure to the repository atmosphere will likely result in organic contaminants on the surface. Contact with the bentonite or with groundwater will result in salt contamination. The canister surface is unlikely to be uniformly contaminated. Therefore, different areas on the surface will wet at different times during the unsaturated phase as the canister cools.

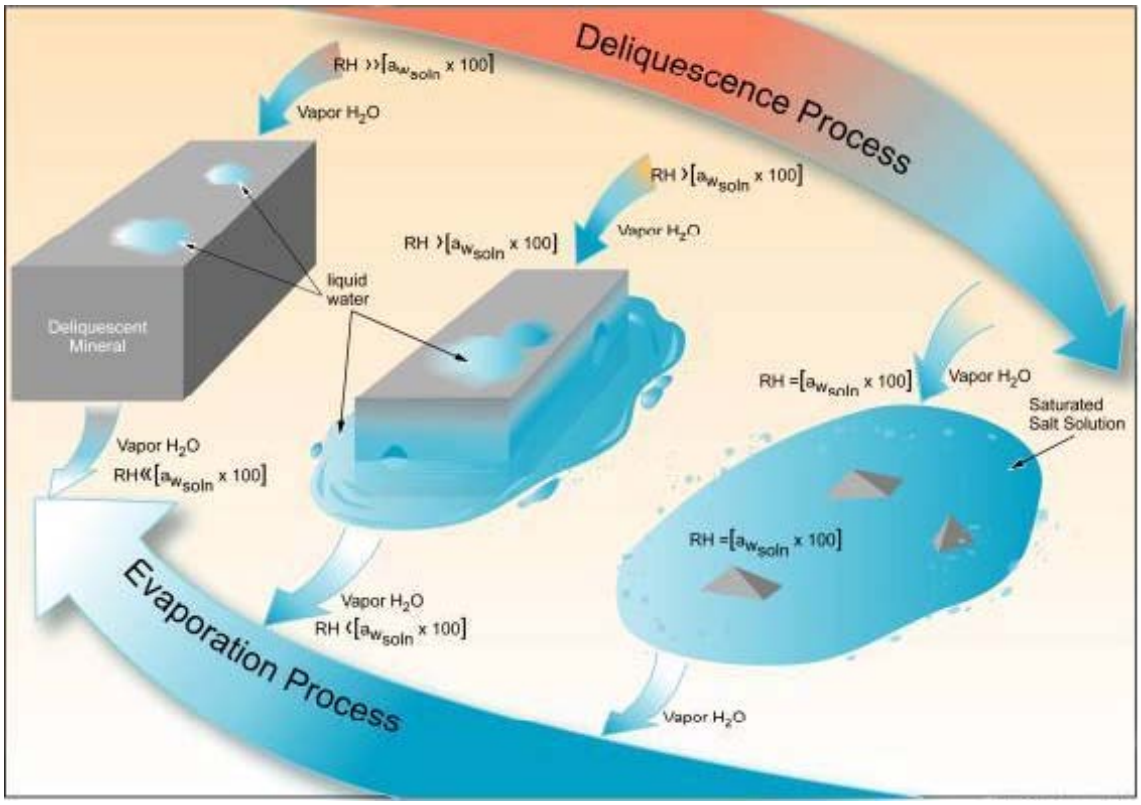

Figure 4-1. *Schematic illustration of the processes of evaporation and deliquescence (BSC 2004).*

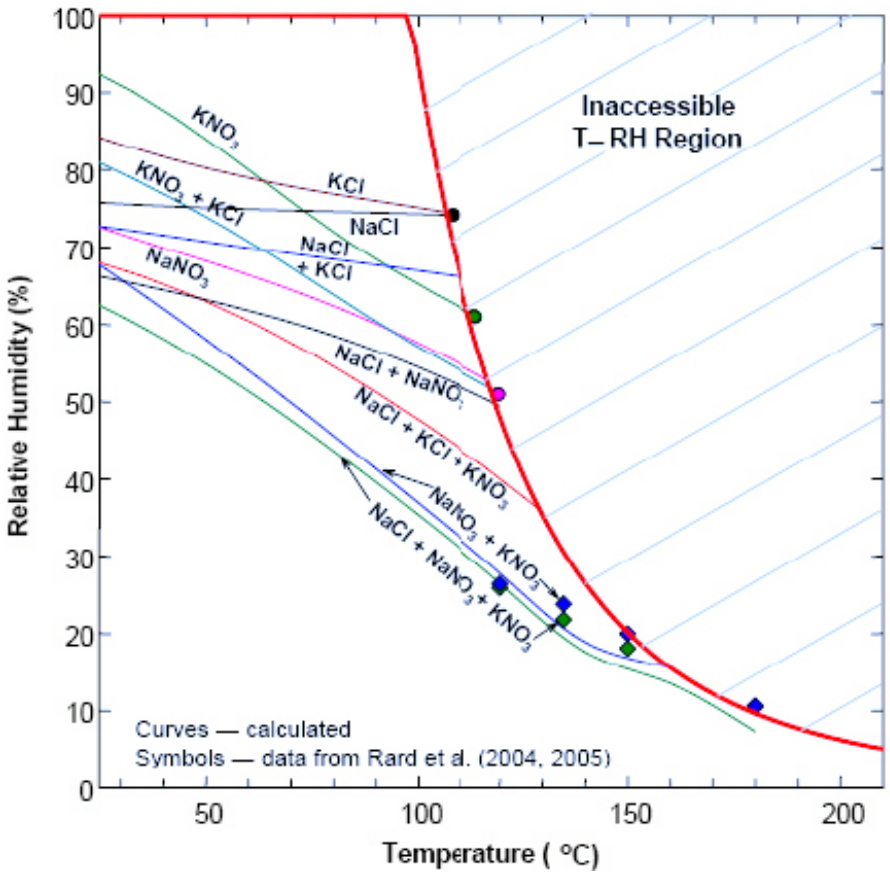

Figure 4-2. *Temperature dependence of the deliquescence relative humidity for various mineral assemblages (after Rard et al. 2005).*

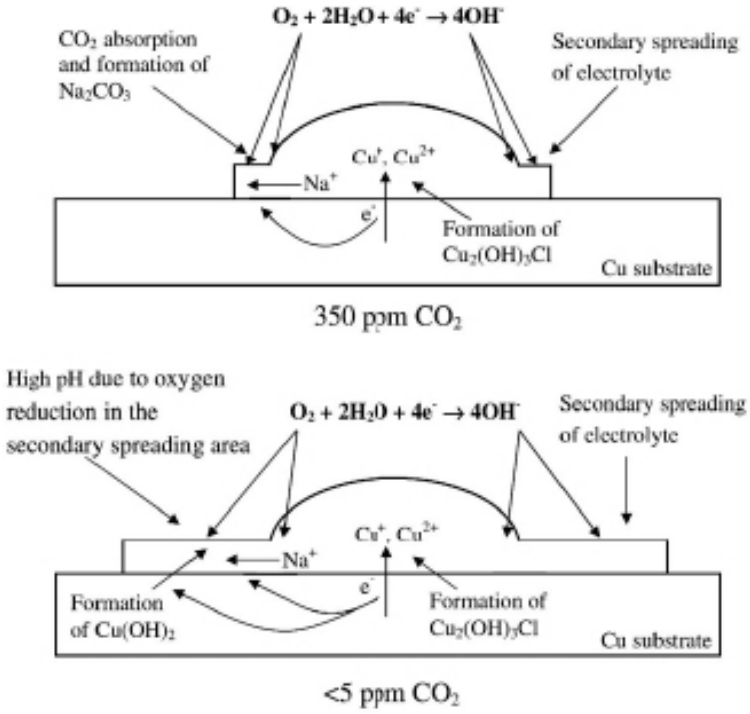

Figure 4-3. *Conceptual model for the atmospheric corrosion of copper contaminated by NaCl in the presence of oxygen and carbon dioxide (Chen et al. 2005).*

Non-uniform wetting of the surface could establish conditions for localised corrosion of the canister. The initial deliquescence of, say, a salt crystal will result in a drop of saturated electrolyte on the surface. The periphery of this droplet (or of microdroplets that form around the main droplet, Zhang et al. 2005) will have greater access to O_2 and will tend to be cathodic, with the centre of the drop acting as the anode (Figure 4-3). This is almost certainly the mechanism by which the localised corrosion observed by Pusch (2008) was initiated, especially since $CaCl_2$ exhibits one of the lowest deliquescence relative humidities of any single salt.

Although localised corrosion may initiate, it is unlikely to propagate very deeply. A major limiting factor is the amount of O_2 trapped in the buffer material. Furthermore, as the relative humidity increases the surface will become more uniformly wetted as less-deliquescent contaminants absorb moisture from the atmosphere. Eventually the entire surface will be wetted and the differential O_2 concentration cell that acted initially as the driving force for localised corrosion will disappear. At this stage the surface will take on a generally roughened appearance as discussed in more detail in Section 5.

4.4 Summary

In summary, information from the literature and the limited experimental data available suggest that the extent of corrosion during the unsaturated phase will have a negligible effect on the canister lifetime. Atmospheric corrosion will be limited because of the generally short duration of exposure to the humid repository atmosphere and because, based on experience from the Äspö HRL, the atmosphere is expected to be relatively non-corrosive. After emplacement, there is the possibility of the initiation of localised corrosion during the early part of the unsaturated transient because of non-uniform wetting of the surface. However, uniform corrosion conditions are expected to be established by the time the bentonite becomes fully saturated. Some further study of this period may be warranted (Section 9).

5 General and localised corrosion of copper

Summary of major changes to the original report

This revised report contains a number of significant changes to the original report, including:

- a discussion of new studies on the initial stages of Cu oxidation and of the effect of bentonite density on the corrosion rate (Section 5.2.1.2),
- a description of recent experimental studies on the corrosion of copper under anoxic conditions, both in Cl^- solutions and in pure water (Section 5.2.2),
- extensive discussion of new experimental and modelling information on the effects of sulphide on the general corrosion of copper during the long-term anoxic phase (Section 5.2.3),
- updated predictions of the time dependence of E_{CORR} and of the corrosion rate of the canister and of the evolution of the repository environment based on the Copper Corrosion Model (CCM) (Section 5.2.4.2),
- a new section on grain boundary and weld corrosion (Section 5.2.5),
- a new section describing the results of *in situ* experiments (Section 5.2.6),
- a discussion of the galvanic corrosion of Cu coupled to cast iron and of the effects of surface defects (Section 5.2.7),
- a new section describing the current thinking that localised corrosion will take the form of surface roughening or uneven general corrosion, rather than discrete pitting attack (Section 5.3.1), and
- a discussion of the effects of an alkaline plume on the localised corrosion of copper canisters (Section 5.3.2).

5.1 Introduction

Following saturation of the repository, the environment surrounding the canister will continue to evolve. As a consequence, the corrosion behaviour of the canister will also change with time. Eventually, however, the environment and the corrosion behaviour will attain a steady state. In general, the evolution in conditions will lead to less aggressive forms of corrosion and the corrosion behaviour of the canister will evolve from an initial period of relatively fast general corrosion accompanied by possible localised corrosion, to a long-term condition of a low rate of general corrosion with no, or little, localised attack.

The evolution of geochemical conditions inside the repository has been discussed in detail in Section 2. For the purposes of this section, the following conditions are assumed. The compacted bentonite is assumed to be saturated with groundwater, so that the mass transport of species to and from the canister surface is by diffusion through water-filled pores and the more-rapid transport of species such as O_2 through vapour-filled pores need not be considered (King and Kolář 1997a). In addition, it is assumed that the bentonite adjacent to the canister surface is always saturated, so that the supply of H_2O does not limit the extent of corrosion. As groundwater saturates the buffer, the pore-water Cl^- concentration will gradually increase. Initially, trapped atmospheric O_2 will create oxidising conditions, but as this O_2 is consumed by (i) corrosion of the canister, (ii) reaction with oxidisable mineral impurities and sulphide in the clay, and (iii) microbial activity, the conditions will become anoxic and subsequently remain so indefinitely. The canister surface temperature will be raised by the decay heat from the spent fuel, which will result in a temperature gradient away from the canister. The canister, and repository, will slowly cool over a period of several thousand years (see Section 2). Thus, during the period considered here, the environmental conditions will evolve from initially warm and oxic, to eventually cool and anoxic.

At the time that the repository saturates, the canister surface will be covered by corrosion products formed during the unsaturated phase (Section 4). It is assumed here that, upon saturation, the canister surface will be covered by a duplex corrosion product layer comprising an inner layer of Cu_2O

and an outer layer of basic Cu(II) salts, most likely either malachite ($Cu_2CO_3(OH)_2$) or atacamite ($CuCl_2{\cdot}3Cu(OH)_2$), depending upon the relative concentrations of CO_3^{2-} and Cl^- in the pore water.

Given this evolution of environmental conditions, the following statements can be made regarding the expected general and localised corrosion behaviour of the canister. Initially, general corrosion will be supported by the reduction of the atmospheric O_2 trapped in the bentonite. Redox conditions will be relatively oxidising and the corrosion potential (E_{CORR}) of the canister surface will be relatively positive. Localised corrosion is possible during this period, in the form of under-deposit corrosion that involves the non-permanent separation of anodic and cathodic processes, leading to a general roughening of the surface (Section 5.3). As the initially trapped O_2 is consumed, the rate of corrosion will become limited by the diffusion of O_2 (or of Cu(II) formed by the homogeneous oxidation of Cu(I) by O_2) to the canister surface. Eventually, conditions will become anoxic and corrosion will be supported by the evolution of H_2 in the presence of sulphide in the clay and groundwater. The rate of corrosion will be limited by the rate of supply of sulphide to the canister surface, and will fall to very low levels indefinitely. Only general corrosion is expected under anoxic conditions.

The evidence for the evolution in the corrosion behaviour described above is discussed in detail below. The available experimental and theoretical evidence is discussed from both a kinetic and thermodynamic viewpoint.

5.2 General corrosion

5.2.1 Kinetic studies of the effects of oxygen and chloride

5.2.1.1 Influence of oxygen

Various aspects of the effect of O_2 on the corrosion of Cu will be considered here. Thermodynamically, the presence of O_2 affects the redox potential in the repository, from which the stable dissolved and solid Cu species can be predicted (as a function of pH). Kinetically, a significant number of studies have been conducted on (i) the mechanism of O_2 reduction on Cu, (ii) the effect of O_2 on the corrosion potential (E_{CORR}) and the corrosion rate (or corrosion current density i_{CORR}), (iii) the homogeneous oxidation of Cu(I) to Cu(II), and (iv) the corrosion behaviour of Cu in compacted clay-based materials.

Initially, the redox conditions in the saturated repository are expected to be determined by the presence of trapped atmospheric O_2 in the pores of the buffer material. Theoretically, even trace amounts of O_2 result in oxidising redox potentials. For example, for a dissolved [O_2] of 8 ppb (i.e. 0.1% of the value for aerated H_2O at room temperature), the redox potential predicted for the couple

$$O_2 + 2H_2O + 4e^- = 4OH^- \qquad 5\text{-}1$$

is +0.76 V_{SHE} (+0.52 V_{SCE}) at pH 7 at 25°C. Examination of the E_H-pH diagram for Cu in 1 mol·dm^{-3} Cl^- solution (Figure 5-1) shows that the thermodynamically stable dissolved species is $CuCl^+$ and the stable solid species is either CuO or $CuCl_2{\cdot}3Cu(OH)_2$, depending upon the activity of Cl^-. As the trapped O_2 is consumed, redox conditions will become more reducing. At some stage in the evolution of repository conditions, some process other than reaction 5-1 will control the redox conditions. Ultimately, the redox potential could lie close to the H_2/H_2O equilibrium line (–0.41 V_{SHE} (–0.65 V_{SCE}) at pH 7 in the presence of 1 atm H_2), especially in the presence of sulphide. During this evolution in E_H, first Cu_2O and then Cu will become the thermodynamically stable solids and $CuCl_2^-$ (and higher complexes) will become the predominant dissolved species.

From a kinetic viewpoint, E_{CORR} and not E_H determines the corrosion behaviour. The E_H value represents the maximum value of E_{CORR}, but partly because reaction 5-1 is highly irreversible (and, therefore, not at equilibrium), E_{CORR} is invariably significantly more negative than the E_H in O_2-containing solutions. Figure 5-2 shows the predicted range of E_{CORR} values for Cu in compacted clay for dissolved O_2 concentrations between 8 ppm (aerated water) and 8 ppb and for Cl^- concentrations between 0.001 mol·dm^{-3} and 1 mol·dm^{-3}. This figure was constructed using a steady-state E_{CORR} model for the corrosion of Cu in O_2-containing Cl^- solutions (King et al. 1995a), under mass-transport conditions similar to those for a Cu canister surrounded by compacted clay (1-cm-thick clay layer, O_2 and $CuCl_2^-$ diffusion coefficients a factor of 100 lower than in solution).

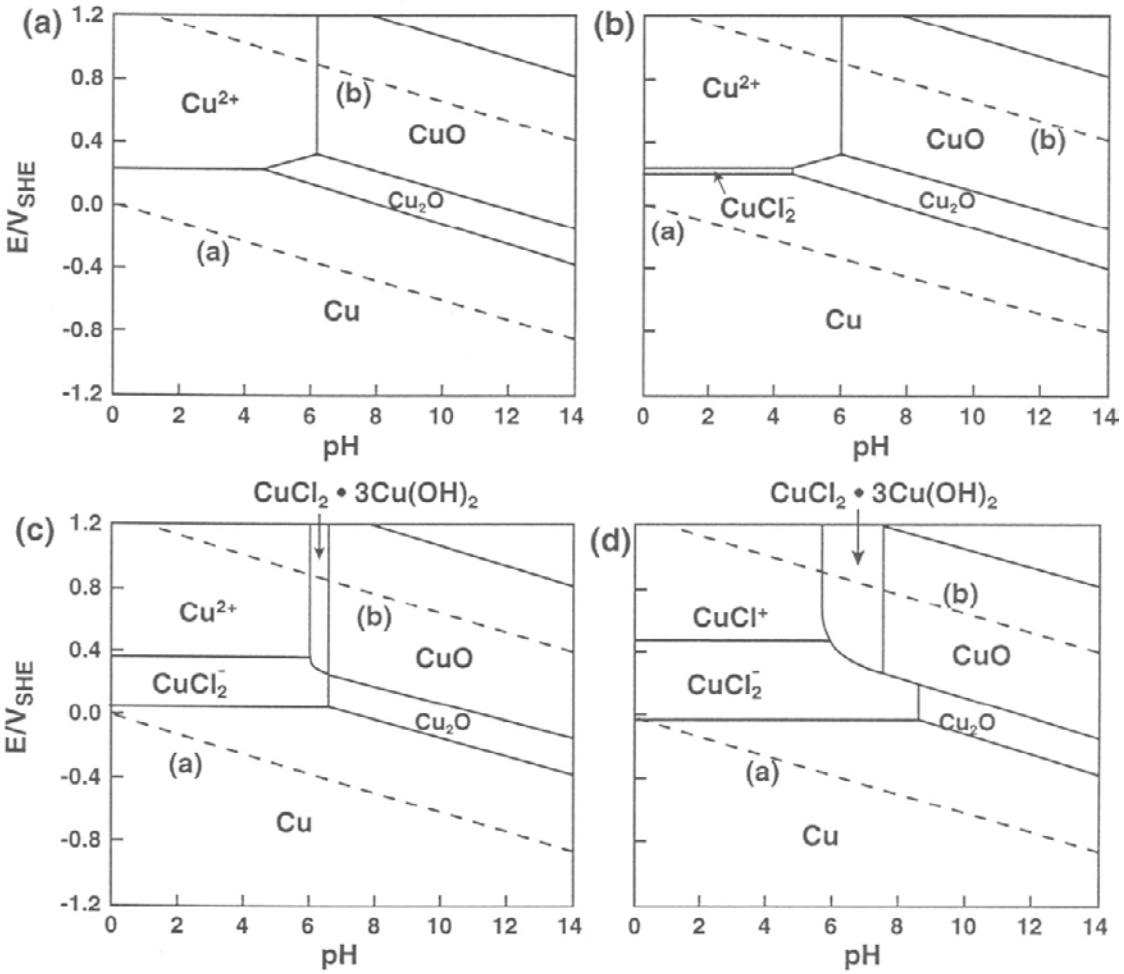

Figure 5-1. *Potential/pH (Pourbaix) diagrams for the system Cu/Cl^-/H_2O at 25°C for various chloride concentrations. (a) 10^{-3} mol·dm^{-3}, (b) 10^{-2} mol·dm^{-3}, (c) 0.1 mol·dm^{-3}, (d) 1.0 mol·dm^{-3}. Figures constructed for a total dissolved Cu activity of 10^{-6} mol·dm^{-3}.*

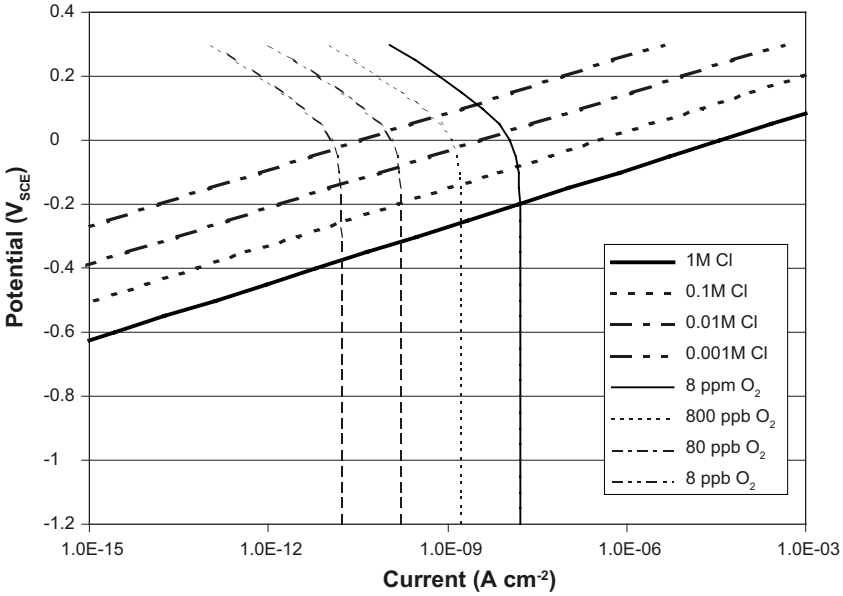

Figure 5-2. *Evans diagram showing the dependence of the corrosion potential of copper on dissolved oxygen and chloride ion concentrations in the presence of compacted clay. Based on the steady-state model of King et al. (1995a) with a clay-layer thickness of 1 cm and O_2 and $CuCl_2^-$ diffusion coefficients a factor of 100 smaller than in bulk solution.*

Thus, in comparison to the E_H value of +0.52 V_{SCE} in solution containing 8 ppb O_2, the predicted E_{CORR} varies between –0.027 V_{SCE} and –0.376 V_{SCE}, depending upon the Cl^- concentration (see Section 5.2.1.2).

The mechanism of the reduction of O_2 on Cu has been studied in detail under well-defined mass-transport conditions (King et al. 1995b, c, Vazquez et al. 1994a, b). The reaction is highly irreversible, and occurs at measurable rates at potentials more negative than approximately –0.3 V_{SCE}. The predominant reaction pathway involves the reduction of O_2 to OH^- ions via four sequential 1-electron transfer steps, according to the overall reaction

$$O_2 + 2H_2O + 4e^- \rightarrow 4OH^- \qquad 5\text{-}2$$

where the arrow indicates the irreversibility of the reaction and distinguishes reaction 5-2 from the equilibrium reaction 5-1. The reaction is catalysed by different Cu surface states. King et al. (1995b, c) suggest catalysis by a Cu(0)/Cu(I) redox couple, whereas Vazquez et al. (1994a, b) propose a sequence of chemical and electrochemical processes involving Cu_2O and CuO surface species.

In general, however, the two groups of investigators are in agreement on the overall mechanism for the reduction of O_2 on Cu. In addition to the overall 4-electron reduction process described above, the reaction is characterised by:

1. slower rates of O_2 reduction on oxide-covered surfaces than on film-free Cu,
2. minimal amounts of H_2O_2 produced as a stable intermediate species,
3. transport-limited currents given by the 4-electron reaction 5-2,
4. first-order kinetics with respect to the concentration of O_2,
5. Tafel slopes more negative than –120 mV in neutral and slightly alkaline solutions.

The last observation is explained by the dependence of the number of surface catalytic sites on the potential. The observed Tafel slope is a consequence of the combined effects of potential on the rate of O_2 reduction and on the number of catalytic surface sites (King et al. 1995c). In neutral solutions, the reduction of O_2 leads to an increase in the interfacial pH due to the formation of OH^- ions. Interfacial pH values as high as pH 10-11 are observed under cathodic polarisation in oxygenated solution. In general, the increase in the interfacial pH depends on the relative rates of O_2 reduction and of the diffusion of OH^- away from the Cu surface. The number of catalytic surface sites for O_2 reduction increases with increasing pH (King et al. 1995c).

The nature of the surface film on the canister surface will affect the rate of O_2 reduction during the saturated phase. The outer layer of the duplex film comprises electrically insulating basic Cu(II) salts. If a continuous layer of these species is formed, the rate of interfacial O_2 reduction will be reduced significantly (Kato et al. 1980a). Generally, however, the outer layer will be porous and non-continuous, so that O_2 reduction can proceed on the inner Cu_2O layer. The rate of the interfacial reaction will depend on the electronic properties of the defected, semi-conducting Cu_2O layer. Although the rate of the interfacial reaction will be slower than on a “bare” Cu surface, the overall rate of O_2 reduction on the canister surface is likely to be controlled by the rate of supply of O_2, as discussed below, rather than by the rate of the surface reaction. A possible consequence of the presence of electrically insulating basic Cu(II) salts is the spatial separation of anodic and cathodic surface reactions, possibly leading to localised corrosion (see Section 5.3.1).

Mechanistic studies of O_2 reduction on Cu are invariably performed in bulk solution involving rapid rates of mass transport to and from the surface. The presence of compacted bentonite will increase the likelihood that the rate of O_2 reduction on the canister surface will be determined by its rate of supply. From Figure 5-2, the O_2 reduction reaction is predicted to be limited by the rate of (steady-state) diffusion across the 1-cm clay layer at potentials more negative than approximately 0 to –0.1 V_{SCE}. Thus, in 1 mol·dm^{-3} Cl^-, the O_2 reduction reaction is transport limited at E_{CORR} at all [O_2]. In 0.001 mol·dm^{-3} Cl^- solution, the O_2 reduction reaction becomes transport limited under freely corroding conditions only at low [O_2] (< ~8 ppb).

Figure 5-2 also shows the effect of O_2 concentration on E_{CORR} and i_{CORR}. As would be expected, both E_{CORR} and i_{CORR} decrease with decreasing [O_2] (Figure 5-3). The dependence of E_{CORR} and i_{CORR} on log [O_2] in 1 mol·dm^{-3} Cl^- is consistent with transport control of both the anodic (Cu dissolution)

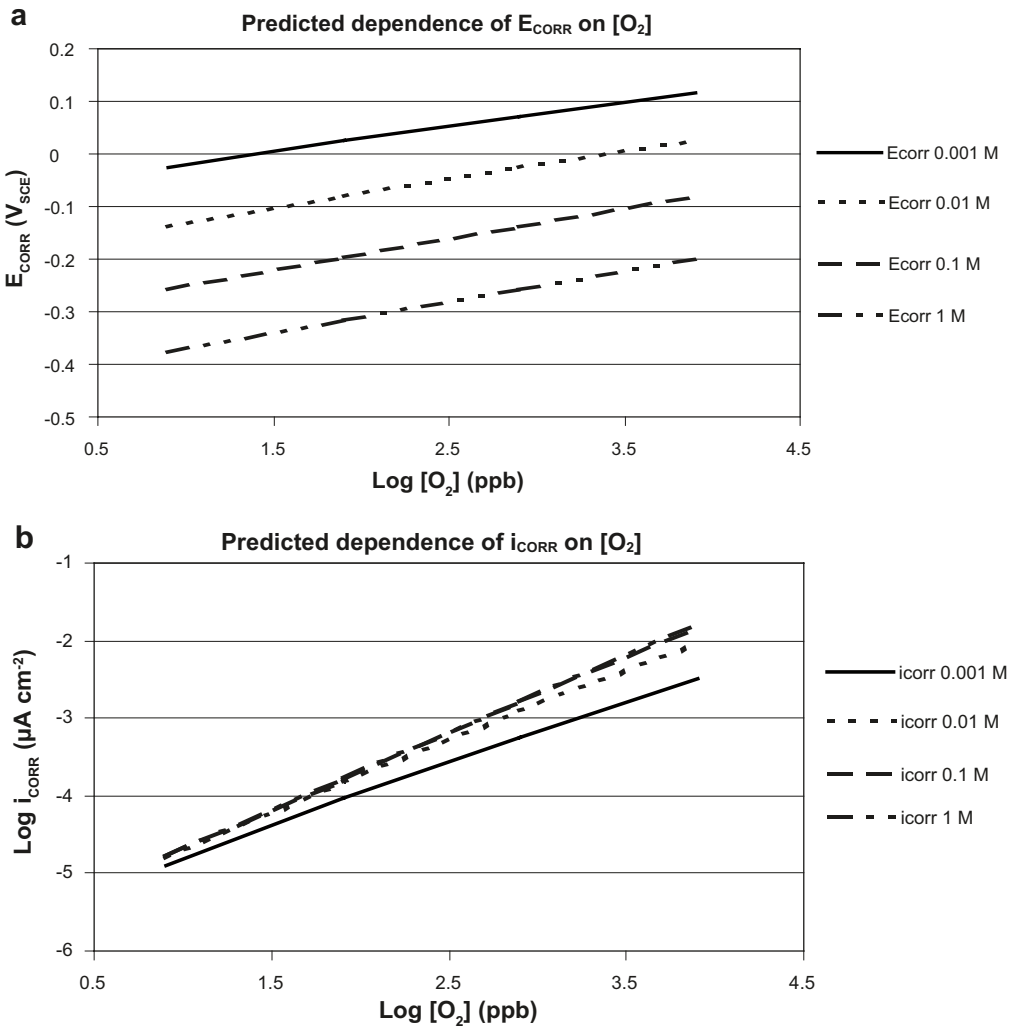

Figure 5-3. *Predicted dependencies of the corrosion potential (E_{CORR}) (a) and corrosion current density (i_{CORR}) (b) on oxygen concentration based on the data in Figure 5-2. Data shown for various [Cl^-].*

and cathodic (O_2 reduction) reactions. Thus, E_{CORR} decreases by 2.3RT/F V for each factor of ten decrease in $[O_2]$ (i.e. by 59 mV/decade) (Power and Ritchie 1981) and the rate of corrosion is first order with respect to $[O_2]$ (i.e. $d\log i_{CORR}/d\log[O_2] = 1$). The dependence of i_{CORR} on $[O_2]$ does not necessarily indicate that the rate of corrosion is O_2-transport limited, however, since the rate of the anodic transport step (the diffusion of $CuCl_2^-$ away from the Cu surface) also decreases with $[O_2]$ due to the decrease of the interfacial $[CuCl_2^-]$ with decreasing E_{CORR}. The extent of transport control of both reactions diminishes with decreasing $[Cl^-]$. In 0.001 mol·dm^{-3} Cl^-, for example, E_{CORR} decreases by only 47 mV per decade decrease in $[O_2]$ (Figure 5-3(a)) and $d\log i_{CORR}/d\log[O_2] = 0.80$ (Figure 5-3(b)), both indications that the O_2 reduction reaction is partially controlled by the rate of the interfacial reaction (reaction 5-2).

In general, the rate of mass transport to and from the canister has a significant effect on E_{CORR}, i_{CORR}, and the nature of the rate-controlling processes for the anodic, cathodic, and overall corrosion reactions. For the equivalent $[O_2]$ and $[Cl^-]$, the steady-state E_{CORR} value in bulk solution (assumed diffusion layer thickness 0.01 cm) is 77 mV more negative than in the presence of clay and the corrosion rate is a factor of ~500 times higher (King et al. 1995a). Unlike the situation in compacted clay, the O_2 reduction reaction is not transport limited at E_{CORR} in bulk solution, but is instead under joint kinetic-transport control. Factors that lead to higher rates of mass transport to and from the canister, therefore, will tend to result in more negative E_{CORR} but higher corrosion rates. Such factors could include lower compaction density and a smaller thickness of bentonite. (Although not considered in this section, partial desiccation of the bentonite would have a complex effect on E_{CORR} and i_{CORR}, since the rate of O_2 diffusion to the canister would increase greatly due to vapour-phase diffusion through partially air-filled pores, but the rate of diffusion of $CuCl_2^-$ would be slowed for the same reason).

An effect of O_2 not included in the mixed-potential model of King et al. (1995a) described above, is the homogeneous oxidation of Cu(I) to Cu(II). As described in the next section, Cu dissolves as Cu(I) at E_{CORR} in Cl^- solutions, yet precipitated Cu(II) salts are invariably observed on the surface of corrosion coupons exposed to compacted bentonite (or bentonite-sand mixtures) (King et al. 1992, 1997a). Cupric species are formed from the homogeneous irreversible oxidation of Cu(I) by O_2, by the reaction (Sharma and Millero 1988)

$$4Cu(I) + O_2 + 2H_2O \rightarrow 4Cu(II) + 4OH^- \qquad 5\text{-}3$$

The overall rate of Cu(I) oxidation is second order, being first order with respect to both [Cu(I)] and [O_2] (Sharma and Millero 1988). The rate constant is a function of pH, temperature and solution composition. The precise speciation of the Cu(I) and Cu(II) species will depend on the composition of the pore water. A significant fraction of the Cu(II) formed by reaction 5–3 will adsorb on the bentonite clay buffer. Other Cu(II) species will precipitate on the canister surface, resulting in a thickening of the outer layer of the duplex Cu_2O/basic Cu(II) salt film formed on the canister surface during the unsaturated phase.

Cupric species can also be reduced on the canister surface, by the reaction

$$Cu(II) + 2Cl^- \rightarrow CuCl_2^- + e^- \qquad 5\text{-}4$$

Chloride stabilises Cu(I) to such a degree that the reaction is irreversible, and the disproportionation of Cu(I) (i.e. 2Cu(I) = Cu(II) + Cu) is not thermodynamically favoured (Peters and Cruser 1965). Like the O_2 reduction reaction, the interfacial reduction of Cu(II) will proceed on the Cu_2O-covered canister surface, but will not occur on the fraction of the surface covered by the insulating basic Cu(II) salts.

A number of workers have studied the corrosion behaviour of Cu in O_2-containing compacted clay environments. Aaltonen and Varis (1993) exposed OFHC and a Cu-0.1%Ag alloy to compacted bentonite saturated with synthetic Finnish groundwaters for periods of up to 2 years. Redox conditions within the open cells were first found to become more reducing as O_2 was rapidly consumed by the corrosion reaction, but then became more oxidising later in the experiment, possibly because of the ingress of atmospheric O_2. The Cu coupons were covered by Cu_2O, CuO and $CuCO_3$ corrosion products (the latter presumably as $CuCO_3 \cdot Cu(OH)_2$), the carbonate salt being favoured over the corresponding basic Cu(II) chloride salt because of the high bicarbonate content of the groundwaters (~600 ppm). Copper concentration profiles were observed in the bentonite at short times, with the Cu diffusing evenly throughout the clay after 2 years. No difference was observed in the corrosion behaviour of the two alloys, although no corrosion rates were given. No evidence for localised corrosion was observed.

Karnland et al. (2000) have reported the results of the examination of coupons from long-term corrosion tests in compacted bentonite at the Äspö Hard Rock Laboratory. The estimated mean corrosion rate after 1-year of exposure was 3 $\mu m \cdot a^{-1}$. As observed by Aaltonen and Varis (1993), Cu diffused into the surrounding bentonite. No indications of pitting attack were observed.

An extensive series of corrosion experiments has been performed as a function of [O_2] and [Cl^-] in compacted bentonite-sand buffer material (to simulate conditions in a Canadian repository) (King et al. 1992, 1997a, Litke et al. 1992). These tests were performed under well-defined 1-D mass-transport conditions, so that the effect of the diffusion of reactants and products to and from the Cu surface could be determined. The rate of consumption of O_2 in the head-space above the experiments was found to decrease with a $t^{1/2}$ dependence, suggesting that the reduction of O_2 was transport limited. However, the corrosion rate was not proportional to the initial [O_2], suggesting the overall rate of corrosion was not cathodically limited. Instead, under the relatively oxidising conditions employed in these tests, the corrosion rate was found to be determined by the diffusion of Cu away from the coupon surface.

As discussed in more detail in the next section, the corrosion behaviour was determined by the speciation of dissolved Cu. Adsorption of Cu(II) by the bentonite clay lowered the interfacial [Cu(II)] concentration, driving further dissolution of the coupon. As a result, higher corrosion rates were observed under conditions that favoured the formation of Cu(II), such as higher [O_2]. In addition,

higher total interfacial [Cu] (i.e. the sum of adsorbed, precipitated and pore-water Cu) and steeper Cu concentration gradients were observed when Cu(II) was formed. Figure 5-4 shows the measured total [Cu] profiles in the compacted bentonite following 30-day corrosion experiments at 95°C with a synthetic groundwater containing ~1 mol·dm^{-3} Cl^- for different initial [O_2]. High interfacial [Cu] and steep concentration gradients were observed in aerated buffer, whereas much lower interfacial [Cu] and shallower Cu profiles were observed with 0.25 vol.% O_2. At the lower [O_2], a greater fraction of the dissolved Cu was in the form of weakly adsorbed $CuCl_2^-$, resulting in lower total [Cu] and a smaller driving force for dissolution.

The dependence of the corrosion rate on [O_2] was lower than that predicted using the steady-state model of King et al. (1995a) described above (Figure 5-3(b)). On average, the corrosion rate was proportional to $[O_2]^{0.47}$, as opposed to the linear dependence predicted by the steady-state electrochemical model. There are two reasons for the difference between the predicted and observed reaction order. First, it is likely that the rate of O_2 diffusion was higher in the compacted bentonite than assumed in the steady-state prediction both because diffusion would have occurred under transient as opposed to steady-state conditions and, possibly, because the bentonite was not totally saturated. Second, a fraction of the O_2 was consumed by the homogeneous oxidation of Cu(I) (reaction 5-3), a reaction not included in the steady-state model. Oxygen consumption by reaction 5-3 was not significant in the room-temperature tests on which the model was based, since the rate of oxidation is 20 times slower at 25°C compared with the experimental temperature of 95°C used in the corrosion tests.

Copper concentration profiles similar to those found experimentally have been observed in seabed clay sediments surrounding a buried bronze cannon (Hallberg et al. 1988, King 1995). Figure 5-5 shows a comparison between the clay sediment [Cu] profiles and a profile measured experimentally in compacted bentonite-sand buffer material (King 1995). In both cases, the interfacial [Cu] is of the order of 10 mg·g^{-1} and the Cu has diffused a maximum distance of ~5 cm. The exposure temperature (7±5°C for the bronze cannon and 100°C for the experimental profile) and exposure period (310 years versus 180 days) were quite different, but the activation energy for the diffusion coefficient derived from the data in Figure 5-5 is very similar to that determined experimentally (~50 kJ·mol^{-1} (King 1995)).

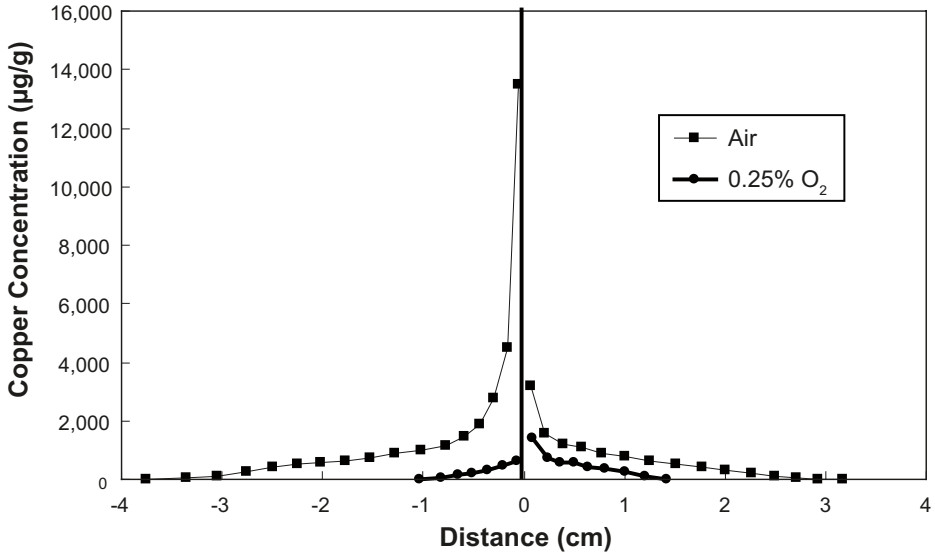

Figure 5-4. *Measured total copper concentration profiles in groundwater-saturated compacted bentonite in contact with a copper coupon following 30 days exposure at 95°c for two initial oxygen concentrations (King et al. 1997a). The Cu coupon was placed in the centre of the clay (dry density 1.2 Mg·m^{-3}). Groundwater Cl^- concentration ~1 mol·dm^{-3}. The clay contained 0.5 wt.% Fe filings added as an O_2 scavenger.*

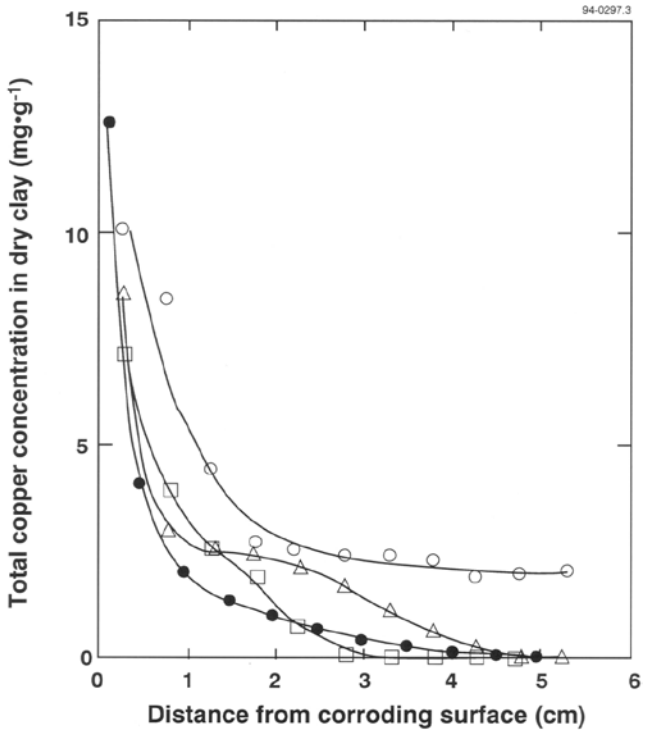

Figure 5-5. *Comparison of copper concentration profiles in sea sediments adjacent to a submerged bronze cannon and a profile observed experimentally in compacted bentonite-sand buffer material in contact with a copper coupon. The sea-sediment profiles (O□Δ) developed over a period of 310 years at a mean ambient temperature of 7±5°C compared with an exposure period of 180 d at 100°C for the buffer material profile (•) (King 1995).*

5.2.1.2 Influence of chloride

A great deal of evidence is available concerning the effect of Cl^- on the corrosion of Cu. The two areas considered in this section are: (i) the electrochemistry of Cu in Cl^- environments, and (ii) the effect of groundwater salinity on the corrosion of Cu in compacted bentonite. The thermodynamic aspects of Cu corrosion in Cl^- solutions are discussed in Section 5.2.2.

Figure 5-1 shows the effect of Cl^- concentration on the relative thermodynamic stability of various solid and dissolved species. Chloride ions stabilise dissolved Cu(I) in the form of complex anions, such as $CuCl_2^-$ and $CuCl_3^{2-}$ (see Section 3). At sufficiently low pH, Cu corrosion is accompanied by the evolution of H_2 in Cl^- solutions, with the critical pH for H^+/H_2O reduction at E_{CORR} increasing with increasing $[Cl^-]$ and temperature. With increasing $[Cl^-]$, the stability of $CuCl_2 \cdot 3Cu(OH)_2$ with respect to Cu_2O and CuO increases, as indicated by the growth in the size of the stability field of the former at the expense of those of the latter species in Figure 5-1.

The electrochemical behaviour of Cu in Cl^- solutions has been extensively studied, in large part because of the widespread use of Cu alloys in sea water and other saline solutions (Kear et al. 2004). The mechanism for the interfacial dissolution reaction has been determined from studies under controlled mass-transport conditions. The most appropriate description of the various chemical and electrochemical steps in the anodic dissolution of Cu is (King et al. 1995a)

$$Cu + Cl^- \leftrightarrow CuCl_{ADS} + e^- \qquad 5\text{-}5(a)$$

$$CuCl_{ADS} + Cl^- \leftrightarrow CuCl_2^- \text{ (surface)} \qquad 5\text{-}5(b)$$

$$CuCl_2^- \text{ (surface)} \xrightarrow{\text{diffusion}} CuCl_2^- \text{ (bulk)} \qquad \text{rds} \qquad 5\text{-}5(c)$$

The adsorbed $CuCl_{ADS}$ species is formed at a potential more negative than that predicted on the basis of the thermodynamic properties of bulk CuCl. Despite earlier assumptions to the contrary, reaction 5-5(a) is not at equilibrium. The rate-determining step (rds) in the overall dissolution reaction is the mass transport of dissolved $CuCl_2^-$ from the surface to the bulk environment (reaction 5-5(c)). Equations 5-5 describe the mechanism of the dissolution of Cu in Cl^- solutions in the so-called "apparent Tafel region," which extends from approximately –0.2 V_{SCE} to a potential of ~0 V_{SCE} depending on the $[Cl^-]$ (Lee and Nobe 1986). Within the apparent Tafel region, this mechanism is valid over a wide range of $[Cl^-]$, ranging from ~0.01 mol·dm^{-3} (Kiss et al. 1971) to > 5 mol·dm^{-3} (Brossard 1983). (At $[Cl^-]$ of 1 mol·dm^{-3} and higher, the higher Cl^- complexes, such as $CuCl_3^{2-}$, become predominant and the stoichiometry in reaction 5-5 changes accordingly). King et al. (1995a) used this reaction mechanism to account for the corrosion behaviour of Cu in O_2-containing Cl^- solutions over a wide range of mass-transport conditions, $[Cl^-]$ and $[O_2]$.

The rate of dissolution of Cu in Cl^- solutions is a function of both the rate of mass transport and of potential. The dependence on the rate of mass transport is a simple consequence of the mass-transport step (reaction 5-5(c)) being rate-determining. As shown in Figure 5-2, the rate of dissolution also increases with increasing potential, as a result of the increase in the interfacial $[CuCl_2^-]$, which increases the driving force for the mass transport of dissolved Cu away from the corroding surface.

The steady-state model of King et al. (1995a) can be used to predict the dependence of E_{CORR} and i_{CORR} on $[Cl^-]$ in compacted clay. Figure 5-6 shows the dependencies on $[Cl^-]$ derived from the Evans diagram in Figure 5-2. The dependence of E_{CORR} on $[Cl^-]$ varies from –105 mV/dec in environments containing 8 ppm O_2 to –116 mV/dec in the presence of 8 ppb O_2 (Figure 5-6(a)). For complete transport control of both anodic and cathodic reactions, the predicted dependence would be –118 mV/dec at 25°C, i.e. $dE_{CORR}/d\log[Cl^-] = 2(2.3RT/F)$, where the factor of 2 corresponds to the complexation of Cu(I) by two Cl^- ions. (Here, Cl^- concentrations have been used instead of the more-correct Cl^- activities, Section 3). The change in $[Cl^-]$ dependence of E_{CORR} with decreasing $[O_2]$ reflects the increasing transport-limitation of the O_2 reduction reaction. The corrosion current density is only weakly dependent on $[Cl^-]$, varying from $[Cl^-]^{0.033}$ for 8 ppb O_2 to $[Cl^-]^{0.23}$ in 8 ppm O_2 (Figure 5-6(b)). The relative independence of i_{CORR} on $[Cl^-]$ suggests that the overall corrosion rate is largely mass-transport limited by the supply of O_2 to the Cu surface. Mass-transport limitation by the diffusion of $CuCl_2^-$ *away* from, or of Cl^- *to*, the Cu surface would result in i_{CORR} being proportional to $[Cl^-]^2$.

Chloride ions play an important role in the formation and properties of surface films on Cu. Cuprous oxide may form via a number of processes in Cl^--containing environments. The initial stages of film formation involve a competition between Cl^- and OH^- for surface sites, followed by the loss of H_2O

$$CuCl_{ADS} + OH^- \leftrightarrow Cu(OH)_{ADS} + Cl^- \qquad 5\text{-}6(a)$$

$$2Cu(OH)_{ADS} \rightarrow Cu_2O + H_2O \qquad 5\text{-}6(b)$$

The extent of Cu_2O formation depends on the relative $[Cl^-]$ and $[OH^-]$ (i.e. pH) and the rate of mass transport, with higher $[Cl^-]$ and rates of mass transport favouring the formation of $CuCl_2^-$, and higher pH favouring Cu_2O formation. Although these processes relate only to the formation of the first few monolayers of Cu_2O, they are nevertheless important in determining the properties of the passivating interfacial Cu_2O layer. The incorporation of CuCl "islands" in the surface Cu_2O film creates defects which are believed to be initiation points for pitting (see Section 5.3).

Copper continues to dissolve through the thin surface layer, especially via defects and cracks in the film. Hydrolysis of dissolved $CuCl_2^-$, or of CuCl produced by the precipitation of dissolved Cu(I), results in further Cu_2O growth

$$2\,CuCl_2^- + H_2O \rightarrow Cu_2O + 2H^+ + 4Cl^- \qquad 5\text{-}7(a)$$

or

$$2CuCl + H_2O \rightarrow Cu_2O + 2H^+ + 2Cl^- \qquad 5\text{-}7(b)$$

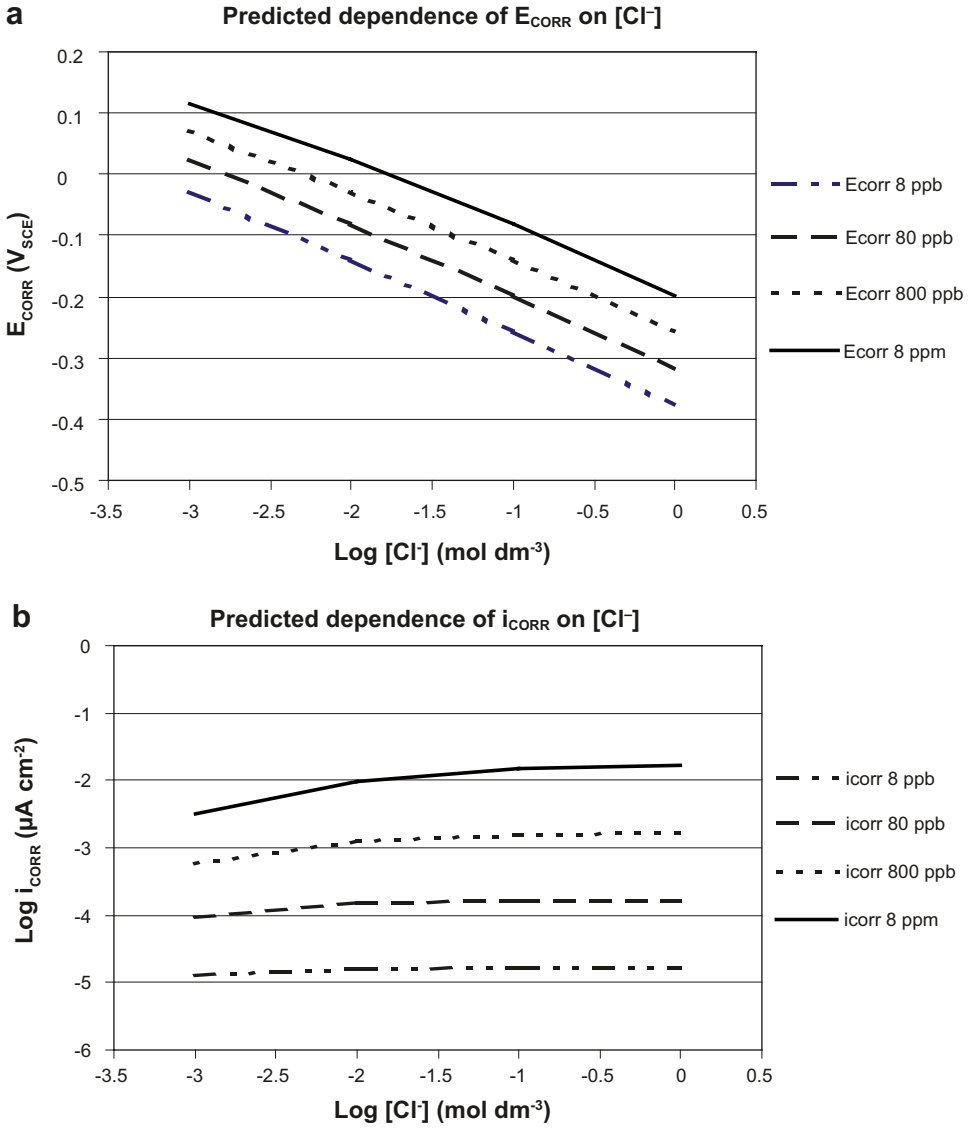

Figure 5-6. *Predicted dependencies of the corrosion potential (E_{CORR}) and corrosion current density (i_{CORR}) on chloride concentration based on the data in Figure 5-2. Data shown for various [O_2].*

In the presence of O_2 in Cl^--containing environments, an outer layer of precipitated $CuCl_2{\cdot}3Cu(OH)_2$ forms on the Cu_2O film. This layer may form by the precipitation of dissolved Cu(II), formed by the homogeneous oxidation of Cu(I) by O_2 (reaction 5-3), once local super-saturation of the environment by Cu(II) is achieved. Evidence for this mechanism comes from the observation of discrete $CuCl_2{\cdot}3Cu(OH)_2$ crystals aligned along linear defects (formed above polishing lines on the Cu surface) on an underlying Cu_2O layer (Figure 5-7(a)). It is possible that Cu dissolved as $CuCl_2^-$ through the defected oxide, with local super-saturation by Cu(II) occurring upon oxidation of the Cu(I) species by O_2. Alternatively, other authors suggest that the $CuCl_2{\cdot}3Cu(OH)_2$ layer forms through the oxidation of the underlying Cu_2O film (Bianchi et al. 1978, Mansfeld et al. 1994), via the overall reaction

$$2Cu_2O + O_2 + 2Cl^- + 4H_2O \rightarrow CuCl_2{\cdot}3Cu(OH)_2 + 2OH^- \qquad 5\text{-}8$$

Reaction 5-8 infers that the outer $CuCl_2{\cdot}3Cu(OH)_2$ layer grows at the expense of the inner Cu_2O film.

Chloride ions will also affect the properties and stability of the precipitated films. The substitution of monovalent Cl^- ions for divalent O^{2-} ions in the Cu_2O lattice creates defects resulting in less-protective films compared with the more-strongly passivating Cu_2O films formed in the absence of Cl^- and/or at higher pH. Depending upon the [Cl^-], Cu_2O films formed in Cl^- solutions may be more susceptible to localised breakdown and pitting attack. At sufficiently high [Cl^-], the surface layer may become so defected that it no longer protects the surface and Cu dissolves actively.

a) Secondary electron image of precipitated $CuCl_2 \cdot 3Cu(OH)_2$ crystals (2) aligned along linear defects in the underlying Cu_2O film (1). Also shown are discrete CuO crystals (3).

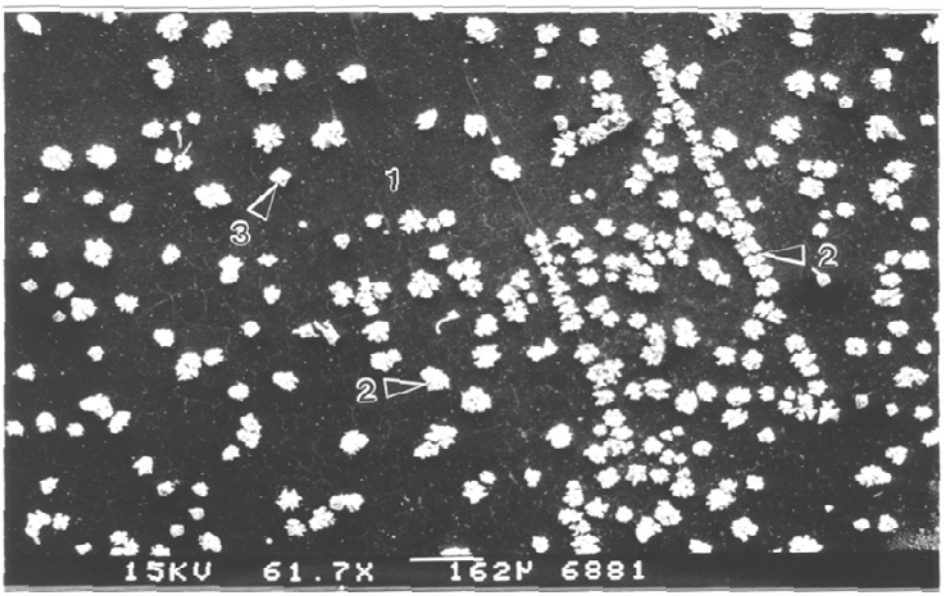

b) Photograph of the duplex corrosion product typical of that formed on copper in groundwater saturated compacted bentonite consisting of an underlying layer of Cu_2O (A) and an upper layer (B) of precipitated basic cupric salts ($CuCl_2 \cdot 3Cu(OH)_2$)

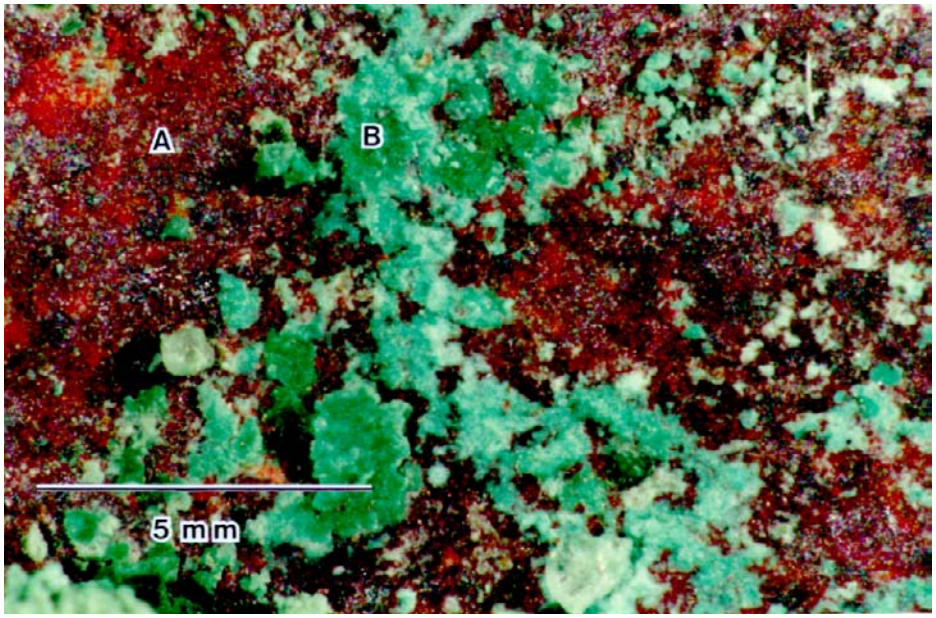

Figure 5-7. *The development of surface films on copper surfaces exposed to saline groundwater and compacted clay buffer material (Litke et al. 1992).*

In contrast to the complex semi-conducting properties of Cu_2O films, $CuCl_2 \cdot 3Cu(OH)_2$ appears to form an electrically insulating layer. In laboratory studies in compacted clay, the surface $CuCl_2 \cdot 3Cu(OH)_2$ layer is discontinuous, exposing the underlying Cu_2O film to the environment (Figure 5-7(b)). Complete coverage by $CuCl_2 \cdot 3Cu(OH)_2$ would passivate the surface (Kato et al. 1980a, b), although usually the interfacial electrochemical processes proceed on the underlying Cu_2O surface (Kato et al. 1980a, b, Schüssler and Exner 1993).

Understanding the properties of oxide films and other precipitated corrosion products is important in predicting the corrosion behaviour of copper canisters. Kvashnina et al. (2007) report results of a preliminary study of the effects of groundwater species on the Cu oxidation state and of the electronic properties of corrosion films. Film changes were measured *in situ* using x-ray absorption spectroscopy (XAS) and resonant inelastic x-ray scattering (RIXS) to monitor the speciation of corroded copper in deaerated solution. Various parameters were considered, including the effects of Cl^-, SO_4^{2-}, and CO_3^{2-}, pH, and the exposure time. Figure 5-8 shows a summary of the effects of these different parameters on the speciation of copper. Increasing time of exposure and, particularly, increasing pH were found to increase the stability of Cu(II), with the cupric state being predominant in dilute Cl^- solutions at pH > 10. Increasing time also resulted in increasing amounts of cupric species. Most interestingly, Kvashnina et al. (2007) reported that cupric species predominated in solutions with high Cl^- concentration (1.5 mol/L). This observation is inconsistent with the known stability of Cu(I)-Cl^- complexes and with the electrochemical behaviour of copper in Cl^- solutions discussed above. It is possible that the copper speciation was affected by atmospheric O_2 leaking into the cell, which then caused the homogeneous oxidation of Cu(I) to Cu(II). This explanation is consistent with the reported observation that the proportion of Cu(II) increases with increasing exposure time.

Although Cl^- may be the predominant groundwater species, the pore water will contain other anions, especially at short times prior to the influx of Cl^-. A major pore-water constituent will be sulphate ions. All the available evidence indicates that the dissolution behaviour of Cu in Cl^-/SO_4^{2-} mixtures will follow the same mechanism as in Cl^- solutions (i.e. reaction 5-5). Kiss et al. (1971) studied the dissolution behaviour of Cu in 0.5 mol·dm^{-3} H_2SO_4 containing 0.007–0.09 mol·dm^{-3} Cl^-, but explained all of their observations in terms of the $CuCl_2^-$ species. King and co-workers (King and Tang 1998, King et al. 1995d) simultaneously determined the fluxes of Cu(I) and Cu(II) produced during the dissolution of a Cu electrode in a 0.1 mol·dm^{-3} Cl^-/0.1 mol·dm^{-3} SO_4^{2-} mixture. Although the addition of SO_4^{2-} shifted the potential at which Cu(II) was produced directly at the surface by ~100 mV in the negative direction, only Cu(I) was detected in the apparent Tafel region, extending to 100–200 mV positive of E_{CORR}. Therefore, there is no evidence that Cu will dissolve directly as Cu(II) in the SO_4^{2-}-enriched pore water in compacted bentonite.

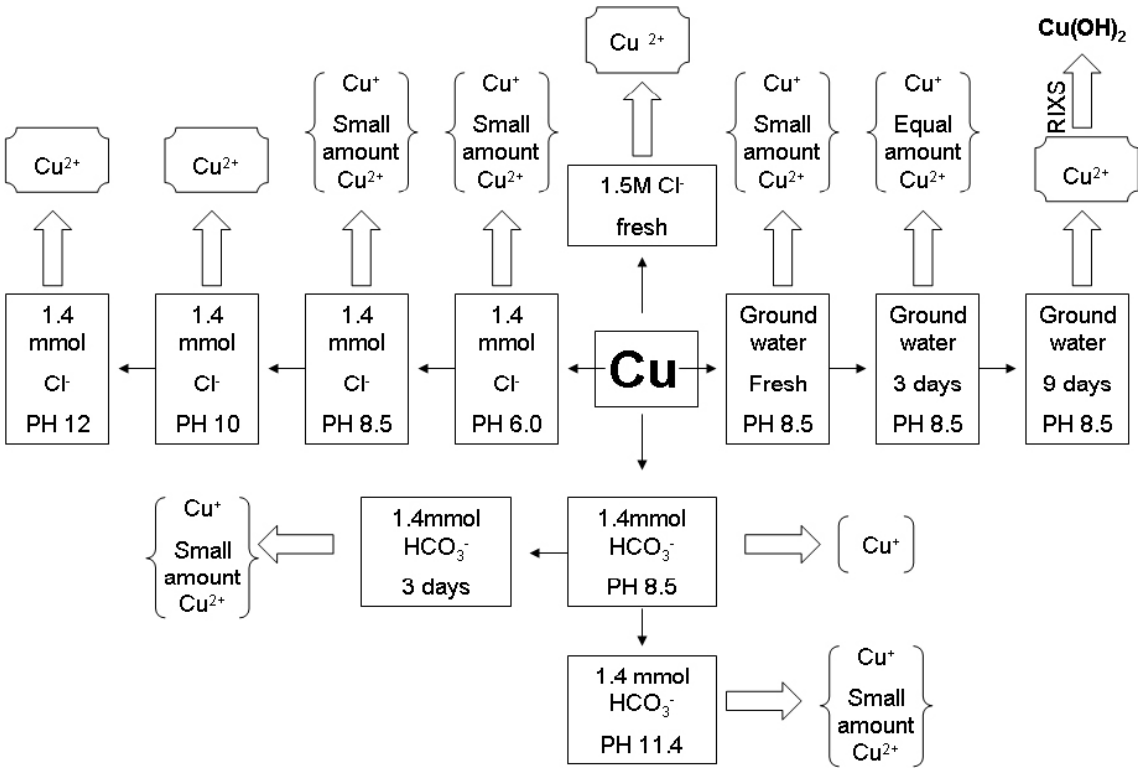

Figure 5-8. *Summary of effects of different groundwater species, pH, and exposure time on the speciation of corroded copper (Kvashnina et al. 2007).*

Another abundant anion in the pore water will be HCO_3^-/CO_3^{2-}. Carbonate does not form strong complexes with Cu(I) and Cu(II) and is not directly involved in the dissolution mechanism. The primary roles of carbonate will be in the formation of surface films and the buffering of the interfacial pH. The basic Cu(II) carbonate salt, $CuCO_3 \cdot Cu(OH)_2$, tends to be more stable than $CuCl_2 \cdot 3Cu(OH)_2$ and forms preferentially in sea water. Both Aaltonen and Varis (1993) and Karnland et al. (2000) observed $CuCO_3 \cdot Cu(OH)_2$, rather than $CuCl_2 \cdot 3Cu(OH)_2$, in laboratory and pilot scale corrosion tests under repository conditions. Another effect of carbonate is to render the surface more passive than in HCO_3^-/CO_3^{2-}-free environments. This could increase the probability of localised corrosion, as discussed in Section 5-3.

A species that may be present in the repository is ammonia, introduced either during repository construction, by microbial activity in the groundwater, or by gas-phase radiolysis of atmospheric N_2. Ammonia is important for the stress corrosion cracking of Cu. Ammonia also forms strong complexes with Cu(I) and Cu(II). Electrochemical studies in Cl^-/NH_3 solutions, however, show that dissolution as $CuCl_2^-$ predominates in 0.1 mol·dm^{-3} Cl^- at pH 7 with total ammonia additions of up to 10^{-2} mol·dm^{-3} (King et al. 1997b). Thus, despite the fact that the Cu(I)-NH_3 complexes are stronger than the equivalent Cu(I)-Cl^- complexes, the latter dominate because of the low $[NH_3]$ in neutral and slightly alkaline solutions. (The pK_a for the NH_3/NH_4^+ equilibrium is 9.3 at 25°C, so that NH_4^+ is the predominant form at pH < 9.3).

Chloride ions also have an effect on the homogeneous oxidation of Cu(I) to Cu(II) by O_2 because the rate constant for reaction 5-3 is a function of salinity (Sharma and Millero 1988). In NaCl solution, the second-order rate constant for the oxidation of Cu(I) is ~100 times larger in 0.1 mol·dm^{-3} Cl^- solution than in 1 mol·dm^{-3} Cl^-. This effect of Cl^- is a result of the stabilising effect of Cu(I)-Cl^- complex formation.

The effect of groundwater salinity on the corrosion behaviour of Cu in compacted bentonite has been reported by King et al. (1997a). Copper coupons were sandwiched between plugs of Na-bentonite compacted to a dry density of 1.2 Mg·m^{-3} and saturated with synthetic groundwaters of three different salinities and at two different $[O_2]$. The experiment was designed such that well-defined 1-D mass-transport conditions were maintained throughout. Tests were conducted at a temperature of 95°C for periods between 10 days and 6 months. The three groundwaters used were representative of those anticipated in a Canadian repository, with $[Cl^-]$ of 0.17 mol·dm^{-3}, 0.97 mol·dm^{-3}, and 2.5 mol·dm^{-3}. A reservoir of groundwater was maintained at the exit side of the compacted clay plugs. These solutions were initially saturated with either air or a 0.2 vol% O_2/N_2 mixture. At the end of the experiments, the clay plugs were sectioned into slices between 1- and 3-mm thick and the total Cu content in each slice determined. The Cu thus determined comprises Cu dissolved in the porewater, precipitated Cu and Cu adsorbed on the clay. Following visual examination of the coupons, the precipitated corrosion products were removed and the corrosion rate determined from the weight loss of the coupon.

The results of the tests suggested an effect of groundwater salinity and $[O_2]$ on the speciation of corroded Cu and a consequent effect on the corrosion behaviour. The tests were divided into those in which Cu(I) appeared to be the predominant oxidation state and those in which there was evidence for Cu(II) species. This classification was based on the visual appearance of the corrosion products (assisted by the bright green colouration of Cu(II) precipitates) and on the shape of the Cu concentration profiles in the clay. Concentration profiles characteristic of Cu(II) species tend to be short and steep with high interfacial [Cu] (King et al. 1992, Litke et al. 1992), similar to that for the aerated solution profile in Figure 5-4. The steep profiles are a consequence of the strong adsorption of Cu(II) by the bentonite clay (Ryan and King 1994). Concentration profiles characteristic of Cu(I) species, on the other hand, are shallow and extended with low interfacial [Cu]. These characteristics can be rationalised if the predominant species is $CuCl_2^-$, which is mobile and weakly adsorbed (leading to extended [Cu] profiles and low interfacial concentrations).

For the various conditions studied, Cu(II) tended to predominate the lower the groundwater salinity and the higher the $[O_2]$. Thus, for the lowest groundwater salinity ($[Cl^-]$ = 0.17 mol·dm^{-3}), the [Cu] profiles and corrosion products exhibited evidence for Cu(II) species for both $[O_2]$. In the highest salinity groundwater ($[Cl^-]$ = 2.5 mol·dm^{-3}), on the other hand, there was no evidence for Cu(II) species in either aerated or 0.2 vol.% O_2/N_2 environments. At the intermediate salinity ($[Cl^-]$ = 0.97 mol·dm^{-3}), Cu(II) predominated in aerated environments, but concentration profiles and corrosion products characteristic of Cu(I) predominated in 0.2 vol.% O_2/N_2.

The relative amounts of Cu(I) and Cu(II) in the various tests can be rationalised based on the stability of Cu(I) in the different environments. The first-order rate constant for the oxidation of Cu(I) (obtained from the product of the second-order rate constant given by Sharma and Millero (1988) and the respective dissolved [O_2]) varies by ~5 orders of magnitude over the range of experimental conditions studied. Thus, the rate of oxidation of Cu(I) in the aerated 0.17 mol·dm^{-3} Cl^- groundwater is ~80,000 times faster than in the high salinity groundwater saturated with 0.2 vol.% O_2/N_2. The respective Cu(I) half-lives are 0.15 s and 12,000 s, respectively. As a general guide, tests in which the calculated Cu(I) half life was < 100 s were characterised by Cu(II) corrosion products and steep [Cu] profiles, whereas those with half-lives > 100 s suggested the predominance of Cu(I) species. The calculated Cu(I) half-lives were estimated based on studies in bulk solution, and the actual half-lives in compacted buffer could be substantially longer because of the effect of the spatial restrictions of the pore network on the collision frequency of O_2 and Cu(I).

Of more interest than the effect of salinity on the Cu concentration profiles and corrosion products is the effect on the corrosion rate. Figure 5-9 shows the results of the three sets of conditions for which tests were performed in all three groundwaters. The results suggest that the corrosion rate *decreases* with increasing salinity. This conclusion can be rationalised on the basis of a Cu-transport rate-determining step (King et al. 1992). If the interfacial dissolution processes are fast with respect to the rate of mass transport *and* are reversible, any process that removes dissolved Cu from the corroding interface will result in a higher corrosion rate. In the case of Cu(I), the only processes removing dissolved Cu from the interface are the relatively slow diffusion through the compacted clay and the precipitation of Cu_2O. For Cu(II), however, dissolved Cu is removed from the interface by adsorption on the bentonite clay, diffusion, precipitation, and reduction to Cu(I) by reaction with Cu. The bentonite has a large capacity to adsorb Cu(II), with the slices of clay nearest the corroding coupon containing as much as 12 mg·g^{-1} Cu, equivalent to adsorption of Cu(II) on 50% of the total exchange sites on the clay. It is interesting to note that the experimental corrosion rates in Figure 5-9, especially at the lower [O_2], are similar to those observed by Karnland et al. (2000) in the long-term pilot scale corrosion tests at Äspö (~3 µm·a^{-1}).

Saario et al. (2004) considered the effect of bentonite density on the corrosion behaviour of copper. Increasing compaction density was found to result in a decrease in corrosion rate, presumably as a consequence of the smaller amount of O_2 and the slower O_2 transport to the corroding surface. Corrosion stopped, however, after ~100 hrs exposure due to the consumption of the initially trapped O_2. Both the corrosion potential and local redox potential remained relatively positive, however. The corrosion potential remained positive because of the presence of Cu(II) species, which may also affect the local redox potential along with other oxidisable species in the system.

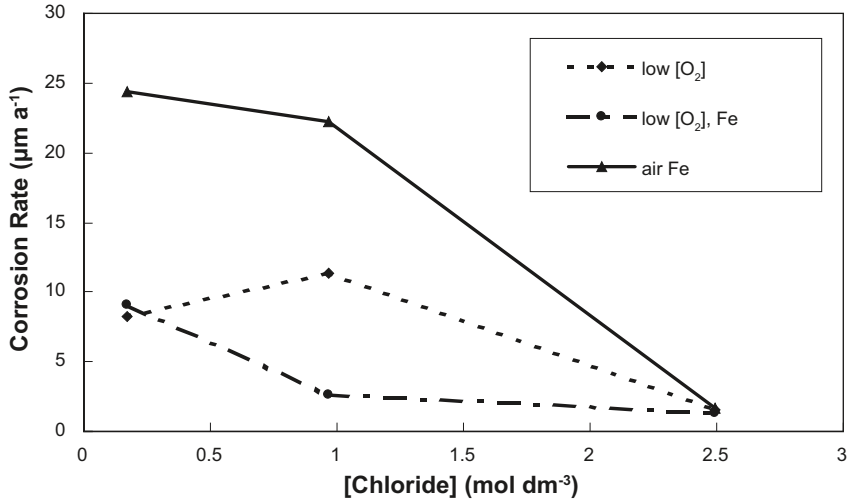

Figure 5-9. *Dependence of the corrosion rate of copper in compacted clay on the salinity of the groundwater. Tests conducted at 95°C for 90 days in groundwater-saturated bentonite clay (dry density 1.2 Mg·m^{-3}). The groundwaters were either initially aerated or equilibrated with a 0.2 vol.% O_2/N_2 (low [O_2]). In some tests, 0.5 wt.% Fe powder was added to the dry clay prior to compaction.*

Figure 5-10 shows the proposed mechanism for the corrosion of Cu in compacted bentonite saturated with saline, O_2-containing groundwaters. Copper dissolves reversibly in the form of $CuCl_2^-$ species. If this species is stable, i.e. at high [Cl^-] and/or low [O_2], $CuCl_2^-$ slowly diffuses away from the Cu surface as the rate-controlling process. In low-salinity groundwaters and/or at high [O_2], Cu(I) is irreversibly oxidised to Cu(II). Cupric species are removed from solution by adsorption and (to a greater extent than Cu(I)) by precipitation. These processes drive further dissolution by slowing down the rate of reduction of Cu(II) to Cu(I). Otherwise, the subsequent increase in the interfacial [$CuCl_2^-$] would inhibit further Cu dissolution because the dissolution of Cu as Cu(I) is reversible. Thus, reactions involving Cu(II) are effectively reversible by virtue of the two coupled *irreversible* reactions, Cu(I) oxidation to Cu(II) by O_2 and Cu(II) reduction to Cu(I) on the Cu surface. Both of these reactions must participate in the mechanism, because otherwise the reactions involving Cu(II) would not be reversible and removing dissolved Cu(II) from the interfacial region would not affect the corrosion rate.

The experimental evidence is not consistent with an O_2 mass-transport limited corrosion reaction. Although O_2 was consumed during the course of the tests at a rate proportional to $t^{1/2}$ consistent with a diffusion-limited O_2 reduction reaction (based on measurement of the remaining [O_2] in a series of tests with different exposure times), the dependence of corrosion rate on [Cl^-] is too large to be explained by the effect of salinity on O_2 solubility (King et al. 1992, 1997a, Litke et al. 1992). Thus, there is no evidence for O_2-transport control of the corrosion of Cu in compacted clay, at least not at the clay density and over the range of [O_2] used in the tests. Theoretically, at some stage in the evolution of repository conditions, the corrosion rate should become limited by the rate of O_2 supply to the canister surface. Based on the results of the experiments discussed here, however, O_2-transport control can only be expected at dissolved [O_2] < ~$2 \cdot 10^{-6}$ mol·dm^{-3}, the concentration in 1 mol·dm^{-3} Cl^- solutions saturated with 0.2 vol.% O_2/N_2 at room temperature.

Contrary to the observed experimental data, the steady-state corrosion model of King et al. (1995a) predicts that the corrosion rate marginally increases with [Cl^-] in aerated solution and is impendent of salinity at lower [O_2]. As discussed in the previous section, the oxidation of Cu(I) to Cu(II) does not appear to have been a significant process in the experiments on which the steady-state model was based. The most likely reason for the difference in observed behaviour at room temperature in NaCl solutions and at 95°C in synthetic groundwater solutions is the effect of temperature on the rate of Cu(I) oxidation by O_2.

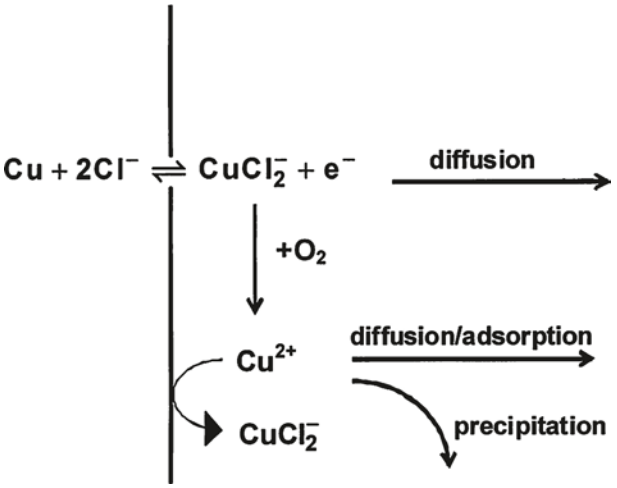

Figure 5-10. *Proposed mechanism for the corrosion of copper in compacted buffer material saturated with saline, O_2-containing groundwater.*

5.2.2 Influence of Cl^- in the absence of oxygen

The corrosion of copper in Cl^- solution with water or protons as the only oxidant can be written as (SKBF/KBS 1983, Swedish Corrosion Institute 1978)

$$Cu(s) + n\ Cl^- + m\ H_2O = CuCl_n(OH)_m^{1-n-m} + (m-1)\ H^+ + ½\ H_2(aq) \qquad 5\text{-}9$$

Appendices I and II give thermodynamic data from which the concentrations of the dissolved species $CuCl_n(OH)_m^{1-n-m}$ can be estimated for various combinations of *n* and *m*. The two sets of data were developed by different authors and differ in the method used to estimate the activity coefficients.

Reaction 5-9 and the two sets of thermodynamic data can be used to predict the concentration of dissolved Cu species in equilibrium with metallic Cu as a function of pH, $[Cl^-]$, and temperature. Calculations were performed for a temperature of 100°C, and for $[Cl^-]$ up to 2 mol/kg at pH 4-11. The activity of water was set to unity although the available data suggest that the correct value at 100°C in 2 mol/kg NaCl is close to 0.93 (Lobo 1989). The ionic strength was set equal to the free chloride concentration without conversion from mol/kg water to mol/L. The values of the parameters in the model for calculation of the activity coefficients were selected to be reasonable and to allow a sensitivity analysis. The values of the activity coefficients are therefore not necessarily exactly those preferred by the original author (see Appendices I and II).

Figure 5-11 shows the isoconcentration curves for the total dissolved copper in a pH- $[Cl^-]$-diagram. The two sets of thermodynamic data used, combined with the different methods for estimation of activity coefficients, give similar results. The results only differ markedly for a total concentration of dissolved copper of lower than 10^{-7} mol/kg.

A copper canister in a repository will be subjected to elevated pressures. Tables 5-1 and 5-2 give the partial molal volumes for the individual reactants and products in reaction 5-9 and for the overall reaction for various combinations of *n* and *m*, respectively. For a change in pressure from 0.1 MPa to 5 MPa (equivalent to the hydrostatic head at a depth of 500 m), the equilibrium constant for reaction 5-9 increases by only ~10%, with the change in the equilibrium dissolved Cu concentration being < 10%. Therefore, the change in pressure in the repository will have little effect on the predicted dissolved Cu concentration.

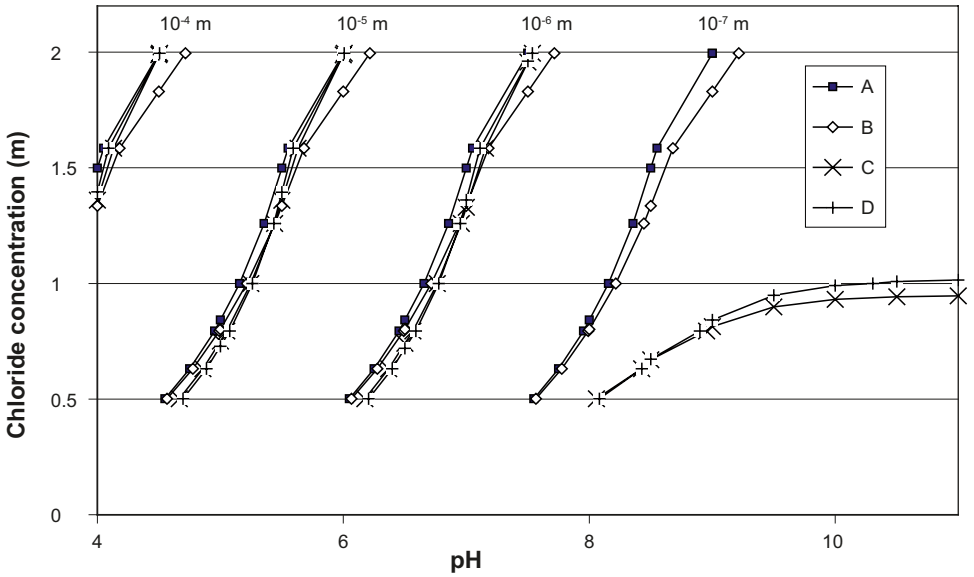

Figure 5-11. *Isoconcentration curves for the total concentration of dissolved copper in equilibrium with metallic copper and stoichiometric concentrations of dissolved hydrogen gas at 100°C.*

Thermodynamic data for $H_2(aq)$ from NBS 82 (HSC Chemistry ver. 3.0) was used in all cases. [NaCl]aq was calculated using log k=–0.45 ($\gamma_{NaCl(aq)}$=1) for all cases.
A: Data from Appendix I, Section 3, activity coefficients from Davies equation using b=0.2.
B: Data from Appendix II, Section 3, activity coefficients from the modified Helgeson equation.
*C: Data from Appendix I, activity coefficients from Davies equation using b=0.1, lg $\gamma(H_2(aq))$=0.094*Im.*
*D: Data from Appendix II, activity coefficients from Davies equation using b=0.3, lg $\gamma(H_2(aq))$=0.094*Im.*

Table 5-1 Partial molal volumes of the reactants and products.

Reactant/product	Partial molal volumes cm^3/mol
Cu(s)	7.1
H^+	0
Cu^+	–10.5
Cl^-	17.9
$CuCl_n(OH)_m^{1-n-m}$	> 0
$H_2(aq)$	~ 0
H_2O	18

Table 5-2 Partial molal volumes of reaction.

ΔVr max cm^3/mol n (Cl^-)	m (OH^-)		
	0	1	2
0	–17.6	–35.6	–53.6
1	–25.0	–43.0	
2	–42.9		
3	–60.8		

Various authors have attempted to determine whether copper corrodes in the absence of O_2. Bojinov and Mäkelä (2003) and Bojinov et al. (2004) report attempts to measure corrosion of copper using an on-line electrical resistance probe in 1 mol/L NaCl solution that initially contained only trace levels of O_2 (< 5 ppb) and which eventually became anoxic. Tests were carried out at room temperature and at 80°C. Corrosion was observed initially as the residual O_2 was consumed, but then virtually stopped as the solution became anoxic, with an estimated O_2 concentration of < 0.001 ppb. At this time, the potential of the copper electrode reached the thermodynamic immunity region (Figure 5-1). Betova et al. (2004) also concluded that the corrosion of copper stopped in compacted bentonite when the O_2 was locally exhausted at the surface and anoxic conditions had been established. These reports, therefore, show no evidence that copper corrodes in concentrated Cl^- solutions at neutral pH, consistent with thermodynamic predictions (Section 3).

Recently, Szakálos et al. (2007) claimed to have detected hydrogen formed by the corrosion of copper in deionised water at temperatures between 8°C and 85°C. Hydrogen gas was detected using an ion pump or as a pressure increase using a pressure gauge. The results show measurable hydrogen generation rates at all temperatures and under all conditions studied. The authors interpreted their observation of corrosion at redox potentials at which metallic copper is thermodynamically stable in terms of the formation of a previously unreported species H_xCuO_y (Szakálos et al. 2007). Powder XRD and secondary ion mass spectrometry (SIMS) were used to identify the H_xCuO_y species which, it is suggested, is thermodynamically stable at E/pH values below the stability line of H_2O. It was claimed that the effect was reproducible, although few details of repeat tests were given.

Hultquist et al. (2008) claim further evidence that water corrodes copper based on differences in the visual appearance of copper samples exposed to water in flasks sealed with either a Pd or Pt membrane. The concept behind the experiments is that H_2 generated by the reduction of water can escape from the Pd-sealed vessel but not from the Pt-sealed flask. After 15 years exposure, the copper exposed to water in the Pd-sealed flask was black and appeared heavily corroded, whilst the Cu exposed in the Pt-sealed flask had apparently retained the bright coppery sheen of freshly polished samples. This visual evidence was used by Hultquist et al. (2008) as further evidence for the corrosion of copper by water and, in particular, as a demonstration that corrosion could be suppressed by a small overpressure (~1 mbar according to Szakálos et al. 2007) of H_2 gas. Hultquist et al. (2009) have published further evidence for the evolution of H_2 from the corrosion of copper by water and have presented molecular dynamic simulations of the Cu-OH system and have estimated a

free energy of formation for the proposed CuOH species responsible for the thermodynamic instability of copper in water, albeit the calculations were performed for an OH radical species rather than the hydroxide anion.

The claims by Hultquist and co-workers are currently being debated. Whilst it is difficult to argue with Hultquist and co-workers' claim that they observed H_2 in the test, it is disturbing that no other researchers have been able to reproduce their results despite three or four attempts to do so. Furthermore, neither the mechanism proposed by Hultquist and co-workers for the generation of H_2 involving a CuOH species nor alternative explanations proposed by others seem to be able to explain the reported observation of H_2 (SSM 2009).

5.2.3 Influence of sulphide

The behaviour of Cu in sulphide-containing environments is important because of the potential for the corrosion of Cu to be supported by the evolution of H_2. Cuprous sulphide (Cu_2S) is thermodynamically stable at potentials below the H_2/H_2O equilibrium line (Pourbaix and Pourbaix 1992). Because of this thermodynamic stability and because of the presence of sulphide minerals in many types of bentonite and in deep Fenno-Scandian Shield groundwaters (Section 2), Cu canisters may be subject to corrosion in the presence of sulphide under the long-term reducing conditions expected to develop in the repository.

Various workers have studied the electrochemical and corrosion behaviour of Cu alloys in sulphide environments. The majority of these studies are associated with corrosion of Cu alloys in polluted seawater. Care should be taken in applying the results of these studies to the corrosion of Cu canisters, however, because most of them involved Cu-Ni alloys (commonly used in marine heat exchangers) and because the particularly aggressive forms of corrosion observed in these applications are associated with *alternating* oxidising and reducing conditions.

Several electrochemical studies of the early stages of film formation on Cu in sulphide environments have been published. As commonly observed in other environments, Cu forms a duplex bilayer corrosion product film in sulphide solutions, comprising an inner layer of Cu_2S (variously reported to be between 0.4 nm (de Chialvo and Arvia 1985) and 25–50 nm thick (Vasquez Moll et al. 1985)) and a thicker outer layer of CuS. Non-stoichiometric sulphides ($Cu_{2-x}S$, with x = 0.08, 0.23, 0.40 and 0.69) may form during the conversion of Cu_2S to CuS. The rate of growth of the CuS layer is believed to be controlled by the rate of transport of sulphide to the surface, which would be a particularly slow process in the compacted bentonite to be used in a repository.

A number of corrosion studies have also examined the role of sulphide on the behaviour of Cu and Cu alloys. Macdonald et al. (1979) also observed a duplex sulphide film on Cu-Ni alloys in deaerated sea water, but suggested the formation of an inner Cu-Ni sulphide and an outer Cu_2S layer. The Cu_2S layer was found to have a lower electrical resistance than the corresponding Cu_2O film formed in the absence of sulphide. Syrett (1981) reported a duplex film comprising an inner layer of Cu_2O, whose growth was hindered at grain boundaries in the underlying Cu-Ni alloy. The presence of sulphide resulted in the formation of an outer Cu_2S and $Cu_{2-x}S$ film due to the precipitation of Cu(I) diffusing through defects in the underlying Cu_2O layer. The reduction of H_2O was thought to occur at the Cu_2O/Cu_2S interface, with the accompanying local increase in pH resulting in growth of the Cu_2O layer. This duplex Cu_2O/Cu_2S layer might be expected to form in a repository once the initially trapped atmospheric O_2 has been consumed and the environmental conditions become more reducing, although other evidence suggests that such a duplex film is not formed but that, upon exposure to sulphide, the Cu_2O converts to Cu_2S (Chen et al. 2010).

Escobar et al. (2001) used X-ray photoelectron spectroscopy to study the nature of films formed on copper in Cl^- solutions containing sulphide ions. Only at very high HS^- concentrations (100 μg/g) or at negative potentials (–0.9 V_{SCE}) did they observe adherent sulphide corrosion products. At more-positive potentials, they observed different forms of Cl^--containing corrosion products with trace amounts of sulphide. These results suggest that the nature of the corrosion products are related to the local chemical and redox conditions, and that the canister will undergo various film formation and transformation processes as the environment within the repository evolves with time.

A number of studies have been performed under freely corroding conditions, with various explanations for the processes determining E_{CORR}. Based on the close correlation between the E_{CORR} of Cu electrodes in deaerated sulphide solutions and the equilibrium potential for the precipitated Cu sulphide covering the electrode, de Chialvo and Arvia (1985) suggested that E_{CORR} was determined by the redox potential between the Cu sulphide and dissolved sulphide in solution. Thus, for Cu_2S-covered surfaces, E_{CORR} was determined by the redox potential for the reaction

$$2Cu + S^{2-} = Cu_2S + 2e^- \qquad 5\text{-}10$$

namely, $E_{CORR} = -1.13 - 0.030 \log[S^{2-}]\ V_{SCE}$. For CuS-covered electrodes, E_{CORR} was determined by the redox potential for the reaction

$$Cu + S^{2-} = CuS + 2e^- \qquad 5\text{-}11$$

namely, $E_{CORR} = -0.94 - 0.030 \log[S^{2-}]\ V_{SCE}$. Implicit in reaction 5-11 is the assumption that CuS is a Cu(II) sulphide, but there is strong spectroscopic evidence (Perry and Taylor 1986) that CuS is a Cu(I) solid, with sulphide present in the form of a polysulphide.

Macdonald et al. (1979) reported some data showing an E_{CORR} dependence on $[HS^-]$ of –29 mV/dec, supporting the mechanism of de Chialvo and Arvia. However, they showed other E_{CORR} data exhibiting different dependences on $[HS^-]$, and themselves suggested that E_{CORR} was a mixed-potential determined by the relative rates of the anodic reaction and the cathodic reduction of H_2O. Mor and Beccaria (1975) also observed a dependence of E_{CORR} on sulphide concentration of ca. –30 mV/dec in artificial sea water for short exposures, but the dependence increased to –40 to –60 mV/dec upon ageing of the surface. This latter dependence is more consistent with a mixed-potential between the anodic reaction and the cathodic reduction of H_2O or HS^- than the redox control suggested by de Chialvo and Arvia (1985). Escobar et al. (1999) also observed a –60 mV/dec dependence of E_{CORR} on $[HS^-]$ at temperatures of 15°C, 25°C and 90°C. Alhajji and Reda (1994) suggested HS^-, rather than H_2O, was the oxidant, with a two-stage cathodic reaction involving

$$HS^- + e^- \rightarrow H_{ads} + S^{2-} \qquad 5\text{-}12(a)$$

followed by

$$S^{2-} + H_2O \rightarrow HS^- + OH^- \qquad 5\text{-}12(b)$$

although the overall reaction is stoichiometrically identical to the reduction of H_2O

$$H_2O + e^- \rightarrow H_{ads} + OH^- \qquad 5\text{-}13$$

Smith and co-workers (Smith et al. 2004, 2006, 2007a, b, 2008, 2009) have recently completed an extensive study of the electrochemistry and corrosion of copper in sulphide environments simulating those expected in a deep geological repository. Experiments were performed with OFP (oxygen-free with added phosphorus) copper in NaCl solutions with the addition of 10^{-4} mol·dm^{-3} to $3 \cdot 10^{-3}$ mol·dm^{-3} total sulphide.

The anodic reaction was found to involve the formation of a Cu_2S film (with trace amounts of digenite $Cu_{1.8}S$). This film is only partially protective and dissolution continues via a two-step process involving an adsorbed intermediate Cu(I)-sulphide species. Detailed studies have been performed of the protectiveness of the film at a sulphide concentration of 10^{-3} mol·dm^{-3} (Smith et al. 2004, 2007a). Two types of behaviour have been observed. In some cases, the film remains intact and film growth is limited and attains a steady-state thickness of ~60 nm. In other cases, this film is defected, possibly due to interfacial stresses, and continues to thicken at a rate of ~10 nm·h^{-1} over the first 48 h (Smith et al. 2004, 2007a).

At potentials close to E_{CORR}, the rate of the interfacial anodic reaction is sufficiently slow that kinetic information about the reaction

$$2Cu + HS^- = Cu_2S + H^+ + 2e^- \qquad 5\text{-}14$$

can be obtained. For example, linear log current-potential (Tafel) behaviour is observed for sulphide concentrations from 10^{-4} mol·dm^{-3} to 0.004 mol·dm^{-3} for the potential range –0.83 V_{SCE} to

–0.99 V_{SCE}. The mean Tafel slope is 37.9 mV (standard deviation 0.9 mV, n = 8). The reaction order with respect to the sulphide concentration can also be determined over this concentration range. The reaction order varies between 1.7 and 1.92 (mean = 1.84, standard deviation 0.08, n = 6) for the potential range –0.85 V_{SCE} to –0.90 V_{SCE}.

These observations are consistent with a 2-step reaction mechanism, in which the first step is a fast 1-electron transfer process

$$Cu + HS^- = Cu(HS)_{ADS} + e^- \qquad \text{fast} \qquad \text{5-15a}$$

followed by a slow second 1-electron process

$$Cu + Cu(HS)_{ADS} + HS^- \rightarrow Cu_2S + H_2S + e^- \qquad \text{slow, rds} \qquad \text{5-15b}$$

The most likely mechanism at the low [HS^-] of interest for the repository is that the cathodic reaction involves the interfacial reduction of HS^- at the Cu surface

$$2HS^- + 2e^- \rightarrow H_2 + 2S^{2-} \qquad \text{5-16a}$$

or the reduction of H_2O

$$H_2O + e^- \rightarrow \tfrac{1}{2}\, H_2 + OH^- \qquad \text{5-16b}$$

An important conclusion from this work is that, for the [HS^-] expected in the repository, the rate of the anodic process is limited by the rate of supply of sulphide to the electrode surface, even in bulk solution. This is strong evidence in support of the assumption that the rate of corrosion of a copper canister in the repository will be limited by the rate of transport of HS^-.

Two sets of E_{CORR} measurements have also been made as a function of sulphide concentration in bulk solution (Smith et al. 2004, 2007a). The two sets of data exhibit different absolute potential values and different dependences on the sulphide concentration. The earliest set of data (referred to here as the original data) exhibit a dependence on the total sulphide concentration ([S_T]) of

$$\left(\frac{dE_{CORR}}{d\log[S_T]}\right)_{original} = -127\,mV/dec \qquad \text{5-17}$$

The more-recent measurements not only exhibit more negative E_{CORR} values (possibly due to improved exclusion of O_2 from the experimental apparatus) but also a smaller dependence on the sulphide concentration

$$\left(\frac{dE_{CORR}}{d\log[S_T]}\right)_{new} = -67\,mV/dec \qquad \text{5-18}$$

Both of these dependences are greater than would be expected for control of the potential by a redox process although, at the higher end of the sulphide concentration range studied, the measured E_{CORR} was similar to the redox potential for reaction 5-10. However, at the lower sulphide levels corresponding to repository conditions, Smith et al. (2007a) concluded that E_{CORR} was determined by a mixed potential with the (rate controlling) anodic component of reaction 5-14 coupled to the cathodic reduction of H_2O or HS^-.

Smith et al. (2008, 2009) have studied the properties of the film(s) formed on copper electrodes in sulphide solutions using a combination of electrochemical impedance spectroscopy (EIS) and scanning electron microscopy (SEM). The EIS data are consistent with a bilayer structure, with an inner defected layer and a thicker outer layer formed by a precipitation process (Smith et al. 2008). In the presence of Cl^-, the Cu_2S film is more or less protective, depending on the [Cl^-]:[HS^-] ratio (Smith et al. 2009). For a [HS^-] of 10^{-3} mol·dm^{-3}, the inner porous $Cu_{1.8}S$ layer becomes covered by a dense, protective outer layer of Cu_2S. However, with increasing [Cl^-], the outer layer becomes more porous and less protective. At a [Cl^-] of 5 mol·dm^{-3}, the outer layer is discontinuous over the surface and is unprotective.

A mixed-potential model is being developed to describe the evolution of E_{CORR} of a copper canister as the repository evolves from initially aerobic to ultimately anoxic in the presence of sulphide (King 2007). Steady-state models have been developed for a combination of possible anodic and cathodic rate-controlling processes for comparison with the experimental data of Smith et al. (2004, 2007a). In bulk solution, the experimental data are consistent with a combination of a kinetically controlled anodic reaction and a constant cathodic current at E_{CORR} in fully deaerated solution (equation 5-18). In the presence of trace levels of O_2, a combination of a transport-limited anodic reaction and the kinetically limited reduction of residual O_2 can explain the observed dependence of E_{CORR} on [HS^-] in equation 5-17. In compacted clay environments, preliminary data are consistent with a transport limited anodic reaction and the kinetically limited cathodic reduction of residual O_2.

The aim of this work is to develop a transient mixed-potential model, referred to as the Copper Sulphide mixed-potential Model (CSM) to predict the time dependence of E_{CORR} as the repository environment evolves. Figure 5-12 shows the reaction scheme on which the model is based. In addition to interfacial reactions involving the dissolution of copper as $CuCl_2^-$ or as Cu_2S, the model also includes redox processes between O_2 and HS^- and the precipitation of FeS.

In a repository, the canister will have been previously exposed to an aerobic environment before being contacted by sulphide and the surface will covered by a Cu_2O film. Smith et al. (2007b) investigated what happens when a pre-oxidised surface is exposed to sulphide. Potential measurements indicate that HS^- rapidly (within 4-10 hours) reaches the underlying copper surface and the potential goes through a rapid transition from approximately –0.4 V_{SCE} to potentials close to the Cu/Cu_2S equilibrium potential (approximately –0.94 V_{SCE} for the HS^- used in the experiments). However, *in situ* Raman studies indicate that the film only slowly converts by a chemical process at the original Cu_2O film/solution interface. Such large potential transitions are often accompanied by galvanic coupling between the oxidation of the substrate (in this case, the oxidation of copper to form Cu_2S) and the reductive dissolution of the pre-existing film (in this case, the reduction of Cu_2O to Cu) and can lead to localised dissolution at defects in the film. However, that does not appear to occur for this system.

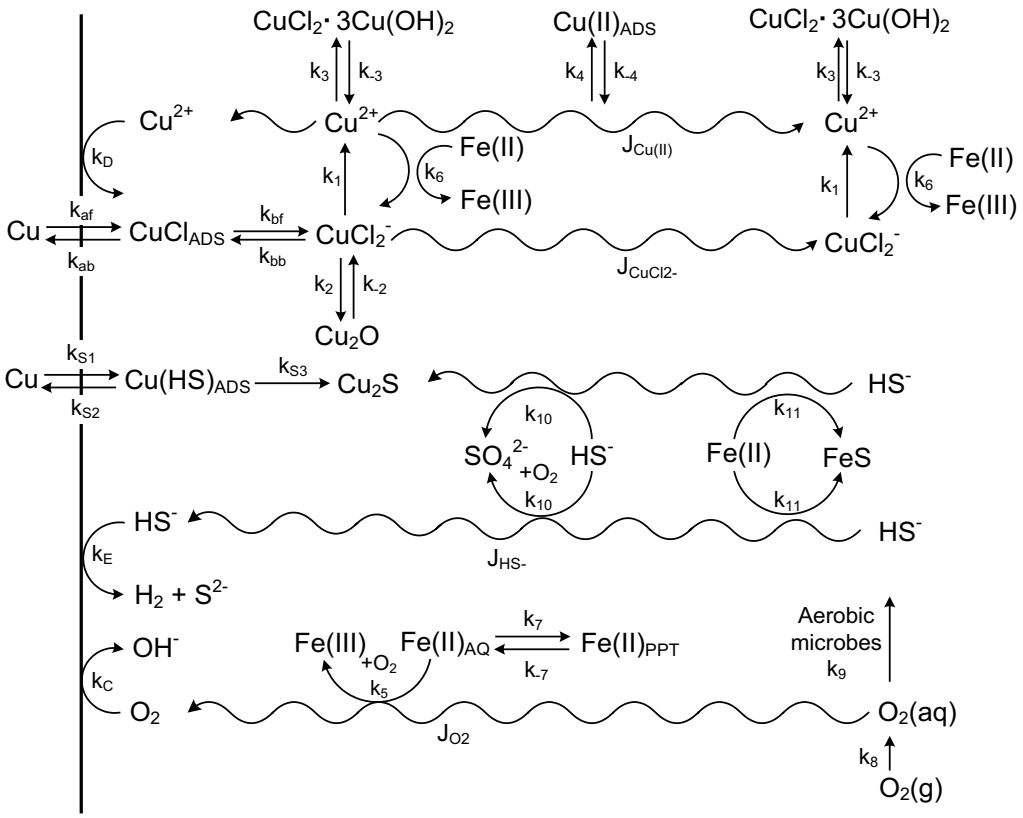

Figure 5-12. *Reaction scheme for the Copper Sulphide Model (CSM) (King 2007).*

A simulation of the evolution of redox conditions in a Swedish/Finnish repository was performed by King and Stroes-Gascoyne (1995), although the experiment was actually performed to determine the effect of sulphate-reducing bacteria on the corrosion of a Cu canister in a Canadian repository. Copper electrodes were exposed to a 1 mol·dm^{-3} NaCl solution under well-controlled mass-transport conditions, either by rotating the electrode in bulk solution or by placing a 0.1-cm-thick layer of compacted bentonite (clay dry density 1.2 Mg·m^{-3}) between the electrode and the bulk solution. The E_{CORR} of the electrode was measured as the purge gas was changed or as sulphide ions were added to the bulk electrolyte. The solution was initially aerated, but the purge gas was sequentially changed to 2 vol.% O_2/N_2, 0.2 vol.% O_2/N_2, and 100% Ar (nominally deaerated). In two experiments, sufficient Na_2S was added to the solution to give a bulk [HS^-] of either 10 µg·g^{-1} or 100 µg·g^{-1}.

Figure 5-13 shows the time dependence of E_{CORR} for three experiments, one in bulk solution and two with a compacted clay electrode. The E_{CORR} of the rotating electrode in bulk solution responded quickly to changes in the purge gas, decreasing with decreasing [O_2] (curve (a)). Under these rapid mass-transport conditions, the anodic reaction is mass-transport controlled and the cathodic reaction is limited by the rate of the interfacial reduction of O_2 at E_{CORR} (King et al. 1995a). Upon the addition of 10 µg·g^{-1} HS^-, E_{CORR} drops immediately by ~500 mV to a value of ca. –0.90 V_{SCE}. Increasing the [HS^-] to 100 µg·g^{-1} resulted in a further 60 mV drop in E_{CORR}. The precipitous drop in E_{CORR} upon the first addition of HS^- can be explained in terms of a switch in the anodic reaction from dissolution as $CuCl_2^-$ to the formation of a Cu_2S surface film, and a switch in the cathodic reaction from the reduction of residual O_2 to the reduction of H_2O (or HS^-). The –60 mV/dec decrease in E_{CORR} with [HS^-] suggests E_{CORR} is determined by the relative rates of Cu dissolution and H_2 evolution, rather than by the redox couple in reaction 5-10 (which would give a –30 mV/dec dependence).

In the presence of compacted clay, a similar decrease in E_{CORR} is observed upon the addition of HS^-, but more slowly as a consequence of the restricted mass-transport conditions. The E_{CORR} of the compacted clay electrode also decreases as the [O_2] is decreased (curves (b) and (c), Figure 5-13). The magnitude of the decrease suggests complete transport control of the anodic and cathodic reactions (see Figure 5-2). Upon the addition of 10 µg·g^{-1} HS^- (point D, curve (c)), E_{CORR} decreases by 10–20 mV but then stabilises for the next 75 hrs. The addition of 100 µg·g^{-1} HS^- (point E, curve (c)) causes a further decrease in E_{CORR} by 50–60 mV followed by a second plateau of ~40 hrs.

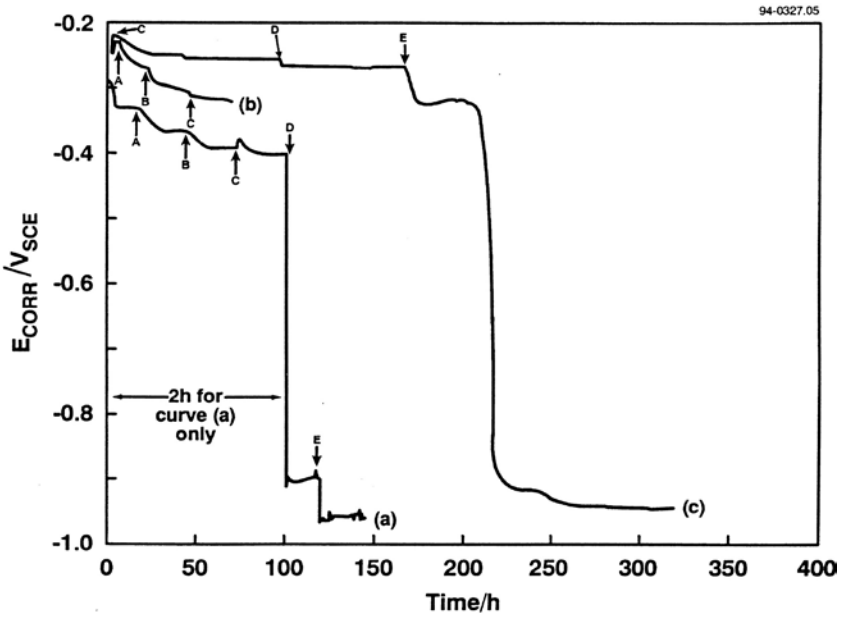

Figure 5-13. *Variation of the corrosion potential of a copper/compacted clay electrode and of a copper rotating disc electrode in 1 mol·dm^{-3} NaCl solution as a function of oxygen and sulphide concentration (King and Stroes-Gascoyne 1995). (a) Rotating disc electrode in bulk solution (the time axis for the first 2 h of this experiment has been expanded by a factor of 50 for clarity); (b) copper/compacted clay electrode in O_2-containing solution only; (c) copper/compacted clay electrode with various [O_2] and sulphide additions. The arrows represent the times at which either the overpurge atmosphere was changed or sulphide additions were made according to: (A) 2 vol.% O_2/N_2; (B) 0.2 vol.% O_2/N_2; (C) Ar; (D) 10 µg·g^{-1} sulphide; (E) 100 µg·g^{-1} sulphide.*

These small decreases in E_{CORR} are thought to be due to the consumption of residual O_2 in the clay layer by reaction with HS^-. After the second plateau period, however, E_{CORR} drops precipitously by ~0.6 V_{SCE} to a final steady-state value virtually identical to that observed in bulk solution at that $[HS^-]$.

Figure 5-14 shows a semi-schematic Evans diagram for the compacted clay experiments in Figure 5-13. In O_2-containing environments, both anodic and cathodic reactions are transport limited at E_{CORR}. Upon the addition of HS^-, the cathodic and anodic reactions change and E_{CORR} shifts to a more negative value as a result. Unlike the changes in $[O_2]$, which cause an immediate change in E_{CORR}, the addition of HS^- to the system only has an effect on E_{CORR} after a delay period. In the case of the transport-limited reduction of O_2, a change in the bulk $[O_2]$ has an immediate effect on the flux of O_2 to the electrode surface, and a consequent immediate effect on E_{CORR}. In the case of HS^-, however, the sulphide must first diffuse to the Cu surface before it can affect a change in E_{CORR}. Thus, sulphide only has an effect because of the formation of Cu_2S corrosion products, which are stable at sufficiently negative redox potentials that corrosion can be supported by hydrogen evolution. Although not conclusive proof, this evidence suggests that the rate of Cu corrosion is controlled by the rate of supply of HS^-. The delay period of 40 hrs between adding 100 $\mu g \cdot g^{-1}$ HS^- and the precipitous drop in E_{CORR} can be used to estimate the effective diffusion coefficient of HS^-. Based on a simple $\sqrt{Dt}$ calculation for the 0.1-cm clay layer, the estimated diffusion coefficient is of the order of $7 \cdot 10^{-8}$ $cm^2 \cdot s^{-1}$, a reasonable value for anionic diffusion in compacted clay.

The variation of E_{CORR} for the clay-covered electrode in Figure 5-13 is the same as that expected for a canister in a Swedish/Finnish repository, albeit on a much shorter timescale. Initially, E_{CORR} will be determined by the relative kinetics of the anodic dissolution of Cu as $CuCl_2^-$ and of the reduction of O_2. As the trapped O_2 is consumed, E_{CORR} will decrease. At some stage during the evolution of the repository environment, the nature of the reactions on the Cu surface will change. In the presence of sulphide, the anodic and cathodic reactions will change to the formation of Cu sulphide films and the evolution of hydrogen. A relatively rapid decrease in E_{CORR} by several hundred mV can be expected, with an ultimate E_{CORR} value in the range of –0.80 V_{SCE} to –1.0 V_{SCE}, depending upon the concentration of HS^- at the canister surface.

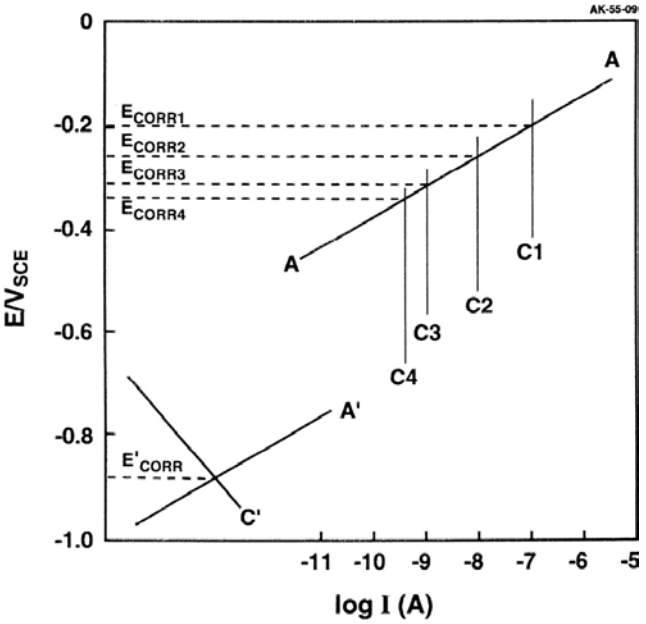

Figure 5-14. *Evans diagram illustrating the variation of E_{CORR} for a clay-covered copper electrode in O_2-containing 1.0 mol·dm^{-3} NaCl and in HS^--containing solution. Line A and lines C1 to C4 are the anodic and cathodic I/E curves predicted from experimental data for an anodic reaction limited by $CuCl_2^-$ diffusion through the clay layer (line A) and for the transport-limited reduction of O_2 for aerated solution (line C1), and for solutions purged with 2 vol.% O_2/N_2 (line C2), 0.2 vol.% O_2/N_2 (line C3) and in nominally deaerated solution (line C4). The various E_{CORR} values marked on the potential axis are the respective corrosion potentials. Lines A' and C' represent the I/E curves for unspecified anodic and cathodic reactions in HS^--containing solution, assumed to have Tafel slopes of 60 mV and –120 mV, respectively. Clay-layer thickness 0.1 cm, electrode surface area 1.0 cm^2.*

As briefly mentioned above, the most serious corrosion in sulphide-polluted sea water arises from alternating aerated and deaerated environments (King 1996a). These alternating conditions may have one of two effects. First, exposure to sulphide environments after initial exposure to an aerated environment (or vice versa) can result in alteration of the corrosion products and spalling of otherwise protective surface films due to volume changes associated with the growth of the altered layer. Thus, truly protective surface films are not stabilised under alternating oxidising and reducing conditions. Second, Cu sulphide films are more catalytic towards the reduction of O_2 than Cu_2O films, due to their more-defective structure. Thus, following the growth of a Cu sulphide film under reducing conditions, the introduction of dissolved O_2 would cause a rapid increase in corrosion rate. In either case, such effects should not occur in a repository, since the environment is expected to evolve from initially aerated to reducing in the long term.

5.2.4 Modelling of general corrosion

Just as there are both thermodynamic and kinetic approaches to describing the effects of O_2, Cl^- and HS^- on the corrosion of Cu, there are thermodynamic and kinetic approaches to predicting the long-term general corrosion behaviour of the canisters in a repository. Canister lifetime predictions based on a thermodynamic description of the corrosion process(es) generally involve an assumption of rapid interfacial kinetics and rate control by the rate of (diffusive) mass transport. Kinetically based lifetime-prediction models combine the finite kinetics of interfacial reactions with possible limitation by mass transport to and from the corroding surface. Thermodynamic models represent a "worst-case" assessment because of the assumption of infinite interfacial kinetics, and produce a conservative estimate of the corrosion rate. Both thermodynamic and kinetic models have been used to predict the lifetimes of Cu canisters in deep geologic repositories.

5.2.4.1 Thermodynamic and mass-transport-limited approach

Werme et al. (1992) describe a mass-transport limited model for predicting the extent of corrosion of copper canisters due to sulphide in a Swedish repository. In a previous assessment (SKBF/KBS 1983), it had been conservatively assumed that all of the sulphide in the bentonite surrounding the canister, plus that formed by microbial activity in the deposition hole, was consumed in the first 1,000 years. Thereafter, sulphide was assumed to diffuse to the canister from the tunnel and from the groundwater. The sources of sulphide in the tunnel were the sulphide impurities in the bentonite and that produced by microbial activity. In the groundwater, the maximum sulphide concentration was assumed to be 1 mg/L, corresponding to that present naturally in the groundwater plus that produced by microbial activity. Table 5-3 gives the predicted depth of corrosion as a function of time due to sulphide from these various sources (SKBF/KBS 1983).

Table 5-3. Predicted time dependence of the depth of corrosion (in mm) due to sulphide from various sources (SKBF/KBS 1983, modified from Werme et al. 1992).

Source of sulphide	Exposure time (yr)			
	10^3	10^4	10^5	10^6
Deposition hole:				
1. from bentonite	0.032	0.032	0.032	0.032
2. from microbial activity in bentonite	0.023	0.023	0.023	0.023
Tunnel:				
1. from bentonite	$3.6 \cdot 10^{-5}$	$3.2 \cdot 10^{-4}$	0.0032	0.032
2. from microbial activity in tunnel	$9.0 \cdot 10^{-6}$	$5.5 \cdot 10^{-5}$	$5.5 \cdot 10^{-4}$	0.0055
Groundwater:				
1. present naturally in groundwater	$9.1 \cdot 10^{-5}$	$8.6 \cdot 10^{-4}$	0.0086	0.086
2. from microbial activity in groundwater	$9.1 \cdot 10^{-5}$	$8.6 \cdot 10^{-4}$	0.0086	0.086

Werme et al. (1992) re-considered the conservative assumption that all of the sulphide in the deposition hole was consumed within 1,000 years. Using a 1-dimensional sulphide consumption model assuming instantaneous consumption of sulphide on the canister surface, they estimated that the sulphide in the deposition hole would be consumed in 850,000 years. The amount of sulphide estimated to be present in the deposition hole (both as an impurity in the bentonite and produced from microbial activity) was higher than that assumed in SKBF/KBS (1983), and gave a maximum depth of corrosion after 850,000 years of just over 1 mm. Until the sulphide in the deposition hole is consumed, there can be no diffusion of sulphide from the tunnel or from the groundwater, since the bentonite pore-water [HS^-] exceeds that in the tunnel or groundwater.

Taxén (Appendix III in King et al. 2001) has considered the following reaction

$$Cu(s) + H^+ + n\ Cl^- \leftrightarrow ½\ H_2(aq) + CuCl_n^{(1-n)} \qquad 5\text{-}19$$

and estimated the mass-transport-limited rate of corrosion of copper in anoxic groundwater with high [Cl^-]. If the interfacial reaction kinetics are fast, the rate of corrosion is limited by the diffusion of either $CuCl_n^{(1-n)}$ or H_2 away from the canister surface. In the absence of other effects, the corrosion rate would be expected to decrease with time as the respective concentration gradients at the canister surface decrease as the two species diffuse through the bentonite.

Any process that maintains a high concentration gradient at the canister surface, however, will maintain a high corrosion rate. Two such processes are the precipitation of $CuCl_n^{(1-n)}$ by sulphides and the oxidation of H_2 by reaction with Fe(III):

$$2CuCl_n^{(1-n)} + MeS \rightarrow Cu_2S(s) + Me(II) + 2nCl^- \qquad 5\text{-}20$$

and

$$½H_2(aq) + Fe(III)(bentonite) \rightarrow H^+ + Fe(II)(bentonite) \qquad 5\text{-}21$$

respectively, where Me(II) is a divalent metal ion. Bentonite may contain up to 0.1 wt.% sulphide, mostly as pyrite (FeS_2). The total Fe content is ~4 wt.%, predominantly as substituted Fe(III) in the montmorillonite lattice and as Fe_3O_4 particles.

Taxén developed a mass-transport-reaction model with cylindrical geometry to calculate the diffusive flux of $CuCl_n^{(1-n)}$ and H_2 away from the canister and, hence, the corrosion rate. The interfacial fluxes of $CuCl_n^{(1-n)}$ and H_2 (J_{Cu} and J_{H2}, respectively) were coupled according to reaction 5-19, such that

$$J_{Cu} = 2J_{H2} \qquad 5\text{-}22$$

The respective concentrations of dissolved Cu and H_2 (C_{Cu} and C_{H2}, respectively) are also linked through an electrochemical equilibrium (k)

$$C_{Cu} \cdot \sqrt{C_{H2}} = k \qquad 5\text{-}23$$

where $k = 1.2 \cdot 10^{-11}$ in 1.0 mol/kg Cl^- at pH7 and 50°C. Reactions between $CuCl_n^{(1-n)}$ and MeS (FeS_2) and between H_2 and Fe(III) were assumed to be instantaneous. The coupled mass-transport-reaction equations were solved using Runge-Kutta techniques.

The bentonite in the deposition hole was simulated by a series of 70 nested cylinders. The canister surface temperature was assumed to be a constant 50°C, with the bentonite at a temperature of 25°C. Only the dichloro Cu(I) complex $CuCl_2^-$ was considered. An initial [Cl^-] of 0.1 mol/kg was assumed in the bentonite, with a constant [Cl^-] of 1.0 mol/kg maintained at the simulated bentonite/rock interface.

Figure 5-15 shows the predicted corrosion rate and depth of corrosion as a function of time for the reference sulphide and Fe(III) concentrations. The corrosion rate increases with time initially as the Cl^- diffuses to the canister surface from the rock (a process that takes of the order of 300–400 years). After this time, the corrosion rate is predicted to decrease with time as the dissolved $CuCl_2^-$ and H_2 diffuse into the bentonite. Simultaneously, the sulphide and Fe(III) contents of the bentonite nearest the canister are reduced by reaction with $CuCl_2^-$ and H_2, respectively, although only a relatively small fraction of the total inventory is consumed within the first 6,000 years shown in Figure 5-15. The total depth of corrosion is negligible, amounting to only ~0.06 μm after 6,000 years (mean rate of 0.01 nm/yr).

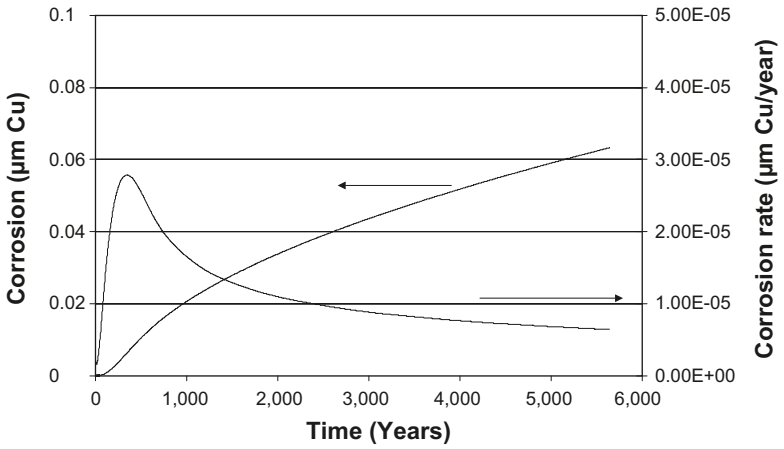

Figure 5-15. *Corrosion depth and corrosion rate as function of time. pH 7.0 50°C, 1.0 mg reactive sulphide and 3 mg reactive Fe(III) per kilogram bentonite.*

Higher sulphide and/or Fe(III) concentrations would lead to higher predicted corrosion rates, since reaction between these species and $CuCl_2^-$ and H_2, respectively, would maintain higher gradients at the canister surface. However, even with a 3,000-fold increase in Fe(III) content and a 100-1,000-fold increase in sulphide content, the maximum depth of corrosion due to reaction 5-19 is predicted to be < 6 µm after 50,000 years (mean of ~0.1 nm/yr). In contrast, the direct sulphidation of the surface by

$$2Cu + HS^- + H^+ = Cu_2S + H_2 \qquad 5\text{-}24$$

results in ~5 times more corrosion after the same period of time (Werme et al. 1992).

5.2.4.2 Kinetic approach

In contrast to the thermodynamically based models used in the Swedish and Finnish programmes, the assessment of the rate of general corrosion in the Canadian programme has been based on both thermodynamic (mass-transport limited) and kinetic models. Three different models have been proposed, each having their particular strengths and weaknesses. The three models are: (i) the Cu(II) mass-transport limited model for oxidising conditions (King and LeNeveu 1992, King et al. 1994), (ii) the steady-state kinetic model of King et al. (1995a), described above, and (iii) the transient kinetic Copper Corrosion Model (CCM) (King and Kolář 1995, 1996a, 2000, 2006a).

The *Cu(II) mass-transport limited model* was developed based on the results of corrosion experiments in compacted buffer material under oxidising conditions (King et al. 1992). Under these conditions, the diffusion of Cu(II) away from the Cu surface limits the rate of corrosion, which is given by

$$\text{Rate} = \frac{2A_{Cu}\rho_d m_0}{\rho_{Cu}(\pi t)^{1/2}}\left(\frac{\varepsilon_e \tau_f D_0}{r}\right)^{1/2} \qquad 5\text{-}25$$

where A_{Cu} and ρ_{Cu} are the atomic mass and density of Cu, ρ_d is the dry density of the buffer material, m_0 is the total concentration of Cu in the buffer immediately adjacent to the canister surface, t is the time, ε_e and τ_f are the effective porosity for mass transport and the tortuosity factor of the buffer, D_0 is the bulk-solution diffusion coefficient of Cu(II), and r is the buffer capacity factor for Cu(II), which is related to the extent of adsorption on the clay. Good agreement was found between corrosion rates predicted from equation 5-25 and the observed corrosion rate of Cu in compacted buffer material for various temperatures (50–150°C), buffer dry densities (1.45–1.79 $Mg \cdot m^{-3}$), and exposure times (1 month – 2 years) (King et al. 1992).

Equation 5-25 was used as the basis for a model to predict the lifetime of Cu canisters in a Canadian repository (King and LeNeveu 1992, King et al. 1994). Implicit in the use of this expression is the assumption that the mechanism does not change over time, i.e. the corrosion rate does not become limited by the supply of O_2 to the canister surface. This is clearly a conservative assumption for a sealed repository and, together with the assumption of infinitely fast interfacial kinetics, this model results in an extremely conservative assessment of the canister lifetimes. Nevertheless, the minimum predicted lifetime for a 25-mm-thick Cu canister (only 16 mm of which was used as the corrosion allowance) in a Canadian repository was of the order of 30,000 yrs. This lifetime was based on a conservative estimate of the interfacial dissolved copper concentration of 0.05 mol·dm^{-3}, calculated from the experimental total copper concentration profiles assuming relatively little adsorbed copper. Predictions based on a more-realistic interfacial Cu concentration of 0.005 mol·dm^{-3} produced lifetimes of ~10^6 yrs, *even for the conservative assumption of an infinite supply of O_2.* The model was also used to predict the corrosion rate for the bronze cannon natural analogue (King 1995), Cu concentrations profiles for which are shown in Figure 5-5. The predicted rate was within a factor of six of the rate estimated for the cannon.

The Cu(II) transport model has a number of advantages and disadvantages. The advantages of the model include: (i) its computational simplicity and the ease with which it can be incorporated into performance assessment models for the entire repository, which generally include a detailed description of the mass-transport conditions, (ii) the limited number of required input parameters, (iii) the experimental basis for the rate equation, and (iv) the conservatism inherent in the model. The disadvantages of the model are: (i) the over-conservatism in the model because of the failure to take into account the limited the availability of O_2, and (ii) the limited amount of output data, comprising only the corrosion rate as a function of time and the total depth of corrosion. To avoid overly conservative lifetime predictions, this model should only be applied to permanently aerobic systems, or to the early stages in the evolution of a sealed repository.

The *steady-state kinetic model* was developed to interpret the results of short-term laboratory electrochemical experiments (King et al. 1995a, b, c). Data from separate electrochemical studies on the anodic dissolution of Cu in Cl^- solutions (King et al. 1995a) and on the reduction of O_2 on Cu (King et al. 1995b, c) were combined with steady-state mass-transport expressions to produce a mixed-potential model capable of predicting E_{CORR} and i_{CORR} for a wide range of mass transport and environmental conditions. Good agreement between predicted and measured E_{CORR} values was demonstrated for $[O_2]$ between $< 10^{-6}$ mol·dm^{-3} and $2 \cdot 10^{-4}$ mol·dm^{-3} and for steady-state mass-transfer coefficients between 10^{-7} cm·s^{-1} and 10^{-2} cm·s^{-1}, the latter achieved using a rotating disc electrode in bulk solution. Of particular relevance for the corrosion of Cu canisters was the application of the model to predict the steady-state E_{CORR} of a Cu electrode separated from a bulk Cl^- solution (simulating saline groundwater) by a 1-cm-thick layer of compacted bentonite clay. In 0.1 mol·dm^{-3} NaCl solution, variously purged with air, 2% O_2/N_2, 0.2% O_2/N_2, and nominally deaerated, the maximum deviation between the predicted and measured steady-state E_{CORR} was 17 mV.

The steady-state model has never been used to predict canister lifetimes, but has instead been used to interpret the results of experimental studies, some of which were described above. As such, the model has certain limitations, the most major being the exclusion of processes involving Cu(II). For example, the steady-state model predicts little dependence of the corrosion rate on $[Cl^-]$ (Figure 5-6(b)), whereas the rate is actually observed to decrease with increasing salinity in tests at elevated temperature (Figure 5-9). The experimental observations have been explained in terms of the effect of Cl^- and O_2 on the Cu(I)/Cu(II) speciation, an effect not included in the steady-state model.

Notwithstanding these limitations, the steady-state model is a useful tool for a number of applications. In addition to the interpretation of the results from short-term laboratory studies at room temperature, the model may also be applicable to the later stages in the evolution of the repository environment, during which processes involving Cu(II) will be less important than they are in the early, oxidising period. As such, the steady-state model complements the Cu(II) transport-limited model described above. A distinct advantage of the steady-state model over the previous model, however, is its ability to predict the E_{CORR}, in addition to i_{CORR}. As will be shown later, comparison of the (predicted) E_{CORR} to critical potentials for localised corrosion is a powerful method for predicting the long-term localised corrosion behaviour of the canister.

The most advanced general corrosion model developed in the Canadian programme, and consequently the one that has proven most useful, is the *transient kinetic Cu corrosion model* (CCM) (King and Kolář 1995, 1996a, 2000, 2006a, King et al. 2008). The CCM is based on the experimentally determined reaction scheme for the corrosion of Cu in compacted buffer with O_2-containing saline groundwater shown in Figure 5-16. This reaction scheme was derived on the basis of (i) corrosion studies in compacted bentonite (King et al. 1992, 1997a, Litke et al. 1992), (ii) electrochemical studies of the anodic dissolution of Cu in Cl^- and Cl^-/SO_4^{2-} solutions (King and Tang 1998, King et al. 1995a, d) and the reduction of O_2 on Cu (King et al. 1995b, c), (iii) the homogeneous oxidation of Cu(I) by O_2 in Cl^- solutions (Sharma and Millero 1988), (iv) the consumption of O_2 by reaction with Fe(II) (Wehrli 1990), and (v) the adsorption of Cu(II) on bentonite and the diffusion of dissolved Cu through compacted buffer (King 1995, Ryan and King 1994). Thus, there is a very substantial experimental database underlying the model.

The mathematical model itself is based on a 1-D description of the various mass-transport barriers in the repository (defined below) and a series of mass-balance equations, one for each of the chemical species in the model. A total of 10 species were considered in the initial version of the model: dissolved O_2, gaseous O_2, Cl^-, $CuCl_2^-$, dissolved Cu(II), Cu(II) adsorbed on clay surfaces, Cu_2O, $CuCl_2 \cdot 3Cu(OH)_2$, dissolved Fe(II) and precipitated Fe(II). The mass-balance equations are of the form

$$\varepsilon_a \frac{\partial c}{\partial t} = \frac{\partial}{\partial x}\left(\varepsilon_e \tau D_0 \frac{\partial c}{\partial x} \right) + \varepsilon_a \sum_i R_i + \sum_i R_i' \qquad 5\text{-}26$$

where c is the pore-water concentration, ε_a is the accessible porosity, and the ΣR_i and ΣR_i' terms represent the sums of the rates of formation and loss of the species in question, respectively. These latter terms account for the various adsorption/desorption, precipitation/dissolution, and redox reactions illustrated in Figure 5-16. Certain species are assumed not to diffuse (i.e. Cu_2O, $CuCl_2 \cdot 3Cu(OH)_2$, adsorbed Cu(II) and Fe(II)(ppt)), so that the respective mass-balance equations contain no diffusive flux term. The spatial and temporal variation of temperature is also included in the model, for which a 1-dimensional heat-conduction equation is written.

The reactions shown in Figure 5-16 are assumed to occur in a spatial grid, bounded on the left-hand boundary by the canister surface and on the right-hand boundary by, generally, a major water-bearing fracture. In between the two boundaries the spatial grid is divided into layers that, for a Canadian repository, describe the layers of compacted buffer and backfill materials, a layer of excavation-disturbed rock and a layer of "intact" rock that act as mass-transport barriers.

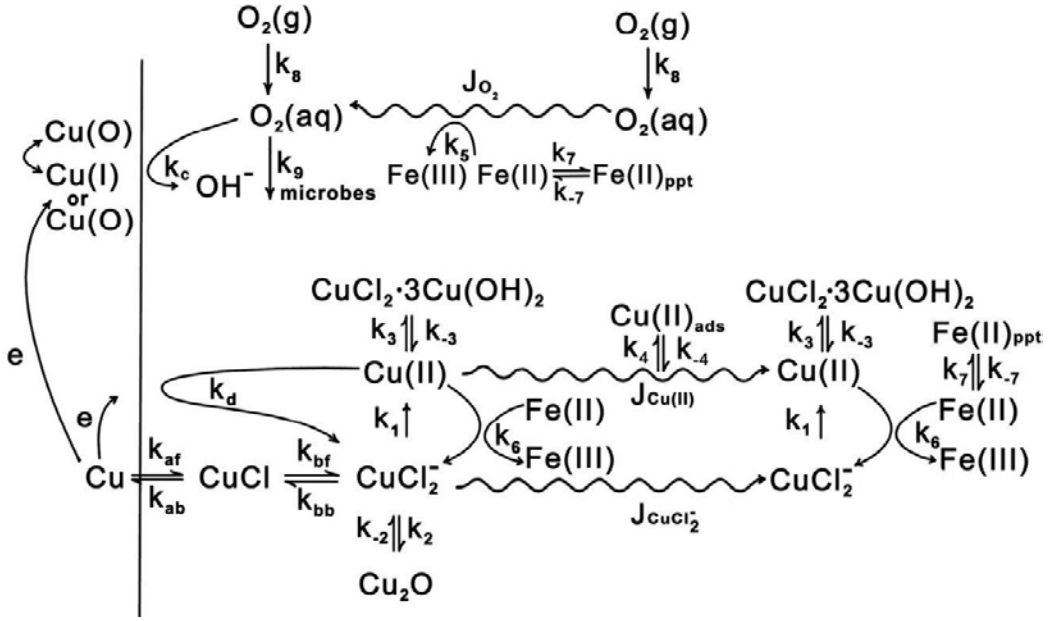

Figure 5-16. *Mechanism for the general corrosion of copper in compacted buffer material with O_2-containing saline groundwater (King and Kolář 2006a).*

The series of ten mass-balance equations (and the heat-conduction equation) are solved subject to various initial and boundary conditions. Of these, the most important from a corrosion viewpoint are the boundary conditions at the canister surface for the species involved in the corrosion reactions, i.e. O_2, Cl^-, $CuCl_2^-$, and dissolved Cu(II). For these species, the electrochemical kinetic expressions describing the rates of reactions 5-2, 5-5 (for both Cl^- and $CuCl_2^-$), and 5-4 are used as flux boundary conditions. These reactions constitute an electrochemical mixed-potential model, enabling the time dependence of the E_{CORR} and i_{CORR} of the canister to be calculated. In this way, the interfacial electrochemical reactions are coupled to the mass-transport, adsorption/desorption, precipitation/dissolution, chemical, and redox processes occurring in the repository. The right-hand boundary conditions are generally defined by the groundwater properties, which enables the effects of, for example, variations in groundwater salinity or of the influx of aerated meteoric water to be determined. It is this coupling of interfacial and near-field processes that makes this form of modelling flexible.

One of the useful features of the CCM is the wide range of output data that are produced. In addition to predicting the time dependence of the E_{CORR} and corrosion rate (i_{CORR}) of the canister, the model also predicts the spatial and time dependence of the concentration of each of the ten chemical species, and of the rate and extent of each of the individual reactions. These latter data can be used, for example, to predict the time dependence of the increase in salinity in the repository, or of the consumption of O_2.

As an example of the predictions from the CCM, Figure 5-17 to 5-19 show various results of a simulation of the evolution of the repository environment and corrosion behaviour of a copper canister in a Canadian repository in granitic host rock (King and Kolář 2006a). For these simulations, the canister was assumed to be surrounded by various compacted clay-based sealing materials, including: 100% bentonite (inner buffer), 50:50 sand:bentonite (outer buffer), a bentonite:illitic clay:aggregate dense backfill, and 50:50 sand:bentonite light backfill. Other mass transport barriers included in the model were the inner and outer EDZ and the near- and far-field rock. The effects of the time-dependent saturation of the sealing materials and rock layers were included in the model by assuming various saturation behaviours for the different sealing materials and rock layers. The inner and outer buffer materials were assumed to initially dry out under the thermal gradient before becoming gradually fully saturated after 200 yrs, with faster saturation of the backfill and rock layers further away from the heat source. In addition to the processes illustrated in Figure 5-16, aerobic microbial activity was simulated using an assumed first-order rate expression for the microbial consumption of O_2, where the rate constant was derived from the simulation of O_2 consumption in the AECL Buffer-Container Experiment (King and Kolář 2006a). However, microbial activity was only allowed in a given layer if the water activity (a_W) exceeded the threshold of 0.96 assumed necessary to sustain microbial activity. Because of the assumption of partially saturated conditions, the initially trapped O_2 is divided between both gaseous and dissolved forms in the model.

Figure 5-17 shows the predicted time dependence of the corrosion potential (E_{CORR}) and corrosion rate (i_{CORR}) of the Cu canister and the extent of corrosion and of each of the supporting cathodic reduction processes. Both E_{CORR} and i_{CORR} decrease during the initial period as the trapped O_2 is consumed (Figure 5-17(a)). The mean predicted corrosion rate over the first year is ~3 $\mu m \cdot a^{-1}$, which is exactly the rate observed by Karnland et al. (2000) at Äspö. The corrosion rate is predicted to increase marginally after ~1 yr, before decreasing again after reaching a peak at ~10–20 yrs. This behaviour is related to the increase in canister temperature and the subsequent cooling once the peak temperature is reached after 10–30 yrs. The corrosion rate decreases after 20–30 yrs both because of the decrease in temperature and the decrease in the rate of supply of oxidants as the repository becomes anoxic. Corrosion finally ceases once all of the oxidant is consumed (see below). At the same time, the E_{CORR} is predicted to decrease (i.e. shift to more-active or more-negative potentials) during the initial period of O_2 consumption, but then increase again after the peak canister temperature is reached. In general, E_{CORR} increases with decreasing temperature, partly explaining the increase in E_{CORR} as the canister cools. However, this positive shift in E_{CORR} is also the result of a change in the predominant cathodic reaction to the reduction of Cu(II). Because the equilibrium potential for the reduction of Cu(II) is more positive than that for O_2 reduction, the value of E_{CORR} (which must lie between the equilibrium potentials for the anodic and cathodic reactions) tends to be more positive if the oxidant is Cu(II).

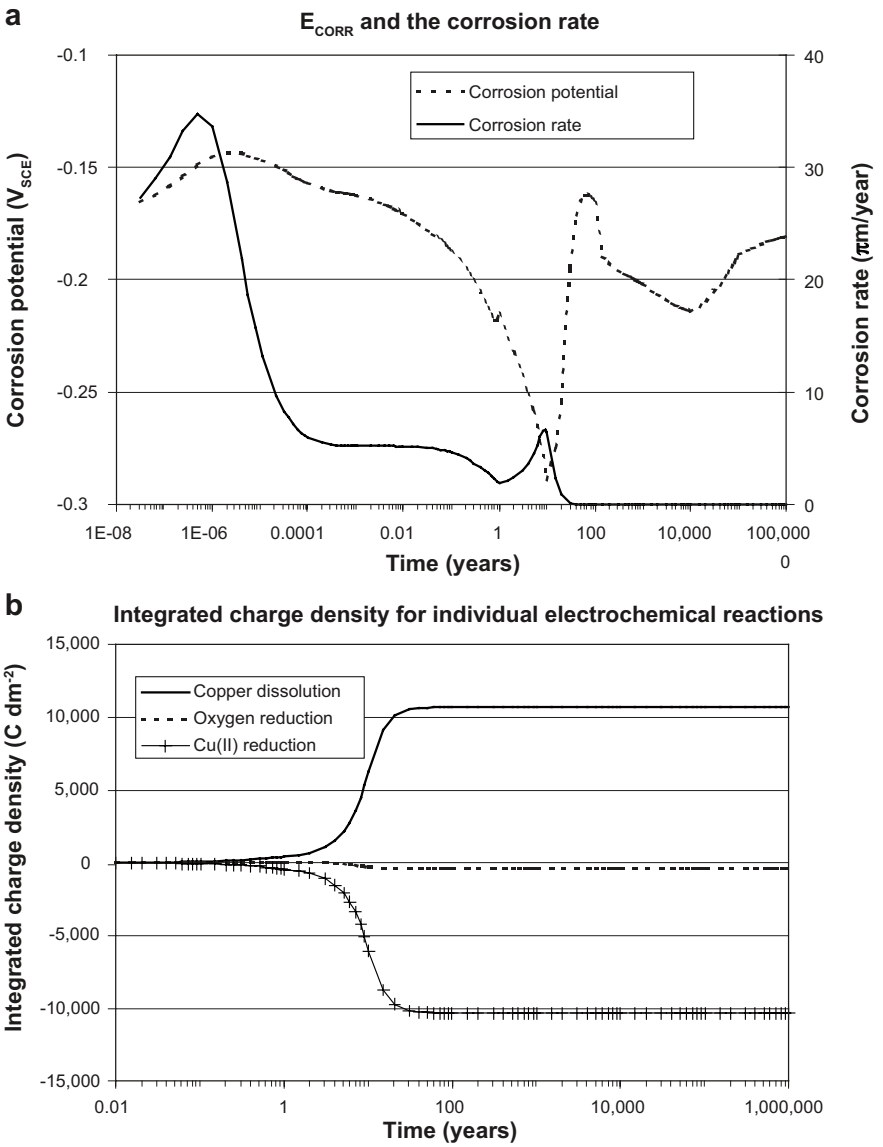

Figure 5-17. *Predicted time dependence of the corrosion potential (E_{CORR}), corrosion rate, and of the extent of the individual interfacial electrochemical reactions of a copper canister in a canadian repository (King and Kolář 2006a). A charge density of 5,000 C·dm^{-2} is equivalent to 37 µm of corrosion.*

The total extent of corrosion amounts to 79 µm (a charge density of 10,000 C·dm^{-2} is equivalent to a depth of corrosion of 74 µm for dissolution as Cu(I), Figure 5-17(b)). Most of the corrosion occurs within the first 30 yrs and thereafter rapidly slows, before effectively stopping after 100–200 yrs. The vast majority (> 96%) of the corrosion is supported by the cathodic reduction of Cu(II) (rate constant k_d in Figure 5-16) rather than the direct reduction of O_2 (rate constant k_c in Figure 5-16). In aerated systems, Cu(II) is typically the oxidant because of the relatively fast kinetics of Cu(I) oxidation to Cu(II) and of the reduction of Cu(II) on the Cu surface.

For this particular simulation, the trapped O_2 in the buffer and backfill is predicted to be consumed in ~200 years (Figure 5-18). (Note: the consumption of trapped O_2 would be expected to be faster with a high-sulphide content bentonite in the deposition holes and if the rate of aerobic microbial respiration is faster than assumed in the calculations). As dissolved O_2 is consumed by the corrosion reaction and other processes, O_2 in the gas phase progressively dissolves in the pore solution. The precise point at which the repository can be said to have become "anoxic" is difficult to define, but here the rapid decrease in the gaseous O_2 inventory at ~200 yrs is taken as an indication of the onset of anoxic conditions.

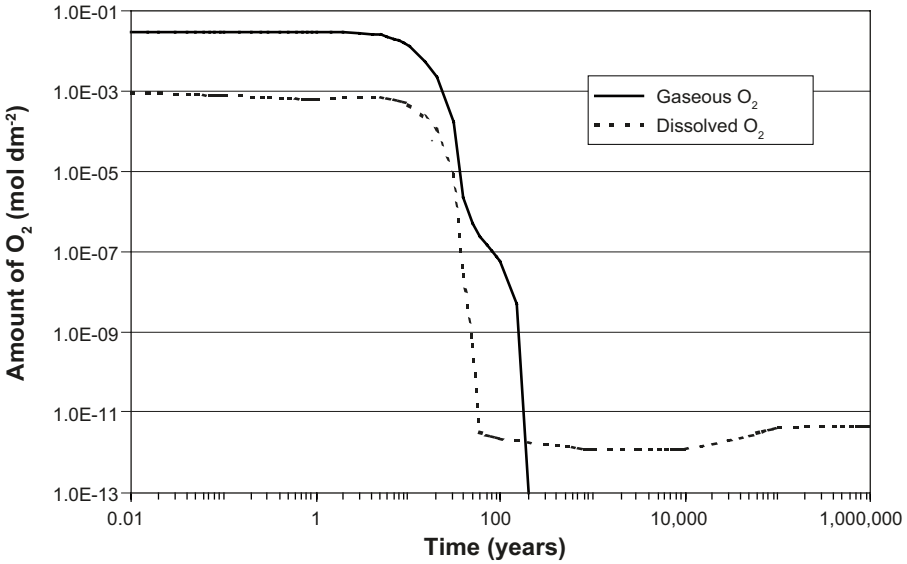

Figure 5-18. *Predicted time dependence of the inventory of gaseous and dissolved oxygen in a canadian repository (King and Kolář 2006a). The inventory of O_2 has units of mol/dm^2 because it is the integrated amount of O_2 in the 1-dimensional geometry of the model.*

Various processes contribute to the consumption of O_2 in the model simulation, including:

1. the interfacial electrochemical reduction of O_2 on the canister surface,
2. the homogeneous oxidation of Cu(I) to Cu(II) by O_2 (rate constant k_1 in Figure 5-16),
3. the homogeneous oxidation of Fe(II) (rate constant k_5 in Figure 5-16), and
4. aerobic microbial respiration (rate constant k_9 in Figure 5-16).

Of the total amount of O_2 initially trapped in the repository, ~90% is predicted to support the corrosion of the canister, either directly by the interfacial reduction of O_2 or indirectly by the oxidation of Cu(I) to Cu(II), which is then reduced on the canister surface. Only ~9% of the initial O_2 is predicted to be consumed by either microbial activity or the oxidation of Fe(II) minerals. The relative lack of importance of the non-corrosion reactions in consuming O_2 is a consequence of:

1. the assumed absence of aerobic microbial activity in the sealing materials at early times because of the desiccation of these materials,
2. the absence of Fe(II) minerals in the inner and outer buffer materials and the light backfill,
3. the rapid diffusion of gaseous O_2 towards the canister in unsaturated buffer material, and
4. the relatively rapid consumption of O_2 at and near the canister surface by the electrochemical reduction reaction and the homogeneous oxidation of Cu(I).

Figure 5-19 shows the spatial distribution of the various homogeneous O_2-consumption processes (i.e. the homogeneous oxidation of Cu(I) and Fe(II) and aerobic microbial respiration). The homogeneous oxidation of Cu(I) occurs within 1 mm of the canister surface as the concentration of Cu(I) is obviously highest at this location (Figure 5-19(a)). In contrast, the oxidation of Fe(II) (Figure 5-19(b)) and aerobic respiration (Figure 5-19(c)) occur further away from the canister. In the case of the oxidation of Fe(II), the majority of the O_2 consumption occurs in the dense backfill, as this is the only sealing material that contains Fe(II) minerals. (As noted above, this analysis would be different if the bentonite contained pyrite impurities). Some O_2 consumption is also predicted to occur in the inner and outer EDZ. Aerobic respiration (Figure 5-19(c)) is limited to the outer buffer and dense backfill, and to a limited extent in the EDZ and rock layers. For the assumed saturation times for the different layers, microbial activity does not occur for much of the important early period because the buffer and backfill are assumed to desiccate to the point that a_W falls below the threshold for microbial activity. Microbial activity is not possible in the 100% bentonite inner buffer at any time based on this criterion.

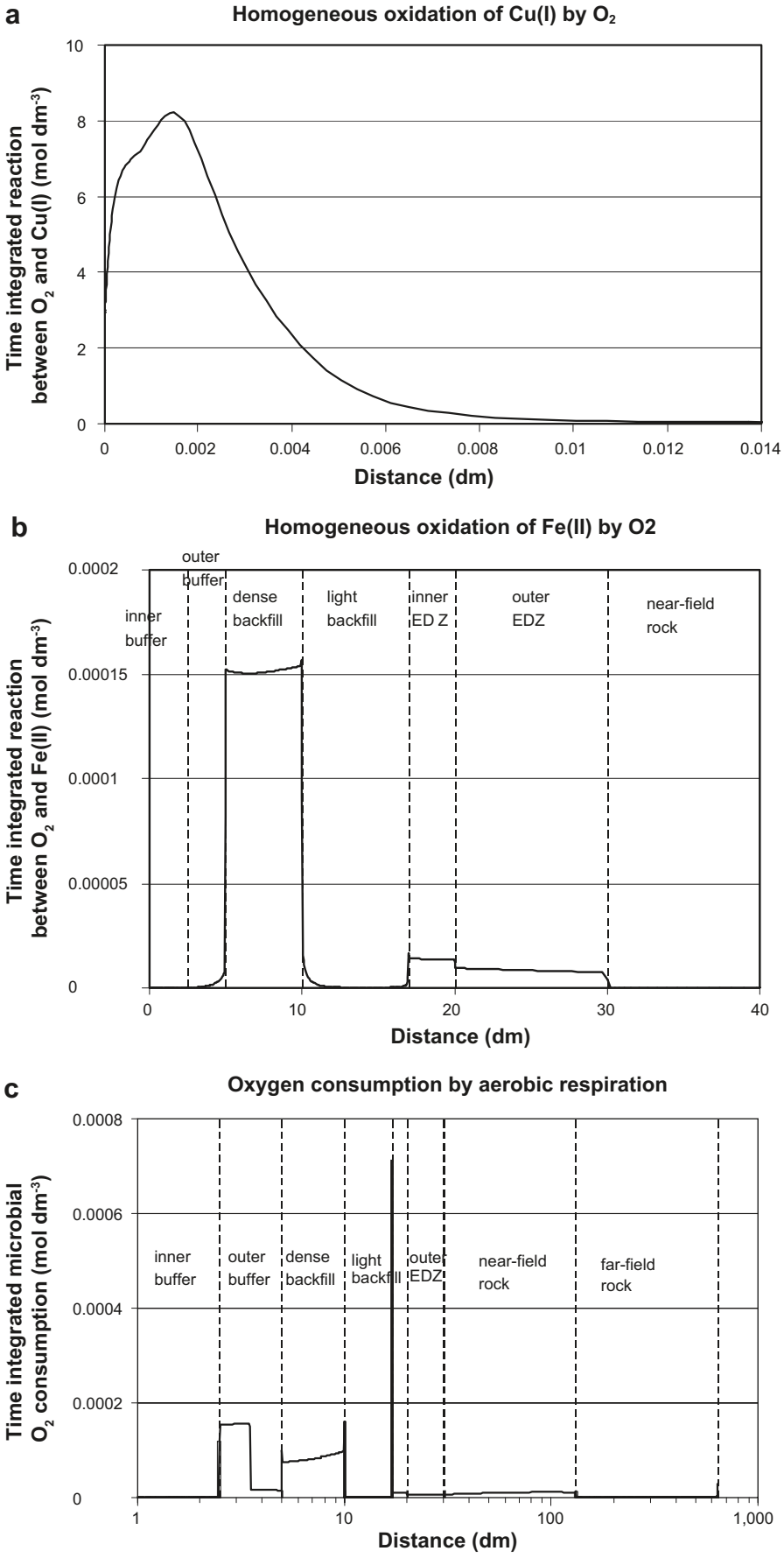

Figure 5-19. *Predicted spatial dependence of the extent of oxygen consumption by homogeneous processes in the near field of a canadian repository (King and Kolář 2006a). The plots show the time-integrated extent of each reaction over the 10^6-year simulation period.*

In addition to predictions of the general corrosion of Cu (King 1996b, King and Kolář 1995, 1996a, 2000, King et al. 2008), the CCM has also been used to predict (i) the evolution of repository redox conditions (King and Kolář 2006a, Kolář and King 1996, King et al. 2008) (Section 2.2.2), (ii) the extent of SCC controlled by the flux of oxidant to the canister surface (King et al. 1999a, b, c), (iii) corrosion prior to saturation of the repository (King and Kolář 1997a) (Section 4.3.1), (iv) the effect of geosphere conditions on the corrosion of Cu canisters (King and Kolář 1997b), (v) the results of Cu corrosion experiments under simulated disposal conditions and of observations from a bronze cannon natural analogue (King and Kolář 1996b), (vi) the probability of pitting of Cu canisters (King and Kolář 2000), and (vii) the results of *in situ* tests at AECL's URL by way of validation of the model (King and Kolář 2006a) (Section 5.2.6).

There are a number of major advantages to the CCM over the other two models described above. First, the CCM is based on an extensive experimental database, lending credibility to the predictions made using the model. Second, unlike the Cu(II) transport model and the steady-state E_{CORR} model, the CCM includes all relevant interfacial, homogenous kinetic, and mass transport processes. Third, the use of electrochemical expressions for the interfacial boundary conditions enables both E_{CORR} and i_{CORR} to be calculated directly, the former being particularly useful for predicting the probability of localised attack and stress corrosion cracking. Finally, the flexibility offered by the coupling of interfacial reactions and processes in the near-field enables many more processes other than the general corrosion of the canisters to be simulated.

The disadvantages of the CCM are its computational complexity, which precludes its use in probabilistic performance assessment calculations, and the large number of required input data. However, most of these parameters are available from the various experimental Cu corrosion studies described above, or from the literature.

In addition to the modelling of general corrosion, variants of the CCM have been developed to predict the extent of microbial activity and the formation of corrosive metabolic by-products (King et al. 2002b, 2003, 2004) and to predict the likelihood of SCC (King and Kolář 2004, 2005, Maak and King 2005). Further details of these two variants of the CCM are given in Sections 2.3.4 and 6.2.2.1 for the microbial and SCC models, respectively.

5.2.5 Weld and grain boundary corrosion

In any welded structure, the regions around the weld, including the weld material itself as well as the heat-affected zone, can be locations of enhanced corrosion susceptibility. Proper attention must be paid to the design of the weld and of the welding procedure in order to minimise such effects. The growth of grains during welding can concentrate impurities at the grain boundary due to a decrease in the relative volumes of the grain body and the grain boundaries (Fennell et al. 2001). Fennell et al. (2001) found no effect of increased grain size on the degree of intergranular corrosion of Cu-OFP in bentonite-equilibrated Äspö groundwater with [Cl^-] of 20 mg/L and 20,000 mg/L, with the pH adjusted to pH 10 using NaOH. In these tests, annealing at a temperature of 650°C for 1 hr was used to cause grain growth to simulate the effect of welding. Experiments were carried out at room temperature in aerated solution, and highly sensitive atomic force microscope measurements were made in an attempt to detect the smallest degree of grain boundary etching. Ryan et al. (1994) found no preferential attack at the weld region of electron-beam welded copper samples exposed to compacted buffer material at 100°C for periods of up to 5 years.

Gubner and co-workers (Gubner and Andersson 2007, Gubner et al. 2006) have studied the corrosion behaviour of welded OFP copper, produced by both electron-bean (EB) and friction-stir welding (FSW) techniques. No significant preferential weld corrosion was observed in either study. Gubner et al. (2006) used a scanning Kelvin probe to characterize possible potential differences between different areas on the weld prior to exposure to ammonium hydroxide solution at 80°C, an environment chosen because it is known to cause grain boundary etching of copper alloys. However, no grain boundary attack was observed after 14 days. A significant potential difference (90–200 mV) was observed between the weld and base metal, with the smaller potential differences for the FSW and the higher potential difference for the EB welded material.

In order to investigate the effect of this potential difference between weld and base material in more detail, Gubner and Andersson (2007) measured galvanic currents between various coupled weld sections. Electrodes were prepared from different locations on a friction-stir weld, a single EB welded sample, and also from the rotating friction stir tool piece itself. The FSW was performed with an "untreated" FSW tool, increasing the probability of contamination of the weld by particles from the tool. This type of weld is unrepresentative of modern FSW technology, in which surface-treated tools are used in order to minimise weld contamination. Coupled galvanic currents were measured in aerated 0.5 mol/L NaCl at pH 6.5, with additional E_{CORR} and polarization measurements in aerated and deaerated 0.01 mol/L and 0.1 mol/L NaCl (pH 8.5).

Overall, there were no indications of preferential corrosion of the weld. Galvanic currents between the weld and base material for FSW were low and no significant potential difference could be detected between the materials. The FSW tool is cathodic to the weld material, so that any particles from the tool that become incorporated into the weld material would be cathodically protected and would not corrode to create locally aggressive conditions (as can occur when Fe particles from carbon steel tools become embedded in fabricated structures).

The conclusion from these studies is that there is no evidence to indicate that the weld region should suffer higher corrosion rates than the rest of the canister shell. Both welding procedures appear to produce welds of acceptable corrosion performance. Of the two techniques, FSW provides better corrosion resistance than EB welding (Gubner and Andersson 2007), possibly because of the minimal grain growth and the absence of any resultant concentration of impurities at the grain boundaries for FSW.

5.2.6 *In situ* experiments

A number of *in situ* corrosion studies have been performed over the past 5–10 years in various national programmes. The most active programme has been that in Sweden where several corrosion-related studies have been performed at the Äspö Hard Rock Laboratory, including the Long Term Test of Buffer Material (LOT) (Karnland et al. 2000), the Canister Retrieval Test (CRT), and a study of atmospheric corrosion of copper in the underground laboratory (Taxén 2004).

The LOT experiments at the Äspö HRL consist of seven test parcels comprising a heater, copper cylinder, and compacted bentonite placed in a borehole for periods of 1–20 years. To date, two pilot tests (parcels S1 and A1) have been removed and examined (Karnland et al. 2000), as has parcel A2, which was also instrumented and monitored during exposure to granitic groundwater for a period of 6 years (Rosborg et al. 2003, 2004a, b, c, 2005).

A total of 8 copper coupons were exposed for a period of 1 year in pilot parcels S1 and A1. The groundwater at the Äspö location is a Na, Ca-based Cl^- solution, with a Cl^- concentration of ~0.18 mol/L (Rosborg et al. 2005). The groundwater itself is anoxic (E_H = –308 mV_{SHE}) but atmospheric O_2 will have been trapped in the test parcels and boreholes upon emplacement of the experiments. After ~1 yr exposure, the surfaces of the coupons were found to be covered by a duplex $Cu_2O/Cu_2CO_3(OH)_2$ (malachite) corrosion product, with significant diffusion of copper into the surrounding bentonite (Karnland et al. 2000). The estimated corrosion rate was 3 µm/yr. These results are similar to those observed by King and co-workers (King et al. 1992, 1997a, Litke et al. 1992) in long-term laboratory tests of copper corrosion in compacted clay. Another important conclusion from these experiments was that the entire surface was corroded and, although there was a tendency for surface roughening, there was no indication of localised corrosion in the form of discrete pits on the surface of any of the coupons. This observation is also consistent with the laboratory observations of King and co-workers and provides supporting evidence that the surface of copper canisters will not be subject to classic localised corrosion, as discussed in more detail below.

Various electrochemical techniques were used to provide real-time monitoring of the corrosion of coupons in the LOT test parcel A2 (Rosborg et al. 2003, 2004a, b, c, 2005). Corrosion rates were monitored using linear polarization resistance, harmonic distortion analysis, and electrochemical noise techniques. Average *in situ* corrosion rates were of the order of ~0.5 µm/yr (Rosborg et al. 2004c). Following decommissioning of the test, corrosion was again found to have been general in nature with an uneven surface morphology, but with no indications of pitting corrosion. Corrosion

products comprised both Cu_2O and γ-$Cu_2(OH)_3Cl$ (paratacamite). Again, these results are in good agreement with the results of long-term laboratory studies on which the corrosion mechanism illustrated in Figure 5-16 is based.

The Canister Retrieval Test was decommissioned in 2006 with the removal of the canister from the borehole after 6 years exposure (Sjöland and Bockgård 2006). Visually, little corrosion of the canister had occurred, as indicated by the appearance of the machining marks on the surface.

Taxén (2004) describes an atmospheric corrosion study at the Äspö HRL designed to determine the likely condition of the canister at the time of emplacement. Copper coupons were exposed to the humid sulphide-containing atmosphere of the HRL with and without compacted bentonite present. Tests were done at ambient temperature and, in the case of the test with bentonite, at 75°C. Corrosion rates were estimated based on mass loss or from electrochemical stripping of the corrosion products under galvanostatic conditions. Corrosion rates were < 0.1 μm/yr, significantly lower than typical surface atmospheric corrosion rates in Sweden, suggesting that the HRL atmosphere is less corrosive than normal surface atmospheres. The only corrosion product detected was γ-$Cu_2(OH)_3Cl$ (paratacamite), although the presence of Cu_2O is also likely and may not have been detected due to sampling artifacts (Taxén 2004).

An experiment similar to the LOT tests, known as the Buffer Coupon Long-term Test (BCLT), was conducted at AECL's Underground Research Laboratory in Canada. Near-horizontal boreholes were drilled in the walls of the URL at the 420-m level and filled with assemblies comprising blocks of compacted sand:bentonite buffer material with embedded copper and other types of coupons (Dixon et al. 2002). The groundwater at this depth is saline, with a total dissolved solids content of ~90 g/L. The experiment was terminated after 1.5 yrs, at which time the bentonite was analysed for the total and acid-soluble copper content and the corrosion rate of the coupons determined by weight loss (Dixon et al. 2004). The mean corrosion rate was estimated to be 0.21 μm/yr.

The results from the BCLT were used to validate the CCM code (King and Kolář 2006a). Based on three different simulations using different assumed mathematical boundary conditions, the predicted corrosion rate varied from 0.17–0.48 μm/yr, in good agreement with the experimentally observed value. Furthermore, the CCM code was able to predict the speciation of dissolved copper. The majority of copper in the bentonite from the experiment (99.8%) was in the acid-soluble form which, based on experimental work by Litke et al. (1992), is known to be Cu(II) adsorbed onto the bentonite clay. The CCM simulations predicted the fraction of Cu(II) species to vary between 52 and 91%. Thus, validation against the results of the BCLT experiment suggest that the CCM is capable of predicting both the corrosion rate and the speciation of dissolved copper in corrosion tests in compacted bentonite.

Corrosion coupons were also included in the FEBEX experiment at the Grimsel test site in Switzerland (Madina et al. 2004). Coupons of various materials, including tough-pitch copper (UBS C11000) were incorporated into heated blocks of bentonite and exposed for a period of 6 yrs. Whilst not primarily a corrosion test, weight-loss corrosion rates were obtained after the experiment and revealed a mean corrosion rate of ~0.7 μm/yr, although the duration of corrosion, and, hence, the maximum corrosion rate, is uncertain.

5.2.7 Miscellaneous corrosion processes

A number of other factors have been raised as possible issues for the long-term corrosion behaviour of copper canisters, including: the effect of Cu-iron galvanic couples on failed canisters, the effect of elevated pressure at repository depth, the effect of surface discontinuities on the corrosion behaviour of the canister, and the effect of methane on the corrosion of copper.

Once the outer copper shell has failed, the inner cast iron vessel will be exposed to groundwater. If the near-field environment still contains O_2 at the time of canister failure, a galvanic couple may develop between the copper shell and cast iron insert, with the iron most likely to be the anode with the reduction of O_2 occurring on the copper cathode. Alternatively, if the environment is anoxic at the time of canister failure then corrosion of the cast iron may proceed in the absence of corrosion of

the copper shell. Regardless, the formation of expansive cast iron corrosion products could induce stress in the failed copper shell which could increase the size of the defect in the shell. Smart et al. (2003, 2004, 2005) have studied the galvanic coupling of copper and cast iron, and found galvanic currents in both aerated and deaerated environments. Apparently polarisation of copper by contact with cast iron is sufficient to induce the reduction of H_2O on copper. However, regardless of the extent of galvanic corrosion, Smart et al. (2003) could find no evidence for an increase in stress due to the expansion of iron corrosion products.

A second factor that may affect the rate of corrosion is the increased pressure at repository depth. However, as discussed in Section 5.2.2, an increase in pressure from 0.1 MPa to 5 MPa will result in a < 10% change in the equilibrium $[CuCl_2^-]$, and a correspondingly small change in the corrosion rate. Mor and Beccaria (1979) observed a small effect of pressure on the anodic and, especially, the cathodic reactions involved in the corrosion of copper in seawater. The effect of pressure on the cathodic reaction is partially due to an increase in the concentration of dissolved O_2 with increasing O_2 partial pressure. Although this might also occur in a repository, due to the increase in pressure due to the development of the hydrostatic head, this effect neither increases the overall amount of O_2 nor the maximum extent of corrosion. In aerated systems over-pressurised with N_2 to a total pressure of ~4 MPa, Escobar et al. (2004) observed no effect of the system pressure on E_{CORR} and, by inference, the corrosion behaviour of copper.

King (2004) considered the effects of surface- and near-surface-breaking defects on the corrosion behaviour of copper canisters. Defects could arise from the welding process or be caused by impacts during handling and emplacement of the canisters. The effects of surface defects on both localised corrosion and stress corrosion cracking were considered. Localised corrosion initiates at a microscopic scale at grain boundaries and other surface defects (Al-Kharafi et al. 1989, de Chialvo et al. 1985, Shalaby et al. 1989). In comparison, surface weld or handling defects would be much larger and will not cause the local spatial separation of anodic and cathodic reactions that characterises localised corrosion. Surface defects, either pits or crack-like features, will lead to stress concentration (in the case of blunt defects) or stress intensification (in the case of crack-like features) and possible increased susceptibility to SCC. However, a sufficient stress or stress intensity is only one factor required for cracking. The main argument against SCC is that the permissive environments for cracking will not develop in the repository (Section 6). Therefore, it was concluded that surface defects are unlikely to compromise the integrity of the canisters.

The presence of high concentrations of methane in deep Finnish groundwaters (up to 400 mL/L (0.018 mol/L), Table 2-3) is expected to have no effect on the corrosion of the canisters. (Similar methane levels have not been reported in Swedish groundwaters (Tables 2-1 and 2-2), but must be considered possible since both Swedish and Finnish repositories would be constructed in the same type of geological formation). Although copper alloys are generally not used in applications involving natural gas, this is because of impurities in the gas, rather than due to the methane itself. Lyle (1993) showed that the corrosion rate of copper in natural gas depends primarily on the H_2S, O_2, and H_2O contents. The sulphur content of natural gas was also correlated with erosion in high-temperature methane-fueled combustion chambers (Walter et al. 1989). Mercaptans, added to impart odour to the gas, may also pose integrity concerns for copper alloys in natural gas facilities. Acidic natural gas combustion products have also been shown to cause corrosion of copper heat exchangers (Bühler 1993). However, in none of these studies is there any evidence that methane itself is deleterious towards copper alloys.

5.2.8 State-of-knowledge of the general corrosion of copper canisters

Much is known about the general corrosion behaviour of Cu under repository conditions. Detailed thermodynamic analyses of possible corrosion reactions have been performed, particularly in the Swedish and Finnish programmes. In Canada, more emphasis has been placed on kinetic studies under well-controlled mass-transport conditions. Combined, these complementary approaches provide a detailed understanding of the general corrosion behaviour of copper canisters under the evolving conditions expected in a repository. The results of laboratory studies have been confirmed by the observations from long-term *in situ* tests under relevant conditions in underground research laboratories.

The most important parameters controlling the rate of general corrosion are: the rates of mass transport of species to and from the canister surface, the availability of O_2, the influx of Cl^- ions from the groundwater, and the supply of sulphide ions to the canister.

In a sealed repository, the extent of general corrosion is limited by the general lack of oxidants. Trapped atmospheric O_2 will support corrosion in the initial stages of the evolution of repository conditions, but the amount of available O_2 is limited and will be partially consumed by reaction with oxidisable minerals (principally sulphide minerals) in the repository. Under reducing conditions, corrosion will be supported by the slow supply of sulphide to the canister surface.

5.3 Localised corrosion

As our general understanding of the corrosion behaviour of copper under repository conditions has improved, so too has our understanding of the possibility of localised corrosion of the canisters. Historically, a conservative approach has been taken because of a lack of evidence from laboratory and *in situ* tests under realistic environmental conditions. In the absence of such information, it was necessary to assume that the canisters might be susceptible to a classical form of pitting attack. Conservative allowances were made for the extent of pitting of the canister. In light of more-recent information obtained under simulated disposal conditions, it is apparent that copper will not undergo pitting in the classical sense of the term, but will instead undergo general corrosion with some unevenness or surface roughening.

Much of the information in this section discusses the classical forms of pitting corrosion and various methods to predict the extent of such damage. This information is provided for historical perspective only and should not be interpreted as reflecting our current understanding of the corrosion behaviour of copper canisters in repository environments.

Localised corrosion refers to a range of corrosion phenomena that result in localised, as opposed to general, attack and which do not fall under the category of environmentally assisted cracking. For pure Cu alloys, which do not undergo dealloying, the most important form of localised corrosion is pitting. Before considering pitting in some detail, two other forms of localised corrosion of Cu will be briefly discussed: crevice corrosion and "ants-nest" corrosion.

Crevice corrosion is of significant concern for many alloy systems, especially passive materials containing alloying elements which strongly hydrolyse and can form locally acidified environments in occluded regions. The hydrolysis of Cu(I), especially when complexed by Cl^-, is weak (Baes and Mesmer 1976), and local acidification in crevices is unlikely to occur. Cupric species hydrolyse more strongly, but, as argued above, the formation of Cu(II) requires the presence of O_2, and is unlikely to occur in occluded regions, such as crevices, where O_2 access is restricted. As a consequence, the crevice corrosion of pure Cu is uncommon, and when it is observed occurs via a differential Cu-ion concentration cell mechanism, with areas exposed to a high Cu-ion concentration acting as cathodic sites supporting the dissolution of areas in contact with a low concentration of dissolved Cu. This form of localised corrosion, however, is inherently self-limiting, because the differential [Cu] cell driving localised corrosion is destroyed by the dissolution itself. In long-term irradiated corrosion tests under the simulated conditions of a Canadian repository, no crevice corrosion was observed on either creviced U–bend of creviced planar samples (Ryan et al. 1994).

Ants-nest corrosion is a peculiar form of corrosion specific to Cu (Corbett and Elliot 2000). It is associated with the presence of formic acid and results in localised dissolution of the material to produce a honeycomb-like ants-nest appearance. The phenomenon appears to be restricted to Cu alloy components in air-conditioning equipment. Ants-nest corrosion can be simulated in the laboratory in the presence of moist air and an organic acid, conditions unlikely to prevail in the repository.

5.3.1 Surface roughening of copper exposed to repository environments

A number of corrosion studies have been performed under conditions that simulate the canister near-field environment. Copper coupons have been exposed to compacted buffer material wetted by (initially) aerated saline pore waters, and exposed for extended periods of time (up to 2 years)

usually at elevated temperature (Aaltonen and Varis 1993, Karnland et al. 2000, King et al. 1992, 1997a, Litke et al. 1992). These experiments simulate the likely environmental conditions soon after emplacement of the canisters and saturation of the buffer material. It is during this period in the evolution of repository conditions that localised corrosion is most likely, since the environment will be oxidising. Furthermore, the pore-water [HCO_3^-] may be significant because of the dissolution of carbonate minerals and the [Cl^-] may be sufficient to cause film breakdown, but not so high as to cause general dissolution of the surface. Thus, short-term lab and field tests can be used to study the period of most aggressive localised corrosion.

Despite the relative aggressiveness of the conditions in such tests, no evidence for pitting has been observed. Thus, both Aaltonen and Varis (1993) and Karnland et al. (2000) report no localised corrosion of Cu exposed to compacted clay over periods of up to 2 years. The only instance of non-uniform corrosion reported under such conditions is the so-called under-deposit corrosion reported by Litke et al. (1992). An example of the surface roughness observed is shown in Figure 5-20. The most important observation from Figure 5-20 is that the entire surface has corroded, albeit to different extents. This, therefore, is not an example of pitting corrosion in the classical sense of permanently separated anodic and cathodic sites. Because the entire surface has corroded, the anodic reaction must have occurred generally across the surface. The non-uniform nature of the attack suggests that either the rate of the anodic reaction was not uniform over the surface or that anodic and cathodic sites were only temporarily spatially separated.

The extent of surface roughening by under-deposit corrosion has been studied in Canada (Brennenstuhl et al. 2002). The electrochemical noise between coupled electrodes, one immersed in bulk solution and the other exposed to a freely swollen 1:1 bentonite:sand mixture, was measured as a function of various factors. Of the various factors studied, temperature, [O_2] and pH had the greatest effect on the extent of localised corrosion. Preliminary results suggested that the degree of localisation of corrosion in a repository should decrease with time as the canister temperature and the [O_2] decrease. A mean roughness of 12.4 μm was predicted, with a maximum peak-to-trough surface roughness of 88 μm.

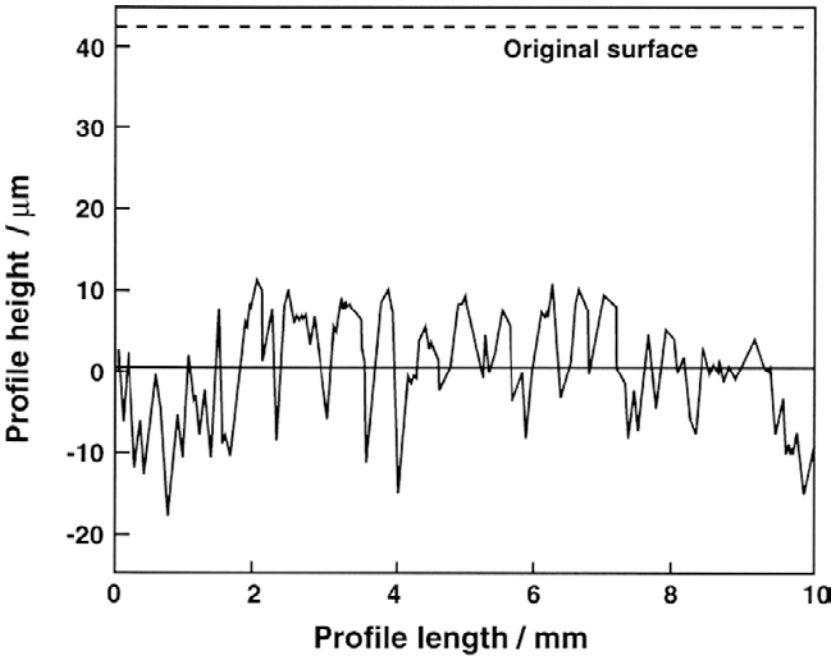

Figure 5-20. *Typical surface profile of stripped copper coupon following exposure to groundwater-saturated compacted buffer material at 50°C for 733 d (Litke et al. 1992).*

5.3.2 Experimental studies of the pitting corrosion of copper

Pitting of Cu has been investigated in relation to a number of different applications of Cu alloys and for various environments. The best-known phenomenon is the pitting of Cu water-distribution pipes. These studies are of limited use for predicting the pitting behaviour of Cu canisters, however, because of the difference in salinity between fresh potable waters and saline pore waters. However, a number of Cu pitting studies have also been reported in Cl^- solutions, with and without the addition of HCO_3^-.

Pitting of Cu water pipes has been studied extensively since the 1960's. At least three types of pitting have been recognised; Types I and II pitting (Mattsson 1980) and a type of pitting apparently induced by microbial activity (Fischer et al. 1988). Types I and II pitting occur under distinctly different conditions, Type I pitting being associated with cold, hard and moderately hard waters free of naturally occurring inhibitors, but containing HCO_3^-, SO_4^{2-}, Cl^- and O_2, and on Cu pipes with a residual surface carbon film remaining from the manufacturing process (Mattsson 1980). Pit initiation involves the formation of a CuCl "pocket" in an otherwise protective Cu_2O film. Dissolution of Cu as $CuCl_2^-$ occurs at the defect produced by the CuCl pocket. The dissolved Cu(I) is oxidised to Cu(II) by O_2 and precipitates forming a crust of $CuCO_3{\cdot}Cu(OH)_2$ and $CaCO_3$. The crust forms an occluded region in which localised dissolution continues. There is some question regarding the location of the cathode, with some favouring a classic mechanism involving the cathodic reduction of O_2 on exposed surfaces outside the pit, and others suggesting that both anodic and cathodic reactions are located within the occluded region formed by the $CuCO_3{\cdot}Cu(OH)_2/CaCO_3$ cap (Campbell 1974, Lucey 1967). A threshold potential for pit propagation has been defined (in terms of the potential of the exposed surface), with a value of between 0.06 V_{SCE} and 0.17 V_{SCE} (Campbell 1974).

Type II pitting is associated with hot potable waters (> 60°C) with a pH < 7.4 and a $[HCO_3^-]:[SO_4^{2-}]$ ratio < 1, and tends to produce pits with a larger depth:width ratio than the approximately hemispherical pits characteristic of Type I pitting. A specific form of Type II pitting has occurred in Japan, in which residual Cl_2 from sterilisation procedures was sufficient to increase the E_{CORR} above the pitting potential of 0.115 V_{SCE} to 0.16 V_{SCE} (Fujii et al. 1984, Kasahara and Komukai 1987, Kasahara et al. 1988, Suzuki et al. 1983).

Although pitting studies in potable waters may not be directly relevant to the pitting of Cu canisters in saline pore waters, the proposed mechanisms provide some insight into the possibility of localised corrosion in a repository. It is useful to consider three phases in the life of a pit; birth, propagation, and death. The initiation of Type I pits is associated with the formation of CuCl underneath a porous Cu_2O layer. The higher $[Cl^-]$ encountered in deep groundwaters may either make pit initiation more likely, or may induce so many defects in the Cu_2O layer that the surfaces dissolves generally (active dissolution) as opposed to locally as pits (passive behaviour).

Oxygen is a pre-requisite for pit propagation. In Type I pitting, O_2 either serves directly as the oxidant supporting pit growth, or oxidises Cu(I) to Cu(II), with the latter species then acting as the oxidant. The reduction of O_2 to OH^- also produces local alkalinity, which supports and maintains the crust over the pit, which in turn maintains local acidity within the pit and sustains pit growth. A decrease in $[O_2]$ would result in less Cu dissolution and an increase in the pit pH, both of which would eventually cause the pit to stop propagating. Pitting of Cu water pipes is only sustained because of the high $[O_2]$ in fresh water and because it is continually replenished by the movement of water in the pipe. This would not be the case for pits on Cu canisters, both because of the limited amount of O_2 available and because of the restricted mass-transport conditions which will limit the supply of O_2 to the corrosion sites. Therefore, pits on Cu canisters will be far more likely to die than those on Cu water pipes.

Studies of the pitting of Cu in concentrated Cl^- and Cl^-/HCO_3^- solutions have been concerned with initiation events and the determination of breakdown potentials (E_b). These experiments are generally performed electrochemically under potential control and, therefore, provide information about film breakdown and pit growth under conditions where the cathodic reaction is not rate limiting. The results have been used to interpret the behaviour of Cu in fresh waters, since concentration of the low levels of Cl^- and HCO_3^- in fresh waters may be a precursor to pit initiation. They are also of use in predicting the possibility of localised corrosion of Cu canisters in more saline conditions.

Figure 5-21 shows the variation of E_b with log [Cl^-] for Cu in Cl^- and Cl^-/ HCO_3^- mixtures from a number of literature studies. There is a wide variation in the data, partly because of the use of different [HCO_3^-] in some of the studies, but also because E_b is a distributed, stochastic parameter. (Excluded from Figure 5-21 are the E_b data from Drogowska et al. (1992) in HCO_3^- -free Cl^- solutions. These authors appear to have misinterpreted the active dissolution of Cu in Cl^- solutions as being due to the breakdown of a protective film (King and Kolář 2000)).

Despite the wide spread in the E_b data in Figure 5-21, the trends observed by various workers are reasonably consistent. In Cl^-/ HCO_3^- mixtures, HCO_3^- promotes passivation, whereas Cl^- promotes pitting. At a constant [HCO_3^-], E_b decreases with increasing [Cl^-] (see, for example, the data of Imai et al. (1996) at [Cl^-] of 0.005, 0.016 and 0.049 mol·dm^{-3} in Figure 5-21). Bicarbonate ions promote passivity more strongly than Cl^- ions promote film breakdown. This can be seen from the results of Drogowska et al. (1992), in which E_b was determined in solutions with equal concentrations of HCO_3^- and Cl^- (the fitted line 3 in Figure 5-21). Thus, E_b increases with increasing concentration (of both Cl^- and HCO_3^-), as opposed to the decrease in E_b with increasing [Cl^-] at constant [HCO_3^-]. For pore-waters containing between 0.001 mol·dm^{-3} and 0.1 mol·dm^{-3} Cl^- and with up to 0.02 mol·dm^{-3} HCO_3^-, E_b will be in the range from approximately –0.1 V_{SCE} to +0.3 V_{SCE}. Higher [HCO_3^-] will lead to more-positive E_b values, especially at lower [Cl^-]. In HCO_3^--free Cl^- solutions, E_b is quite positive, consistent with the trend towards active dissolution in Cl^--solutions.

There have been relatively few systematic studies of the effect of pH on E_b. The E_b values shown in Figure 5-21 were determined in the pH range 7–9. Laz et al. (1992) report a linear dependence of E_b on pH in the range pH 7–11 in 1 mol·dm^{-3} $NaClO_4$, with E_b increasing with pH (dE_b/dpH = 27 mV) presumably because of the greater stability of the passive layer with increasing pH. In alkaline solutions (pH > 12), the passive layer comprises an inner layer of Cu_2O and an outer passivating layer of either $Cu(OH)_2$ (at temperatures less than 35°C) or CuO (T > 35°C) (Shoesmith and Lee 1977). However, Cl^- ions will compete with OH^- ions for surface adsorption sites and for complexation of dissolved Cu ions, thus interfering with the film formation process. Chloride will stabilise Cu(I) species, possibly preventing the formation of the passive Cu(II) outer layer. Thus, the structure of the film in alkaline saline environments, and the propensity for localized corrosion, will depend on whether the surface is exposed to alkaline environments prior to being exposed to Cl^- ions, or vice versa.

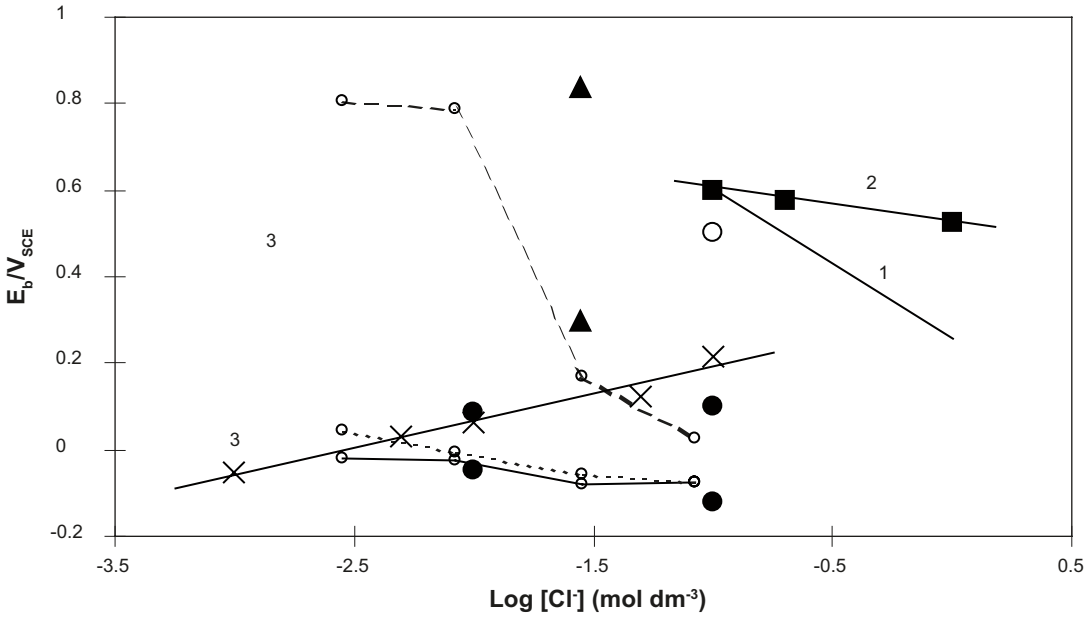

Figure 5-21. *Dependence of pitting (breakdown) potential E_b on chloride concentration in Cl^- solutions and in Cl^-/HCO_3^- mixtures at 25°C. The data were recorded potentiodynamically but have been corrected to zero scan rate to aid inter-comparison (as described by King 2002). No correction has been made for the variation of E_b with pH. Data from references (○) Qafsaoui et al. (1993), (▲) Sridhar and Cragnolino (1993), (●) Thomas and Tiller (1972a, b), (■) Nishikata et al. (1990), (×) Cl^-/ HCO_3^- mixtures of Drogowska et al. (1992), (-○-) Imai et al. (1996). Line 1 based on expression from de Chialvo et al. (1985), line 2 fitted to data of Nishikata et al. (1990), line 3 fitted to Drogowska et al. (1992) Cl^-/ HCO_3^- data.*

King (2002) considered the effect on the localised corrosion of copper of an increase in pore-water pH due to an alkaline plume from cementitious material in the repository. If the pore-water pH increases prior to the establishment of anoxic conditions, the canister surface will passivate as the pore-water pH exceeds a value of ~pH 9. Passivation will result from the formation of a duplex $Cu_2O/Cu(OH)_2$ film. Experimentally, the corrosion potential is found to correspond to the equilibrium potential for the $Cu_2O/Cu(OH)_2$ couple under oxic conditions, or by the Cu/Cu_2O redox couple under anoxic conditions (in the absence of sulphide) (King 2002 and references therein). Pitting corrosion is only likely to occur early in the evolution of the repository environment, whilst the canister is still relatively cool (< 40°C), whilst there is still O_2 available to support localised corrosion, and prior to the increase in pore-water pH and salinity. The subsequent increase in canister surface temperature, pore-water pH and salinity, and decrease in $[O_2]$ will make pit initiation less likely, although the canister will remain passive provided the pore-water pH is maintained above pH 9. The higher the pore-water pH, the more strongly the canister is passivated and the less likely the surface is to undergo localised attack because the difference between the breakdown and corrosion potentials increases with pH (King 2002). If the pore-water salinity increases prior to the increase in pH, there could be a period of active canister corrosion before passivation occurs. Under these circumstances, the corrosion potential will be a true mixed potential, determine by the relative kinetics of Cu dissolution as $CuCl_2^-$ and of the reduction of O_2.

In the presence of sulphide, the development of anoxic conditions and an increase in pore-water sulphide concentration will result in the formation of a Cu_2S surface film. Increasing pH due to an alkaline plume will tend to enhance the protectiveness of this film, because of the decrease in solubility of Cu_2S. At the same time, pitting corrosion will become less likely, since the corrosion potential will shift to more-negative values and the pitting potential to more-positive values with increasing pH. As in sulphide-free environments, therefore, there appears to be little threat to the integrity of the canister from an increase in pore-water pH (King 2002).

There are relatively few studies of the effect of temperature on E_b. Thomas and Tiller (1972b) report a linear decrease in E_b with increasing temperature, of approximately –0.8 V/°C. Of more importance than the absolute value of E_b is the difference between E_b and E_{CORR}, which Thomas and Tiller reported was constant because of the corresponding decrease of E_{CORR} with increasing temperature. Conversely, Drogowska et al. (1994) reported a substantial increase in E_b with increasing temperature, amounting to +7.2 mV/°C. Sridhar and Cragnolino (1993) reported a tendency away from localised corrosion to general corrosion with increasing temperature, which would imply an increasing value of $(E_b - E_{CORR})$ with increasing temperature.

A related parameter to E_b is the repassivation potential E_{rp}. Whereas E_b is the potential at which pits initiate, E_{rp} can be viewed as the potential at which propagating pits cease to grow. Widely used as a criterion for localised corrosion in the U.S. Yucca Mountain project, the use of E_{rp} is proposed as a more conservative measure of pitting susceptibility than E_b since E_{rp} is invariably more negative than E_b and should be subject to less scatter compared with the potential for the stochastic pit initiation process. Relatively few values of E_{rp} have been reported for Cu in relevant conditions. Sridhar and Cragnolino (1993) report E_{rp} values of 0.37 V_{SCE} and 0.07 V_{SCE} for Cu in solutions containing 0.14 mol·dm^{-3} HCO_3^-, 0.028 mol·dm^{-3} Cl^-, and either $2 \cdot 10^{-4}$ mol·dm^{-3} or 0.01 mol·dm^{-3} SO_4^{2-}, respectively.

There have been a number of studies of the passivation of Cu in HCO_3^- solutions. In Cl^--free solutions, passivation proceeds via the formation of a thin interfacial layer of $CuCO_3$ (formed from either Cu_2O or $Cu(OH)_{ADS}$ precursors), with the eventual precipitation of basic Cu(II) carbonate ($CuCO_3 \cdot Cu(OH)_2$) (Pérez Sánchez et al. 1990, 1993). These processes will be hindered in Cl^--containing solutions because of the competition between Cl^- and HCO_3^- for the interfacial $Cu(OH)_{ADS}$ species. Sirkiä et al. (1999) have identified a bilayer film structure on Cu in neutral HCO_3^- solutions, comprising an inner layer of semi-conducting Cu_2O and an outer layer of Cu(II) species. At relatively modest potentials (at which Cu(I) is the stable species), the rate of the anodic reaction is limited by the transport of ionic defects through the interfacial Cu_2O film. With increasing potential, and presumably also in the presence of Cl^- (although this was not investigated in this study), the number of charge carriers in the Cu_2O film increases, and the rate of oxidation becomes partially controlled by the rate of charge transfer reactions on the defected Cu_2O layer. Based on electrochemical studies, Imai et al. (1996) have classified the behaviour of Cu in Cl^-/ HCO_3^- mixtures

as being either active, passive, or active-passive (the latter characterised by a limited passive range). In HCO_3^- solutions, passive behaviour was observed for concentrations ≥ 0.016 mol·dm^{-3} (1,000 mg/L), with either active or active-passive behaviour at lower [HCO_3^-]. The addition of Cl^- promoted active-passive behaviour, especially for [Cl^-] ≥ 0.01 mol·dm^{-3} (~300 mg/L). Sulphate ions were also found to promote the breakdown of passive films formed in HCO_3^- solutions, although SO_4^{2-} was less aggressive than Cl^-.

Localised corrosion of Cu has been reported in sea water polluted by sulphide, but only under conditions of alternating aerated and deaerated conditions. As discussed above, cyclic redox conditions can disrupt the otherwise protective surface film (either Cu_2O or Cu_2S/CuS). In marine applications, disruption of the surface film is exacerbated by flow effects, which further destabilise the protective layer. Such alternating redox conditions are not expected in a repository.

Vasquez Moll et al. (1985) considered the breakdown of sulphide films on Cu and the onset of localised dissolution. An E_b value of –0.74 V_{SCE} was reported in 0.01 mol·dm^{-3} HS^-, which shifted to more-positive values with decreasing HS^- concentration. Thus, E_{CORR} is ~200 mV more negative than E_b in sulphide solutions, based on the E_{CORR} values in sulphide solutions in Figure 5-13. Escobar et al. (1999) observed pitting on Cu-OF samples in sulphide solutions at a potential of –0.218 V_{SCE}. Pitting was observed in 0.001 mol·dm^{-3} sulphide, but to a smaller degree if passivating species such as HCO_3^- ions were also present. This lead Escobar et al. (1999) to suggest that a threshold sulphide concentration might exist below which pitting does not occur. In addition, the potentials at which these studies were performed are many hundreds of mV more positive than those likely in a repository, also making pitting of copper canisters unlikely. Provided conditions within the repository remain reducing, therefore, localised corrosion due to the breakdown of the protective Cu_2S film seems unlikely, although the possibility of the spatial separation of anodic and cathodic sites (the reduction of H_2O on the conducting Cu_2S film coupled to anodic dissolution at defects in the surface layer) has yet to be resolved.

5.3.3 Modelling approaches for the pitting corrosion of copper

No detailed predictive model for the type of surface roughening that is expected to occur on the canisters has been developed. Much of the discussion in this section is of various methods for predicting the initiation and/or growth of pits. As noted above, our current understanding is that the canisters will not be subject to pitting in the classical sense of the term, and the information given below is provided for historical perspective only.

The approach taken to model the long-term localised corrosion behaviour of the canister depends on the nature of the available data. If the pitting mechanism is known then detailed mechanistic models can be developed. Such models can provide information about either the initiation or growth of pits. Alternatively, if E_b and E_{CORR} data are available, the probability of pit initiation can be predicted. Finally, measured pit depths can be statistically or otherwise analysed and predictions of pit growth on canisters made based on the depths of pits from shorter exposure periods.

Taxén (1996, 2000, 2002a, b) and Taxén and Puigdomenech (2001) have described a model for the growth of pits based on mass transport and chemical equilibrium principles. Continued growth of the pit is contingent on the transport of reactants to the base of the pit, where the anodic reaction is located, and the transport of dissolved Cu out of the pit (Figure 5-22). Both solid and dissolved corrosion products are assumed to form within the pit. If sufficient Cu is not transported out of the pit, the corrosion products in the pit become so dense and non-porous that growth is stifled and the pit dies.

Mass transport into and out of the pit is by a combination of diffusion and migration and is simulated by a 1-D mass-balance equation of the form

$$j_i = -\frac{c_i D_i}{RT} \cdot \frac{\partial \mu_i}{\partial x} \qquad 5\text{-}27$$

where j_i, c_i and D_i are the flux, concentration and diffusion coefficient of species i, and μ_i is the chemical potential, given by

$$\mu_i = \mu_i^0 + RT \ln a_i + z_i F\Phi \qquad 5\text{-}28$$

where a is the activity, z is the charge, F is Faradays constant and Φ is the electrical potential. The pit geometry is simulated by a series of hemispherical shells (with a constant surface area:thickness ratio) describing both the pit in the metal and the cap of porous corrosion products (Figure 5-23). Chemical reactions between various species are assumed to be fast relative to the rate of mass transport, so that equilibrium chemical conditions can be used.

The fraction of corrosion products precipitating as a solid compared with the fraction that are transported out of the pit is decisive in determining whether the pit can continue to grow. Based on the relative molar volumes of Cu and of either Cu_2O or CuCl, a certain fraction of the corrosion products must be transported out of the pit to avoid starvation of the pit. If Cu_2O is precipitated within the pit, ≥ 40% of the corroded Cu must be transported out of the pit for continued pit propagation. If CuCl forms within the pit, this fraction is even larger (≥ 70%).

If ≥ 40% of the corrosion products are to be transported out of the pit, local acidification within the pit is necessary to avoid precipitation of the corrosion products. Acidification results from the formation of Cu_2O

$$2Cu + H_2O = Cu_2O + 2H^+ + 2e^- \qquad 5\text{-}29$$

The equilibrium expression for reaction 5-29 defines a combination of potential and pH for the formation of Cu_2O, the lower the pH the higher the potential, and vice versa. The potential at which the transported fraction of the corroded copper is equal to 40% is termed the minimum potential for pit propagation. Potential drops in the solution caused by diffusion potentials and the passage of current were added. Activity coefficients were calculated as a function of ionic strength using the Davies' method (Section 3.5.1).

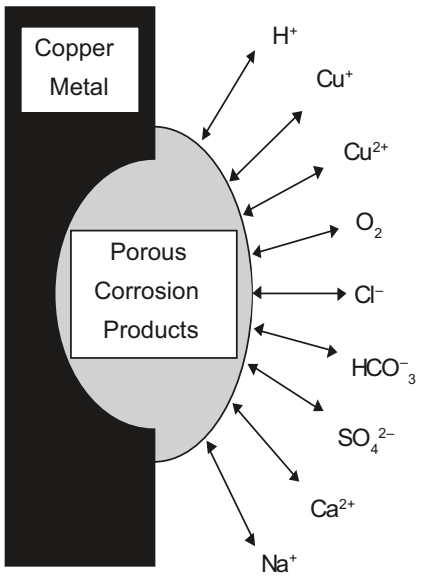

Figure 5-22. *Schematic illustration of the site of a corrosion pit in copper with aqueous species diffusing and migrating.*

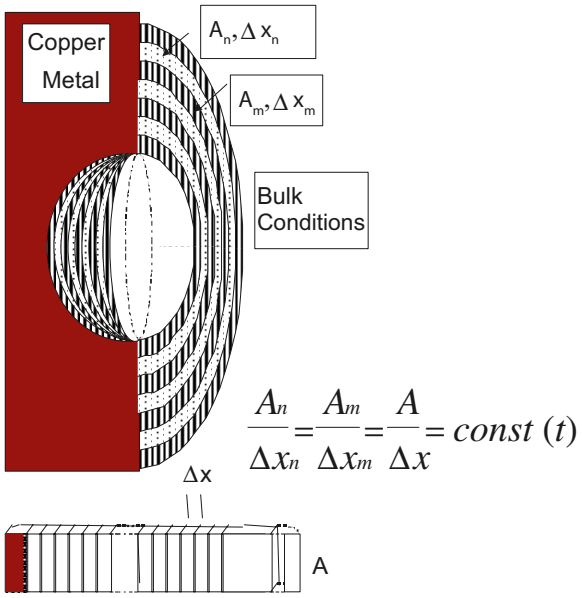

Figure 5-23. *Description of the site of a corrosion pit as consisting of thin shells. A is the cross-sectional area and Δx the thickness of the shell.*

Figure 5-24 shows the predicted conditions of potential and [Cl^-] for pit propagation. A number of conclusions about the role of various components in the water in the pitting process were drawn from the calculations:

- The pH of the bulk water outside the corrosion pit has a small influence on the minimum potential for pit propagation. The stability of the cuprous oxide against oxidation decreases with increasing pH. The potential window where reduction at a cuprous oxide surface can drive the anodic dissolution in a corrosion pit decreases with increasing pH. Pitting of copper is less likely to occur at high pH values.
- Expressing the difference between the minimum potential for propagation of a corrosion pit and the upper potential for stability of cuprous oxide as a margin against pitting, it is found that for a given pore-water composition, the value of this margin increases with temperature. Pitting is less likely to occur at higher temperatures.
- Of the common anions, chloride is the most aggressive species towards copper. Strong complex formation of chloride with monovalent copper allows high copper concentrations in contact with corroding copper metal. The chloride concentration is decisive for the value of the minimum pitting potential of copper. Using the margin against pitting as a criterion, it is found that the value of this margin decreases with increasing chloride concentration. Pitting is, according to this criterion, more likely to occur in waters with high chloride concentrations.
- Carbonate forms strong complexes with divalent copper. Carbonate is more aggressive at the higher pH of the bulk than at the lower pH in a corrosion pit. A high carbonate concentration may facilitate the anodic reactions in general corrosion. The buffering capacity of bicarbonate at moderately low pH values facilitates the transport of acidity out of the pit. An increased transport rate for protons, in the form of carbonic acid, favours the formation of cuprous oxide in the pit rather than the competing formation of aqueous copper species. A high carbonate concentration may increase the value of the minimum pitting potential and decrease the value of the upper stability potential for cuprous oxide. Pitting is less likely to occur in water with high carbonate concentrations.
- Sulphate forms a complex with divalent copper. Sulphate is aggressive towards copper in a corrosion pit and almost inert with respect to the general corrosion. Pitting is more likely to occur in waters with high sulphate concentrations.

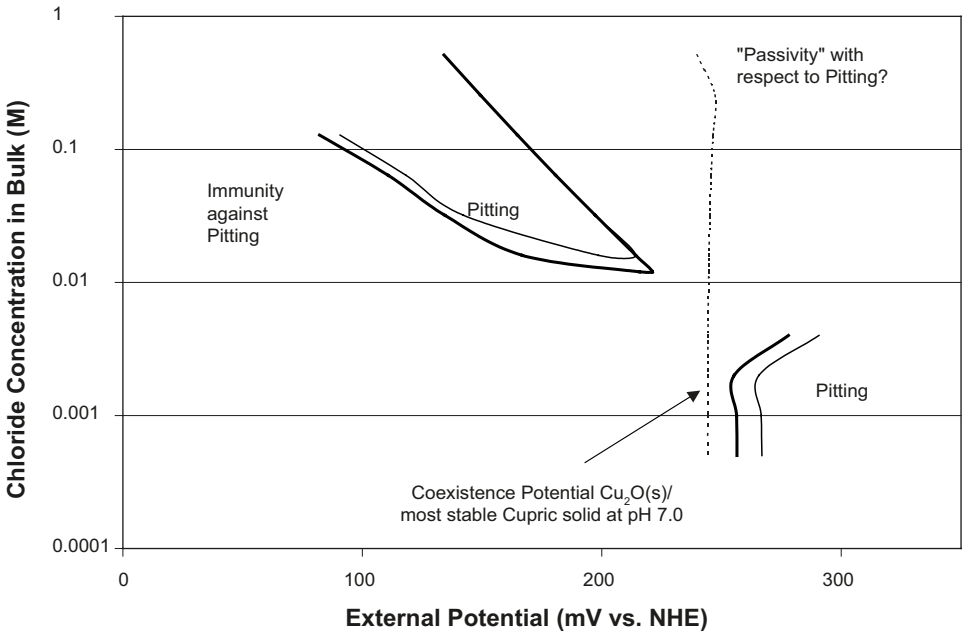

Figure 5-24. *Potential – chloride concentration diagram identifying conditions for pit propagation. The thick line indicates that the fraction of the oxidised copper which is transported away from the site of the oxidation as aqueous species is equal to 0.4, the thin line indicates conditions corresponding to the transported fraction equal to 0.5.*

- Calcium may have an indirect beneficial effect. For a water with a high sulphate concentration, pitting is less likely to occur if the calcium concentration is of the same magnitude or higher.
- Oxygen at low concentrations can also give potentials higher than the minimum pitting potential. The influence at the site of the pit of the direct oxidation of monovalent copper to divalent has a small influence on the minimum pitting potential.
- Corrosion pits where the transport of copper is dominated by monovalent copper may lead to precipitation of large amounts of porous cuprous oxide in and outside the cavity. Where the transport is dominated by divalent copper, precipitation, in the form of basic salts, occurs at higher pH values and outside the cavity.
- Precipitation in the cavity decreases the aqueous cross sectional area available for diffusion and migration to a higher extent than precipitation outside the cavity. Pits where the precipitation occurs mainly outside the cavity have higher growth rates.
- Factors favouring the type of pits dominated by monovalent copper are high chloride contents in the bulk water and high temperature. Factors favouring the type of pits dominated by divalent copper are a high sulphate concentration, low concentrations of other salts and a high potential.
- Pitting of copper has been observed in waters with a composition and temperature such that the minimum pitting potential is in a range where cuprous oxide is not stable at the pH of the bulk water.
- Pitting of copper is possible in a wide range of solution compositions. In some waters a corrosion pit will not propagate unless the cuprous oxide at the external surface is stabilised or if there is electronic contact with a conducting, more noble phase.
- Limits of the propagation rates for corrosion pits in copper can be given only as conditional depending on the corrosion potential.
- In waters with chloride contents approaching that of sea water, pitting is possible with high propagation rates and at high pH values.

For saline solutions with a Cl^- concentration > 0.02 mol·dm^{-3}, the model can be simplified and analytical expressions used to define the minimum pitting potential and the fraction of Cu transported out of the pit (tf) as a function of pit pH, bulk [Cl^-] and total carbonate concentration. Figure 5-25 shows the predicted fraction of transported Cu as a function of pit pH for two different bulk [Cl^-]. For pit propagation, the pH inside the pit must be less than ~pH 5, with a corresponding minimum pitting potential of 0.17–0.19 V_{SHE} (–0.07 to –0.05 V_{SCE}, respectively) (bulk total carbonate concentration of 0.064 mol·dm^{-3}). Figure 5-26 shows the distribution of predicted minimum pitting potentials as a function of [Cl^-] and total carbonate concentration (to convert the NHE scale in Figure 5-26 to the SCE scale used in Figure 5-21, subtract 0.24 V from the NHE scale). The predicted minimum pitting potentials are 100–200 mV lower than the observed E_b values in Figure 5-21. The predicted temperature dependence of the minimum pitting potential is similar to that observed by Thomas and Tiller, amounting to –1.4 mV/°C.

Taxén (1991) has also developed a pit propagation model for Cu in reducing conditions in the presence of sulphide. The pit growth rate was assumed to be limited by the rate of supply of HS^- to the base of the pit by diffusion through either the buffer material or through a porous deposit of precipitated Cu_2S in the pit (Taxén 1991). Two pit geometries were considered: a cylindrical pit of radius r_p, in which the sides of the pit are passive and dissolution only occurs at the pit bottom, and a hemispherical pit. In both cases, diffusion within the pit and within a hemispherical region of buffer adjacent to the pit mouth was assumed to be at steady state. Under these conditions, the pit growth rate was limited by the slower of the two diffusion processes (diffusion through the buffer or diffusion within the pit), which, given that the pit was assumed to be coupled to a semi-infinite hemisphere of buffer, is likely to be the supply of HS^- to the pit mouth. The assumption of steady-state concentration profiles underestimates the flux of HS^- during the transient period when the [HS^-] gradient will be much steeper. To overcome this problem, the steady-state concentration profiles were assumed to be established at an undefined time t_0, at which time the pit depth was p_0. The analyses performed predicted the growth of the pit during the subsequent steady-state period. For a bulk [HS^-] of 1 μg.g^{-1} and a pre-existing pit depth of 0.5 cm, the pit was predicted to grow by a further 0.5 to 1.1 cm in the subsequent 10^5 years.

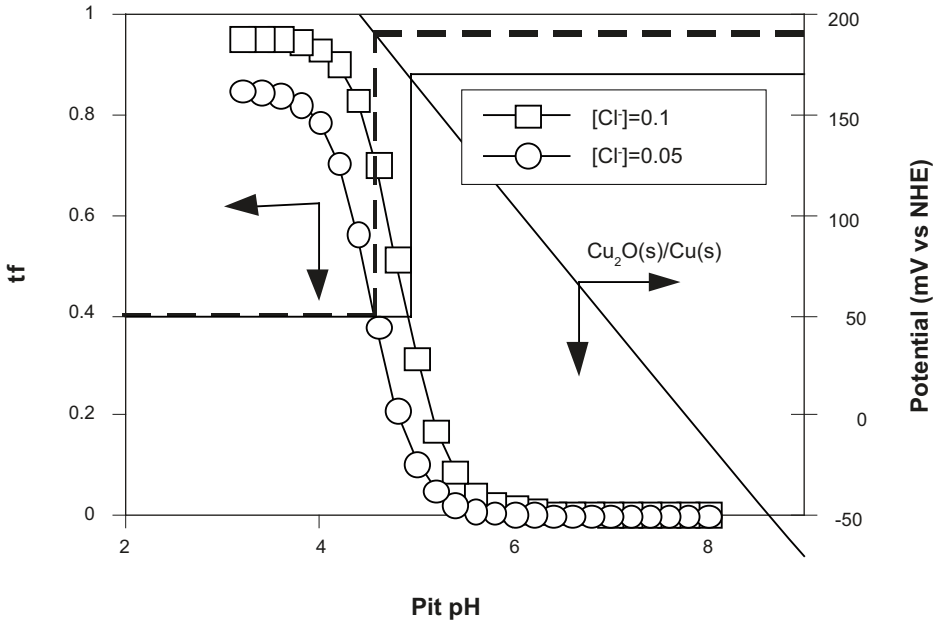

Figure 5-25. *Calculated values of the fraction of Cu transported out of the pit (tf) as a function of the local pH at 25°C and bulk* $[CO_2]_{tot} = 0.064$ *mol·dm*$^{-3}$.

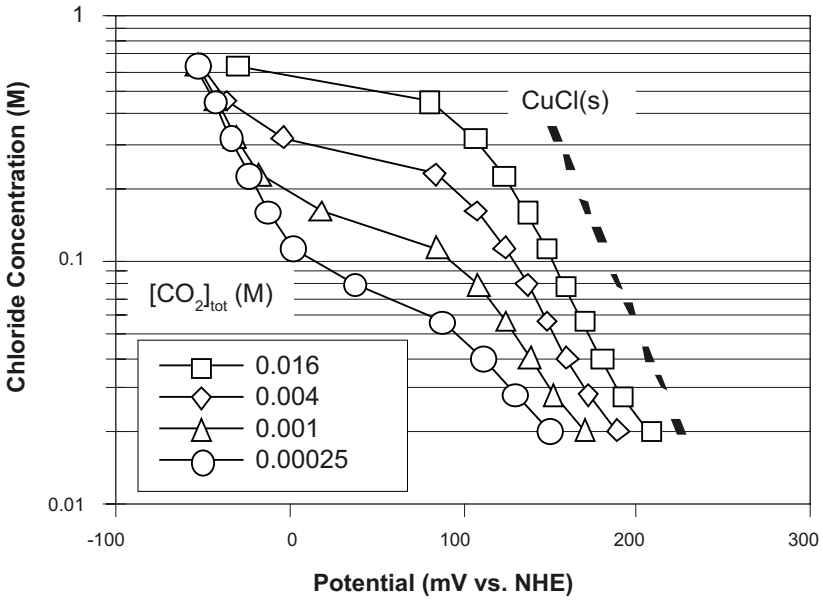

Figure 5-26. *Predicted minimum pitting potential as a function of the bulk chloride concentration at 25°C for various bulk total carbonate concentrations.*

King and Kolář (2000) have proposed a conceptual model to account for the type of surface roughening observed on Cu exposed to compacted buffer material illustrated in Figure 5-20. In this model (Figure 5-27), pits initiate stochastically over the surface and grow at a rate inversely proportional to the pit size, based on the assumption that the area of the cathode supporting pit growth is constant. Pit death, as a result of the accumulation of corrosion product on either the anodic or cathodic sites, would also be simulated by a stochastically distributed pit death parameter. A series of such randomly distributed pit initiation, growth and death processes would result in the type of roughened surface observed experimentally. Some information on pit initiation rates is available (Qafsaoui et al. 1993), but no data currently exists on the distribution of pit growth and death rates under repository conditions.

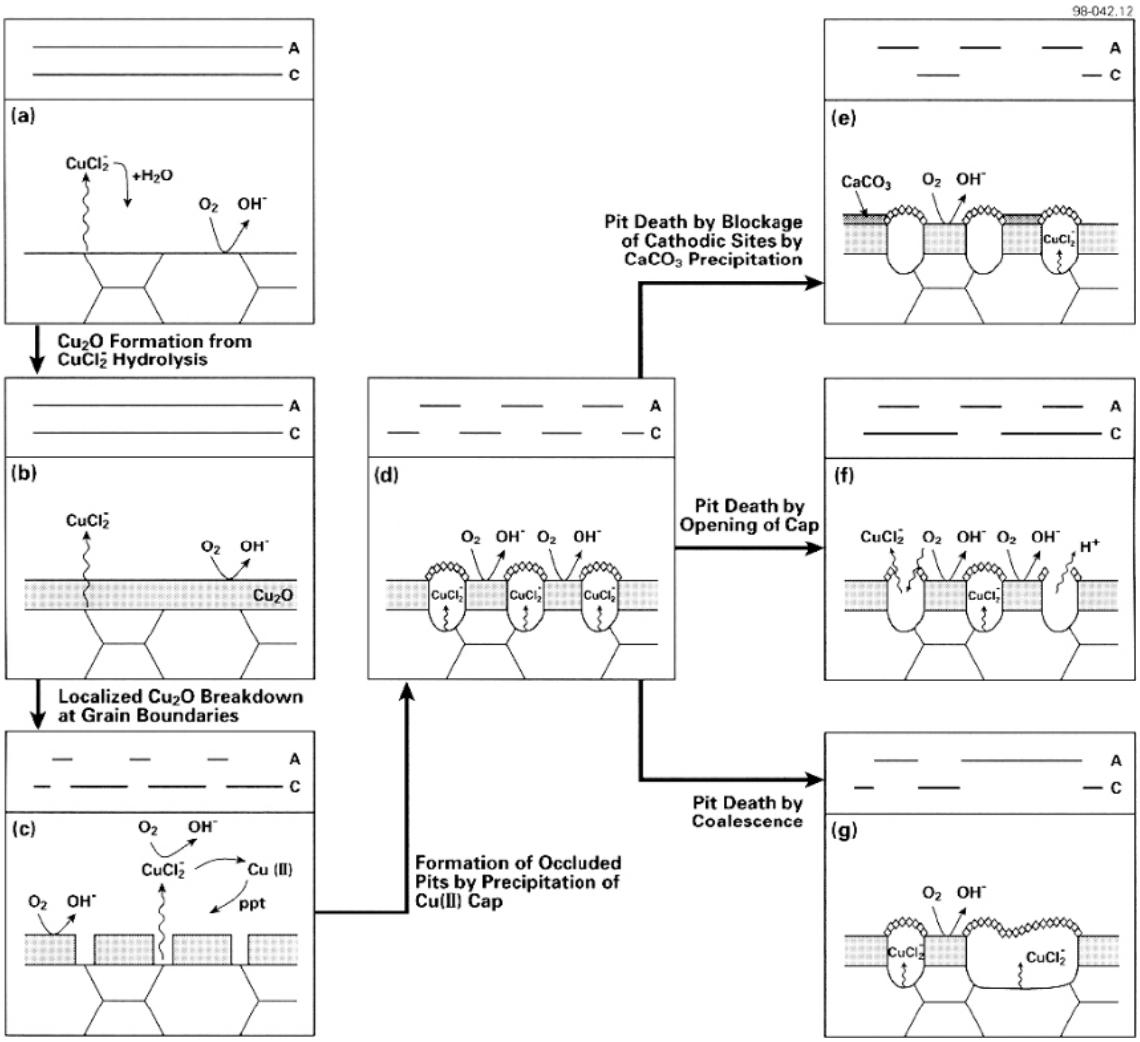

Figure 5-27. *Illustration of a conceptual model for surface roughening of the form observed on copper surfaces exposed to repository conditions (King and Kolář 2000). A and C denote the anodic and cathodic reactions with the location and length of the lines representing the respective surfaces over which these reactions occur.*

An alternative approach to modelling the localised corrosion behaviour of the canister is to predict the probability of pit initiation based on observed E_b values. This approach requires a knowledge of the variation of E_b with environmental conditions and of the time dependence of E_{CORR} for a canister. Figure 5-28 shows a comparison of the value of E_b as a function of pH in Cl^- and Cl^--free solutions with the predicted E_{CORR} for a copper canister in a Canadian repository (shown a a function of time in the figure). The predicted E_{CORR} values are plotted as a function of the predicted interfacial pH (King and Kolář 2005). It is apparent that the predicted E_{CORR} is at least 250 mV more negative than the measured E_b values, so that pitting should not occur at any time, consistent with the recent observations of Karnland et al. (2000) and with the laboratory observations of Litke et al. (1992) (Figure 5-20).

The final approach to predicting the extent of localised corrosion on Cu canisters is to make projections based on observed pit depths. Because pitting has not been observed on Cu exposed to simulated repository conditions, pit depth data have been taken for this purpose from literature studies of the long-term burial of Cu alloys (Romanoff 1989) and from an analysis of pit depths on archaeological artifacts (Bresle et al. 1983). Whilst the environmental conditions and Cu alloys are different from those in a repository, these studies offer the great advantage of having been "conducted" over long periods of time. The long-term soil corrosivity measurements of Romanoff (1989) were conducted for times up to 14 years. The Bronze Age artifacts studied by Bresle et al. (1983) had been exposed to the environment for an estimated period of 3,000 years.

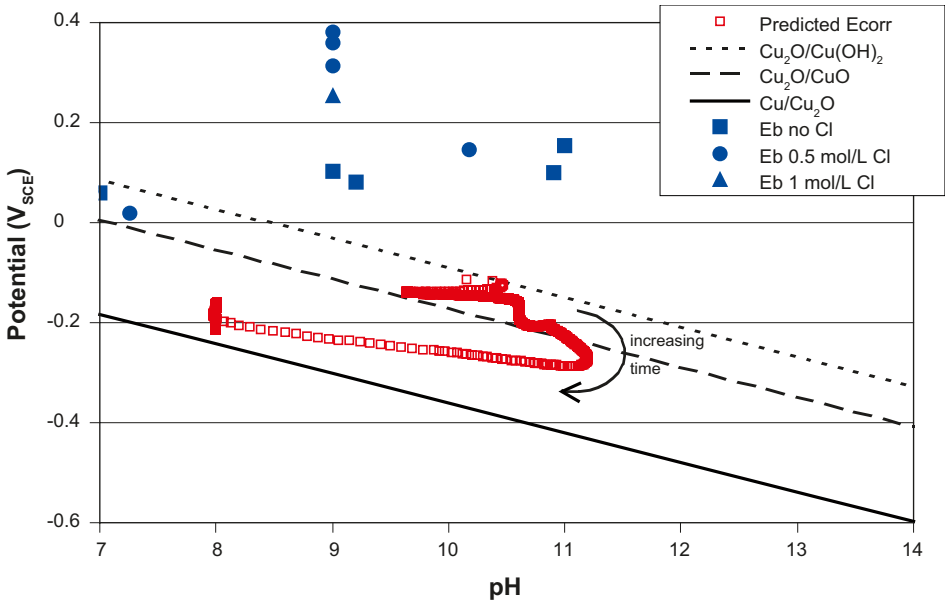

Figure 5-28. *Comparison of film breakdown (pitting) potentials for copper in chloride solutions as a function of pH with the predicted variation of the corrosion potential and interfacial pH for a copper canister in a canadian deep geological repository.*

In the Swedish and Finnish programmes, these pit depth data have been used to estimate a pitting factor (Mattsson 1980, SKBF/KBS 1983, Swedish Corrosion Institute 1978, 1983, Werme et al. 1992). The pitting factor (PF) is the ratio of the maximum pit depth (as measured from the original surface) to the depth of general corrosion and has a value > 1 (PF = 1 corresponds to general corrosion). The maximum pit depth on a canister is then estimated by multiplying the depth of general corrosion, determined by some other means, by the PF. For the earliest predictions of canister lifetimes (Mattsson 1980, Swedish Corrosion Institute 1978), a conservative PF value of 25 was used, based on the most severe case of pitting reported in the literature (Romanoff 1989). Subsequent analysis of the archaeological artifacts (Bresle et al. 1983), supported by the modelling studies of Taxén described above, have lead to the adoption of a more realistic PF of 5 (SKBF/KBS 1983, Werme et al. 1992, Wersin et al. 1994a). The consequences of these various PF values on the predicted canister lifetimes are discussed in Section 8.2.1.

An alternative use of the same pit depth data has been developed in the Canadian programme (King and Kolář 2000, King and LeNeveu 1992). The data were analysed using extreme-value statistics, in which the deepest pit on a collection of samples (or within a given area of the surface of one or more samples) of the same exposure time is fitted to an extreme-value distribution of the form

$$F(x) = \exp[-\exp(-ax + b)] \qquad 5\text{-}30$$

where F(x) is the cumulative probability that the depth of the deepest pit is less than or equal to a depth x, a is the scale (or shape) parameter, and b/a is the location parameter of the distribution. The fitting procedure produces vales for a and b for a given set of data for a given exposure period. Fitting several sets of data with different exposure periods gives the time dependence of the scale and location parameters. Then, the cumulative probability of a pit of a given depth on a canister as a function of time can be determined from equation 5-30 and the time dependences of a and b/a.

Fitting of the Romanoff and Bresle et al. data to equation 5-30 indicated that whilst the scale parameter was relatively independent of exposure time, the location parameter increased with time. Figure 5-29 shows the predicted time dependence of b' (the value of b normalised to an area of 5.76 m^2, the surface area of a Canadian dual-wall canister (Johnson et al. 1996, King 1996b)). Based on this time dependence, the maximum pit depth on a canister can be predicted. Figure 5-30 shows the maximum pit depth as a function of time, based on a probability of 10^{-11} that the pit will be deeper than the given depth (i.e. a probability of $< 10^{-6}$ for any of the $\sim 10^5$ canisters in the Canadian repository considered in the analysis). Thus, after a period of 10^6 years, the maximum pit depth on any of the canisters was predicted to be 7.6 mm, for this assumed probability.

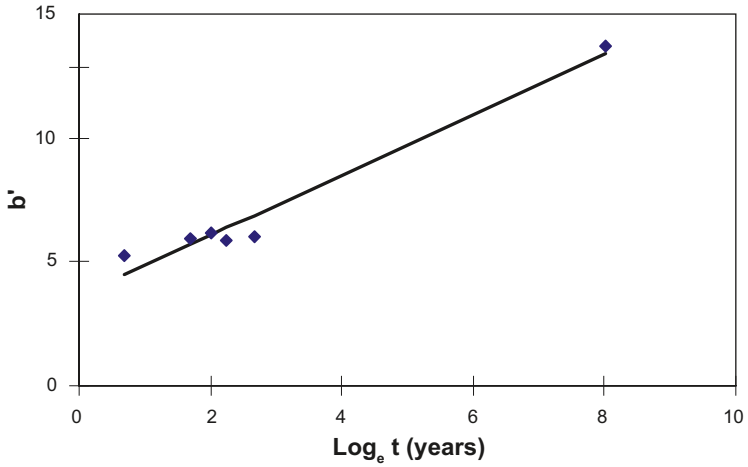

Figure 5-29. *Predicted time dependence of the pit depth extreme value distribution fitting parameter b (b' is the value of b normalised to a surface area of 5.8 m^2).*

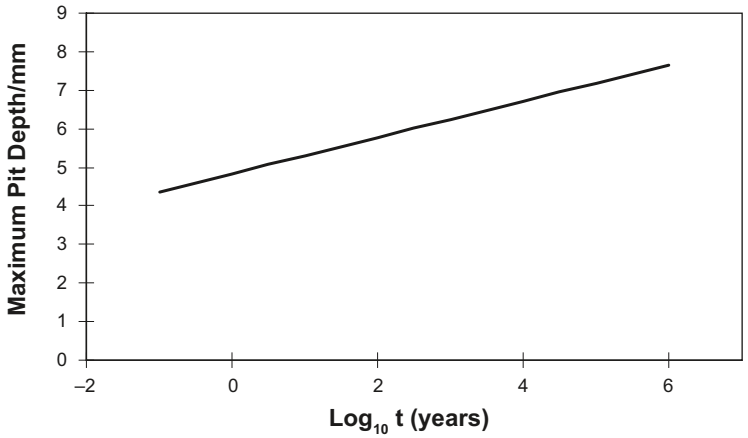

Figure 5-30. *Predicted maximum pit depth on a copper canister as a function of time (assumed canister surface area 5.76 m^2).*

Unlike the critical potential approach to pitting, neither the pitting factor nor the extreme-value analysis approach allows for pit death. Propagation is assumed to continue indefinitely regardless of the evolution in the repository environment, albeit at a diminishing rate in the extreme-value approach. The slope of Figure 5-30 suggests the pit growth rate follows a $t^{0.47}$ time dependence.

5.3.4 State-of-knowledge of the pitting corrosion of copper canisters

Various experimental and modelling approaches have been developed to study the pitting of Cu. Although the extensive database on the pitting of Cu water pipes provides some useful mechanistic information, the results of corrosion tests carried out in the laboratory and in underground research facilities under simulated repository conditions suggest that canisters will not undergo classical pitting, but rather a form of under-deposit corrosion, in which there is no permanent separation of anodic and cathodic sites.

The mechanistic Cu pitting studies indicate that an oxidant (either O_2 or Cu(II)) is a pre-requisite for pit propagation. Since the near-field environment in the repository will evolve from initially oxidising to ultimately reducing, this implies that pitting will only be possible (if at all) in the early stages of the repository life. Thus, the environment within the repository is evolving to one in which only general corrosion will occur. In addition, the difficult problem of predicting localised corrosion is made easier by the fact that predictions only have to be made for the early oxidising period.

Given this evolution in localised corrosion behaviour with repository conditions, the most suitable pitting models are those that include the possibility of pit death. Of the currently available models, only those based on a critical potential (either for pit initiation or pit propagation) are capable of predicting when pitting may cease to be an active degradation mechanism in the repository, although the amount of suitable data, particularly re-passivation potentials, is limited. For analyses based on literature pit depth data (either the pitting factor or extreme-value approaches) it is implicitly assumed that pits propagate indefinitely. Predictions of pit depth based on these latter two approaches must be considered conservative. An alternative, and perhaps more appropriate method of prediction, is to assume a certain degree of roughness which is then added to the predicted depth of general corrosion.

6 Stress corrosion cracking

Summary of changes to stress corrosion cracking section

Stress corrosion cracking (SCC) of copper canisters continues to be an area of active research in a number of national programmes, including Finland, Sweden, and Canada. The following updates have been made to the SCC section:

- The entire section (Section 6 in the new report) has been renumbered as a result of combining the old Sections 4 and 5 into a single section in the revised report.
- A more-detailed discussion of the scientific basis for the surface mobility model has been included (Section 6.1.1(d)).
- Copper SCC studies since 2001 have been summarised, with an emphasis on studies performed in support of nuclear waste disposal programmes (Section 6.1.2).
- Tables 6-1(a), (b), (c) have been updated with studies since 2001 and a new Table 6-1(d) has been added.
- A fault-tree approach to predicting the possibility of SCC of copper canisters is introduced (Section 6.2.2.1 and Figures 6-8 and 6-9).
- The possibility of SCC during the long-term anaerobic phase in the evolution of the repository environment is discussed (Section 6.2.2.1).
- A number of figures summarizing experimental observations of SCC in ammonia, acetate, and nitrite solutions (Figure 6-1) have been added.

6.1 Literature studies of the SCC of pure coppers

The SCC of Cu alloys is the oldest form of environmentally assisted cracking known, dating from the "season-cracking" of brass munitions in the mid-late 19th Century. Apart from the SCC of stainless steel in chloride solutions, the cracking behaviour of Cu and Cu alloys has probably been studied more than any other form of SCC. A number of reviews of the likely SCC behaviour of Cu canisters have been written (Farmer et al. 1988, King 1996c, King and Litke 1997, King and Newman 2010, Ikeda and King 2001, Saario et al. 1999), on which this section has been based.

The three pre-requisites for SCC are a susceptible material, a tensile stress, and a suitably aggressive environment. The proposed canister material cannot be claimed to be immune to SCC, since pure coppers, especially those containing phosphorus, have been shown to be susceptible. Tensile stresses on the canister surface are possible during various stages in the evolution of the repository environment, either due to external loads or from residual manufacturing stresses. Finally, the possibility that known SCC agents, i.e. ammonia, nitrite, or acetate, may be present in the repository cannot be excluded. Therefore, the possibility of SCC of Cu canisters must be considered.

Of all corrosion processes, SCC is probably the most complex and the most difficult to predict. The extensive database on the SCC of pure coppers is summarized in the first section, followed by a discussion of the expected long-term SCC behaviour of Cu canisters in a deep underground repository.

The SCC of pure coppers has been reported to be caused by ammonia, acetate, nitrite, and recently also by sulphide ions. Table 6-1 summarizes the various literature studies on the SCC of pure coppers in these different environments, with an emphasis on studies associated with the SCC of Cu canisters.

Literature studies of the stress corrosion cracking of copper

Table 6-1 (a). Stress corrosion cracking in ammonia environments.

Environment	Solution	Proposed Mechanism*	Comments**	Reference
Tarnishing ammonia	Moist ammonia atmosphere	FRAD	IGSCC following rupture of Cu_2O film. Increasing susceptibility with increasing P content, as well as of other alloying elements (Zn, As, Sb, Si, Ni and Al).	Thompson and Tracy (1949)
Non-tarnishing ammonia	15 mol·dm^{-3} ammonia, pH ~13, 0.04 mol·dm^{-3} Cu(II)	FRAD	IGSCC following rupture of Cu_2O film.	Pugh et al. (1966), Pugh (1979)
Ammonia	Flowing moist air containing ammonia, 0.5–108 mg/L ammonia	–	OFP Cu (0–1,500 ppm P), various stress levels, various grain sizes. Evidence for threshold P content of 50–80 ppm, evidence for threshold ammonia concentration, susceptibility increases with grain size	Sato and Nagata (1978)
Tarnishing ammonia	0.05 mol·dm^{-3} ammonia	TR	Crack advance by rupture of adherent Cu_2O layer. Cracking only observed at ammonia concentrations ≤ 0.05 mol·dm^{-3}. TGSCC.	Suzuki and Hisamatsu (1981)
Non-tarnishing ammonia	15 mol·dm^{-3} ammonia, pH 12.5–13, 0.008–0.03 mol·dm^{-3} Cu(II)	FIC	TGSCC induced by nanoporous Cu layer produced by the rapid nucleation of etch pits. Nanoporous layer only produced under limited range of conditions of strain rate and high dissolution rates.	Sieradzki and Kim (1992)
Ammonia	Mattsson's solution[1)] containing various Cu^{2+} concentrations	–	OFE[2)] (UNS C10100) and OFP Cu. Constant displacement experiments in compacted buffer material. No cracking observed.	King et al. (1999a)
Ammonia	Deaerated synthetic brackish and saline Olkiluoto groundwater plus 1–100 mg/L ammonia, 100°C, pH 7	–	OFP Cu (45 ppm P), base and electron-beam welded material. SSRT,[3)] 10^{-6} s^{-1}. No cracking observed.	Arilahti et al. (2000)
Ammonia	Aerated 0.06 mol·dm^{-3} ammonia, room temperature	–	OFP Cu (35–45 ppm P), 20% cold worked. Constant load, K_I = 32 MPa·m$^{1/2}$. No cracking observed, general dissolution.	Pettersson and Oskarsson (2000)
Ammonia	Bentonite equilibrated synthetic groundwater containing 0.5 mg/L ammonia	–	OF and OFP Cu (40 ppm Cu). SSRT, $4 \cdot 10^{-7}$ s^{-1}. No cracking observed at potentials between –0.10 and –0.25 V_{SCE}.	Rosborg (1998), Rosborg and Werme (2001)
Ammonia	NH_4OH solution (0.07–2.0 mol·dm^{-3}), with and without added Cu^{2+} and/or anodic polarisation. Chloride ions added to some tests.	–	OFP Cu, constant extension rate using sub-size CT[4)] specimens, SCC observed at E_{CORR} values between –0.2 V_{SCE} and –0.27 V_{SCE}. Chloride inhibits SCC at sufficient concentration.	Ikeda and Litke (2004, 2008)

Table 6-1(b). Stress corrosion cracking in acetate solutions.

Environment	Solution	Proposed Mechanism*	Comments**	Reference
Cupric acetate	0.025 mol·dm^{-3} Cu(II) acetate	TR	IGSCC due to rupture of Cu_2O film. Illumination inhibits tarnish growth and cracking.	Escalante and Kruger (1971)
Sodium acetate	0.1 mol·dm^{-3} acetate and conditions of pH and E under which oxide formed	FIC	TGSCC cleavage-like cracking believed to be induced by the rupture of a thin Cu_2O layer.	Cassagne et al. (1990)
Sodium acetate	1–100 mg/L acetate added to deaerated saline and highly saline ground water	–	OFP Cu, SSRT. No SCC observed.	Kinnunen (2006)
Sodium acetate	0.001–0.5 mol·dm^{-3} acetate, solution adjusted to pH 9, with and without the addition of Cu^{2+} and/or anodic polarisation, with and without added Cl^-	–	OFP Cu, constant extension rate using sub-size CT specimens, cracking observed at E_{CORR} greater than ~0.05 V_{SCE}, Cl^- inhibits SCC	Ikeda and Litke (2008), Litke and Ikeda (2006, 2008)

Table 6-1(c). Stress corrosion cracking in nitrite solutions.

Environment	Solution	Proposed Mechanism*	Comments**	Reference
$NaNO_2$	Aerated 1.0 mol·dm^{-3} NO_2^- at E_{CORR}	FRAD	TGSCC during slow-strain experiments. Film rupture caused by deformation at slip steps.	Pednekar et al. (1979)
$NaNO_2$	Aerated 1.0 mol·dm^{-3} NO_2^- E = 0 V_{SCE}, 25–40°C	FIC	Sustained TGSCC only under conditions of dynamic strain. Cracking stopped within 10–20 μm under constant load conditions.	Sieradzki et al. (1984)
$NaNO_2$	Aerated 0.3 mol·dm^{-3} NO_2^- at 80°C, E_{CORR} (–0.05 V_{SCE}) and +0.10 V_{SCE}, OFHC[5] Cu	–	TGSCC following initiation at grain boundaries. Fracture surfaces cleavage-like with evidence for crack arrest markings.	Aaltonen et al. (1984)
$NaNO_2$	Various NO_2^- concentrations (pH 9), E and T.	FRAD or FIC	TGSCC following initiation at grain boundaries. Evidence for threshold E and NO_2^- concentration below which cracking does not occur. Activation energy for crack growth 21 kJ·mol^{-1}. Cleavage-like fracture surfaces with crack arrest markings.	Yu and Parkins (1987)
$NaNO_2$	0.001–1.0 mol·dm^{-3} NO_2^- concentration room temperature and 80°C and various E. OFHC and phosphorus-deoxidized Cu	FRAD or FIC	TGSCC. Evidence for threshold E and NO_2^- concentration, possibly associated with a minimum crack-tip current density of 0.1 mA·cm^{-2}. Lower susceptibility at 80°C. OFHC and PDO[6] Cu behaved identically.	Benjamin et al. (1988)
$NaNO_2$	1.0 mol·dm^{-3} NO_2^-, pH 9, E between E_{CORR} (–0.07 V_{SCE}) and +0.05 V_{SCE}	FIC	TGSCC cleavage-like cracking believed to be induced by the rupture of a thin Cu_2O layer.	Cassagne et al. (1990)
$NaNO_2$	1 mol·dm^{-3} NO_2^-, ~pH 7.5, 0 to +0.10 V_{SCE}	FRAD or TR	TGSCC. Maximum susceptibility at E corresponding to formation of Cu_2O film.	Uchida et al. (1991)
$NaNO_2$	Various NO_2^- concentrations, E and T	–	TGSCC of OF Cu (UNS C10200). Cracking observed at E_{CORR} at 23°C, but not at 90°C. Anodic polarization induced cracking at both temperatures.	Beavers and Durr (1992)
$NaNO_2$	0.3 mol·dm^{-3} $NaNO_2$, synthetic saline groundwater, pH 9.3, room temperature and 80°C, various E	–	OFP Cu, SSRT, 1.5·10^{-8}–5·10^{-6} s^{-1}, TG initiation and IG propagation, aim of study to demonstrate use of potential threshold approach to canister modelling	Rosberg and Svensson (1994)
$NaNO_2$	Various NO_2^- concentrations at E_{CORR} in aerated pH 9.0 solution	–	TGSCC of OFE Cu using constant extension rate technique. Evidence for crack coalescence and discontinuous crack growth.	King and Litke (1997)
$NaNO_2$	0.1 mol·dm^{-3} $NaNO_2$ (pH 9.0), various oxidant fluxes	–	TGSCC of OFE and OFP Cu as a function of oxidant supply. Constant extension rate tests. Modelling of canister lifetimes based on oxidant supply to canister.	King et al. (1999 b, c)
$NaNO_2$	Various NO_2^- concentrations (pH 9.0), various Cl^- concentrations	–	TGSCC of OFE Cu. Inhibitive effect of Cl^- at certain Cl^- concentration and NO_2^-:Cl^- concentration ratios. Constant extension rate technique.	King et al. (1999a)
$NaNO_2$	0.15–0.3 mol·dm^{-3}, aerated, room temperature and 80°C	–	OFP Cu (35–55 ppm P), annealed and 10–20% cold work, pre-cracked compact-tension specimens, constant load, various K_I, determined crack growth rate as a function of K_I, Cu_2O identified in crack, K_{ISCC} ~30 MPa·m$^{1/2}$	Pettersson and Oskarsson (2000)
$NaNO_2$	Deaerated 0.1 mol·dm^{-3}, pH 9, room temperature, galvanostatic control, Cl^- ion additions	FRAD	OFP Cu, base and electron-beam welded material, SSRT and constant load, pre-cracked compact-tension specimens. SCC susceptibility decreased with decreasing nitrite or increasing Cl^- concentrations, data consistent with threshold potential.	Ikeda and Litke (2000, 2008)

Table 6-1(c). Stress corrosion cracking in nitrite solutions.

Environment	Solution	Proposed Mechanism*	Comments**	Reference
$NaNO_2$	0.3 mol·dm^{-3}, room temperature, potentiostatic control	–	OF and OFP Cu, SSRT, $4 \cdot 10^{-7}$ s^{-1}. Mixture of IGSCC and TGSCC observed. Reduction in ductility potential dependent. Evidence for threshold potential of –0.10 V_{SCE}.	Rosborg (1998), Rosborg and Werme (2001)
KNO_2	1 mol·dm^{-3} NO_2^-, 45°C and 75°C	–	Semi-hard DHP[7] Cu (yield strength 220 MPa), constant load. IGSCC observed at stresses below yield stress, threshold stress ~25 MPa	Mori et al. (2003, 2005), Schwentenwein et al. (2002)
$NaNO_2$	0.1 mol·dm^{-3} NO_2^-, pH 7	–	OFP Cu, constant extension rate and constant displacement tests, acoustic emission and fractography. Threshold stress intensity factors and J-integrals determined for both crack initiation and crack growth stages.	Khanzin and Nikulin (2005)
$NaNO_2$	0.001–0.1 mol·dm^{-3} NO_2^-, pH 9, additions of 0–0.01 mol·dm^{-3} Cl^-, 100–130°C	–	OFP Cu, constant extension rate using sub-size CT specimens. Both increased temperature and the presence of Cl^- found to decrease the susceptibility to SCC.	Ikeda and Litke (2007)

Table 6-1(d). Stress corrosion cracking in other environments.

Environment	Solution	Proposed Mechanism[1]	Comments[2]	Reference
Sulphide-containing seawater	0–0.01 mol·dm^{-3} Na_2S in deaerated synthetic seawater, natural pH	–	PDO Cu (45 ppm P), SSRT. Evidence for cracking at sulphide concentrations above 0.005 mol·dm^{-3}.	Taniguchi and Kawasaki (2008)
Cupric nitrate	1 mol·dm^{-3} $Cu(NO_3)_2$	Surface mobility	Pure Cu wires, SSRT. SCC observed under conditions of equilibrium between metal and dissolved metal ions, but Cu_2O film likely to be present.	Farina et al. (2005)

* FRAD, FIC, TR and SM refer to film-rupture/anodic-dissolution, film-induced cleavage, tarnish-rupture and surface-mobility mechanisms, respectively.

** IGSCC and TGSCC denote intergranular and transgranular stress corrosion cracking, respectively.

[1] 1 mol/L NH_4^+, 0.05 mol/L Cu^{2+}, pH 7.2.

[2] Oxygen-free electronic.

[3] Slow strain rate test.

[4] Compact tension.

[5] Oxygen-free high-conductivity.

[6] Phosphorus deoxidised.

[7] Deoxidised high-residual-phosphorus.

6.1.1 Mechanisms proposed for the SCC of pure coppers

Various mechanisms have been proposed to account for SCC in general, some of which have been specifically proposed for the SCC of Cu (King 1996c, King and Newman 2010, Ikeda and King 2001). Determining the mechanism(s) controlling crack initiation and/or growth is not simply of academic interest, but is necessary for developing predictive models for Cu canisters and for justifying long-term predictions of SCC behaviour.

The four mechanisms proposed to account for the SCC of Cu in various environments are (King and Newman 2010): (a) the film-rupture/anodic-dissolution (FRAD) mechanism, (b) the tarnish-rupture (TR) mechanism, (c) film-induced cleavage (FIC), and (d) the surface-mobility (SM) model.

a) Film-rupture/anodic–dissolution model

There are a number of variants of the film-rupture/anodic-dissolution model (e.g. the slip dissolution model), but in each one crack advance occurs by dissolution following the rupture of a protective film at the crack tip. Anodic dissolution at the crack tip is supported by cathodic reactions on the

crack walls or on surfaces outside the crack. An important implication for the SCC of Cu canisters is that, if cracking occurs, it will stop once all the oxidant in the repository has been consumed. Thus, the probability of SCC is highest during the early aerobic period in the evolution of repository conditions, gradually becoming less likely as conditions become anoxic.

The FRAD mechanism has been proposed to account for the SCC of Cu in ammonia and nitrite solutions (Tables 6-1(a) and 6-1(c)).

Theoretical expressions have been derived to predict the crack growth rate for the FRAD mechanism. Under rapid straining conditions the crack tip is maintained oxide-free at all times, and the crack grows continuously with a velocity (v) determined by the crack-tip anodic current density (i_{CT})

$$v = i_{CT} \frac{M}{zF\rho} \qquad 6\text{-}1$$

where M is the atomic mass of Cu, z is the valence of dissolved metal, F is the Faraday constant, and ρ is the density of Cu. If the crack-tip strain rate ($\dot{\varepsilon}_{CT}$) is slow, the crack tip periodically repassivates and the crack advances discontinuously at a rate given by

$$v = \frac{Q_F}{\varepsilon_C} \dot{\varepsilon}_{CT} \frac{M}{zF\rho} \qquad 6\text{-}2$$

where Q_F is the charge density corresponding to crack advance and ε_C is the critical strain for film rupture.

The impact of evolving redox conditions will be to either diminish the crack-tip current density (under high strain rate conditions and continuous crack growth) or to decrease the charge density at the crack tip between repassivation events (under slow strain rate conditions and discontinuous crack growth). Although the overall amount of oxygen in the repository may be limited, the crack-tip current density can be high because of the small surface area of the crack tip compared with the potentially large cathodic surface area available to support oxygen reduction.

b) Tarnish-rupture mechanism

The tarnish-rupture mechanism has long been associated with the SCC of Cu alloys because of the observation of SCC of Cu and brasses in so-called tarnishing ammonia solutions. The TR mechanism differs from the FRAD mechanism in that crack advance occurs by rupture of the oxide, rather than by dissolution following oxide rupture. By inference, therefore, cracking is discontinuous and the rate of crack growth is limited to the rate of film growth. The TR mechanism has been proposed to account for cracking in ammonia, acetate, and nitrite environments (Table 6-1).

The crack velocity is given by

$$v = C\left(\frac{\dot{\varepsilon}_{CT}}{\varepsilon_C}\right)^{1/n} \qquad 6\text{-}3$$

where C and n are constants describing the kinetics of tarnish growth, with n = 2 for parabolic kinetics and n = 3 for a cubic growth law.

Crack growth requires oxidation of the Cu to form the oxide, and a corresponding supply of oxidant to support corrosion. Implicitly, therefore, the rate of crack growth for a Cu canister will decrease with time as the rate of oxide growth decreases with the evolution of the repository environment.

c) Film-induced cleavage model

In the FIC model, a crack initiates in a surface film and is projected into the underlying ductile metal, inducing a cleavage-like crack. Formation of the surface layer in which the crack initiates requires oxidation of the surface, but the overall size of each crack event is typically ~10 times the thickness of the initiating film. Thus, a small amount of corrosion can lead to a crack many times deeper than the depth of oxidation. The FIC mechanism has been proposed for the SCC of Cu in

ammonia and acetate environments (Tables 6-1(a) and 6-1(b)), for which the initiating layers were proposed to be either a nanoporous Cu layer or a thin Cu_2O film, respectively.

The crack velocity for a FIC mechanism is given by

$$v = (j + L)\left(\frac{\dot{\varepsilon}_{CT}}{\varepsilon_C}\right) \qquad 6\text{-}4$$

where j is the length of the cleavage crack and L is the thickness of the initiating film.

Whilst crack growth by an FIC mechanism also requires a supply of oxidant, and therefore should be limited as the repository becomes anoxic, relatively deep cracks could be produced from a small amount of corrosion because ~90% of the crack advance does not require the support of a corresponding cathodic reaction.

For the FIC mechanism, as for the discontinuous FRAD (equation 6-2) and TR (equation 6-3) models, cracking may also cease if the crack-tip strain rate becomes negligible. This may occur on a canister after the outer Cu shell has deformed onto the inner cast-iron insert.

d) Surface-Mobility Model

The SM model was developed by Galvele (1987) and has been proposed for the SCC of brass and copper.

Crack advance is a result of the removal of atoms (or the introduction of vacancies) at the crack tip due to surface diffusion. The crack velocity is given by

$$v = \frac{D_S}{L'}\left[\exp\left(\frac{\sigma \cdot b^3}{kT}\right) - 1\right] \qquad 6\text{-}5$$

where D_S is the surface self-diffusion coefficient, L' is the diffusion distance of the atoms (or vacancies), σ is the elastic surface stress at the crack tip, b is the atomic size, k is Boltzmann's constant and T is the absolute temperature.

According to the SM model, the crack velocity is never zero, since D_S is always finite. This poses some problems for Cu canisters, since even small crack velocities could produce significant cracks over the timescales of interest. Surface oxidation (corrosion) increases the crack velocity by producing adsorbed atoms (adatoms) with higher surface diffusivities than that of the pure metal. There is no explicit relationship between the rate of oxidation and the crack velocity.

The SM model has been the subject of some controversy since its first introduction. Recently, King and Newman (2010) reviewed the model and the history of the discussions in the technical literature between the proponents of the model and other researchers who have questioned its scientific basis. The SM model has been criticized on two major grounds; first, the expression used for estimating the effect of stress on the decrease in vacancy formation energy is appropriate for the bulk solid rather than the surface and, second, the model does not take into account capillary closure effects for sharp cracks. If equation 6-5 is reformulated taking these two effects into account, the resultant crack velocity for copper would be of the order of 10^{-20} m/s, which is vanishingly small even on repository timescales (King and Newman 2010).

6.1.2 SCC of pure coppers

6.1.2.1 Environmental effects

There are a number of ways in which the repository environment will impact the SCC behaviour of the canisters. The four main influences of the environment are: (i) the presence of an SCC agent, (ii) redox conditions, (iii) the influx of Cl^- ions, and (iv) temperature.

SCC agents and redox conditions

Various mechanisms have been proposed for the SCC of Cu in ammonia (Table 6-1(a)). The FRAD mechanism has been proposed in both tarnishing and non-tarnishing environments, the only differ-

ence being that a *visible* oxide is formed in tarnishing solutions, since a Cu_2O oxide is undoubtedly formed at the crack tip in both environments. The actual oxidant in these systems is believed to be Cu(II)-NH_3 complexes (e.g. Cu $(NH_3)_5^{2+}$), rather than O_2. However, the presence of O_2 is a pre-requisite for SCC, since in practical examples Cu(II) is produced by the homogeneous oxidation of Cu(I) by O_2. Suzuki and Hisamatsu (1981) proposed a TR mechanism to explain their observations. Under rapid dissolution conditions, Sieradzki and Kim (1992) were able to generate a nanoporous etch-pitted layer, which they suggested induced cracking via an FIC mechanism.

The effect of ammonia concentration has been reported in a number of studies. Many studies have been conducted in concentrated (15 mol·dm^{-3}) ammonia solutions, since such concentrated electrolytes could be formed by the absorption of ammonia vapour in thin surface water films. Others have used the standard Mattsson's solution, comprising 1 mol·dm^{-3} ammonia at various pH values and added Cu(II) as the oxidant. Sato and Nagata (1978) reported a systematic study of the effect of ammonia concentration, but failed to define an absolute threshold concentration, although the incidence of SCC at concentrations of 0.5 mg/L ($3 \cdot 10^{-5}$ mol·dm^{-3}) was much less than at higher concentrations. Suzuki and Hisamatsu (1981) report that SCC only occurred at concentrations *below* 0.05 mol·dm^{-3}, but do not report a lower concentration limit. Pettersson and Oskarsson (2000) did not observe SCC of OFP Cu during constant load tests on pre-cracked specimens in 0.06 mol·dm^{-3} ammonia. Based mainly on the results of Sato and Nagata (1978), Saario et al. (1999) proposed a lower threshold ammonia concentration of ~0.5 mg/L. Rosborg (1998) and Rosborg and Werme (2001) reported no SCC of OFP Cu in a bentonite equilibrated synthetic groundwater containing 0.5 mg/L ammonia.

To determine whether SCC could occur in deep Finnish groundwaters, Arilahti et al. (2000) performed a series of SSRT in synthetic Olkiluoto groundwaters at 100°C with additions of between 1 and 100 mg/L ammonia. Both base metal and EB-welded OFP (45 ppm P) were tested. The deaerated groundwaters contained either 3,700 mg/L or 17,000 mg/L Cl^- ions and ~1 mg/L sulphide (TDS of ~8,300 mg/L and ~30,000 mg/L, respectively). The estimated pH of the solution at the experimental temperature of 100°C was ~pH 7. No SCC was observed in either groundwater for either material, regardless of the ammonia concentration. Based on the elongation-to-failure and fractography, the samples suffered purely ductile failure, with no evidence for brittle environmentally-assisted cracking.

Based on the requirement to form a Cu_2O film, Saario et al. (1999) argued that the minimum potential for cracking is given by the equilibrium potential for the reaction

$$2Cu + H_2O \Leftrightarrow Cu_2O + 2H^+ + 2e^- \qquad 6\text{-}6$$

which is equal to –0.002 V_{SHE} at pH 8 at 25°C and –0.11 V_{SHE} at the same pH at 80°C. These threshold potentials are consistent with the failure to observe SCC in ammonia-containing deaerated Olkiluoto groundwaters at 80°C, for which the E_{CORR} was in the range –0.35 to –0.46 V_{SHE} (Arilahti et al. 2000). Pettersson and Oskarsson (2000) failed to observe SCC in aerated 0.06 mol·dm^{-3} ammonia, even though the E_{CORR} value of ~0.15 V_{SHE} at room temperature was above the threshold potential.

Ikeda and Litke (2004) studied the SCC of OFP copper in 0.07 to 2.0 mol·dm^{-3} ammonia solutions at pH 11–12 at room temperature. The solutions were naturally aerated and, in some cases, $4–8 \cdot 10^{-3}$ mol·dm^{-3} Cu(II) ions, which were found to improve the reproducibility of the results. Tests were performed under either freely corroding conditions or with anodic polarisation to simulate a given flux of oxidants to the canister surface. The effect of Cl^- ions was also examined. Under the aggressive loading conditions of the constant extension rate testing used, SCC was observed in 1 mol·dm^{-3} NH_4OH solution with the addition of Cu(II) ions, although not under all conditions. Factors that tended to produce cracking were the presence of Cu(II) and the absence of anodic polarisation. No cracking was observed in either 0.07 mol·dm^{-3} or 2.0 mol·dm^{-3} NH_4OH. In 1.0 mol·dm^{-3} solution, the addition of 0.5 mol·dm^{-3} Cl^- inhibited cracking, but a Cl^- concentration of 0.1 mol·dm^{-3} did not. An important indicator of cracking appeared to be the solution redox potential, with SCC only observed at E_h values more positive than –0.25 V_{SCE}, corresponding to a corrosion potential in the range –0.27 V_{SCE} to –0.22 V_{SCE}. Ikeda and Litke (2004) correlated the conditions for cracking with the E-pH conditions for a duplex Cu_2O/CuO layer.

The results of various SCC studies in ammonia environments are shown in Figure 6-1(a) superimposed on a Pourbaix (E-pH) diagram that also shows the equilibrium lines for Cu/Cu_2O, Cu_2O/CuO, and $Cu_2O/Cu(OH)_2$. Instances when SCC did and did not occur are indicated.

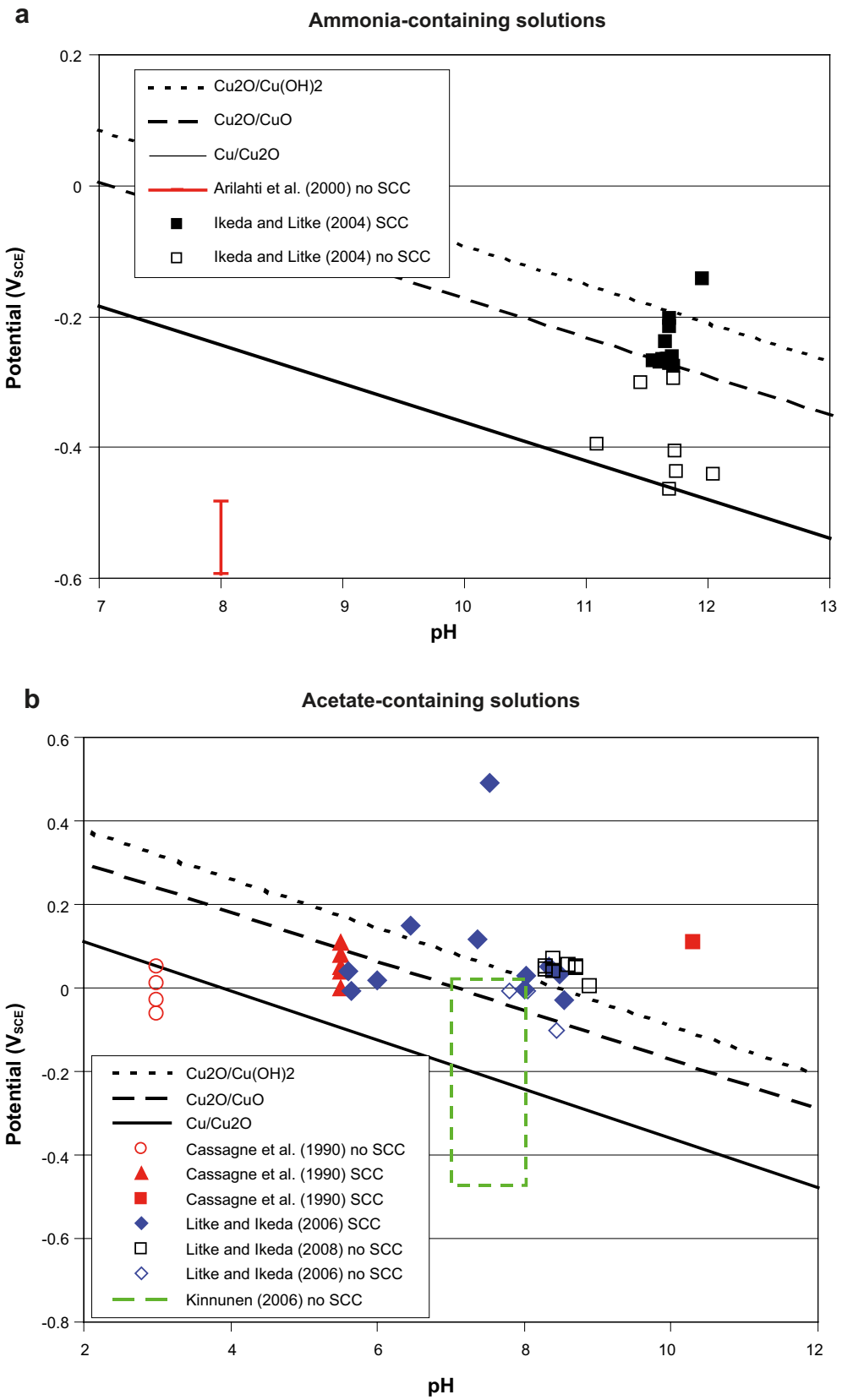

Figure 6-1. *Effect of potential and pH on the observed cracking behaviour of copper. (a) ammonia, (b) acetate, (c) nitrite solutions. The sloping dotted, dashed, and solid lines indicate the equilibrium lines for the $Cu_2O/Cu(OH)_2$, Cu_2O/CuO, and Cu/Cu_2O couples, respectively. Experimental observations of both cracking and no cracking are shown.*

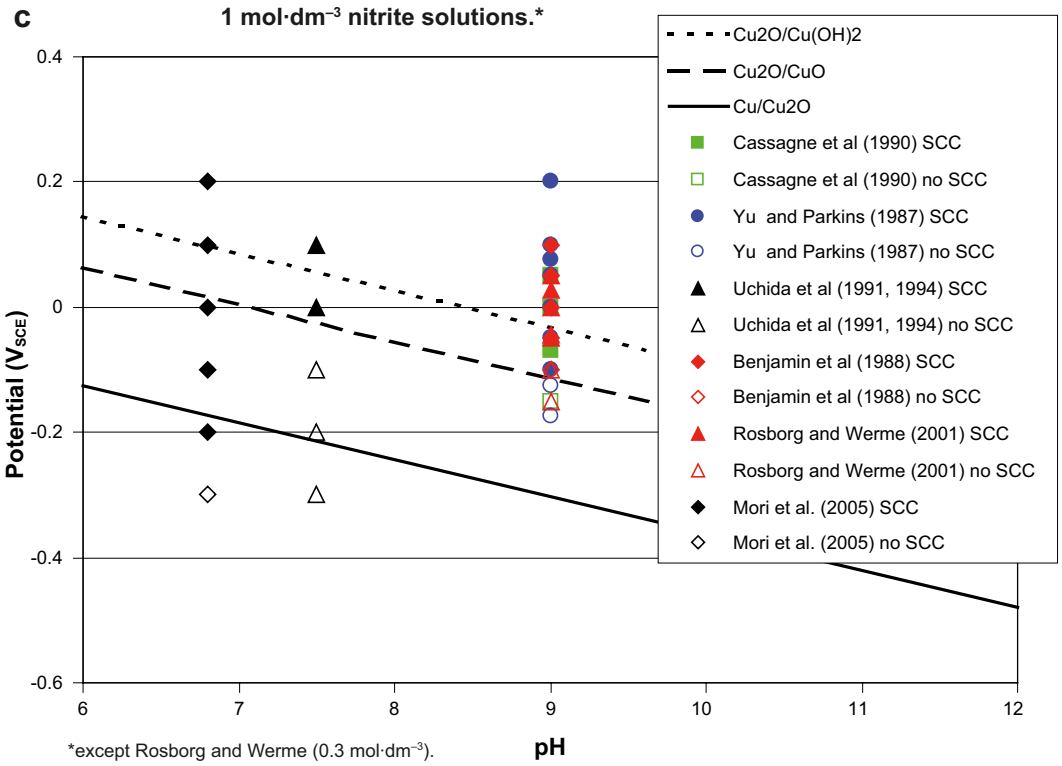

Figure 6-1 continued. *Effect of potential and pH on the observed cracking behaviour of copper. (a) ammonia, (b) acetate, (c) nitrite solutions. The sloping dotted, dashed, and solid lines indicate the equilibrium lines for the $Cu_2O/Cu(OH)_2$, Cu_2O/CuO, and Cu/Cu_2O couples, respectively. Experimental observations of both cracking and no cracking are shown.*

There is a significant amount of information in the literature on the SCC of Cu in acetate solutions (Table 6-1(b)). Both TR and FIC mechanisms have been proposed. There is no information available regarding the minimum [OAc^-] for cracking, although the threshold concentration, if there is one, must be below the concentration of 0.05 mol·dm^{-3} acetate (0.025 mol·dm^{-3} $Cu(OAc)_2$) used by Escalante and Kruger (1971). The use of this solution implies that Cu(II) can act as an oxidant in support of cracking. Cassagne et al. (1990) associated the onset of cracking with the formation of a Cu_2O film.

There have been a number of recent studies of the SCC of copper in acetate solution in various national nuclear waste programmes. Kinnunen (2006) used SSRT to study the SCC of OFP copper base metal and electron-beam welded samples in synthetic saline groundwaters (Cl^- concentrations of 0.23 mol·dm^{-3} and 1.5 mol·dm^{-3}) containing 1 mg/L to 100 mg/L acetate ($1.7\cdot10^{-5}$ mol·dm^{-3} to $1.7\cdot10^{-3}$ mol·dm^{-3}). No indications of SCC were found, presumably partly because of the relatively low concentrations of acetate, especially compared to the high concentrations of inhibitive Cl^- ions, but primarily due to the fact that, like Arilahti et al. (2000), Kinnunen (2006) used deaerated solutions to simulate the long-term anaerobic conditions in the repository. It is evident from these results that SCC would only be expected to occur in acetate and ammonia solutions in the presence of an oxidant. In the Canadian programme, Litke and Ikeda (2006, 2008) were unable to establish reproducible conditions for cracking in solutions ranging from 0.01 mol·dm^{-3} to 0.5 mol·dm^{-3}. Tests were conducted at open-circuit potential and under anodic polarisation in fully aerated solution, with and without the addition of Cu(II) to the solution, at pH values between pH 5.6 and pH 9, with and without Cl^- ions, and using various extension rates. Although evidence for secondary cracking was observed on the fracture surfaces, failure was predominantly ductile in nature. It was suggested that a corrosion potential greater than +0.05 V_{SCE} was necessary for SCC (Litke and Ikeda 2006, 2008).

Figure 6-1(b) summarises the results of SCC studies in acetate-containing solutions of various concentrations.

There is considerably more information available regarding the transgranular SCC (TGSCC) of Cu in NO_2^- solutions (Table 6-1(c)). Many of the reported studies in NO_2^- solutions have stemmed from the academic interest in the Cu/ NO_2^- system and the mechanistic information it provides. In addition, a significant number of studies have been performed in connection with the use of Cu canisters. As in ammonia environments, however, there is no agreement on the mechanism of SCC.

The work of Benjamin et al. (1988) and Yu and Parkins (1987) identified threshold $[NO_2^-]$ and E below which SCC was not observed during short-term SSRT. Figure 6-2 shows the dependence of the ductility of oxygen-free high-conductivity (OFHC) and phosphorus-deoxidized (PDO) Cu in $NaNO_2$ solutions as a function of E and $[NO_2^-]$ at room temperature. The results suggest a threshold E of approximately –0.1 V_{SCE} and a threshold $[NO_2^-]$ of ~0.003 mol·dm^{-3} below which SCC was not observed. This threshold potential is supported by data from Yu and Parkins (Figure 6-3), Rosborg and Svensson (1994), Rosborg (1998) and Rosborg and Werme (2001). The E_{CORR} value in aerated solution is positive of this threshold potential, and SCC is observed under freely corroding conditions (Pednekar et al. 1979, Aaltonen et al. 1984, Cassagne et al. 1990).

In Canada, studies have been performed under controlled current density conditions to simulate a given flux of oxidants to the canister surface (King and Litke 1997, King et al. 1999a, b ,c, Ikeda and Litke 2000, 2007). Constant extension rate (CERT) and constant load tests were performed on pre-cracked compact-tension specimens made from an oxygen-free Cu and from as-received and electron-beam welded OFP Cu. As expected, the crack growth rate decreased with decreasing current density, but not in a linear manner. Both annealed base metal and welded OFP Cu were susceptible to cracking. Cracking was inevitably observed under the aggressive CERT loading conditions, but was not observed in all constant-load tests. The potentials measured on the galvanostatically controlled samples were more positive than the threshold potential of –0.1 V_{SCE}. Increasing $[Cl^-]$ and temperature reduced the susceptibility to cracking and promoted ductile behaviour. In the case of the elevated temperature tests (100°C and 130°C), this observation is, in part at least, due to the effect of temperature on the yield strength of the material (Ikeda and Litke 2007).

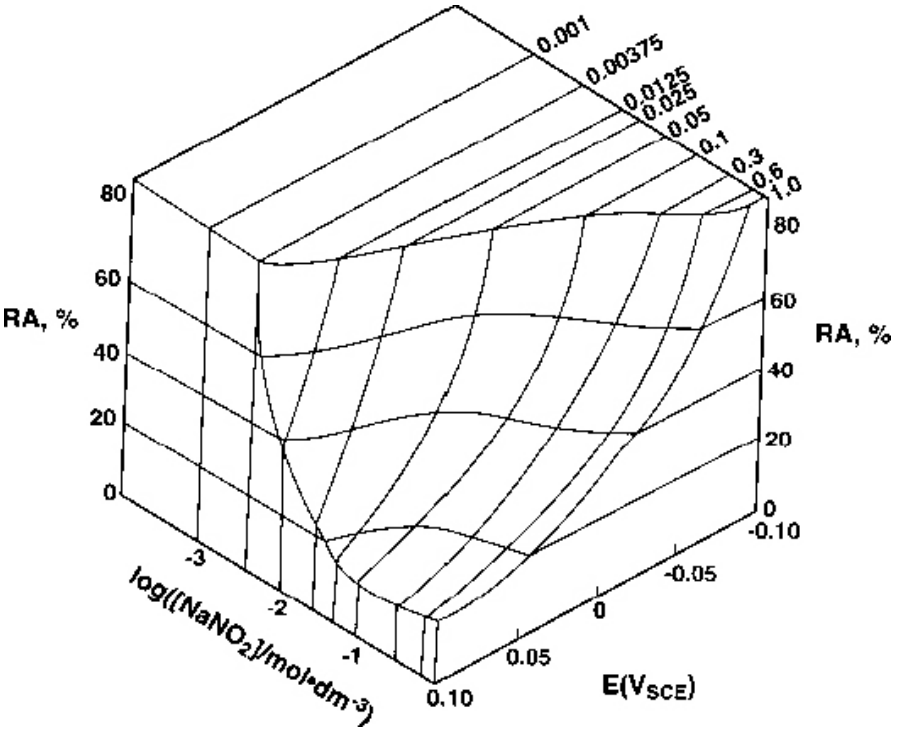

Figure 6-2. *Dependence of the percentage reduction in area (%RA) of smooth oxygen-free high-conductivity and phosphorus-deoxidized copper tensile specimens during slow strain testing in $NaNO_2$ solutions as a function of potential (E) (Benjamin et al. 1988). The data suggest a threshold nitrite concentration ($[NaNO_2]$) and a threshold potential below which SCC is not observed.*

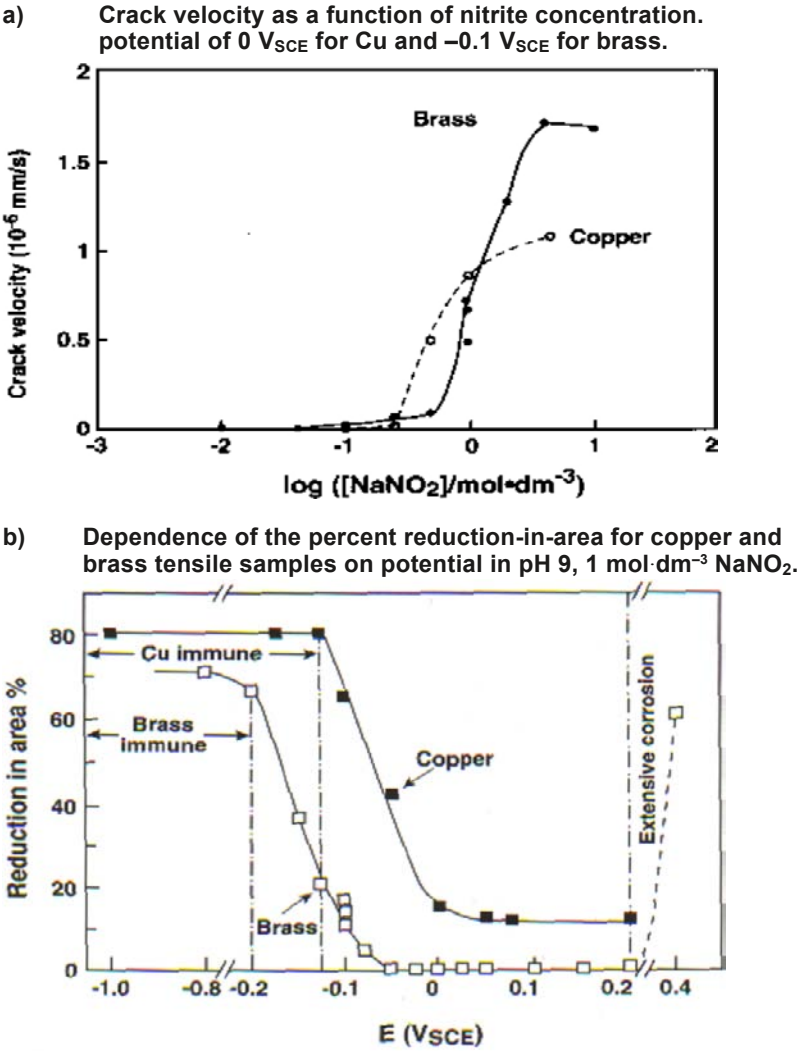

Figure 6-3. *Evidence for a threshold nitrite concentration and threshold potential for the stress corrosion cracking of copper and brass in $NaNO_2$ at room temperature (Yu and Parkins 1987).*

Khanzin and Nikulin (2005) used acoustic emission (AE) and fractography to study the SCC of OFP copper in 0.1 mol·dm^{-3} $NaNO_2$ (pH 7.0) at room temperature. Through careful analysis of the AE signals and of features on the fracture surfaces, the authors were able to distinguish the initiation stage from the subsequent crack growth behaviour. Threshold stress intensity factors (K_I) and J-integrals (J_I) were estimated for initiation (K_I = 10.5 MPa·$m^{1/2}$, J_I = 114.6 kJ·m^{-2}) and crack growth (K_I = 29.3 MPa·$m^{1/2}$, J_I = 578 kJ·m^{-2}).

Mori and co-workers (Mori et al. 2003, 2005, Schwentenwein et al. 2002) have reported the SCC of semi-hard DHP (deoxidized high-residual phosphorus) copper in 1 mol·dm^{-3} KNO_2 at temperatures of 45°C and 75°C. Unlike the transgranular cracking reported above, Mori and co-workers observed intergranular cracking (IGSCC) at stresses significantly below the yield stress. The threshold stress for IGSCC was found to be ~25 MPa, compared with a yield stress of 220 MPa. At stresses above yield, the crack path changed from intergranular to transgranular. Cracking was associated with the observation of a tenorite (CuO) layer on the surface of the samples. Chemical dissolution at grain boundaries is thought to promote the intergranular form of cracking observed in these tests.

Figure 6-1(c) summarises the results of SCC studies in nitrite-containing solutions.

Although the vast majority of the reports of SCC of copper have been in one of these three environments, there are a few reports of cracking in other solutions. Farina et al. (2005) reported the cracking of pure copper in a solution of 1 mol·dm^{-3} $Cu(NO_3)_2$. It was claimed that the copper surface was in equilibrium with the dissolved Cu^{2+} ions but, as noted by King and Newman (2010), a Cu_2O

oxide film would have formed at the expected pH of the tests (pH 5–6). The pH and open-circuit potential of the experiments was not reported by Farina et al. (2005), but the redox conditions were presumably oxidising.

In contrast to the oxidising conditions used by Farina et al. (2005), Taniguchi and Kawasaki (2008) used SSRT to study the SCC of PDO copper in sulphide-containing synthetic seawater solution. Examination of the fracture surfaces and of the gauge length indicated microcracks (< 50 μm in length) at sulphide concentrations greater than $5 \cdot 10^{-3}$ mol·dm^{-3}. Attack was intergranular in nature. Only single experiments were reported and there was non-systematic variation in the strain-to-failure suggesting some scatter in the data, as generally observed for SSRT.

Effect of chloride Ions

Chloride ions diffusing into the repository from the groundwater will tend to promote general dissolution over localized corrosion of the canister. As a consequence, the possibility of SCC should diminish as the bentonite pore water in contact with the canister becomes more saline. The effects of Cl^- on the SCC behaviour of Cu have not been studied in detail, but some studies have been reported and information is also available from the effect of Cl^- on Cu_2O film stability and the competitive complexation of Cu(I) by Cl^- and NH_3.

Figure 6-4 shows the results of CERT tests with OFP Cu in 0.1 mol·dm^{-3} $NaNO_2$ with additions of varying amounts of Cl^- to the solution (data taken from King et al. 1999a). The specimens were maintained at a constant current density (to simulate the flux of oxidant to the canister) and the corresponding potential recorded. The crack velocity was estimated from the extension of the fatigue pre-crack, but was not corrected for the extension due purely to ductile tearing (indicated in Figure 6-4 by the horizontal line in air). The crack velocity decreases slightly with increasing [Cl^-] for chloride concentrations of up to 0.01 mol·dm^{-3}. At higher [Cl^-], the crack velocity falls to that in air (i.e. pure ductile tearing) and the measured potential drops by ~250 mV to more active values. Thus, the decrease in SCC susceptibility is a result of the shift from passive to active dissolution. Similar behaviour is observed with decreasing [NO_2^-] in 0.01 mol·dm^{-3} chloride containing solution. In this case, the transition between passive and active potentials and from high to low crack growth rates occurs for a [NO_2^-] between 0 mol·dm^{-3} and 10^{-3} mol·dm^{-3}. These results indicate that Cu canisters exposed to saline groundwaters will be less susceptible to SCC in nitrite solutions. These earlier results were subsequently corroborated by Ikeda and Litke (2007).

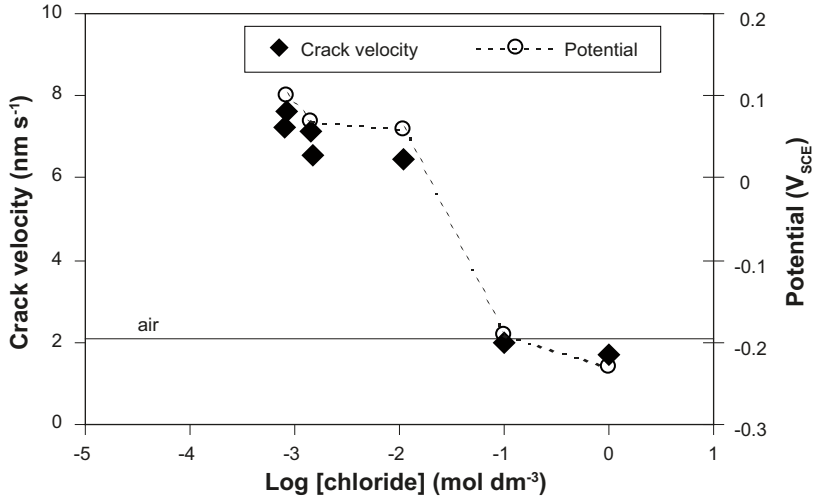

Figure 6-4. *Effect of chloride ion concentration on the crack velocity and potential of OFP copper specimens in 0.1 mol·dm^{-3} $NaNO_2$ at room temperature. The OFP specimens were maintained at a constant current density of 1 μA·cm^{-2} and the corresponding potential is shown in the figure. Crack velocities were estimated from surface crack extension rates, with the value determined in air corresponding to crack extension due to ductile tearing of the pre-cracked compact tension specimens. The current density of 1 μA·cm^{-2} simulates the maximum flux of O_2 to the canister surface during the aerobic phase.*

Similarly, Cl^- would be expected to inhibit the SCC of Cu in ammonia solutions. Ikeda and Litke (2004, 2008) report the inhibition of SCC in 1 mol·dm^{-3} NH_4OH solution by the addition of 0.5 mol·dm^{-3} Cl^-. Arilahti et al. (2000) observed no SCC of OFP Cu in deaerated Olkiluoto groundwaters at 100°C with between 1 and 100 mg/L ammonia, i.e. in excess of the threshold concentration of ~0.05 mg/L suggested by Saario et al. (1999). The synthetic groundwaters contained either 3,700 mg/L (~0.1 mol·dm^{-3}) or 17,000 mg/L (~0.5 mol·dm^{-3}) Cl^-, and had a pH of ~7.

Chloride ions will compete with NH_3 for the complexation of Cu(I) and will also inhibit Cu_2O film formation. King et al. (1999d) report the effects of ammonia on the dissolution of Cu in Cl^- solutions and on Cu_2O film formation. At pH 7 at room temperature, Cl^- ions dominate the dissolution behaviour for ammonia concentrations < 180 mg/L (< 0.01 mol·dm^{-3}). The concentration at which the formation of $Cu(NH_3)_2^+$ becomes important decreases with increasing pH, because of the effect of pH on the speciation of dissolved ammonia (at room temperature, NH_3 predominates at pH values > 9.25 (Tromans 1997)). At 100°C, the relative importance of Cl^- and NH_3 on the dissolution of Cu will depend on the temperature dependence of the stabilities of the respective complex ions and of the dissociation constant for NH_3/NH_4^+. Thus, the failure of Arilahti et al. (2000) to observe cracking may have been a result of the competition between Cl^- and NH_3. In effect, at sufficiently high [Cl^-], the dissolution behaviour of Cu in Cl^-/ammonia mixtures is essentially the same as in Cl^--only solutions, in which SCC is not observed. This implies that the threshold ammonia concentration for SCC will be higher in saline groundwaters than in the ammonia solutions reported in the literature on which the threshold proposed by Saario et al. (1999) was based.

Litke and Ikeda (2006, 2008) and Ikeda and Litke (2008) also report an inhibitive effect of Cl^- on the SCC of copper in acetate solutions. As in NO_2^- and NH_3 environments, the inhibition of SCC is coincident with an active shift in E_{CORR}.

Chloride ions inhibits SCC of Cu in all three SCC environments (nitrite, acetate, and ammonia) because of the effect on the formation and stability of Cu_2O films. As discussed in more detail in Section 5, Cl^- ions inhibit Cu_2O film formation by competing with OH^- ions for surface sites (CuOH is a precursor to Cu_2O formation). Furthermore, the incorporation of Cl^- ions into an existing Cu_2O layer (as may form on a canister surface prior to emplacement in the repository) increases the defect density of the oxide and tends to promote general dissolution over localized corrosion. A defected Cu_2O layer will be less protective, and, therefore, less likely to support SCC, than a Cu_2O film formed in Cl^--free environments. Although the effect of Cl^- ions on the stability of Cu_2O films has not been demonstrated for the SCC of pure Cu, there is evidence that the inhibitive effect of Cl^- on the SCC of brass is due to an effect on the film stability (King 1996c).

Temperature

All available experimental evidence suggests that Cu becomes less susceptible to SCC with increasing temperature. Benjamin et al. (1988) reported that the range of potentials over which SCC was observed for both OFHC and PDO Cu in aerated 0.6 mol·dm^{-3} $NaNO_2$ was narrower at 80°C than it was at 20°C. Under freely corroding conditions, this effect was most likely a result of the lower dissolved O_2 concentration in the open experimental vessel at the higher temperature. However, lower susceptibility was also observed at potentials away from the corrosion potential, suggesting a real effect of temperature on the SCC susceptibility. Beavers and Durr (1992) also observed a beneficial effect of increased temperature on the SCC of oxygen-free Cu (UNS C10200) in $NaNO_2$ solutions. Transgranular cracking was observed at the open-circuit potential during slow strain rate testing in 0.005 mol·dm^{-3} and 1 mol·dm^{-3} nitrite solutions at 23°C, but not at 90°C. Ikeda and Litke (2007) also found increased ductility at elevated temperatures (100°C and 130°C) in nitrite solutions.

In addition to lower susceptibility in nitrite solutions with increasing temperature, there is a large body of evidence to suggest that Cu is not susceptible to SCC in deep Fenno-Scandian groundwaters at elevated temperature. Aaltonen et al. (1984), Benjamin et al. (1988) and Rosborg and Svensson (1994) all failed to observe SCC of Cu in natural and synthetic groundwaters at 80°C. Yunker (1990) did not observe SCC of Cu alloys in irradiated J-13 water (a dilute synthetic groundwater based on conditions at the Yucca Mountain site in the U.S.) and moist air at either 95°C or 150°C. Beavers and Durr (1992) failed to induce SCC in J-13 water or the vapour phase above it at 90°C. Comparable experiments at room temperature were not performed in either of these latter two studies.

The apparent decrease in SCC susceptibility with increasing temperature may be the result of several factors. First, in Cl^- solutions, increasing temperature promotes general dissolution of the surface resulting in negative shifts in E_{CORR}. A similar negative shift in E_{CORR} occurs in aerated nitrite solutions (Benjamin et al. 1988). Second, there is some evidence to suggest that the range of potentials for SCC shifts to more positive values with increasing temperature. For example, in 0.6 mol·dm^{-3} $NaNO_2$, the threshold potential for SCC shifts from approximately –0.1 V_{SCE} at 20°C to ~+0.1 V_{SCE} at 80°C. This positive shift in threshold potential with temperature and the corresponding negative shift in E_{CORR} (from approximately 0–0.04V_{SCE} in aerated solution at 20°C to –0.09 V_{SCE} at 80°C) is sufficient to render OFHC and PDO Cu immune to SCC at E_{CORR} in aerated solution at 80°C, whereas cracking is observed at E_{CORR} in aerated solution at room temperature (Benjamin et al. 1988).

6.1.2.2 Effect of material properties

The material properties known to have an effect on the SCC of pure Cu are: (i) phosphorus content and (ii) grain size. In addition, consideration must be given to possible differences between base metal and welded material.There have been two systematic studies of the effect of P content of pure Cu on the SCC behaviour in ammonia environments (Thompson and Tracy 1949, Sato and Nagata 1978). In both cases, tests were performed in moist atmospheres with ammonia vapour. Figure 6-5

a) Dependence of time-to-failure on p content (Thompson and Tracy 1949).

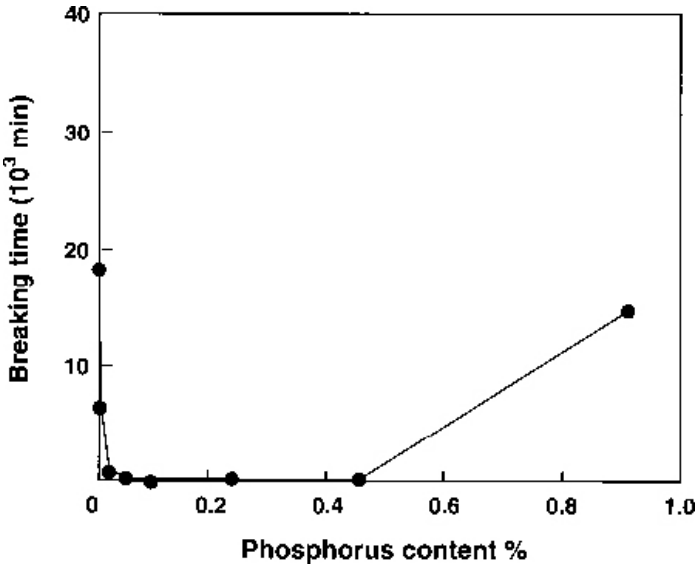

b) Effect of p content and applied tensile stress on SCC of Cu (Sato and Nagata 1978).

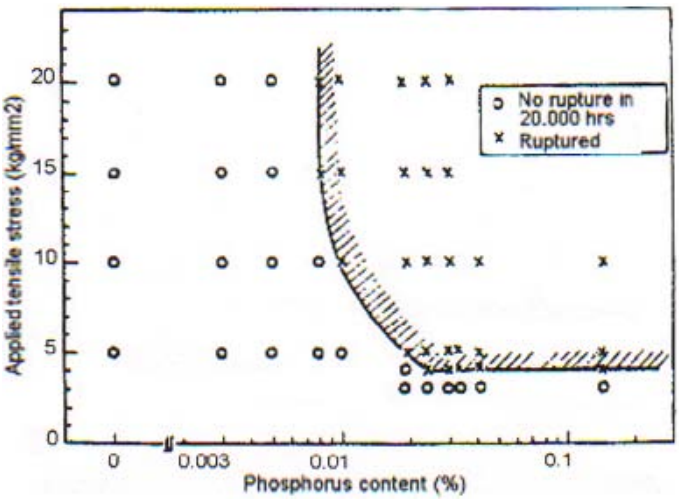

Figure 6-5. *Effect of phosphorus content on the SCC of copper in moist ammonia atmospheres.*

shows the results from the two studies. Thompson and Tracy (1949) report a ductility minimum at a P content of ~0.014 wt.% (140 ppm), with a measurable decrease in ductility for P contents as low as 40 ppm. These results are broadly in line with the later findings of Sato and Nagata, who found a threshold P content of between 50 and 80 ppm P. In contrast to these studies in ammonia environments, Benjamin et al. (1988) found no difference between the behaviour of OFHC and PDO Cu (P content unknown) in a range of nitrite solutions and a synthetic Swedish groundwater.

Grain size can affect both the initiation and propagation of SCC. In general, initiation of cracking is favoured by a smaller grain size (Yu et al. 1987), whereas crack propagation is favoured by larger grains. Much of the evidence for the effect of grain size on the SCC of Cu alloys comes from studies on α-brass. The exception is the study of Sato and Nagata (1978) in moist ammonia atmospheres. Figure 6-6(a) shows the dependence of failure (ruture) time of Cu-300 ppm P tensile samples in a

a) Effect of grain size on the time-to-rupture by SCC of a Cu-300 ppm P alloy in moist air in contact with 49 mg/L ammonia (Sato and Nagata 1978).

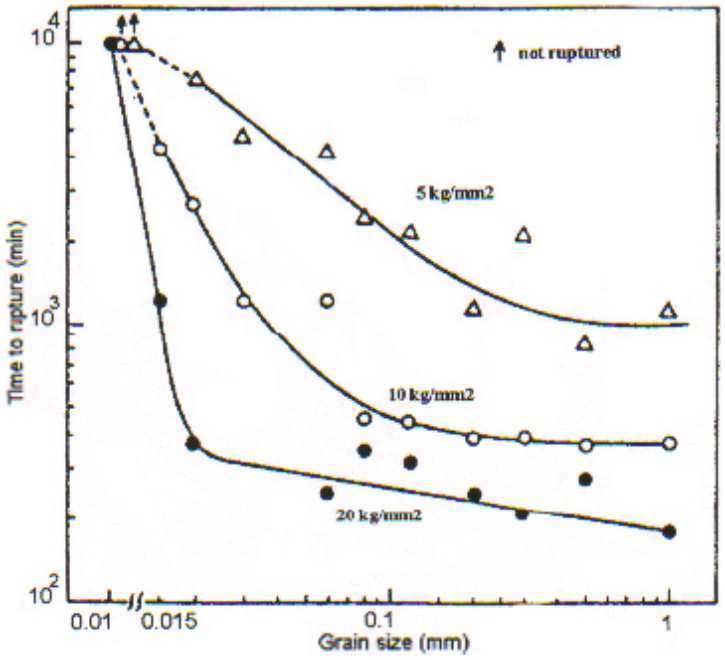

b) Effect of grain size on the time-to-failure by intergranular SCC of Cu-30Zn in moist ammonia atmospheres (Pugh et al. 1969).

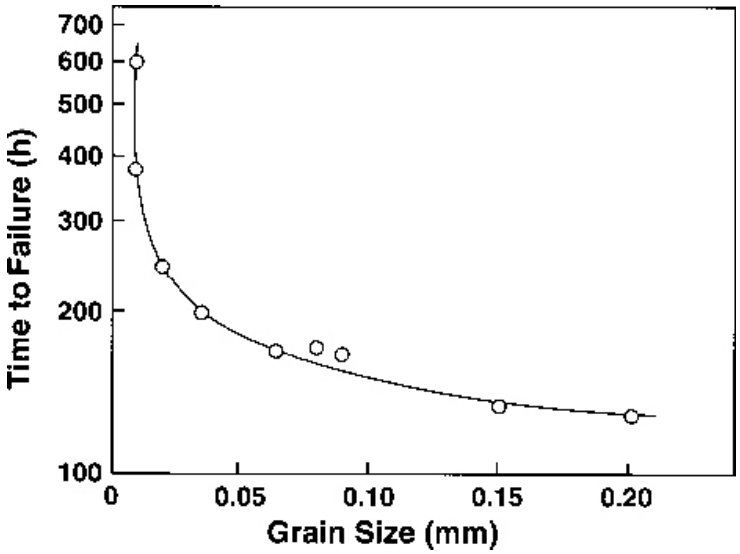

Figure 6-6. *Effect of grain size on the SCC of copper alloys.*

moist ammonia atmosphere for various applied tensile stresses. The susceptibility increases with increasing grain size, suggesting that the effect of grain size on crack propagation outweighs its effect on crack initiation. Alloys with grain sizes of ~10 μm were relatively immune, but the susceptibility increased significantly for grain sizes of between 10 and 100 μm, and became relatively insensitive for larger grain sizes. A similar trend has been observed for α-brass (Figure 6-6(b)), with a significant increase in susceptibility between grain sizes of 10 μm and 100 μm.

No study has yet shown a significant difference in the SCC behaviour of base metal and electron-beam (EB) welded OFP Cu. Arilahti et al. (2000) did not observe cracking for either the base metal or EB-welded OFP Cu in deaerated synthetic Olkiluoto groundwaters with 1–100 mg/L ammonia at 100°C. The respective grain sizes of the base and welded materials were 190–260 μm and 260–430 μm. Thus, the grain size of both materials is within the range where no difference based on grain size would be expected (Figure 6-6). Ikeda and Litke (2000) report a lower stress intensity factor for crack growth (K_{ISCC}) for EB-welded OFP Cu than for the base metal, but reported similar crack growth rates for the two materials. Again, the grain size of the two materials were > 250 μm.

Pettersson and Oskarsson (2000) introduced various degrees of cold work into annealed OFP Cu samples and studied their SCC behaviour in nitrite solutions. The use of cold-worked material was partly for experimental convenience, as annealed samples suffered extensive plastic deformation. In SSRT experiments, samples with 20% cold work were marginally more susceptible than annealed specimens (13% elongation-to-failure for cold-worked material versus 15% for annealed), although the difference in the ductility in air was much greater (17% and 48% for the cold-worked and annealed material, respectively). Mori and co-workers (Mori et al. 2003, 2005, Schwentenwein et al. 2002) also introduced cold work to PDO samples and found intergranular SCC at stresses significantly below the yield strength (threshold stress ~25 MPa compared with a yield strength of 220 MPa). The behaviour of this semi-hard copper is unusual, both in terms of the crack path and the low value of the threshold stress. Because the nature of this material is quite different from the more ductile material from which the canister will be fabricated, care should be taken in drawing inferences from the work of Mori et al. for the performance of the canister.

6.1.2.3 Stress-related effects

Canisters will be subject to both applied stresses (from swelling of the buffer and from hydrostatic loading) and a residual stress (from the non-heat-treated final closure weld). Stress effects on SCC are usually reported in terms of the stress-dependence of crack initiation and crack growth or, for pre-cracked specimens, as a stress intensity factor. The applied stress, and the consequent strain, may affect both the cracking process(es) and/or result in creep of the material.

Pettersson and Oskarsson (2000) reported the results of a fracture-mechanics study of the SCC of OFP Cu. Figure 6-7(a) shows a schematic illustration of the dependence of crack velocity on stress intensity factor (K_I). In Region I, the crack velocity is a strong function of K_I. A threshold stress intensity factor (K_{Ith}) may exist, below which the crack velocity is truly zero. A more practical threshold value is the K_{ISCC}, which may be experimentally measured. In Region II, crack growth is limited by non-mechanical factors (e.g. the environment), and in Region III mechanical overload occurs.

In Region I, the crack velocity (v) depends on K_I

$$v = C \cdot (K_I)^n \qquad 6\text{-}7$$

where C and n are constants. By fitting their data to this expression, Pettersson and Oskarsson (1997, 2000) proposed that the crack growth rate in $NaNO_2$ solutions could be described by

$$v = 5.2 \cdot 10^{-24} (K_I)^{11} \qquad 6\text{-}8$$

where v is in $mm \cdot s^{-1}$ and K_I is in $MPa \cdot m^{1/2}$. (Data from various sources, employing various $[NO_2^-]$ and potentials were used to develop equation 6-8). Further studies have indicated an approximate K_{ISCC} value for cold-worked material of ~30 $MPa \cdot m^{1/2}$ (Figure 6-7(b)).

Conditional stress intensity factors for crack growth of annealed and EB-welded OFP Cu have been estimated in the Canadian programme (Ikeda and Litke 2004, 2007, 2008, Litke and Ikeda 2006, 2008). In this case, true stress intensities could not be calculated because the test-specimens

a) Schematic illustration of the effect of stress intensity on crack velocity.

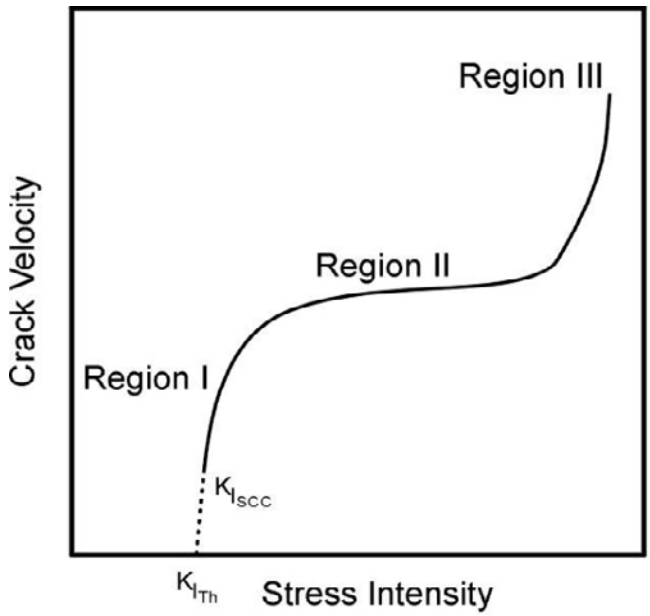

b) Experimental measurements of the effect of stress intensity factor (K) on the crack growth rate (da/dt) for OFP copper in sodium nitrite solutions (Pettersson and Oskarsson 2000).

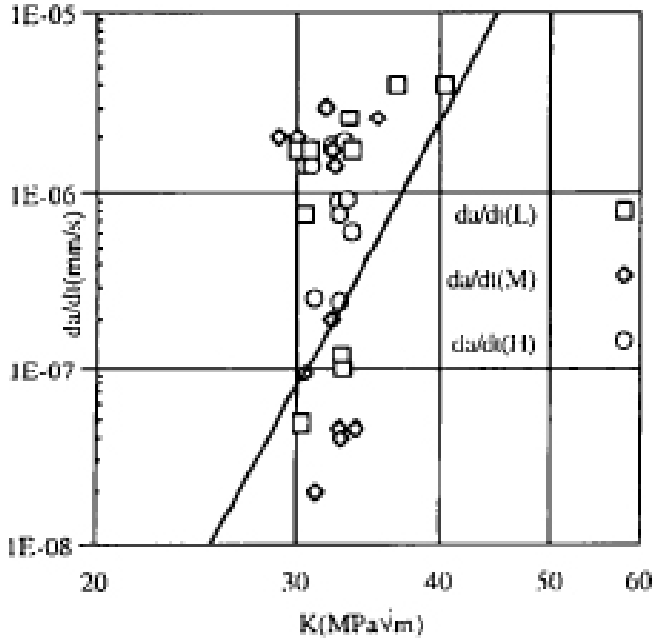

Figure 6-7. *Effect of stress intensity on SCC crack growth.*

were of sub-standard size, due primarily to the low yield strength of the material (as opposed to the cold-worked material used by Pettersson and Oskarsson (2000)). The parameter determined (K_Q) is the estimated stress intensity at which cracks started to grow during the constant extension rate tests on pre-cracked compact-tension specimens. For the base metal, an upper bound for K_Q was estimated to be ~22 MPa·m$^{1/2}$. That of the EB-welded material was much lower, but this could have been an artifact due to the method used to estimate the load at which crack growth occurred and the much shorter elastic deformation range for the welded material (Ikeda and Litke 2000). Khanzin and Nikulin (2005) reported threshold stress intensity factors for crack initiation and growth of 10.5 MPa·m$^{1/2}$ and 29.3 MPa·m$^{1/2}$, respectively. Reviewing the data of Hietanen et al. (1996), King et al. (1999a) and Pettersson and Oskarsson (2000) in nitrite solutions, Rosborg and Werme (2001) noted the difficulty in defining a K_{ISCC}, since the values reported in these various studies ranged from 16–30 MPa·m$^{1/2}$.

On un-cracked specimens, the equivalent parameter is the threshold stress for crack initiation and/or growth. There have been relatively few reports of the threshold stress for the SCC of Cu and none in simulated repository conditions. Saario et al. (1999) report a threshold stress of 120 MPa for Cu in 1 mol·dm^{-3} $NaNO_2$ at room temperature, and suggest a much smaller value (~40 MPa) in ammonia environments. This latter value comes from the study of Sato and Nagata (1978), who studied the SCC of Cu-P alloys in moist ammonia atmospheres. For example, the results in Figure 6-5(b) suggest a threshold load of ~3 kg·mm^{-2}, equivalent to a stress of ~30 MPa.

King (2004) considered the effects of surface-breaking defects on both the localised corrosion and SCC behaviour of copper canisters. Stress concentration at pits could lead to crack initiation under some circumstances, but the stress intensity factor for the resultant cracks, or for pre-existing crack-like discontinuities, will be smaller than the minimum threshold stress intensity factor (K_{ISCC}) for copper reported in the literature. Therefore, any cracks that do initiate will tend to become dormant.

The impact of the applied stress is to cause strain at the crack tip. This strain may have both detrimental and beneficial effects. Strain at the crack tip will rupture protective oxide films, or prevent their formation in the first place) (FRAD and TR mechanisms, equations 6-2 and 6-3) or initiate cracks which then propagate into the underlying ductile material (the FIC mechanism, equation 6-4). The theoretical crack growth expressions for each of these mechanisms suggest that the crack velocity will increase with crack-tip strain rate. This is indeed found to be the case, as reported by Benjamin et al. (1998) and Yu and Parkins (1987) for OFHC and PDO Cu in nitrite solutions, although Rosborg and Svensson (1994) found cracking to be most evident at an intermediate strain rate in their tests in aerated 0.3 mol·dm^{-3} $NaNO_2$. This latter observation is consistent with a FRAD mechanism, for which the optimum balance between the crack-tip repassivation and film-rupture processes can be established at an intermediate strain rate.

Strain at the crack tip may also be in the form of creep. Although creep could rupture protective films at the crack tip, sustaining crack growth, it could also blunt cracks by relieving the stress at the crack tip. Stress relief through creep is more likely at higher temperatures. Creep of the Cu shell could be a significant factor, both in terms of the mechanical stability and the SCC behaviour of the canister. A number of creep studies have been performed on OFP Cu (Andersson et al. 1999, Henderson 1994, Henderson et al. 1992), but no detailed analysis of the interaction of creep and SCC has been performed. There are indications, however, in the results of Pettersson and Oskarsson (2000) that crack-tip creep will slow crack growth. In at least two of the reported tests, the crack growth rate under constant load conditions decreased with time, presumably as a result of creep at the crack tip.

6.2 Approaches to predicting the SCC behaviour of copper canisters

6.2.1 General approaches to predicting the SCC of copper canisters

Two broad approaches have been taken to predict the SCC behaviour of Cu canisters. The first is that there exist threshold values for various environmental, material and mechanical parameters, below which the crack growth rate is zero. The other approach has been to assume that the crack growth rate is always finite, but that it is so small that failure of the canister by SCC does not occur within the required lifetime. There are advantages and disadvantages to each approach.

An example of the threshold approach is that proposed by Saario et al. (1999), in which various "boundary conditions" were defined for the SCC of Cu in nitrite and ammonia environments. For example, threshold potentials for SCC can be defined based either on experimental data or on thermodynamically calculated potentials for the formation of the requisite Cu_2O or other type of film. Threshold concentrations (particularly for nitrite) and stresses can also be defined. The true threshold stress intensity factor (K_{Ith}, Figure 6-7(a)) can also be used to define conditions under which the crack growth rate is zero.

The advantage of the "threshold" approach is that it defines an absolute set of conditions under which SCC will not occur. The disadvantage of this approach is that the threshold values may need to be determined over a wide range of conditions, and it is difficult to guarantee that the crack

growth rate is zero. For instance, it is currently impossible to measure crack velocities of less than ~10^{-9} mm·s^{-1}. However, a crack growing at this rate would penetrate a 50-mm-thick canister in < 1,600 years. Thus, if threshold values are to be used, they must be soundly based on mechanistic principles (e.g. the potential at which a Cu_2O or some other film grows), and should be used with a suitable margin of safety (e.g. E_{CORR} should be a minimum of X volts below the threshold potential). Long-term exposure tests can be used to support lifetime predictions based on this approach.

In the alternative approach, the crack growth rate is measured under accelerated conditions, from which predictions are made about the crack growth rate for the canister using suitable extrapolation techniques. Pettersson and Oskarsson (2000) have proposed such an approach, based on fracture-mechanics principles (Figure 6-7(a)). A similar "limited-propagation" model has also been proposed in Canada (King and Litke 1997), in which the crack growth rate is estimated as a function of the evolving conditions in the repository.

The advantages of the limited-propagation approach are that it (i) avoids the problems associated with defining threshold parameters and (ii) tends to provide a conservative assessment. The disadvantages are that long extrapolations may be required because tests must be greatly accelerated in order to measure crack growth rates, and that as a consequence, the predictions may be too conservative. Extrapolation of experimental data is aided by the use of mechanistic models which provide a basis for the extrapolation.

6.2.2 Specific approaches to predicting the SCC of copper canisters

Various approaches have been taken towards, or proposed for, the prediction of the long-term SCC behaviour of Cu canisters. Here, the various approaches are categorized according to the three pre-requisites for SCC: a suitable environment, a susceptible material, and a sufficient tensile stress.

6.2.2.1 Approaches based on the repository environment

Since more is known about the effect of environmental parameters on the SCC of Cu than the effects of stress or material properties, the majority of attempts at predicting the long-term behaviour of copper canisters have been based on the environmental conditions in the repository. Of the two general approaches to predicting SCC discussed above (the threshold and growth rate approaches), most of the assessments performed to date have involved the concept of one or more threshold environmental conditions.

An important consideration when making predictions of the long-term SCC behaviour is the evolution of environmental conditions in the repository. Since all SCC mechanisms involve some degree of oxidation of the metal (apart from the intrinsic susceptibility of the SM model), the probability of SCC will diminish with time as conditions become anoxic (Section 6.1.2.1). Thus, as with other forms of localized and general corrosion (see Section 5), SCC should be a relatively short-term phenomenon. As a consequence, what seems at first to be a formidable task of guaranteeing that a Cu canister will not fail by SCC over a period of at least 100,000 years simplifies into one of demonstrating that SCC will not cause canister failure over a much shorter time period of, perhaps, a few hundred years.

Saario et al. (1999) started the development of an SCC model based on the concept of threshold parameters (or boundary conditions (Saario et al. 1999)) for SCC. Thus, a threshold concentration and critical potential (E_{SCC}) are defined for each SCC agent (nitrite, acetate, and ammonia). Then, provided the concentration of these species at the canister surface and the canister corrosion potential are below the respective threshold values, SCC will not occur.

Threshold concentrations and E_{SCC} values have been estimated based on a survey of the available literature and theoretical considerations. Based primarily on the studies of Parkins and co-workers (Benjamin et al. 1988, Yu and Parkins 1987), the threshold NO_2^- concentration for the SCC of pure Cu alloys is ~0.001 mol·dm^{-3} (equivalent to 46 mg/L NO_2^-). From the same studies, duplicated subsequently by others (Saario et al. 1999), E_{SCC} in nitrite environments is ~0.1 V_{SHE} (–0.14 V_{SCE}). In comparison, the *maximum* [NO_2^-] in deep Finnish groundwaters is ~0.02 mg/L (Table 2-4). Since there is no other significant source of nitrite in the repository (assuming nitrite blasting residues can be avoided or only persist in the vicinity of the deposition hole for a short period of time), it can be

concluded that nitrite-induced SCC of Cu canisters will not occur. In addition, the long-term redox conditions in the groundwater (E_H of –0.2 to –0.3 V_{SHE}, Anttila et al. 1999a, b) are more-negative than E_{SCC}. (The thermodynamic redox potential represents the maximum value of E_{CORR}).

King and co-workers (King and Kolář 2004, 2005, Maak and King 2005) have developed this concept of relating the SCC susceptibility to the evolution of the repository environment in more detail. The approach is based on a decision tree (Figure 6-8) that defines the various pre-requisites for SCC of copper canisters.

The first pre-requisite for SCC is that the potential and interfacial pH exceed a threshold value defined by the Cu_2O/CuO equilibrium line. This threshold is based on the observation that virtually all instances of cracking reported in the literature (regardless of whether in ammonia-, acetate-, or nitrite-containing solutions) occur at potentials and pH values above this equilibrium line (Figure 6-1 and discussed in Section 6.1.2.1). It is not suggested that a duplex Cu_2O/CuO film is present at the crack tip or is in any way directly involved in the cracking processes. Indeed, the potential at the crack tip is likely to be more negative (due to iR effects) and the pH more acidic (due to hydrolysis of copper ions inside the crack) than that required for the formation of a Cu(II) film. However, it does appear that the external E and pH conditions in the bulk solution outside the crack can be used to predict whether cracking could occur, even though the cracking process itself will be largely determined by the local environment inside the crack.

Prediction of the external potential (E_{CORR}) and pH is performed with a variant of the Copper Corrosion Model, referred to as the Copper Corrosion Model for Stress Corrosion Cracking (CCM-SCC) (King and Kolář 2004, 2005). Figure 6-9 shows the predicted variation of E_{CORR} and the interfacial pH superimposed on a Pourbaix diagram showing the equilibrium lines for the various copper oxide/hydroxide equilibria. The locus of points represents the time evolution in the repository over a period of 10^6 years as the O_2 initially trapped in the pores of the buffer and backfill materials is consumed and conditions become less oxidising. In fact, the threshold conditions defined by the Cu_2O/CuO equilibrium are predicted to be exceeded for only the first three years following repository closure. (The CCM-SCC model simulates the period starting from the point at which the buffer and backfill have been emplaced and the repository has been sealed to prevent any additional O_2 ingress). Therefore, based on this criterion alone, the period of SCC susceptibility is predicted to be short in comparison to the lifetime of the canister.

The next pre-requisite in the decision tree is whether the known SCC agents (ammonia, acetate, and nitrite) are present at the canister surface in sufficient concentration to produce cracking. A possible source of such species is microbial activity in the repository, with the metabolic by-products then diffusing to the canister surface. However, calculations using the CCM microbial model (Section 2.3.4) suggest that the maximum concentration of such species reaching the canister surface will be $< 10^{-10}$ mol·dm^{-3} (King and Kolář 2006b, King et al. 2002b, 2003, 2004), from which it can be concluded that SCC will not occur even for the early period when the combination of E and pH is in the permissive range.

The decision tree contains further pre-requisites related to the inhibitive effect of Cl^- ions, the increase in ductility at elevated temperature, and the requirement for a tensile stress (Figure 6-8), each of which further reduce the probability of cracking.

The decision tree approach discussed above is largely based on the argument that SCC is only possible during the early aerobic period because crack growth requires a certain degree of oxidation. However, the SM model for SCC (Galvele 1987) implies an inherent susceptibility of metals to crack growth in the absence of anodic dissolution. In addition, the observations of SCC in sulphide solutions (Taniguchi and Kawasaki 2008) raises the question of whether cracking could occur during the long-term anaerobic phase. King and Newman (2010) considered the possibility of SCC during the anaerobic phase and concluded that there is no credible evidence to support such a suggestion. First, as detailed above (Section 6.1.1), the SM model in the form proposed by Galvele and co-workers appears to be incorrectly formulated. When corrected for the effects of stress on the decrease in vacancy formation energy for surfaces and for capillary closure effects for sharp cracks, the SM model predicts insignificant crack growth rates (of the order of 10^{-20} m·s^{-1}), regardless of whether surface diffusion is enhanced by dissolution or not.

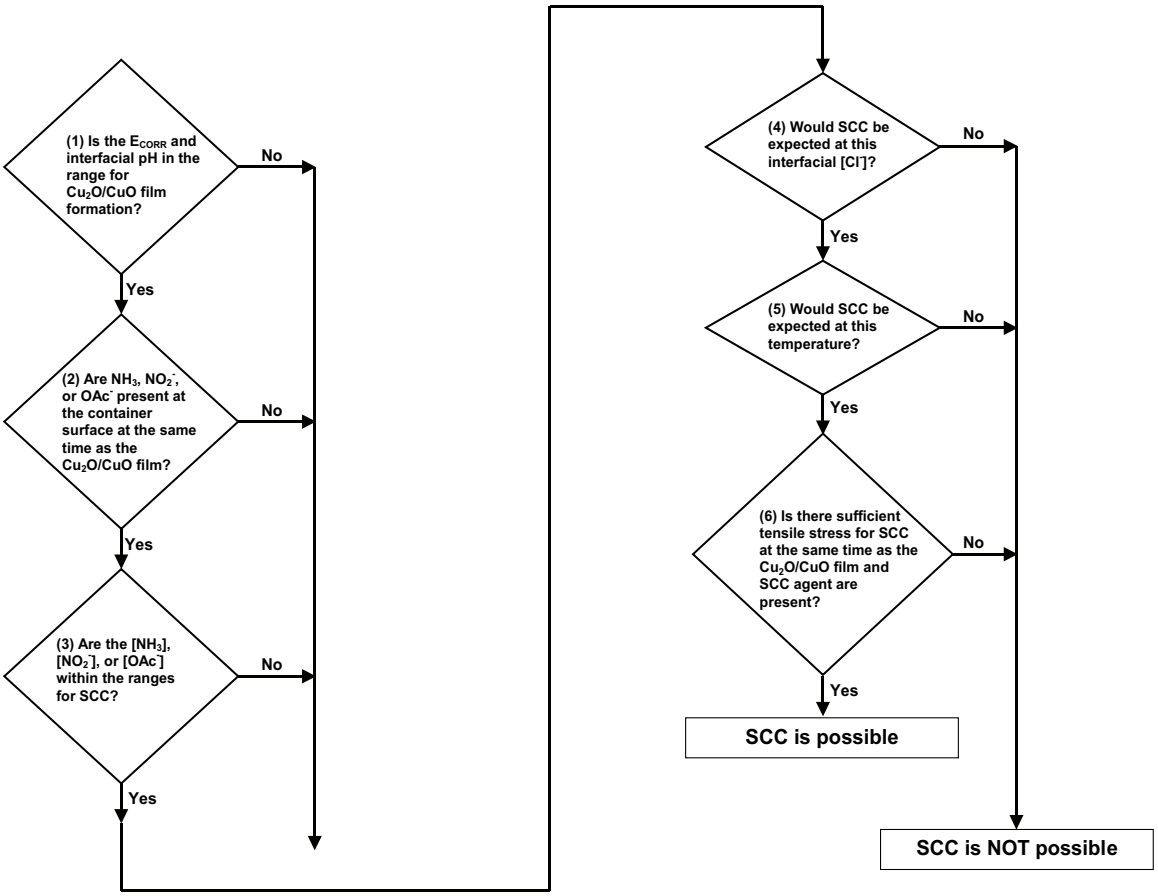

Figure 6-8. *Fault tree approach to predicting the possibility of stress corrosion cracking of copper canisters (King and Kolář 2004).*

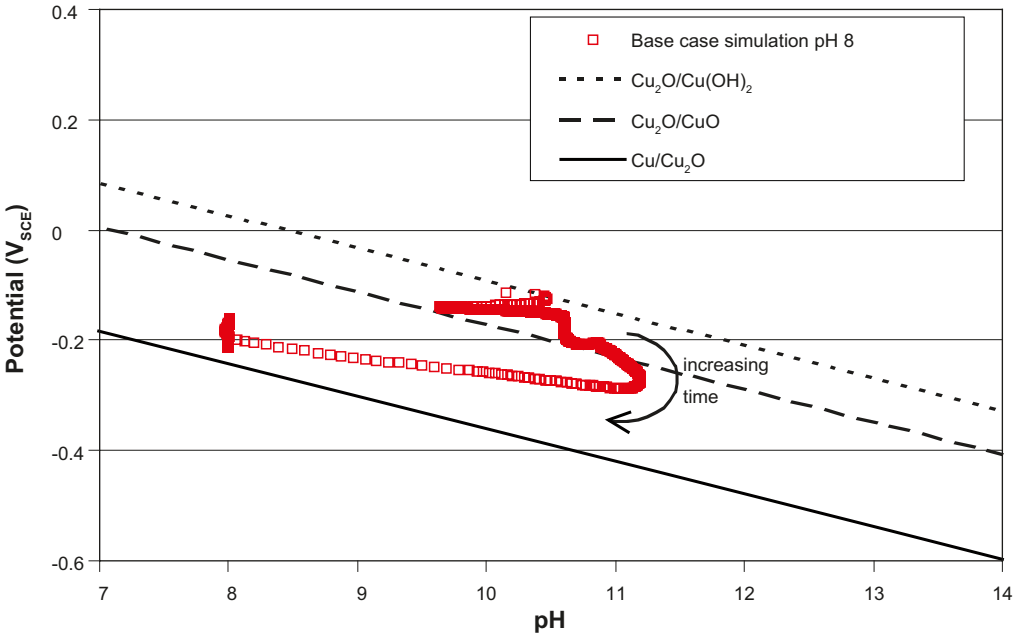

Figure 6-9. *Predicted time dependence of the corrosion potential and interfacial pH for a copper canister in a repository based on the copper corrosion model for stress corrosion cracking (King and Kolář 2005, Maak and King 2005). Each point represents the predicted corrosion potential for an individual time step in the simulation. The spacing of the time steps increases according to an arithmetic series from as short as a few seconds at early times to as long as 20,000 years after 10^6 years.*

King and Newman (2010) also argued that sulphide would not lead to cracking of canisters in a repository by any of the other SCC mechanisms (Section 6.1.1). The rate of general corrosion during the anaerobic phase will be determined by the rate of supply of HS^- to the canister surface, partly because of the presence of highly compacted bentonite. Consequently, the interfacial [HS^-] will be small and the concentration of sulphide at the tip of any crack will be effectively zero. Therefore, HS^- will not reach the crack tip to support cracking by either FRAD or TR mechanisms. Crack growth by the FIC mechanism also requires a certain degree of sulphidation at the crack tip to produce a film, but in addition to the requirement for HS^- at the crack tip, the properties of the film formed must also be suitable for generation of the cleavage crack. However, the available evidence (Smith 2007) suggests that the Cu_2S films are not adherent and, therefore, are unlikely to sustain a FIC mechanism.

In conclusion, therefore, there is no evidence to suggest that SCC will continue beyond the initial aerobic period when the necessary oxidants (O_2 or Cu(II)) are present in the repository.

6.2.2.2 Approaches based on the canister material

There has been no attempt to argue that SCC of Cu canisters will either not occur or will be limited in extent based on the properties of the canister material. Based on the P content and grain size of the proposed alloy, it is difficult to claim that the canister would be immune to SCC. For example, the proposed P content of 30–80 ppm exceeds the threshold P contents for SCC in ammonia environments reported by both Thompson and Tracy (1949) and Sato and Nagata (1978) (Figure 6-5). In addition, the possibility of large grain sizes in the annealed canister shell, as a consequence of EB welding, also renders the material potentially more-susceptible to SCC (Figure 6-6), although the use of friction-stir welding (which does not cause excessive grain growth) would minimise the impact of increased grain size.

6.2.2.3 Approaches based on the effect of stress

Several stress-related arguments can be made regarding the susceptibility of Cu canisters to SCC. These arguments include: (i) the existence of a threshold stress for SCC, (ii) crack exhaustion due to compressive stresses in the canister wall, (iii) the detection of sub-critical flaws based on fracture mechanics principles, (iv) the time dependence of the crack-tip strain rate, and (v) the effect of creep on stress relaxation.

There is relatively little information available regarding the threshold stress for SCC of Cu in relevant environments. Only two values were reported by Saario et al. (1999) (140 MPa in 1 mol·dm^{-3} $NaNO_2$ at room temperature, and ~40 MPa in moist ammonia atmospheres). It is likely that the outer Cu shell will undergo some plastic deformation with inevitably some tensile component on the canister surface, making it difficult to claim that the sum of the applied and residual stresses will not exceed the threshold stress for SCC.

Saario et al. (1999) have suggested that a propagating crack will stop growing because of compressive stresses in the Cu shell. Whilst it is true that the tensile and compressive stresses must be balanced through the canister wall, the actual distribution of stresses is difficult to predict and may change with time in response to deformation of the Cu shell. Therefore, no attempt has been made to argue that SCC will be limited by the presence of compressive stresses in the canister wall.

Based on their crack growth rate measurements as a function of stress intensity factor (equation 6-8), Pettersson and Oskarsson (1997) predicted the size of the deepest sub-critical defect that would lead to canister failure within a given period of time. These authors used the limited-propagation approach, rather than rely on a threshold stress intensity factor for SCC (K_{ISCC}), even though their own data could be used to estimate a K_{ISCC} value. Based on a crack growth rate of $3 \cdot 10^{-12}$ mm·s^{-1} (equivalent to ~10 mm crack growth in 100,000 years and, therefore, insufficient to lead to canister failure), Pettersson and Oskarsson estimated a corresponding stress intensity factor of 12 MPa·m$^{1/2}$ that could not be exceeded on the canister surface. For an assumed maximum tensile stress of 100 MPa, this stress intensity factor corresponds to a defect size of ~5 mm. Because such a deep defect would be readily detectable by inspection, Pettersson and Oskarsson argued that the actual defect size and the corresponding stress intensity would be smaller than 12 MPa·m$^{1/2}$ so that the maximum crack depth after 100,000 years would be < 10 mm.

Rosborg and Werme (2001) have reviewed all the available data relating the crack velocity to K_I. Given the wide range of K_{ISCC} values estimated from the various studies (16–30 MPa·$m^{1/2}$), they concluded that predicting the long-term SCC behaviour based on the existence of a threshold K_I for SCC would be difficult.

A stress-based argument proposed in the Canadian program, but never developed further, was that the period of crack-tip strain will be limited. Crack-tip strain (or stress, in the case of the SM model) is a crucial factor in supporting crack growth for all SCC mechanisms (equations 6-2 to 6-5). If a thick inner steel or cast iron insert is used to support the external load (as in the Swedish/Finnish canister design), strain of the outer Cu shell is only possible until such time that the initial gap between the outer canister shell and cast iron insert is closed by deformation of the Cu shell. Once the gap has been closed, deformation of the Cu shell will only be possible by creep. Thus, the strain (deformation) rate of the Cu shell, and, hence, also at the tip of any crack in the shell, will be high initially as the hydrostatic load increases, but will then diminish considerably after the collapse of the shell onto the inner cast iron insert. It might be possible to argue, therefore, especially in conjunction with other limiting factors such as either the combination of E_{CORR} and the interfacial pH or the interfacial concentration of SCC agent at the canister surface, that SCC will either not occur or will do so for such a short time that the canister will not fail.

The final stress-related argument against the SCC of a Cu canister is based on the creep behaviour of the Cu shell. Creep is a result of tensile stress and serves to relieve the stress through deformation of the material. One of the prime requirements for specification of the material for the outer Cu shell is that it should have a suitable creep rate and creep failure strain. Much work has gone into the specification of a suitable alloy composition (Andersson et al. 1999, Henderson 1994, Henderson et al. 1992). The crack growth rate under possible repository conditions will be so slow that creep processes will relieve crack-tip stresses before crack growth can occur. In this way, creep of the Cu shell will preclude any possible SCC.

6.3 Summary of the stress corrosion cracking of copper canisters

As stated at the beginning of this section, there is extensive experience with, and knowledge of, the SCC of Cu alloys. Considerable effort has gone into studying the mechanism of SCC of Cu canisters.

The three pre-requisites for SCC are a susceptible material, a tensile stress, and a suitably aggressive environment. The proposed canister material cannot be claimed to be immune to SCC, since pure coppers, especially those containing phosphorus, have been shown to be susceptible. Tensile stresses on the canister surface are possible during various stages in the evolution of the repository environment, either due to external loads or from residual manufacturing stresses. Finally, it is not possible to exclude the possibility that known SCC agents, i.e. ammonia, nitrite, or acetate, may be present in the repository. Therefore, the possibility of SCC of Cu canisters must be considered.

As with other forms of corrosion, the available evidence indicates that the probability of SCC of a Cu canister will diminish with time as the repository environment evolves. Because of this, the difficult task of predicting the SCC behaviour of components with design lifetimes of the order of 100,000 years is reduced to a simpler task of predicting the SCC behaviour over the much shorter duration of aggressive conditions (perhaps of the order of tens to hundreds of years). Conditions will be at their most suitable for SCC early in the evolution of the repository environment. Oxidant will be available in the form of trapped atmospheric O_2 and/or Cu(II) produced by corrosion of the canister. Ammonia, and possibly acetate ions, will be present in the groundwater and, possibly as a result of human activity during construction (Saario et al. 1999), although it is unlikely that sufficient SCC agent, including nitrite, will be present at the canister surface to cause SCC. Furthermore, the beneficial effects of Cl^- ions will not be fully felt until the bentonite pore water has equilibrated with the groundwater. During this early period, the outer Cu shell may also be subject to considerable strain as the hydrostatic load develops and the Cu shell is deformed onto the inner cast iron insert. As the available oxidant is consumed, as the pore water becomes more saline, and as the buffer material saturates and restricts the transport of SCC agents from the groundwater to the canister surface, the probability of SCC will diminish accordingly. Only the decrease in repository temperature with time

will tend to render the canister more susceptible to SCC. The period of highest SCC susceptibility is not known with certainty, but is likely to be of the order of tens or hundreds of years.

In addition to there being a low probability of SCC during the initial warm, aerobic period, there is no evidence to suggest that cracking can be sustained during the long-term anaerobic phase in the absence of oxidants or due to the presence of sulphide. Although the surface mobility model predicts an inherent susceptibility to SCC for all metals in the absence of dissolution, the correctly formulated crack growth expression predicts vanishingly small crack propagation rates (< 0.1 μm in 100,000 years). Furthermore, no HS^- will reach the crack tip as the rate of corrosion of the canister surface by sulphide is transport limited due to the slow rate of supply of HS^- through compacted bentonite. The absence of sulphidation at the crack tip precludes crack growth based on the film-rupture, tarnish-rupture, or film-induced cleavage mechanisms. Film-induced cleavage can also be ruled out because the properties of the non-adherent sulphide films formed on copper will not support the generation of a cleavage crack in the underlying copper.

7 Corrosion induced by radiation effects

Summary of changes to section on the effects of γ-radiation

There have been relatively few studies of the effects of radiation on the corrosion of copper published since the original report. Therefore, only minimal changes have been made to this section, including:

- The addition of a reference to new calculations of the electron radiation level on the outside of a copper canister.
- A discussion of a recent study of the effects of γ-radiation on copper electrodes.
- Reorganisation of the section, including a new section on the effect of γ-radiation on the corrosive environment.

7.1 Effect of γ-radiation on the corrosive environment

The corrosion environment will be determined by the groundwater chemistry at the disposal site and the chemical properties of the buffer and backfill. In addition to these factors, the near field environment will, for the first few hundred years after disposal, also be influenced by the γ-radiation field outside the canister. The radiation is dominated by the decay of ^{137}Cs, which has a half-life of 30 years.

Lundgren (2004) re-estimated the external γ-radiation field for a copper canister with a cast iron insert based on a calculation of the flux of secondary electrons. The *average* dose rate was found to be 0.1 Gy/h, similar to the average γ dose rate calculated earlier using a point-kernel technique (Lundgren 1998) which gave a *maximum* dose rate of 0.5 Gy/h. With a ^{137}Cs half-life of 30 years, the dose rate will have dropped to negligible levels after a few hundred years.

The main effect of γ-radiation on the corrosion behaviour of the copper canister will be through radiolysis of the gases and the aqueous solutions that are present close to the canister surface. Radiolysis will produce oxidizing and reducing radicals and molecular species. In pure water, the oxidizing species include radicals, such as OH•, and molecular species, such as O_2, H_2O_2 and O_2^-. The reducing species will include H, e_{aq}^- and H_2. In a closed system, a steady state will develop rapidly and the net production of radiolytic species would cease. Calculations by Sunder and Christensen (1993) show that steady state is reached after about 20 hours. The concentrations of oxidants are then in the range 10^{-12} to 10^{-10} mol·dm^{-3} for a dose rate of 1 Gy/h. However, these calculations are for a system in which there is no reactive interface (i.e. the corroding canister surface) consuming radiolysis products. Consequently, the total yield and relative amounts of the various radiolysis products may differ.

The canister near field in the repository cannot be regarded as closed. Gaseous hydrogen is mobile and will escape from the near field faster than the dissolved oxidizing species, resulting in a mildly oxidizing environment. The oxidants, on the other hand, may be consumed through oxidation processes, e.g. by oxidising Fe(II) in the bentonite or dissolved Fe^{2+} in the pore water or supporting corrosion of the canister. The overall effect of radiolysis on the near-field redox conditions will depend, therefore, on the relative mobility and reactivity of the oxidising and reducing species.

In groundwater, other species may also be produced depending on the composition of the solution. For example, in highly saline solutions, chloride species are produced (Cl_2^-, Cl_2, ClO^- etc.) and at high carbonate concentration the carbonate radical may form ($CO•_3^-$). During radiolysis of moist air, nitrogen oxides (and as a consequence, nitric oxide) will be produced.

7.2 Corrosion in air in the presence of γ-radiation

Experimental studies of the effects of γ-radiation on corrosion have been performed within the Yucca Mountain Project in the U.S. for corrosion in moist air (see e.g. Yunker and Glass (1986) and Reed and Van Konynenburg (1991)).

Yunker and Glass reported results from the exposure of oxygen free copper to an air/water vapour mixture at 150°C and to vapour-saturated air at 95°C in a γ-radiation field of 10^5 rad/h (10^3 Gy/h). This dose rate is a factor of 10,000 higher than the expected average surface dose rate on the canister. For exposures of about half a year, the corrosion rate at 150°C was about 1 μm/yr and at 95°C, it was about 4 μm/yr. The difference could be due to differences in relative humidity at the two temperatures.

Reed and Van Konynenburg (1991) performed experiments in both dry air and at 40% relative humidity at almost the same temperatures as Yunker and Glass. The dose rates were 0.021 Mrad/h (210 Gy/h) at 94°C and between 0.011 and 0.015 Mrad/h (110–150 Gy/h) at 152°C. The experiments were run for about 75 days. The observed corrosion rates ranged from about 1 μm/yr to 3 μm/yr. The dominant corrosion product at the longer exposure times seems to have been cuprite (Cu_2O).

Apart from a possible increase in the corrosion rate due to strongly oxidizing species being formed through radiolysis of water in air, there is also the possibility of the radiolytic formation of nitrogen oxides and nitric acid. Reed et al. (1990) confirmed formation of nitrogen oxides in the gas phase at all temperatures (90°C, 120°C and 150°C) and for both dose rates that were used in the experiments (0.7 kGy/h and 2 kGy/h). They also identified basic cupric nitrate ($Cu_2NO_3(OH)_3$) as a lesser component in the corrosion products, but only at lower relative humidity (< 15% RH). The dose rates used in the experiments are at least a factor of 1,000 higher than the maximum surface dose rate for the canister.

Marsh (1990) used a simple method to make a rough calculation of the quantity of nitric acid produced. The rate of formation is given by

$$\frac{d[HNO_3]}{dt} = \frac{G \cdot V \cdot \rho \cdot D_o}{A_v} \cdot e^{\frac{-0{,}693 \cdot t}{T}} \qquad 7\text{-}1$$

where G is the G value for HNO_3 (in number of molecules/eV), V the irradiated air volume (dm^3), ρ the density of air (g/dm^3), D the initial dose rate (eV/g·year), A_v Avogadro's number, t the time (years) and T the half-life (years) of the radiation source. If it is assumed that the γ-radiation has a half-life of 30 years (corresponding to ^{137}Cs), G = 0.02 molecules/eV and an air gap of 5 cm exists around the canister (V = 825 dm^3), then the production rate for nitric acid in the repository will be 0.002 mol/year. This is a very small quantity, which will have a negligible effect on the life of the canister.

The corrosion rates measured in the presence of γ-radiation are not higher than what one would expect for corrosion of copper in unirradiated moist air (see Section 4) indicating that the influence of radiation will be negligible even at dose rates considerably higher than the maximum surface dose rate for the canister.

7.3 Corrosion in water in the presence of γ-radiation

Corrosion in irradiated water has been performed by Nagra in Switzerland (Simpson 1984) and by AECL in Canada (see e.g. King and Litke 1987), and also within the Yucca Mountain Project (Yunker and Glass 1986). Corbel et al. (2003) report the effects of high γ-dose rates on copper electrodes. AECL has also published a review of the effects of γ-radiation on the corrosion of high level waste canister materials (Shoesmith and King 1999).

Yunker and Glass (1986) report copper corrosion rates in a fresh water of low ionic strength irradiated with 10^3 Gy/h for about 200 days. Whilst initially higher, the rate eventually attains a nearly constant value of about 2 μm/y after a few months. What appears to be the same data are also reported by Kass (1990), who also presents data in the absence of radiation showing that the

radiation has a very small effect, if any, on the corrosion of pure copper. The rates measured without irradiation are, in fact, slightly higher than those obtained with irradiation.

At much lower dose rates (13 Gy/h) Simpson (1984) finds lower corrosion rates in the presence of radiation than without irradiation. This observation is corroborated by King and Litke (1987). They used dose rates in the range 14 to 27 Gy/h for irradiation of copper in a saline solution (about 1 mol·dm^{-3} chloride) at 150°C. The experiments were performed in aerated and deaerated solutions and the corrosion rates were about a factor of four lower in the presence of radiation. King and Litke attributed this to the more protective nature of the surface film formed in irradiated solutions. Furthermore, they saw no effect of radiation on the corrosion potential. The corrosion rates (weight loss) were, however, very high, probably because of the high solution volume to surface area ratio in the tests. In deaerated solutions, however, King and Litke saw no difference in the corrosion rate in irradiated and unirradiated solutions.

Corbel et al. (2003) γ-irradiated copper electrodes in aerated synthetic clay water solution at an absorbed dose rate of 800 Gy/h. The clay solution had a total dissolved solids content of 2.3 g/L with a Cl^- concentration of 0.035 mol/L. The corrosion potential (E_{CORR}) of the copper electrode was found to increase by ~40 mV after 16 h of irradiation, an increase that was only partly reversed 4 days after removing the ^{60}Co source. The corrosion rate increased from 2 µm/y without radiation to 59 µm/y with radiation. The authors measured H_2O_2 concentrations in solution of between $5 \cdot 10^{-5}$ mol/L (15 min after the start of irradiation) to $3 \cdot 10^{-6}$ mol/L (70 hr after the start of irradiation). Although these results suggest increased corrosion rates in the presence of radiation, the relevance of this work to a copper-cast iron canister in saline groundwater is unclear because of (i) the high dose rates used in the tests, (ii) the use of aerated solution, and (iii) the use of a dilute clay water solution. The positive effect of irradiation on the corrosion rate observed by Corbel et al. (2003) is in contrast to the lack of any effect reported by Yunker and Glass (1986). This difference may be the result of the short exposure time in the experiments of Corbel et al. (2003) (Yunker and Glass also reported higher corrosion rates at short times) or differences in the solution composition between the two studies.

Available information shows that there is no evidence for enhanced corrosion rates caused by γ-radiation except, possibly, at high dose rates (> 100 Gy/h). At dose rates in the range of 10–100 Gy/h, the experimental data seem to indicate a lower corrosion rate in the presence of radiation.

8 Implications for the canister service life

Summary of changes made to the section on canister service life

Since the original report, there has been no change in the general conclusion that copper canisters will not suffer corrosion failures in periods of less than 10^6 years under design conditions (Werme et al. 2004). Indeed, the additional knowledge obtained in the intervening 8–9 years has strengthened that conclusion. New assessments have been carried out in Sweden (SKB 2006a, b), Switzerland (Johnson and King 2003), and Canada (King 2005). Table 8-1 has been updated accordingly.

8.1 Introduction

Formal assessments of the long-term corrosion behaviour of Cu canisters and predicted canister lifetimes have been presented in five countries. Sweden was the first country to propose the use of copper canisters in 1978 (Swedish Corrosion Institute 1978), since when various assessments have been published in Sweden and Finland (SKBF/KBS 1983, SKB 2006a, b, Swedish Corrosion Institute 1983, Werme 1992, 2001, Werme et al. 1992, Wersin et al. 1994a, Raiko and Salo 1999). In 1996, Canada presented a case study of the use of Cu canisters (Johnson et al. 1996), which has been subsequently extended to include sedimentary host rock (King 2005). Japan also considered the use of Cu canisters for the disposal of vitrified waste (JNC 2000). Finally, Switzerland are considering the KBS-3 method with copper-a cast iron canister as a back-up to the principal carbon steel candidate canister design (Johnson and King 2003).

Table 8-1 summarises the various assessments of the long-term corrosion behaviour of Cu canisters and, where given, the predicted canister lifetimes. A more detailed discussion of the predictions is given below.

8.2 Lifetime predictions from various international programmes

8.2.1 Sweden/Finland

The corrosion processes considered in the Swedish/Finnish studies include: general corrosion under oxic and anoxic conditions, localised corrosion (pitting), microbially influenced corrosion (MIC), and stress corrosion cracking (SCC). Of these processes, detailed analyses have been performed for general corrosion and localised corrosion. Microbial effects are limited to the reduction of SO_4^{2-} to HS^-. Stress corrosion cracking is believed to be unlikely, either because the maximum concentration of SCC agents and the corrosion potential lie below their respective threshold values for SCC, or because the creep rate will exceed the crack growth rate (Section 6).

A combined mass-balance/mass-transport approach was taken in predicting the long-term corrosion behaviour in the original Swedish/Finnish canister lifetime assessments (SKBF/KBS 1983, Swedish Corrosion Institute 1978, Swedish Corrosion Institute 1983, Werme et al. 1992). The corrosion assessment was divided into an initial period of aerobic (oxic) corrosion, followed by a longer period of corrosion under anaerobic (anoxic) conditions. During both periods, general corrosion and pitting were assumed to be possible.

In the 1983 assessment (SKBF/KBS 1983, Swedish Corrosion Institute 1983, and later revisited by Werme et al. 1992), corrosion during the aerobic period was supported by all of the trapped O_2 in the buffer material and a small fraction (~1%) of that in the backfilled tunnels above the deposition holes, the remainder being consumed by reaction with Fe(II) minerals. Radiolytically produced oxidants were also considered. The combined general corrosion due to trapped O_2 and radiolytic oxidants was estimated to be 0.084 mm, virtually all of which occurred in the first 1,000 years. Pitting was assessed using a pitting factor (PF), with a realistic value of 2 and a conservative value of 5. Thus, the maximum penetration due to general corrosion and pitting during the initial aerobic phase was estimated to be between 0.17 mm and 0.42 mm, for a PF of 2 and 5, respectively.

During the long-term anaerobic phase, corrosion was supported by HS^- from a number of sources. Sulphide was present naturally in the MX-80 bentonite in the deposition hole and tunnel and in the groundwater. These sources of HS^- were assumed to be supplemented by the microbial reduction of SO_4^{2-} in the deposition hole, tunnel and groundwater. The corrosion rate was assumed to be limited by the rate of supply of HS^- to the canister surface. After 10^6 yrs, an additional 0.27 mm of general corrosion was predicted due to HS^-, of which ~40% was of microbial origin. As for the aerobic phase, a PF of 2 or 5 was applied, to produce a maximum additional depth of corrosion (general and pitting) of 0.53 mm (PF = 2) to 1.33 mm (PF = 5).

Adding the estimated depths of corrosion for the aerobic and anaerobic periods produces an estimate of the total amount of corrosion on a Cu canister over a period of 10^6 yrs. For realistic (PF = 2) and conservative (PF = 5) pitting assessments, the maximum predicted depth of general and localised corrosion was 0.70 mm and 1.75 mm, respectively (Table 8-1). Such a depth is negligible compared with the proposed canister wall thickness of 50 mm, from which it was concluded that the expected canister lifetime would be > 10^6 yrs (SKBF/KBS 1983, Swedish Corrosion Institute 1983, Werme et al. 1992, Raiko and Salo 1999).

A slightly different approach to predicting the corrosion rates of Cu canisters in a Swedish/Finnish repository was taken by Wersin et al. (1994a). A steady-state mass transport-reaction model was used, in which the repository system was described by compartments representing the buffer, canister, and a compartment in which various fast and slow chemical and mass-transport processes were assumed to occur. As in the previous assessments, the evolution of repository conditions was divided into an aerobic and an anaerobic period. For each period, the rate of general corrosion was predicted based on a series of coupled chemical and mass-transport processes for various possible corrosion reactions.

In the aerobic period, the corrosion rate was predicted to be $7 \cdot 10^{-6}$ mm·yr^{-1}. Through a series of sensitivity analyses, the rate-determining process was shown to be the diffusion of Cu(II) away from the canister surface. Thus, any parameter which lead to an increase in the rate of Cu(II) diffusion (such as changes to the CO_3^{2-} concentration and pH, which affect the solubility of precipitated $CuCO_3 \cdot Cu(OH)_2$) resulted in an increase in corrosion rate, whereas parameters which did not affect Cu(II) transport (such as the dissolved O_2 concentration) were predicted to have no effect. Because of the independence of the corrosion rate on $[O_2]$, the extent of corrosion during the aerobic period was estimated by multiplying the predicted corrosion rate by the length of the aerobic period. Pitting corrosion was again estimated using a pitting factor (PF). Wersin et al. (1994a) proposed a so-called "realistic" estimate of the extent of general corrosion plus pitting during the aerobic period of 0.003 mm, based on a 65-yr aerobic period and a PF of 5. A conservative estimate was also provided, based on a 10-times higher corrosion rate, a PF of 100, and a 280-yr-long aerobic period, giving a maximum corrosion depth of 2 mm.

During the anaerobic period, corrosion was assumed to be supported by either the reduction of Fe(III) (produced from the dissolution of $Fe(OH)_3$ impurities in the bentonite) or of H_2O/H^+ in the presence of HS^-. The predicted corrosion rates for corrosion supported by Fe(III) and HS^- were $5 \cdot 10^{-8}$ mm·yr^{-1} and $4 \cdot 10^{-6}$ mm·yr^{-1}, respectively. Pitting corrosion was believed to be less severe during the anaerobic phase, so Wersin et al. (1994a) used smaller PF factors than for the aerobic period and assumed "realistic" and conservative PF values of 2 and 5, respectively. Consequently, over a period of 10^6 yrs, the minimum and maximum depths of general corrosion plus pitting were estimated to be 0.1 mm (PF = 2, Fe(III)-supported corrosion) and 20 mm (PF = 5, HS^--supported corrosion), respectively.

Combining the estimated corrosion depths for the aerobic and anaerobic periods, Wersin et al. (1994a) estimated realistic and conservative corrosion depths after 10^6 yrs of 0.1 mm and 22 mm, respectively. Compared with the reference wall thickness of 50 mm, it was concluded that the canister lifetime would be > 10^6 yrs (Table 8-1).

A new estimate of the canister lifetime was made based on the information contained in the original version of this report (King et al. 2001, 2002a). Using the analysis of Werme et al. (1992) as the basis for the estimate, two new factors were taken into account. First, since microbial activity was

considered unlikely in highly compacted bentonite, the microbially mediated reduction of SO_4^{2-} to HS^- was assumed not to occur in the deposition hole. In the analysis of Werme et al. (1992), microbially produced HS^- in the deposition hole resulted in 0.023 mm general corrosion in 10^6 yrs. Second, the analysis presented in Section 5.2.4.1 suggests that corrosion of Cu supported by the reduction of H_2O may occur at high Cl^- concentrations. The mass-transport-limited corrosion rate depends on the HS^- and Fe(III) content of the bentonite, since these species are assumed to react with the corrosion products $CuCl_2^-$ and H_2, respectively, maintaining steep concentration gradients at the canister surface. However, for HS^- and Fe(III) concentrations of 1 $\mu g \cdot g^{-1}$ and 3 $\mu g \cdot g^{-1}$, respectively, the additional corrosion is < 0.001 mm in 10^6 yrs (Figure 5-15).

The analysis by King et al. (2001, 2002a) predicts slightly less general and localised corrosion than the previous analysis of Werme et al. (1992). The decrease in the extent of general corrosion during the anoxic period, due to the absence of microbial reduction of SO_4^{2-} in the deposition hole, is much greater than any incremental corrosion due to the dissolution of Cu as $CuCl_2^-$ supported by the reduction of H_2O. Therefore, using the previous analysis of Werme et al. (1992) to estimate the depth of general corrosion due to the initially trapped O_2, radiolysis products, and HS^- (present in the bentonite in the deposition hole and tunnel, in the groundwater itself and produced by microbial activity in the tunnel and groundwater only), the maximum depth of general corrosion in the new analysis is 0.33 mm after 10^6 yrs, compared with 0.35 mm in the previous assessment. As a consequence of using pitting factors to assess the depth of localised corrosion (realistic PF = 2, conservative PF = 5), the predicted depth of localised corrosion is also lower for this new assessment. The overall canister lifetime is predicted to be > 10^6 yrs (Table 8-1).

The most recent assessment of the canister lifetime was performed in support of the SR-Can safety assessment (SKB 2006a, b). For the expected evolution of conditions within the repository, the canister was predicted to be subject to only 20–30 µm of general corrosion due to the initially trapped O_2 (Table 8-1), the remainder being consumed by microbial reactions and the oxidation of Fe(II) minerals. An additional maximum of 3 mm of general corrosion could be caused by the sulphide present in the deposition hole. Finally, sulphide diffusion to the canister surface from the groundwater could result in an additional < 1 mm of corrosion over 10^5 yrs. Unlike previous assessments, no allowance was made for pitting, but instead the degree of surface roughening was estimated to be ±50 µm. Microbial activity might be possible in the buffer material before the development of the swelling pressure but, based on measurements of the kinetics of sulphide production, the estimated amount of corrosion that could result is only 4 µm. Finally, SCC was not considered because of the limited tensile stress and the absence of appropriate environmental conditions for cracking. Based on this analysis, canister lifetimes of > 10^6 yrs would be expected (Table 8-1). This corrosion analysis applies to both the Forsmark and Laxemar sites.

Higher HS^- concentrations than the 1.6 mg/L used for the SR-Can assessment (SKB 2006b) are possible in the groundwater (maximum 12 mg/L) and backfill (43 mg/L) at the Olkiluoto site (Pastina and Hellä 2006). However, since the rate of mass transport of HS^-, and hence the corrosion rate, is proportional to the sulphide concentration, the canister would still not fail within 10^5 years even if such high HS^- concentrations were sustained.

Other cases were considered, including the case of erosion of the bentonite and rapid transport of sulphide from the groundwater to the canister surface (SKB 2006a, b). In this scenario, a portion of the compacted bentonite in the borehole is chemically "eroded" by dissolution of the clay in dilute glacial melt waters that are presumed to reach repository depth. Erosion of part of the bentonite results in a reduction in bentonite density and, hence, an increase in the diffusivity of species towards and away from the canister, including HS^- ions in the groundwater. However, buffer erosion is expected to only affect a limited number of boreholes (SKB 2006a, b). As a result of the higher flux of HS^- for the affected boreholes, between 10 and 37 canister failures are predicted after 10^6 yrs for the Forsmark site (SKB 2006a). A similar scenario at Olkiluoto is taken into account in the long-term safety assessment as a low-likelihood, or disturbance, scenario. Preliminary scoping calculations suggest that in the case of advective conditions in the buffer (for example, due to chemical erosion) and high concentrations of sulphide in the groundwater (44 mg/L), less than 10 canisters are expected to fail in 10^6 years.

8.2.2 Canada

As in the Swedish/Finnish assessments, general corrosion and pitting were assumed to be the two major processes leading to corrosion of the canister in a Canadian repository (Johnson et al. 1996). Microbial effects were considered to be possible, but were thought to contribute no more than 1 mm of additional corrosion, and were not part of the detailed assessment. Reasoned arguments were used to claim that the canisters would not be subject to SCC, because of (i) limited strain of the canister wall, (ii) the lack of SCC agents in the repository, (iii) the general lack of oxidants, and (iv) the inhibitive effects of Cl^- ions.

Whilst it was recognised that the repository environment would evolve over time, the aerobic and anaerobic phases were not distinguished as in the Swedish/Finnish assessments. The extent of general corrosion was predicted using the 1-dimensional coupled reaction-diffusion model described in Section 5.2.4.2. The repository was described by a series of layers representing buffer, backfill, excavation-disturbed rock, and a layer of sparsely fractured rock. By using electrochemical expressions for the mathematical boundary conditions at the canister surface, it was possible to predict the effect of the evolving repository environment on the corrosion potential (E_{CORR}) and corrosion current density (i_{CORR}) of the canister (Figure 5-17). General corrosion of the canister was predicted to stop once all of the initially trapped O_2 (and the Cu(II) produced by the oxidation of $CuCl_2^-$ by O_2) had been consumed, since there is no sulphide in either the Avonlea bentonite specified for a Canadian repository or in deep Canadian Shield groundwaters. The absence of sulphide minerals in the clay resulted in a longer aerobic phase, predicted to be a maximum of 2,000–3,000 yrs in duration. Most of the trapped O_2, however, was calculated to be consumed by reaction with Fe(II) minerals, so that the maximum depth of general corrosion was predicted to be only 0.011 mm (Johnson et al. 1996).

Pitting corrosion was assumed to be possible at all times during the evolution of the repository environment. The depth of the deepest pit on any of the 60,000 canisters in the repository was estimated using an extreme-value statistical analysis of literature pit-depth data (Section 5.3.2). The data included in the analysis were from long-term burial studies and from a study of Bronze Age archaeological artifacts (Bresle et al. 1983). The maximum estimated pit depth was 6 mm after 10^6 yrs. This estimate of maximum pit depth was considered to be conservative because pitting was assumed to continue indefinitely, despite the fact that the aerobic period lasted only a few thousand years.

The maximum depth of general corrosion and pitting for a copper canister in granitic host rock was predicted to be 6.0 mm after 10^6 yrs. Since the reference wall thickness was 25 mm, canisters were predicted to have a lifetime of > 10^6 yrs (Table 8-1).

A similar approach was subsequently taken for the prediction of the lifetime of copper canisters in a sedimentary host-rock formation (King 2005). The major differences between the two host rock environments are the higher salinity and lower hydraulic conductivity of the sedimentary formation, the latter potentially resulting in slower saturation of the repository. For copper, the higher Cl^- can be considered beneficial to the corrosion behaviour as it promotes general dissolution over localised corrosion or SCC (Sections 5.2.1.2 and 6.1.2.1). Furthermore, the lower water activity associated with the higher salinity was considered to make microbial activity less likely. Although the longer saturation time would result in a longer period of atmospheric corrosion, and the associated possibility of localised attack, the amount of oxidant (atmospheric O_2) in the repository was considered to be independent of the nature of the host rock and dependent only on the repository design (and, specifically, the volume and initial degree of saturation of the clay-based sealing materials). As a consequence, King (2005) concluded that the depth of general corrosion due to the initially trapped O_2 would be 0.17 mm, with an additional 0.1 mm (realistic) or 6 mm (conservative) of localised attack. The "realistic" value was based on the argument that any localised attack would take the form of surface roughening only, with the "conservative" estimate based on the same extreme-value statistical analysis adopted by Johnson et al. (1996). Stress corrosion cracking was excluded based on (i) the limited period of sufficient tensile stress, (ii) the absence of SCC agents, (iii) an E_{CORR} value below the threshold potential, and (iv) the inhibitive effect of Cl^-. Microbiologically influenced corrosion was not included in the assessment because of the use of highly compacted 100% bentonite in the repository and the high salinity pore water in the host rock. As a consequence of these arguments, the predicted lifetime for the 25-mm-thick copper canister was predicted to be > 10^6 yr (King 2005).

8.2.3 Japan

Although no formal lifetime prediction has been made for a Cu canister in a Japanese repository, the maximum depth of corrosion has been assessed (JNC 2000). As in the Swedish/Finnish and Canadian programmes, the two corrosion processes considered were general corrosion and pitting. Although it was believed that microbial activity would be limited by nutrient availability, it was implicitly included in the assessment through the production of HS^- from the reduction of SO_4^{2-}. Stress corrosion cracking was not considered because the maximum concentrations of ammonia, nitrite and acetate ions in the repository were assumed to be below the threshold values for cracking. The assessment was similar to that used in Sweden and Finland, but with more-conservative assumptions. A number of repository designs were considered, employing various amounts of buffer and backfill materials. These different designs resulted in a range of values for the predicted corrosion damage.

General corrosion was assumed to be caused by O_2 trapped in the buffer and backfill materials, and by HS^- in the buffer and groundwater. It was conservatively assumed that all of the O_2 in the deposition holes and tunnels would lead to corrosion of the canister. Depending upon the repository design, this resulted in between 0.6 mm and 3.6 mm of general corrosion. For HS^--induced corrosion, it was assumed that all of the SO_4^{2-} in the buffer and backfill was reduced to HS^- by sulphate-reducing bacteria, and that the groundwater itself contained 0.03 mol·dm^{-3} HS^-. The rate of corrosion was assumed to be limited by the rate of diffusion of HS^- to the canister surface. Over a 1,000-yr period, the additional corrosion due to HS^- was 0.2–1.1 mm from the SO_4^{2-} in the buffer material and 8.1 mm due to HS^- in the groundwater. Thus, after 1,000 yrs, the maximum depth of general corrosion due to both O_2 and HS^- was predicted to be 9–13 mm, depending upon the repository design (Table 8-1).

The extent of pitting corrosion was assessed using both a pitting factor and the extreme-value analysis approach described above. For the pitting factor approach, a PF of 3 was used. For the extreme-value analysis, the maximum pit depth after 1,000 yrs was predicted to be 2.2 mm.

The overall extent of general corrosion and pitting after 1,000 yrs was predicted to be 27–39 mm from the PF approach and 11–15 mm based on the extreme-value pitting analysis. These estimates are highly conservative, due mainly to the very high groundwater HS^- concentration used in the assessment and to the assumption that all the SO_4^{2-} in the buffer and backfill is reduced to HS^-.

8.2.4 Switzerland

Carbon steel is the primary canister material being considered by Nagra for the Swiss high-level waste/spent nuclear fuel disposal programme (Johnson and King 2003). However, in case there is a need for longer-lived containment, consideration is also being given to a copper-cast iron canister design similar to the Swedish/Finnish concept. The nature of the corrosion analysis was similar to that carried out in Sweden and Finland, and involved a combination of mass-balance and mass-transport estimates of the extent of corrosion by O_2 and sulphide (Table 8-1). Based on a mass-balance argument, the amount of corrosion due to O_2 was estimated to be < 100 µm. Transport of sulphide from the bentonite and host rock would cause a further 0.9 mm of corrosion in 10^5 yrs. As with the latest SKB analysis, localised corrosion in the form of pitting was not expected to occur and instead an allowance of < 100 µm was made for surface roughening. A conservative estimate of < 5 mm was also provided as an alternative analysis, based on a pitting factor of 5 (Table 8-1). No allowance was made for microbial effects because of the claim that microbial activity would not be possible in the highly compacted bentonite. Similarly, SCC was excluded from consideration because of the limited period of stress, the absence of SCC agents, the general absence of oxidants, and the inhibitive effects of Cl^- ions (Johnson and King 2003). Based on this analysis, canister lifetimes of > 10^5 yrs would be expected.

8.3 Conclusions

There are certain similarities and certain distinct differences between the various assessments of the lifetimes of Cu canisters. In both the early Swedish/Finnish and Canadian assessments, general corrosion and pitting were believed to be the processes most likely to result in corrosion of the

canister. In a Swedish/Finnish repository, HS^- (or, rather, H_2O/H^+ in the presence of HS^-) is the most prevalent oxidant. In a Canadian repository, trapped O_2 is the major oxidant. Different approaches have been used to assess the extent of general corrosion and pitting. Both mass-balance and detailed kinetic modelling have been used to model general corrosion. For pitting, empirical pitting factors and statistical analyses have been used. Despite these differences in repository conditions, and in the approaches taken to make long-term predictions, the predicted canister lifetimes exceed 10^6 years in all cases.

It is interesting to note that for the most-recent lifetime assessments in Switzerland (Johnson and King 2003), Canada (King 2005), and Sweden (SKB 2006a, b), no allowance is made for pitting corrosion, but instead a surface roughening factor of 50–100 μm is used. This change in approach to localised corrosion stems from the improved understanding of the nature of the corrosion processes under repository conditions.

Based on these analyses, it is apparent that corrosion is not the limiting factor in determining the canister design wall thickness.

Table 8-1. Comparison of predictions of long-term corrosion behaviour and canister lifetimes.

Country	General corrosion	Localised corrosion	Microbially influenced corrosion	Stress corrosion cracking	Predicted lifetime	Reference
Sweden/Finland[1)]	0.05 mm in 10^6 yrs (realistic) 4 mm in 10^6 yrs (conservative)	0.05 mm in 10^6 yrs (realistic) 16 mm in 10^6 yrs (conservative)	–	–	> 10^6 yrs	Wersin et al. (1994a)
Sweden/Finland[1)]	0.35 mm in 10^6 yrs	0.35 mm in 10^6 yrs (realistic) 1.4 mm in 10^6 yrs (conservative)	SRB assumed to reduce SO_4^{2-} to HS^-	Maximum possible nitrite concentration below threshold for SCC	> 10^6 yrs	Swedish Corrosion Institute (1983), SKBF/KBS (1983), Werme et al. (1992)
Sweden/Finland[1)]	0.33 mm in 10^6 yrs	0.33 mm in 10^6 yrs (realistic) 1.3 mm in 10^6 yrs (conservative)	SRB assumed to reduce SO_4^{2-} to HS^- in tunnel and groundwater only	SCC does not occur based on threshold potential and concentrations of SCC agent, and because creep is faster than SCC	> 10^6 yrs	King et al. (2001, 2002a)
Sweden SR-Can	20–30 μm due to O_2, 3 mm due to sulphide in deposition hole (maximum); < 1 mm in 10^5 yrs due to sulphide in groundwater	±50 μm due to surface roughening	Sulphide production in buffer prior to full saturation possible; 4 μm corrosion in 1,000 yrs (maximum)	SCC not included because of limited tensile stress, absence of SCC agents, insufficiently positive E_{CORR}, and inhibitive effects of Cl^-	> 10^6 yrs	SKB (2006a, b)
Canada[2)]	0.011 mm in 10^6 yrs	6 mm in 10^6 yrs	Limited impact; additional wall loss of 1 mm in 10^6 yrs (maximum)	SCC not included because of limited period of stress, absence of SCC agents, general lack of oxidant, and inhibitive effects of Cl^-	> 10^6 yrs	Johnson et al. (1996)
Canada[2)]	0.17 mm in 10^6 yrs due to trapped O_2	0.1 mm in 10^6 a (realistic) based on surface roughening 6 mm in 10^6 a (conservative) based on extreme-value analysis	Not included because of the use of 100% bentonite in repository and assumption of no microbial activity in host rock	SCC not included because of limited period of stress, absence of SCC agents, E_{CORR} below threshold value, and inhibitive effects of Cl^-	> 10^6 yrs	King (2005)
Japan	9–13 mm in 10^3 yrs, depending on repository design	18–26 mm in 10^3 yrs based on pitting factor of 3; 2 mm in 10^3 yrs based on extreme-value analysis	SRB assumed to reduce allSO_4^{2-} to HS^-	Maximum concentrations of ammonia, nitrite and acetate less than threshold concentrations	None given	JNC (2000)
Switzerland[1)]	< 100 μm due to O_2 0.9 mm in 10^5 yrs due to sulphide	< 100 μm due to surface roughening (best estimate); 5 mm based on pitting factor of 5 (conservative)	Not included due to absence of microbial activity in compacted bentonite.	SCC not included because of limited period of stress, absence of SCC agents, general lack of oxidant and inhibitive effects of Cl^-	> 10^5 yrs	Johnson and King (2003)

[1)] Reference canister wall thickness of 50 mm.

[2)] Reference canister wall thickness of 25 mm.

9 Areas for further research

Studies of copper corrosion under repository conditions have been going on since 1977 and a large amount of information has been gathered during this period. A number of lifetime assessments have been performed over the years, as discussed in detail in Section 8. The conclusion from these assessments is that copper canisters will have a very long lifetime in the repository environment and that corrosion is highly unlikely to be a limiting factor for lifetimes exceeding 100,000 years. The canister is an important barrier in the overall multi-barrier system, and also, in case of local failure, as a barrier against the release of radionuclides to the near field. It is important, therefore, that research into the corrosion behaviour of copper should continue in order to maintain a high level of certainty about the expected excellent long-term corrosion performance of the canister.

King et al. (2001, 2002a) defined a number of areas requiring further research. The progress made in the intervening period in addressing these areas is summarised below. In addition, a limited number of new, or continuing, areas of further research are identified in this revised version of the report.

9.1 Review of progress on areas for further research identified by King et al. (2001, 2002a)

Measurement and prediction of the evolution of environmental conditions

There have been a number of experimental and modelling studies of the evolution of the near-field environment over the past 8–9 years, particularly with regard to the evolution of redox conditions (Section 2.5). Puigdomenech et al. (2001) have considered the various O_2 consumption processes in a repository in granitic media, including microbial processes and reaction with oxidisable minerals. In addition, Muurinen (2006b) has evaluated the rate of O_2 consumption as part of the LOT project at the Äspö Hard Rock Laboratory. Both experimental measurements and numerical simulations indicate that the timescale for oxygen depletion in individual KBS-3V deposition holes is no more than a few hundred years at most, and could be as little as a few years. King and Kolář (2006a) have also modelled the evolution of near-field conditions for a Canadian-design repository. The relative contributions of canister corrosion, reaction with Fe(II), and microbial activity to the consumption of the initially trapped O_2 was considered.

The results of these and earlier studies appear to provide a consistent picture of the evolution of the near-field conditions. The initial aerobic phase is expected to be of limited duration (of the order of years to tens of years) based on both experimental and theoretical (modelling) evidence. There has been less effort in relating this evolution of environmental conditions to the evolution of the corrosion behaviour of the canister, the one exception being the modelling work of King and Kolář (2000, 2006a) in the Canadian programme.

Measurement and prediction of corrosion potentials in highly compacted bentonite

The development of a mixed-potential model to predict the corrosion potential (E_{CORR}) of copper containers in the presence of sulphide is currently in progress (Section 5.2.3). The model accounts for the various electrochemical, mass transport, redox, precipitation, and sorption reactions of importance for the corrosion of copper in compacted bentonite with sulphide-containing chloride pore waters (King 2007). The aim of the work is to predict the evolution of the E_{CORR} as the initially trapped O_2 is consumed and as HS^- from various sources begins to dominate the corrosion behaviour.

Experimental measurements of E_{CORR} will be needed to validate the mixed-potential model being developed. Although some measurements of E_{CORR} in bulk solution have been reported in sulphide-containing Cl^- solutions (Smith 2007), there are very few published data in compacted bentonite systems.

Possible microbial activity in highly compacted bentonite

Much effort has been expended over the past 5–10 years on the study of microbial activity in compacted bentonite, the results of which are summarised in Section 2.3. It is clear that compacted bentonite is an inhospitable environment for microbial activity. However, Masurat and Pedersen (2004) and Masurat et al. (2010b) found that active microbes can survive in compacted bentonite and measured the rate of sulphate reduction using radiotracer techniques. The sulphide production rate was of the order of 10^{-13} mol mm^{-2}·day^{-1} and was found to be inversely related to the swelling pressure, although no threshold swelling pressure of bentonite density was determined. SKB (2006b) have included an allowance of 4 μm for SRB activity in the buffer in the SR-Can safety assessment (see Section 8).

Work in Canada has focussed on the water activity as the limiting factor for microbial activity in compacted bentonite (Stroes-Gascoyne et al. 2006, 2007a, b). Regardless of whether the water activity is adjusted by varying the bentonite density (i.e. via the suction potential) or by varying the pore-water salinity (i.e. via the osmotic potential), there is strong evidence for a threshold water activity of 0.96 below which microbes undergo a decrease in the viable population.

Although there is no consensus regarding the physiological mechanism involved, there is general agreement that a dry density ≥ 1.6 Mg/m^3 or a swelling pressure ≥ 2 MPa is sufficient to preclude microbial activity in saturated compacted bentonite. Pedersen and co-workers (Masurat and Pedersen 2004, Pedersen et al. 2000a, b) believe the forces and constrictions imposed upon the microbes by the swelling clay are responsible for suppressing microbial activity, whereas Stroes-Gascoyne and co-workers (Stroes-Gascoyne et al. 2006, 2007a, b) believe the effect is the result of the low water activity. Where the two schools of thought differ is in the possibility of microbial activity in unsaturated bentonite prior to the establishment of the swelling pressure. Regardless, it is apparent that the extent of possible microbiologically influenced corrosion of copper canisters is small and that this form of corrosion does not represent a threat to the integrity of the canisters (King 2009).

Stress corrosion cracking

Progress has been made in the understanding of the stress corrosion cracking (SCC) of copper canisters since the original report was published. In addition to various experimental studies in ammonia-, acetate-, and nitrite-containing environments, the results of which are summarised in Section 6.1, an approach to predicting the period of susceptibility to SCC has also been developed (Section 6.2.2.1, King and Kolář 2004, 2005, Maak and King 2005). It is apparent that, during the early aerobic phase in the evolution of the repository environment, the period of susceptibility to SCC is short and it is highly unlikely that the required conditions of potential, interfacial pH, and SCC-inducing species will be present simultaneously (King and Newman 2010).

The issue of whether SCC is possible during the long-term anaerobic phase has also been addressed (Section 6.2.2.4). Taniguchi and Kawasaki (2008) have presented evidence for the SCC of copper in sulphide solutions above a concentration of ~$5 \cdot 10^{-3}$ mol·dm^{-3}. King and Newman (2010) have reviewed the mechanistic evidence for SCC under anaerobic conditions and concluded that of the four mechanisms proposed for the cracking of copper, three (the slip-dissolution, tarnish-rupture, and film-induced cleavage mechanisms) will not be operative in the presence of sulphide, either because HS^- will not enter the crack or because (in the case of film-induced cleavage) copper sulphide films will be insufficiently adherent to support crack initiation. In the case of the surface mobility model, King and Newman (2010) argue that the crack propagation rate expression has been incorrectly formulated and, in its corrected version, would predict vanishingly small crack growth rates (amounting to < 1 μm in 10^{-6} years).

An experimental programme of mechanistic studies of the SCC of copper, especially under anaerobic conditions, has been established at the University of Toronto. However, based on the evidence available to date it appears that the SCC of copper canisters is extremely unlikely at any stage during their service life.

Corrosion during water saturation

There has been no experimental work specifically directed towards the effect of unsaturated conditions on the corrosion behaviour of copper. As discussed in Section 4, King (2006) reviewed the mechanism of corrosion under unsaturated conditions. As the repository saturates, salt contaminants on the surface of the canister will deliquesce at a critical temperature and relative humidity determined by the nature of the salt. Local separation of anodic and cathodic sites is possible following this initial wetting if O_2 is still present. As the relative humidity continues to increase, however, the surface will progressively wet more uniformly, until the entire surface is wetted and corrosion is general in nature.

Although unintentionally, Pusch (2008) studied the corrosion of copper in unsaturated bentonite (Section 4.2.2). Some localisation of the attack was observed as predicted theoretically. In the repository, the localised attack will cease as both the degree of saturation increases and the O_2 concentration decreases.

There appears to be a sound understanding of the mechanism of corrosion in unsaturated bentonite, which is supported by the limited available evidence. Because of the limited amount of O_2 in the repository, any initial localisation of attack will be limited.

Copper corrosion in highly saline groundwaters

At sufficiently high Cl^- concentration, copper could become thermodynamically unstable in water (Section 5.2.2). Various attempts have been made to measure the corrosion rate of copper under strictly anoxic conditions (Bojinov et al. 2004, Betova et al. 2004, Bojinov and Mäkelä 2003). Great care was taken to exclude O_2 from the system, although some corrosion due to residual O_2 was inevitably observed during the experiments. Once the trace levels of O_2 had been consumed, however, there was no evidence for continued corrosion (Section 5.2.2). There is no evidence, therefore, that copper corrodes in concentrated Cl^- solutions at neutral pH, consistent with thermodynamic prediction.

Effect of discontinuities

A study was performed to determine whether surface discontinuities, such as crack-like features or pits, might affect the corrosion behaviour of the canister (King 2004). It was concluded that such features would not influence the localised corrosion behaviour since the initiation of pits occurs on a microscopic, rather than a macroscopic scale (Section 5.2.7). Furthermore, surface "pits" or cracks would not, in themselves, lead to an increased susceptibility to SCC, since stress concentration (in the case of pits) or stress intensification (in the case of pre-existing crack-like defects) is only one of several factors required to sustain SCC.

Properties of Cu_2O films

No specific study of the properties of Cu_2O films and their effect on the corrosion behaviour of copper canisters has been performed since the original report.

Corrosion in saline solutions at high pH

The possibility of enhanced susceptibility to localised corrosion because of passivation of the copper canister by alkaline pore waters resulting from the use of cementitious materials in the repository was investigated by King (2002). It was found that increased pH actually renders the surface less susceptible to localised corrosion because the difference between the pitting or repassivation potential and E_{CORR} increases with increasing pH (Section 5.3.2).

Therefore, in the unlikely event that an alkaline plume from the leaching of cementitious materials should reach the canister surface, there will be no detrimental impact on canister performance.

Corrosion due to differential bentonite properties

Saario et al. (2004) considered the effect of bentonite density on the corrosion behaviour of copper (Section 5.2.1.2). Increasing compaction density was found to result in a decrease in corrosion rate, presumably as a consequence of the smaller amount of available O_2 and the slower O_2 transport to the corroding surface. Corrosion stopped, however, after ~100 hrs exposure due to the consumption of the initially trapped O_2.

There has been no investigation of the effect of differential bentonite swelling on the establishment of localised corrosion cells on the canister surface.

9.2 New and continuing areas of further research

Stress corrosion cracking

Stress corrosion cracking of copper continues to be an area of interest (Section 6). Recent work suggesting that SCC of copper can be induced by sulphide (Taniguchi and Kawasaki 2008) requires further investigation, although the currently available evidence suggests that there is no mechanistic reason why copper canisters surrounded by compacted bentonite should be susceptible to cracking during the anaerobic phase in the evolution of the repository environment (King and Newman 2010).

Under aerobic conditions (i.e. in the presence of dissolved O_2 or Cu(II)), the bulk environmental conditions under which SCC has been observed correspond to the equilibrium potential and pH for Cu_2O/CuO formation (Section 6.2.2.1). The reasons for this apparent correlation needs to be understood and the relationship between conditions at the crack tip and those in the bulk environment investigated, which may also provide a better understanding of the mechanism involved.

Residual stresses in seals

High residual stresses in the copper weld are not desirable from a long-term safety point of view because of the potential for early canister failure. Residual stress levels have been measured for both friction-stir welds (FSW) (Raiko et al. 2010) and electron-beam welds (EBW) (Gripenberg 2009). For FSW, the residual stresses on the outer surface tend to be compressive with values up to –60 MPa, with smaller compressive (and, in some cases, slightly tensile) stresses on the inside of the canister. Tensile stresses are found mid-wall. In contrast, EBW tend to exhibit tensile residual stresses up to 70 MPa, balanced by compressive stresses in the adjacent base metal. (Gripenberg 2009).

Surface roughening

It is now apparent that copper exposed to disposal environments undergoes "uneven general corrosion" or surface roughening, rather than pitting corrosion (Section 5.3). The corrosion allowance necessary for surface roughening is typically < 100 μm, compared with the several mm required when estimating the maximum pit depth using a pitting factor or extreme-value analysis (Section 5.3). Although there is strong experimental evidence for surface roughening, both from laboratory studies and from large-scale *in situ* tests, there is relatively little mechanistic understanding of how this form of corrosion evolves over time. A combination of experimental and mathematical modelling could be used to address this gap.

Additional surface roughness measurements could be obtained from long-term *in situ* experiments.

Laboratory experiments could involve the study of the distribution of anodic and cathodic sites on corroding surfaces, and how it evolves as the environment evolves. Information on the birth, growth, and death of such features could be used in a stochastic surface roughening model.

Properties of Cu_2O films

Cuprous oxide (Cu_2O) films formed on the canister surface may exhibit a wide range of behaviour, including semi-conducting properties and the susceptibility to localized breakdown and corrosion.

The properties of such films may be important in determining the localized and SCC behaviour of the canister. The effects of pore-water species, such as chloride and sulphide ions, on the properties of such films should be evaluated.

Corrosion in bentonite

Although we have a good conceptual understanding of the corrosion mechanism under unsaturated conditions, we have no direct evidence of the corrosion consequences for the canister. Measurement of the spatial distribution of anodic and cathodic processes as a function of relative humidity and surface contamination levels would indicate the extent of localised corrosion that is possible during this period.

There has been no investigation of the effect of differential bentonite swelling on the establishment of localised corrosion cells on the canister surface. Differential swelling could allow faster O_2 transport to some areas of the canister, which would then tend to act as cathodes and possibly support local anodic dissolution at adjacent areas in contact with more highly compacted bentonite. Such an effect is likely to be quite localized as the resistance of the bentonite would prevent large-scale coupling of anodic and cathodic regions, but is worthy of further study.

In situ experiments

The results of large-scale *in situ* tests are proving useful in validating the models and mechanisms derived on the basis of short-term laboratory experiments. The results from existing tests may provide additional validation for corrosion models. Future large-scale tests should be planned with post-test analysis and model validation in mind.

Corrosion by H_2O

Recently, Hultquist and co-workers have published several papers claiming the generation of hydrogen due to the corrosion of copper in water (Hultquist et al. 2008, Szakálos et al. 2007). Whilst the basis for this mechanism is not clear (Section 5.2.2), there is a need to determine whether the claims made in these papers are correct. Although it is well known that surface intermediate species are formed on copper under electrochemical polarisation, it is not clear that these species are stable and can sustain H_2O reduction. This problem is amenable to experimental study and to theoretical analysis via the incorporation of adsorbed surface species into traditional Pourbaix diagrams. No other research group has been able to reproduce the H_2 observed by Hultquist and co-workers. It is necessary to understand why these authors apparently observe H_2 and others do not.

Mixed-potential models for copper canisters

The corrosion potential is a fundamental parameter in corrosion science that can be used to interpret and predict the corrosion behaviour of the canister. Although mixed-potential models exist to predict the E_{CORR} of a copper canister in the repository (Section 5.2.4.2), these models have not been adequately validated, partly as a result of the relative lack of E_{CORR} measurements in compacted bentonite. Because these models also predict the evolution of the near-field environment, there is an opportunity to validate other aspects of the models through simulation of the results from various laboratory and *in situ* experiments.

Completion of the Copper Sulphide Model and the prediction of the E_{CORR} of copper canisters exposed to sulphide-containing repository environments is planned for 2010 (Section 5.2.3). As with other mixed-potential modelling, a more extensive validation of the CSM against experimental or analogue data should be performed.

Assessment of copper corrosion in dilute glacial melt water

Under some proposed scenarios, dilute glacial melt water could reach repository depth and chemically erode the bentonite buffer. The copper canisters would then be exposed to dilute aqueous environments with relatively high rates of mass transport. The focus of the current review is primarily saline solutions and restrictive mass transport conditions. The implications for the performance of the canister of the intrusion of dilute glacial melt waters should be reviewed.

References

SKB's (Svensk Kärnbränslehantering AB) publications can be found at www.skb.se/publications.

Aaltonen P, Varis P, 1993. Long term corrosion tests of OFHCcoppers in simulated repository conditions – final report. Report YJT9305, Nuclear Waste Commission of Finnish Power Companies.

Aaltonen P, Hänninen H, Kemppainen M, 1984. Stress corrosion testing of pure OFHC-copper in simulated groundwater conditions. Report YJT8421, Nuclear Waste Commission of Finnish Power Companies.

Ageskog L, Jansson P, 1999. Heat propagation in and around the deep repository. Thermal calculations applied to three hypothetical sites: Aberg, Beberg and Ceberg. SKB TR-99-02, Svensk Kärnbränslehantering AB.

Ahonen L, 1995. Chemical stability of copper canisters in deep repository. Report YJT9519, Nuclear Waste Commission of Finnish Power Companies.

Ahonen L, 2001. Appendix II in this report.

Alhajji J N, Reda M R, 1994. The conflicting roles of complexing agents on the corrosion of copper-nickel alloys in sulfide polluted seawater. Journal of the Electrochemical Society, U141, pp 1432–1439.

Al-Kharafi F M, Shalaby H M, Gouda V K, 1989. Pitting of copper under laboratory and field conditions. British Corrosion Journal, 24, pp 284–290.

Anderson C, Jakobsson A-M, Pedersen K, 2006a. Influence of in situ biofilm coverage on the radionuclide adsorption capacity of subsurface granite. Environmental Science & Technology, 41, pp 830–836.

Anderson C, Pedersen K, Jakobsson A-M, 2006b. Autoradiographic comparisons of radionuclide adsorption between subsurface anaerobic biofilms and granitic host rocks. Geomicrobiology Journal, 23, pp 15–29.

Andersson H, Seitisleam F, Sandström R, 1999. Influence of phosphorous and sulphur as well as grain size on creep in pure copper. SKB TR-99-39, Svensk Kärnbränslehantering AB.

Andersson C-G, Eriksson P, Westman M, Emilsson G, 2004. Status report, canister fabrication. SKB TR-04-23, Svensk Kärnbränslehantering AB.

Andersson J, Ahokas H, Hudson J A, Koskinen L, Luukkonen A, Löfman J, Keto V, Pitkänen P, Mattila J, Ikonen A T K, Ylä-Mella M, 2007. Olkiluoto site description 2006. Report Posiva 2007-3, Posiva Oy, Finland.

Anttila P, Ahokas H, Front K, Hinkkanen H, Johansson E, Paulamäki S, Riekkola R, Saari J, Saksa P, Snellman M, Wikström L, Öhberg A, 1999a. Final disposal of spent nuclear fuel in Finnish bedrock – Olkiluoto site report. Posiva 9910, Posiva Oy, Finland.

Anttila P, Ahokas H, Front K, Hinkkanen H, Johansson E, Paulamäki S, Riekkola R, Saari J, Saksa P, Snellman M, Wikström L, Öhberg A, 1999b. Final disposal of spent nuclear fuel in Finnish bedrock – Hästholmen site report. Posiva 9908, Posiva Oy, Finland.

Appelo C A J, Postma D, 2005. Geochemistry, groundwater and pollution. 2nd ed. Leiden: Balkema.

Arcos D, Grandia F, Domènech C, 2006. Geochemical evolution of the near field of a KBS-3 repository. SKB TR-06-16, Svensk Kärnbränslehantering AB.

Arilahti E, Bojinov M, Mäkelä K, Laitinen T, Saario T, 2000. Stress corrosion cracking investigation of copper in groundwater with ammonium ions. Posiva Working Report 200046, Posiva Oy, Finland.

Auqué L F, Gimeno M J, Gómez J B, Puigdomenech I, Smellie J, Tullborg E-L, 2006. Groundwater chemistry around a repository for spent nuclear fuel over a glacial cycle. Evaluation for SR-Can. SKB TR-06-31, Svensk Kärnbränslehantering AB.

Baes C F, Mesmer R E, 1976. The hydrolysis of cations. New York: Wiley.

Banwart S, Tullborg E-L, Pedersen K, Gustafsson E, Laaksoharju M, Nilsson A-C, Wallin B, Wikberg P, 1996. Organic carbon oxidation induced by largescale shallow water intrusion into a vertical fracture zone at the Äspö Hard Rock Laboratory (Sweden). Journal of Contaminant Hydrology, 21, pp 115–125.

Barton P B, Bethke P M, 1960. Thermodynamic properties of some synthetic zinc and copper minerals. American Journal of Science, 258A, pp 21–34.

Beavers J A, Durr C L, 1992. Stress-corrosion cracking studies on candidate container alloys for the tuff repository. Report NUREG/CR5710, U.S. Nuclear Regulatory Commission.

Benjamin L A, Hardie D, Parkins R N, 1988. Stress corrosion resistance of pure coppers in ground waters and sodium nitrite solutions. British Corrosion, 23, pp 89–95.

Betova I, Heinonen J, Kinnunen P, Lilja C, Ruokola E, Saario T, 2004. Application of an on-line corrosion probe and a reference electrode for copper corrosion studies in repository conditions. In: Oversby V M, Werme L O (eds). Scientific basis for nuclear waste management XXVII: symposium held in Kalmar, Sweden, 15–19 June 2003. Warrendale, PA: Materials Research Society. (Materials Research Society Symposium Proceedings 807), pp 429–434.

Beverskog B, Puigdomenech I, 1998. Pourbaix diagrams for the system copper-chlorine at 5–100°C. SKI Report 98:19, Statens kärnkraftinspektion (Swedish Nuclear Power Inspectorate).

Bianchi G, Fiori G, Longhi P, Mazza F, 1978. "Horse shoe" corrosion of copper alloys in flowing sea water: mechanism, and possibility of cathodic protection of condenser tubes in power stations. Corrosion, U34, pp 396–406.

Bojinov M, Mäkelä K, 2003. Corrosion of copper in anoxic 1M NaCl solution. Posiva Working Report 200345, Posiva Oy, Finland.

Bojinov M, Laitinen T, Mäkelä K, Snellman M, Werme L, 2004. Corrosion of copper in 1 M NaCl under strictly anoxic conditions. In: Oversby V M, Werme L O (eds). Scientific basis for nuclear waste management XXVII: symposium held in Kalmar, Sweden, 15–19 June 2003. Warrendale, PA: Materials Research Society. (Materials Research Society Symposium Proceedings 807), pp 459–464.

Brennenstuhl A M, McBride A, Ramamurthy S, Davidson R, 2002. The effects of microstructural and environmental factors on underdeposit corrosion of oxygen-free phosphorus-doped copper. Report 06819-REP-01200-10079, Ontario Power Generation, Nuclear Waste Management Division, Canada.

Bresle A, Saers J, Arrhenius B, 1983. Studies in pitting corrosion on archaeological bronzes. Copper. SKBF/KBS TR 83-05, Svensk Kärnbränsleförsörjning AB.

Brossard L, 1983. Anodic dissolution of copper in concentrated LiCl solution at pH between 3 and 7. Journal of the Electrochemical Society, U130, pp 403–405.

Brown A D, 1990. Microbial water stress physiology: principles and perspectives. Chichester: Wiley.

Bruno J, Acros D, Duro L, 1999. Processes and features affecting the near field hydrochemistry. Groundwater-bentonite interaction. SKB TR-99-29, Svensk Kärnbränslehantering AB.

BSC, 2004. Engineered barrier system: physical and chemical environment model. Bechtel SAIC Company report to U.S. DOE, ANL-EBS-MD-000033 Rev 02.

Bühler K, 1993. Die Rolle der Begleitstoffe von Abgaskondensaten aus der Erdgasverbrennung bei der Korrosion von Wärmetauschern (Impurity constituents of flue gas condensates and their significance for the corrosion of heat exchangers). Werkstoffe und Korrosion, 44, pp 289–294.

Börgesson L, Hernelind J, 1999. Coupled thermo-hydro-mechanical calculations of the water saturation phase of a KBS-3 deposition hole. Influence of hydraulic rock properties on the water saturation phase. SKB TR-99-41, Svensk Kärnbränslehantering AB.

Campbell H S, 1974. A review: pitting corrosion of copper and its alloys. In: Staehle R W, Brown B F, Kruger J, Agrawal A (eds). Localized corrosion: proceedings of a conference, Williamsburg, Virginia, 6–10 December 1971. Houston, TX: National Association of Corrosion Engineers, pp 625–638.

Cassagne T B, Kruger J, Pugh E N, 1990. Role of the oxide film in the transgranular stress corrosion cracking of copper. In: Lisagor W B, Crooker T W, Leis B N (eds). Environmentally assisted cracking: science and engineering, ASTMSTP1049, Philadelphia, PA: American Society for Testing and Materials, pp 59–75.

Chen J, Qin Z, Shoesmith D W, 2010. Kinetics of corrosion film growth on copper in neutral chloride solutions containing small concentrations of sulphide. Journal of the Electrochemical Society, 157, pp C338–C345.

Chen Z Y, Persson D, Nazarov A, Zakipour S, Thierry D, Leygraf C, 2005. In situ studies of the effect of CO_2 on the initial NaCl-induced atmospheric corrosion of copper. Journal of the Electrochemical Society, 152, pp B342–B351.

Corbel C, Féron D, Roy M, Maurel F, Wasselin-Trupin V, Hickel B, 2003. Effect of irradiation on long term alteration of oxides and metals in aqueous solutions. In: Féron D, Macdonald D D (eds). Prediction of long term corrosion behaviour in nuclear waste systems: proceedings of an international workshop, November, Cadarache, France. London: Maney Pub. (European Federation of Corrosion Publications 36), pp 484–502.

Corbett R A, Elliot P, 2000. Ant-nest corrosion – digging the tunnels. Corrosion/2000, NACE International, Houston, Texas, Paper 646.

Crawford M B, Wilmot R D, 1998. Normal evolution of a spent fuel repository at the candidate sites in Finland. Posiva 98-15, Posiva Oy, Finland.

de Chialvo M R G, Arvia A J, 1985. The electrochemical behaviour of copper in alkaline solutions containing sodium sulphide. Journal of Applied Electrochemistry, 15U, pp 685–696.

de Chialvo M R G, Salvarezza R C, Vasquez Moll D, Arvia A J, 1985. Kinetics of passivation and pitting corrosion of polycrystalline copper in borate buffer solutions containing sodium chloride. Electrochimica Acta, 30, pp 1501–1511.

Dixon D A, Ikeda B M, StroesGascoyne S, 2004. Final report on the buffer coupon long-term test. Report 06819REP0120010140R00, Ontario Power Generation, Nuclear Waste Management Division.

Dixon D A, Snider G R, Ikeda B M, Kaatz R H, Kohle C L, Haugen K A, Betteridge J S, 2002. Installation of the buffer coupon long-term test at Atomic Energy of Canada Limited's Underground Research Laboratory. Report 06819REP0130010045R00, Ontario Power Generation, Nuclear Waste Management Division.

Domènech C, Arcos D, Bruno J, Karnland O, Muurinen A, 2004. Geochemical model of the granite-bentonite-groundwater at Äspö (LOT expiriment). In: Oversby V M, Werme L O (eds). Scientific Basis for Nuclear Waste Management XXVII: symposium held in Kalmar, Sweden, 15–19 June 2003. Warrendale, PA: Materials Research Society. (Materials Research Society Symposium Proceedings 807), pp 855–860.

Drogowska M, Brossard L, Ménard H, 1992. Copper dissolution in $NaHCO_3$ and $NaHCO_3$ + NaCl aqueous solutions at pH 8. Journal of the Electrochemical Society, 139, pp 39–47.

Drogowska M, Brossard L, Ménard H, 1994. Comparative study of copper behaviour in bicarbonate and phosphate aqueous solutions and effect of chloride ions. Journal of Applied Electrochemistry, U24, pp 344–349.

Ekendahl S, Pedersen K, 1994. Carbon transformations by attached bacterial populations in granitic ground water from deep crystalline bed-rock of the Stripa research mine. Microbiology, 140, pp 1565–1573.

Ekendahl S, Arlinger J, Ståhl F, Pedersen K, 1994. Characterization of attached bacterial populations in deep granitic groundwater from the Stripa research mine with 16S-rRNA gene sequencing technique and scanning electron microscopy. Microbiology, 140, pp 1575–1583.

Eriksson S, 2008. Äspö Hard Rock Laboratory. Prototype repository. Analysis of microorganisms, gases, and chemistry in buffer and backfill, 2004–2007. SKB IPR-08-01, Svensk Kärnbränslehantering AB.

Escalante E, Kruger J, 1971. Stress corrosion cracking of pure copper. Journal of the Electrochemi cal Society, 118, pp 1062–1066.

Escobar I S, Silva E, Silva C, Ubal A, 1999. Study of the effect of sulfide ions on the corrosion resistance of copper for use in containers for high-level waste. In: Eltringham G A, Piret N L, Sahoo M (eds). Proceedings of 4th International Conference Copper 99 – Cobre 99. Vol. I. Warrendale, PA: Minerals, Metals, and Materials Society, pp 371–386.

Escobar I, Silva C, Silva E, Werme L, 2001. Sulfide corrosion of copper cansiter for spent fuel disposal. In: Nuclear waste containment materials. Papers related to the SKB waste disposal programme presented at the Materials Research Society Spring Meeting, April 19, 2001. SKB TR-01-25, Svensk Kärnbränslehantering AB, pp 25–31.

Escobar I, Silva E, Lamas C, Silva C, Werme L, 2004. Effects of the environmental pressure in the corrosion potential of the copper that will be used as container of high level radioactive waste. In: Oversby V M, Werme L O (eds). Scientific basis for nuclear waste management XXVII: symposium held in Kalmar, Sweden, 15–19 June 2003. Warrendale, PA: Materials Research Society. (Materials Research Society Symposium Proceedings 807), pp 453–458.

Farina S B, Duffó G S, Galvele J R, 2005. Stress corrosion cracking of copper and silver, specific effect of the metal cations. Corrosion Science, 47, pp 239–245.

Farmer J C, Van Konynenburg R A, McCright R D, Gdowski G E, 1988. Survey of degradation modes of candidate materials for high-level radioactive-waste disposal containers. Volume 4. Stress corrosion cracking of copper-based alloys. Report UCID21362 Vol 4, Lawrence Livermore National Laboratory, California.

Fennell P A H, Graham A J, Smart N R, Sofield C J, 2001. Grain boundary corrosion of copper canister material. SKB TR-01-09, Svensk Kärnbränslehantering AB.

Fischer W, Hänßel I, Paradies H H, 1988. First results of microbial induced corrosion of copper pipes. In: Sequeira C A C, Tiller A K (eds). Microbial Corrosion-1. London: Elsevier, pp 300–327.

Fujii T, Kodama T, Baba H, 1984. The effect of water quality on pitting corrosion of copper tube in hot soft water. Corrosion Science, 24, pp 901–912.

Galvel J R, 1987. A stress corrosion cracking mechanism based on surface mobility. Corrosion Science, 24, pp 1–33.

Grenthe I, Wanner H, Östhols E, 2000. Guidelines for the extrapolation to zero ionic strength. Thermochemical Data Base Project, TDB-2. Le Seine-St. Germain: OECD/NEA. [Online]. Available at: http://www.oecd-nea.org/dbtdb/guidelines/tdb2.pdf.

Gripenberg H, 2009. Residual stress investigation of copper plate and canister EB-welds: Complementary results. Posiva Working Report 2009-21, Posiva Oy, Finland.

Gubner R, Andersson U, 2007. Corrosion resistance of copper canister weld material. SKB TR-07-07, Svensk Kärnbränslehantering AB.

Gubner R, Andersson U, Linder M, Nazarov A, Taxén C, 2006. Grain boundary corrosion of copper canister weld material. SKB TR-06-01, Svensk Kärnbränslehantering AB.

Hallberg R O, Ostlund P, Wadsten T, 1988. Inferences from a corrosion study of a bronze cannon, applied to high level nuclear waste disposal. Applied Geochemistry, 3, pp 273–280.

Harned H S, Owen B B, 1958. The physical chemistry of electrolytic solutions. 3rd ed. New York: Reinhold.

Haveman S A, Pedersen K, 2002a. Distribution of culturable microorganisms in Fennoscandian Shield groundwater. FEMS Microbiology Ecology, 39, pp 129–137.

Haveman S A, Pedersen K, 2002b. Microbially mediated redox processes in natural analogues for radioactive waste. Journal of Contaminant Hydrology, 55, pp 161–74.

Haveman S A, Pedersen K, Routsalainen P, 1999. Distribution and metabolic diversity of microorganisms in deep igneous rock aquifers of Finland. Geomicrobiology Journal, 16, pp 277–294.

Helgeson H C, Kirkham D H, Flowers G C, 1981. Prediction of the thermodynamic properties of electrolytes at high pressures and temperatures. In: Rickard D T, Wickman F E (eds). Chemistry and geochemistry of solutions at high temperatures and pressures. Oxford: Pergamon Press.

Henderson P J, 1994. Creep of copper. In: International Seminar on Design and Manufacture of Copper Canisters for Nuclear Waste, Sollentuna, April 1994. Paper IM3112.

Henderson P J, Österberg J-O, Ivarsson B, 1992. Low temperature creep of copper intended for nuclear waste containers. SKB TR 92-04, Svensk Kärnbränslehantering AB.

Hietanen S, Ehrnstén U, Saario T, 1996. Environmentally assisted cracking behaviour of copper in simulated ground water. STUK-YTO-TR 105, Radiation and Nuclear Safety Authority (STUK), Finland.

Hökmark H, 2004. Hydration of the bentonite buffer in a KBS-3 repository. Applied Clay Science, 26, pp 219–233.

Hultquist G, Szakálos P, Graham M J, Sproule G I, Wikmark G, 2008. Detection of hydrogen in corrosion of copper in pure water. In: Proceedings of the 17th International Corrosion Congress, Las Vegas, 6–10 October 2008. Houston, TX: NACE International, paper 3884.

Hultquist G, Szakálos P, Graham M J, Belonoshko A B, Sproule G I, Gråsjö L, Dorogokupets P, Danilov B, Aastrup T, Wikmark G, Chuah G K, Eriksson J C, Rosengren A, 2009. Water corrodes copper. Catalysis Letters, 132, doi: 10.1007/s10562-009-0113-x.

Humphreys P, Johnstone T, Trivedi D, Hoffmann A, 1995. The biogeochemical transport code DRINK: a mechanistic description. In: Murakami T, Ewing R C (eds). Scientific basis for nuclear waste management XVIII: symposium held in Kyoto, Japan, 23–27 October 1994. Pittsburgh, PA: Materials Research Society. (Materials Research Society Symposium Proceedings 353), pp 211–218.

Hunter K S, Wang Y, Van Cappellen P, 1998. Kinetic modelling of microbially-driven redox chemistry of subsurface environments: coupling transport, microbial metabolism and geochemistry. Journal of Hydrology, 209, pp 53–80.

Ikeda B M, King F, 2001. State of knowledge on stress corrosion cracking of copper for used-fuel disposal containers. Report 06819REP0120010058R00, Ontario Power Generation, Nuclear Waste Management Division, Canada.

Ikeda B M, Litke C D, 2000. The effect of oxidant flux, nitrite concentration and chloride concentration on the stress corrosion cracking behaviour of non-welded and electron-beam welded copper. Report 06819REP0120010049R00, Ontario Power Generation, Nuclear Waste Management Division, Canada.

Ikeda B M, Litke C D, 2004. Status report for 2003 on stress corrosion cracking of OFP copper in ammonia. Report 06819-REP-01300-10078, Ontario Power Generation, Nuclear Waste Management Division, Canada.

Ikeda B M, Litke C D, 2007. Stress corrosion cracking of copper in nitrite/chloride mixtures at elevated temperatures. NWMO TR-2007-04, Nuclear Waste Management Organization, Canada.

Ikeda B M, Litke C D, 2008. The effect of high chloride concentration on stress corrosion cracking behaviour of copper. NWMO TR-2008-12, Nuclear Waste Management Organization, Canada.

Imai H, Fukuda T, Akashi M, 1996. Effects of anionic species on the polarization behavior of copper for waste package material in artificial ground water. In: Murphy W A, Dieter A K (eds). Scientific basis for nuclear waste management XIX: symposium held in Boston, Massachusetts, USA, 27 November – 1 December 1995. Pittsburgh, PA: Materials Research Society. (Materials Research Society Symposium Proceedings 412), pp 589–596.

JNC, 2000. H12: project to establish the scientific and technical basis for HLW disposal in Japan. Supporting Report 2. Repository design and engineering technology. JNC TN1410 2000-003, Japan Nuclear Cycle Development Institute.

Johnson L H, King F, 2003. Canister options for the disposal of spent fuel. Nagra Technical Report NTB 02-11, National Cooperative for the Disposal of Radioactive Waste, Switzerland.

Johnson L H, LeNeveu D M, King F, Shoesmith D W, Kolář M, Oscarson D W, Sunder S, Onofrei C, Crosthwaite J L, 1996. The disposal of Canada's nuclear fuel waste: A study of postclosure safety of in-room emplacement of used CANDU fuel in copper containers in permeable plutonic rock: volume 2: vault model. AECL11494-2, COG96552-2, Atomic Energy of Canada Limited.

Kalyuzhnaya M G, Khmelenina V N, Kotelnikova S, Holmquist L, Pedersen K, Trotsenko Y A, 1999. Methylomonas scandinavica, sp. nov, a new methanotrophic psychrotrophic bacterium isolated from deep igneous rock ground water of Sweden. Systematic and Applied Microbiology, 22, pp 565–72.

Karnland O, Birgersson M, 2006. Montmorillonite stability. With special respect to KBS-3 conditions. SKB TR-06-11, Svensk Kärnbränslehantering AB.

Karnland O, Sandén T, 2000. Long term test of buffer material at Aspo Hard Rock Laboratory, Sweden. In: Smith R W, Shoesmith D W (eds). Scientific basis for nuclear waste management XXIII: symposium held in Boston, Massachusetts, USA, 29 November – 2 December 1999. Warrendale, PA: Materials Research Society. (Materials Research Society Symposium Proceedings 608), pp 173–178.

Karnland O, Sandén T, Johannesson L-E, Eriksen T E, Jansson M, Wold S, Pedersen K, Motamedi M, Rosborg B, 2000. Long term test of buffer material. Final report on the pilot parcels. SKB TR-00-22, Svensk Kärnbränslehantering AB.

Kasahara K, Komukai S, 1987. Case studies of pitting corrosion of copper tubes in central hot-water supply systems. Corrosion Engineering, 36, pp 453–459.

Kasahara K, Komukai S, Fujiwara T, 1988. Preventing copper-pipe pitting in central hot water supply by residual-chlorine UV photolysis. Corrosion Engineering, 37, pp 361–370.

Kass J, 1990. Evaluation of copper, aluminum bronze, and copper-nickel container material for the Yucca Mountain Project. In: Shoesmith D W (ed). Corrosion of nuclear fuel containers: proceedings of a workshop. AECL-10121, Atomic Energy of Canada Limited, pp 87–108.

Kato C, Ateya B G, Castle J E, Pickering H W, 1980a. On the mechanism of corrosion of Cu9.4Ni1.7Fe alloy in air saturated aqueous NaCl solution. I. Kinetic investigations. Journal Electrochemical Society, 127, pp 1890–1896.

Kato C, Castle J E, Ateya B G, Pickering H W, 1980b. On the mechanism of corrosion of Cu9.4Ni1.7Fe alloy in air saturated aqueous NaCl solution. II. Composition of the protective surface layer. Journal of the Electrochemical Society, 127, pp 1897–1903.

Kear G, Barker B D, Walsh F C, 2004. Electrochemical corrosion of unalloyed copper in chloride media – a critical review. Corrosion Science, 46, pp 109–135.

Khanzin V G, Nikulin S A, 2005. Assessment of copper resistance to stress-corrosion cracking in nitrite solutions by means of joint analysis of acoustic emission measurements, deformation diagrams, qualitative and quantitative fractography, and non-linear fracture mechanics. SKB TR-05-15, Svensk Kärnbränslehantering AB.

Kindred J S, Celia M A, 1989. Contaminant transport and biodegradation. 2. Conceptual model and test simulations. Water Resources Research, 25, pp 1149–1159.

King F, 1995. A natural analogue for the long-term corrosion of copper nuclear waste containers – reanalysis of a study of a bronze cannon. Applied Geochemistry, 10, pp 477–487.

King F, 1996a. Microbially influenced corrosion of copper nuclear fuel waste containers in a Canadian disposal vault. AECL-11471, COG-94–519, Atomic Energy of Canada Limited

King F, 1996b. A copper container corrosion model for the in-room emplacement of used CANDU fuel. AECL-11552, COG96105, Atomic Energy of Canada Limited.

King F, 1996c. The potential for stress corrosion cracking of copper containers in a Canadian nuclear fuel waste disposal vault. AECL11550, COG9694, Atomic Energy of Canada Limited.

King F, 2002. Corrosion of copper in alkaline chloride environments. SKB TR-02-25, Svensk Kärnbränslehantering AB.

King F, 2004. The effect of discontinuities on the corrosion behaviour of copper canisters. SKB TR-04-05, Svensk Kärnbränslehantering AB.

King F, 2005. Overview of the corrosion behaviour of copper and steel used fuel containers in a deep geologic repository in the sedimentary rock of the Michigan Basin, Ontario. Report 06819-REP-01300-10101, Ontario Power Generation, Nuclear Waste Management Division, Canada.

King F, 2006. Review and gap analysis of the corrosion of copper containers under unsaturated conditions. Report 06819REP0130010124R00, Ontario Power Generation, Nuclear Waste Management Division, Canada.

King F, 2007. Mixed-potential modelling of the corrosion of copper in the presence of sulphide. Posiva Working Report 2007-63, Posiva Oy, Finland.

King F, 2009. Microbiologically influenced corrosion of nuclear waste containers. Corrosion, 65, pp 233–251.

King F, Kolář M, 1995. Prediction of the lifetimes of copper nuclear waste containers under restrictive masstransport and evolving redox conditions. Corrosion/95, NACE International, Houston, Texas, Paper 425.

King F, Kolář M, 1996a. A numerical model for the corrosion of copper nuclear fuel waste containers. In: Murphy W A, Dieter A K (eds). Scientific basis for nuclear waste management XIX: symposium held in Boston, Massachusetts, USA, 27 November – 1 December 1995. Pittsburgh, PA: Materials Research Society. (Materials Research Society Symposium Proceedings 412), pp 555–562.

King F, Kolář M, 1996b. Mechanistic modelling of the corrosion behaviour of copper nuclear fuel waste containers. In: Proceedings of international conference on deep geological disposal of radioactive waste. Toronto, ON: Canadian Nuclear Society, pp 5–39 – 5–50.

King F, Kolář M, 1997a. Corrosion of copper containers prior to saturation of a nuclear fuel waste disposal vault. AECL11718, COG96566I, Atomic Energy of Canada Limited.

King F, Kolář M, 1997b. The effect of geosphere conditions on the lifetimes of copper containers. AECL11717, COG96565I, Atomic Energy of Canada Limited.

King F, Kolář M, 2000. The copper container corrosion model used in AECL's second case study. Report 06819REP0120010041R00, Ontario Power Generation, Nuclear Waste Management Division, Canada.

King F, Kolář M, 2004. Theory manual for the copper corrosion model for stress corrosion cracking of used fuel disposal containers CCM-SCC.0. Report 06819-REP-01300-10095-R00, Ontario Power Generation, Nuclear Waste Management Division, Canada.

King F, Kolář M, 2005. Preliminary assessment of the stress corrosion cracking of used fuel disposal containers using the CCM-SCC.0 model. Report 06819REP0130010103R00, Ontario Power Generation, Nuclear Waste Management Division, Canada.

King F, Kolář M, 2005. Preliminary assessment of the stress corrosion cracking of used fuel disposal containers using the CCMSCC.0 model. Report 06819-REP-01300-10103, Ontario Power Generation, Nuclear Waste Management Division, Canada.

King F, Kolář M, 2006a. Simulation of the consumption of oxygen in long-term in situ experiments and in the third case study repository using the copper corrosion model CCM-UC.1.1. Report 06819REP0130010084R00, Ontario Power Generation, Nuclear Waste Management Division, Canada.

King F, Kolář M, 2006b. Consequences of microbial activity fopr corrosion of copper used fuel containers – analyses using the CCM-MIC.0.1 code. Report 06819REP0130010120R00, Ontario Power Generation, Nuclear Waste Management Division, Canada.

King F, LeNeveu D, 1992. Prediction of the lifetimes of copper nuclear waste containers. In: Proceedings of Conference on Nuclear Waste Packaging, FOCUS '91. American Nuclear Society, La Grange Park, IL, pp 253–261.

King F, Litke C D, 1987. The corrosion of copper in synthetic groundwater at 150°C. Part I. The results of short term electrochemical tests. Technical Record TR-428, Atomic Energy of Canada Limited.

King F, Litke C D, 1997. Stress corrosion cracking of copper - report on experimental methodologies and preliminary results. Report 06819REP012000010 R00, Ontario Hydro Nuclear Waste Management Division, Canada.

King F, Newman R C, 2010. Stress corrosion cracking of copper canisters. SKB TR-10-04, Svensk Kärnbränslehantering AB.

King F, Stroes-Gascoyne S, 1995. Microbially influenced corrosion of nuclear fuel waste disposal containers. In: Proceedings of the 1995 International Conference On Microbially Influenced Corrosion, New Orleans, Louisiana, 8–10 May. Houston: NACE International, pp 35/1–35/14.

King F, Tang Y, 1998. The anodic dissolution of copper in chloride-sulphate groundwaters. Report 06819-REP-01200-0058 R00, Ontario Hydro Nuclear Waste Management Division, Canada.

King F, Litke C D, Ryan S R, 1992. A mechanistic study of the uniform corrosion of copper in compacted Na-montmorillonite/s and mixtures. Corrosion Science, 33, pp 1979–1995.

King F, Litke C, Ryan S, LeNeveu D, 1994. Predicting the longterm corrosion behaviour of copper nuclear fuel waste containers. In: Parkins R N (ed). Life prediction of corrodible structures. Houston, TX: NACE International, pp 497–512.

King F, Litke C D, Quinn M J, LeNeveu D M, 1995a. The measurement and prediction of the corrosion potential of copper in chloride solutions as a function of oxygen concentration and masstransfer coefficient. Corrosion Science, 37, pp 833–851.

King F, Quinn M J, Litke C D, 1995b. Oxygen reduction on copper in neutral NaCl solution. Journal of Electroanalytical Chemistry, 385, pp 45–55.

King F, Litke C D, Tang Y, 1995c. Effect of interfacial pH on the reduction of oxygen on copper in neutral $NaClO_4$ solution. Journal of Electroanalytical Chemistry, 384, pp 105–113.

King F, Tang Y, Quinn M J, Litke C D, 1995d. The effects of dissolved oxygen concentration and masstransport conditions on the dissolution behaviour of copper nuclear waste containers. Corrosion/95, NACE International, Houston, TX, Paper 424.

King F, Ryan S R, Litke C D, 1997a. The corrosion of copper in compacted clay. AECL11831, COG97319I, Atomic Energy of Canada Limited.

King F, Greidanus G, Jobe D J, 1997b. Dissolution of copper in chloride/ammonia mixtures and the implications for the stress corrosion cracking of copper containers. AECL11865, COG97412I, Atomic Energy of Canada Limited.

King F, Litke C D, Ikeda B M, 1999a. The effect of oxidant supply and chloride ions on the stress corrosion cracking of copper. Report 06819REP0120010013R00, Ontario Power Generation, Nuclear Waste Management Division.

King F, Litke C D, Ikeda B M, 1999b. The stress corrosion cracking of copper containers for the disposal of high-level nuclear waste. Corrosion/99, NACE International, Houston, Texas, Paper 482.

King F, Litke C D, Ikeda B M, 1999c. The stress corrosion cracking of copper nuclear waste containers. In: Wronkiewicz D J, Lee J H (eds). Scientific Basis for Nuclear Waste Management XXII: symposium held in Boston, Massachusetts, 30 November – 4 December 1998. Warrendale, PA: Materials Research Society. (Materials Research Society Symposium Proceedings 556)

King F, Greidanus G, Jobe D J, 1999d. Dissolution of copper in chloride/ammonia mixtures and the implications for the stress corrosion cracking of copper containers. AECL11865, COG-97-412-I, Atomic Energy of Canada Limited.

King F, Ahonen L, Taxén T, Vuorinen U, Werme L, 2001. Copper corrosion under expected conditions in a deep geologic repository. SKB TR-01-23, Svensk Kärnbränslehantering AB.

King F, Ahonen L, Taxén T, Vuorinen U, Werme L, 2002a. Copper corrosion under expected conditions in a deep geologic repository. Posiva 2002-01, Posiva Oy, Finland.

King F, Kolář M, Stroes-Gascoyne S, 2002b. Theory manual for the microbiological copper corrosion model CCM-MIC.0. Report 06819REP0120010091R00, Ontario Power Generation, Nuclear Waste Management Division, Canada.

King F, Kolář M, Stroes-Gascoyne S, 2003. Preliminary simulations of the long-term activity of microbes in a deep geologic repository using CCM-MIC.0 and the implications for corrosion of copper containers. Report 06819REP0120010116R00, Ontario Power Generation, Nuclear Waste Management Division, Canada.

King F, Kolář M, Stroes-Gascoyne S, Maak P, 2004. Model for the microbiological corrosion of copper containers in a deep geologic repository. In: Oversby V M, Werme L O (eds). Scientific basis for nuclear waste management XXVII: symposium held in Kalmar, Sweden, 15–19 June 2003. Warrendale, PA: Materials Research Society. (Materials Research Society Symposium Proceedings 807), pp 811–816.

King F, Kolář M, Maak P, 2008. Reactive-transport model for the prediction of the uniform corrosion behaviour of copper used fuel containers. Journal of Nuclear Materials, 379, pp 133–141.

Kinnunen P, 2006. Stress corrosion cracking investigations of copper in groundwater with acetate ions. Posiva Working Report 200618, Posiva Oy, Finland.

Kinzelbach W, Schäfer W, 1991. Numerical modeling of natural and enhanced denitrification processes in aquifers. Water Resources Research, 27, pp 1123–1135.

Kiss L, Farkas J, Korosi A, 1971. Ionization of metals and the neutralization of the metal ions on the rotating ring disk electrode. VII. Dependence of the anodic dissolution of copper on the concentration of the chloride ions. Acta Chimica Hungary, 68, pp 359–370.

Kolář M, King F, 1996. Modelling the consumption of oxygen by container corrosion and reaction with Fe(II). In: Murphy W A, Dieter A K (eds). Scientific basis for nuclear waste management XIX: symposium held in Boston, Massachusetts, USA, 27 November – 1 December 1995. Pittsburgh, PA: Materials Research Society. (Materials Research Society Symposium Proceedings 412), pp 547–554.

Kotelnikova S, Pedersen K, 1998. Distribution and activity of methanogens and homoacetogens in deep granitic aquifers at Äspö Hard Rock Laboratory, Sweden. FEMS Microbiology Ecology, 26, pp 121–34.

Kubaschewski O, Alcock C B, Spencer P J, 1993. Materials thermochemistry. 6th ed. Oxford: Pergamon Press.

Kvashnina K O, Butorin S M, Modin A, Soroka I, Marcellini M, Guo J-H, Werme L, Nordgren J, 2007. Changes in electronic structure of copper films in aqueous solutions. Journal of Physics: Condensed Matter, 19, 226002.

Kyle J E, Eydal H S C, Ferris F G, Pedersen K, 2008. Viruses in granitic groundwater from 69 to 450 m depth of the Äspö hard rock laboratory, Sweden. The ISME Journal, 2, pp 571–574.

Langmuir D, 1997. Aqueous environmental geochemistry. Upper Saddle River, NJ: Prentice Hall.

Laz M M, Souto R M, González S, Salvarezza R C, Arvia A J, 1992. Pitting corrosion of polycrystalline annealed copper in alkaline sodium perchlorate solutions containing benzotriazole. Journal of Applied Electrochemistry, 22, pp 1129–1134.

Lee H P, Nobe K, 1986. Kinetics and mechanisms of Cu electrodissolution in chloride media. Journal of the Electrochemical Society, 133, pp 2035–2043.

Lempinen A, 2006. Thermo-hydro-mechanical analysis of KBS-3V deposition hole. Ph.D. thesis. In preparation.

Leygraf C, Graedel T E, 2000. Atmospheric Corrosion. New York: Wiley-Interscience.

Litke C D, Ryan S R, King F, 1992. A mechanistic study of the uniform corrosion of copper in compacted claysand soil. AECL10397, COG91304, Atomic Energy of Canada Limited.

Litke C D, Ikeda B M, 2006. The effect of acetate concentration, chloride concentration, and applied current on stress corrosion cracking of OFP copper. Report 06819-REP-01300-10005, Ontario Power Generation, Nuclear Waste Management Division, Canada.

Litke C D, Ikeda B M, 2008. The stress corrosion cracking behaviour of copper in acetate solutions. NWMO TR-2008-21, Nuclear Waste Management Organization, Canada.

Lobo V M M, 1989. Handbook of electrolyte solutions. Amsterdam: Elsevier.

Lucey V F, 1967. Mechanism of pitting corrosion of copper in supply waters. British Corrosion Journal, 2, pp 175–185.

Lundgren K, 1998. Kontroll av strålskärmsberäkningar för kopparkapsel (in Swedish). Rapport 97-0028R, ALARA Engineering AB, Sweden.

Lundgren K, 2004. Final disposal of fuel – electron radiation outside copper canister. SKB TR-04-06, Svensk Kärnbränslehantering AB.

Luukkonen A, 2001. Groundwater mixing and geochemical reactions – An inverse-modelling approach. In: Luukkonen A, Kattilakoski E (eds). Äspö Hard Rock Laboratory. Groundwater flow, mixing and geochemical reactions at Äspö HRL. Task 5. Äspö Task Force on groundwater flow and transport of solutes. SKB IPR-02-41, Svensk Kärnbränslehantering AB, Part III.

Luukkonen A, 2004. Modelling approach for geochemical changes in the Prototype repository engineered barrier system. Posiva Working Report 2004-31, Posiva Oy, Finland.

Luukkonen A, Nordman H, 2007. Reactive transport predictions for an Olkiluoto final repository tunnel unit. Posiva Working Report 2007-81, Posiva Oy, Finland.

Luukkonen A, Pitkänen P, Partamies S, 2005. Evaluation of Olkiluoto hydrogeochemical data in 3D – with a proceeding of recent geochemical interpretation results. Posiva Working Report 2005-72, Posiva Oy, Finland.

Lyle F F, 1993. Experimental evaluation of copper corrosion by constituents of natural gas. Final report, September 1988 – March 1993. Report PB93193621/XAB, Southwest Research Institute.

Löfman J, 2005. Simulation of hydraulic disturbances caused by the decay heat of the repository in Olkiluoto. Posiva 2005-7, Posiva Oy, Finland.

Löfman J, Poteri A, 2008. Groundwater flow and transport simulations in support of RNT-2008 analysis. Posiva Working Report 2008-52, Posiva Oy, Finland.

Maak P, King F, 2005. A model for predicting stress corrosion cracking behaviour of copper containers in a deep geologic repository. In: Van Iseghem P (ed). Scientific basis for nuclear waste management XXIX: proceedings of a meeting held in Ghent, Belgium, 12–16 September 2005. Warrendale, PA: Materials Research Society. (Materials Research Society Symposium Proceedings 932), pp 837–844.

Macdonald D D, Syrett BC, Wing S S, 1979. The corrosion of CuNi alloys 706 and 715 in flowing sea water. IIEffect of dissolved sulfide. Corrosion, 35, pp 367–378.

Madina V, Azkarate I, Insausti M, 2004. Corrosion of several components of the "in-situ" test perfomed in a deep geological granite disposal site. In: Proceedings of the 2nd International Workshop on Prediction Of Long Term Corrosion Behaviour in Nuclear Waste Systems, Nice, France, September 2004, European Federation of Corrosion.

Mansfeld F, Liu G, Xiao H, Tsai C H, Little B J, 1994. The corrosion behavior of copper alloys, stainless steels and titanium in seawater. Corrosion Science, 36, pp 2063–2095.

Marsh G P, 1990. A preliminary assessment of the advanced cold process canister. AEA-InTec-0011, AEA Industrial Technology, Harwell Laboratory, UK.

Masurat P, 2006. Potential for corrosion in disposal systems for high level radioactive waste by Meiothermus and Desulfovibrio. Ph.D. thesis. University of Gothenburg, Sweden.

Masurat P, Pedersen K, 2004. Microbial sulphide production in compacted bentonite at the commencement of long-term disposal of high-level radioactive waste. In: Oversby V M, Werme L O (eds). Scientific basis for nuclear waste management XXVII: symposium held in Kalmar, Sweden, 15–19 June 2003. Warrendale, PA: Materials Research Society. (Materials Research Society Symposium Proceedings 807), pp 805–810.

Masurat P, Eriksson S, Pedersen K, 2010a. Evidence for indigenous sulphate-reducing bacteria in commercial MX-80 Wyoming bentonite. Applied Clay Science, 47, pp 51–57.

Masurat P, Eriksson S, Pedersen K, 2010b. Miocrbial sulphide production in compacted Wyoming bentonite MX80 under in situ conditions relevant to a reposiotry for high-level radioactive waste. Applied Clay Science, 47, pp 58–64.

Mattsson E, 1980. Corrosion of copper and brass: practical experience in relation to basic data. British Corrosion Journal, 15, pp 6–13.

Miley H A, Evans U R, 1948. Oxidation of copper in air. In: Evans U R. Metallic corrosion, passivity and protection. 2nd ed. London: Arnold.

Moll H, Stumpf T H, Merroun M, Rossberg A, Selenska-Pobell S, Bernhard G, 2004. Time-resolved laser flourescence spectroscopy study of the interaction of Curium(III) with Desulfovibrio aespoeensis DSM 10631^{T}. Environmental Science & Technology, 38, pp 1455–1459.

Mor E D, Beccaria A M, 1975. Behaviour of copper in artificial sea water containing sulphides. British Corrosion Journal, 10, pp 33–38.

Mor E D, Beccaria A M, 1979. Effects of temperature on the corrosion of copper in seawater at different hydrostatic pressures. Werkstoffe und Korrosion, 30, pp 551–558.

Mori G, Scherer D, Schwentenwien S, 2003. Requirements for initiation of intergranular SCC in DHP-copper tubes. Corrosion/2003, NACE International, Houston, Texas, Paper 03511.

Mori G, Scherer D, Schwentenwien S, Warbichler P, 2005. Intergranular stress corrosion cracking of copper in nitrite solutions. Corrosion Science, 47, pp 2099–2124.

Motamedi M, Pedersen K, 1998. Desulfovibrio aespoeensis sp. nov. a mesophilic sulfate-reducing bacterium from deep groundwater at Äspö hard rock laboratory, Sweden. International Journal of Systematic Bacteriology, 48, pp 311–315.

Muurinen A, 2001. Development and testing of analysis methods for bentonite porewater. Posiva Working Report 2001-7, Posiva Oy, Finland.

Muurinen A, 2003. Chemical conditions in the A0 parcel of the long-term test of buffer material in Äspö (LOT). Posiva Working Report 2003-32, Posiva Oy, Finland.

Muurinen A, 2006a. Ion concentration caused by an external solution into the porewater of compacted bentonite. Posiva Working Report 2006-96, Posiva Oy, Finland.

Muurinen A, 2006b. Chemical conditions in the A2 parcel of the long-term test of buffer material in Äspö (LOT). Posiva Working Report 2006-83, Posiva Oy, Finland.

Muurinen A, Lehikoinen J, 1999. Porewater Chemistry in compacted bentonite. Posiva 99-20, Posiva Oy, Finland.

Nielsen M E, Pedersen K, Fisk M, Istok J, 2006. Microbial nitrate respiration of lactate at in situ conditions in groundwater from a granitic aquifer situated 450 m underground. Geobiology, 4, pp 43–52.

Nishikata A, Itagaki M, Tsuru T, Haruyama S, 1990. Passivation and its stability on copper in alkaline solutions containing carbonate and chloride ions. Corrosion Science, 31, pp 287–292.

Paloneva M, 2009. The effects of gaseous methane on groundwater flow in crystalline bedrock. M.A. thesis. Helsinki University of Technology, Faculty of Information and Natural Sciences, unpublished.

Parkhurst D L, Appelo C A J, 1999. User's guide to PHREEQC (version 2): a computer program for speciation, batch-reaction, one-dimensional transport, and inverse geochemical calculations. Water-Resources Investigations Report 99-4259, U.S. Geological Survey, Denver, Colorado.

Pastina B, Hellä P, 2006. Expected evolution of a spent fuel repository at Olkiluoto (revised). Posiva 2006-5, Posiva Oy, Finland.

Pedersen K, 2000. Äspö Hard Rock Laboratory. The microbe site. Drilling, instrumentation and characterisation. SKB IPR-00-36, Svensk Kärnbränslehantering AB.

Pedersen K, 2001. Diversity and activity of microorganisms in deep igneous rock aquifers of the Fennoscandian Shield. In: Fredrickson J K, Fletcher M (eds). Subsurface microbiology and biogeochemistry. New York: Wiley-Liss, pp 97–139.

Pedersen K, 2002. Microbial processes in the disposal of high level radioactive waste 500 m underground in Fennoscandian shield rocks. In: Keith-Roach M J, Livens F R (eds). Interactions of microorganisms with radionuclides. Amsterdam: Elsevier, pp 279–311.

Pedersen K, 2005a. Äspö Hard Rock Laboratory. The MICROBE framework: Site descriptions, instrumentation, and characterization. SKB IPR-05-05, Svensk Kärnbränslehantering AB.

Pedersen K, 2005b. Äspö Hard Rock Laboratory. MICROBE. Analysis of microorganisms and gases in MICROBE groundwater over time during MINICAN drainage of the MICROBE water conducting zone. SKB IPR-05-29, Svensk Kärnbränslehantering AB.

Pedersen K, 2005c. The deep intraterrestrial biosphere. In: Gadd G M, Semple K T, Lappin-Scott H M (eds). Micro-organisms and earth systems: advances in geomicrobiology. Cambridge: Cambridge University Press, pp 233–245.

Pedersen K, 2006. Microbiology of transitional groundwater of the porous overburden and underlying shallow fractured bedrock aquifers in Olkiluoto 2004, Finland. Posiva Working Report 2006-9, Posiva Oy, Finland.

Pedersen K, 2008. Microbiology of Olkiluoto groundwater, 2004–2006. Posiva 2008-2, Posiva Oy, Finland.

Pedersen K, 2010. Analysis of copper corrosion in compacted bentonite clay as a function of clay density and growth conditions for sulfate-reducing bacteria. Journal of Applied Microbiology, 108, pp 1094–1104.

Pedersen K, Ekendahl S, 1990. Distribution and activity of bacteria in deep granitic groundwaters of southeastern Sweden. Microbial Ecology, 20, pp 37–52.

Pedersen K, Ekendahl S, 1992a. Incorporation of CO_2 and introduced organic compounds by bacterial populations in groundwater from the deep crystalline bedrock of the Stripa mine. Journal of General Microbiology, 138, pp 369–376.

Pedersen K, Ekendahl S, 1992b. Assimilation of CO_2 and introduced organic compounds by bacterial communities in ground water from Southeastern Sweden deep crystalline bedrock. Microbial Ecology, 23, pp 1–14.

Pedersen K, Arlinger J, Ekendahl S, Hallbeck L, 1996. 16S rRNA gene diversity of attached and unattached groundwater bacteria along the access tunnel to the Äspö Hard Rock Laboratory, Sweden. FEMS Microbiology Ecology, 19, pp 249–262.

Pedersen K, Motamedi M, Karnland O, Sandén T, 2000a. Cultivability of microorganisms introduced into a compacted bentonite clay buffer under high-level radioactive waste repository conditions. Engineering Geology, 58, pp 149–161.

Pedersen K, Motamedi M, Karnland O, Sandén T, 2000b. Mixing and sulphate-reducing activity of bacteria in swelling compacted bentonite clay under high-level radioactive waste repository conditions. Journal of Applied Microbiology, 89, pp 1038–1047.

Pedersen K, Arlinger J, Eriksson S, Hallbeck A, Hallbeck L, Johansson J, 2008. Numbers, biomass and cultivable diversity of microbial populations relate to depth and borehole-specific conditions in groundwater from depths of 4-450 m in Olkiluoto, Finland. The ISME journal, 2, pp 760–775.

Pednekar S P, Agrawal A K, Chaung H E, Staehle R W, 1979. Transgranular cracking of copper in 1M NaNO2 solution. Journal of the Electrochemical Society, 126, pp 701–702.

Pérez Sánchez M, Barrera M, González S, Souto R M, Salvarezza R C, Arvia A J, 1990. Electrochemical behaviour of copper in aqueous moderate alkaline media containing sodium carbonate and bicarbonate and sodium perchlorate. Electrochimica Acta, 35, pp 1337–1343.

Pérez Sánchez M, Souto R M, Barrera M, González S, Salvarezza R C, Arvia A J, 1993. A mechanistic approach to the electroformation of anodic layers on copper and their electroreduction in aqueous solutions containing $NaHCO_3$ and Na_2CO_3. Electrochimica Acta, 38, pp 703–715.

Perry D L, Taylor J A, 1986. X-ray photoelectron and Auger spectroscopic studies of Cu_2S and CuS. Journal of Materials Science Letters, 5, pp 384–386.

Peters D G, Cruser S A, 1965. Cathodic chronopotentiometry of copper(I) and copper(II) in chloride media. Journal of Electroanalysis Chemistry, 9, pp 27–40.

Pettersson K, Oskarsson M, 1997. A study of stress corrosion crack growth in copper for nuclear waste canister application. TRITAMAC0611, The Royal Institute of Technology, Materials Research Center, Stockholm, Sweden.

Pettersson K, Oskarsson M, 2000. Stress corrosion crack growth in copper for waste canister applications. In: Smith R W, Shoesmith D W (eds). Scientific basis for nuclear waste management XXIII: symposium held in Boston, Massachusetts, USA, 29 November –2 December 1999. Warrendale, PA: Materials Research Society. (Materials Research Society Symposium Proceedings 608), pp 95–101.

Pinnel M R, Tompkins H G, Heath D E, 1979. Oxidation of copper in controlled clean air and standard laboratory air at 50°C and 150°C. Applications of Surface Science, 2, pp 558–577.

Pitkänen P, Partamies S, 2007. Origin and implications of dissolved gases in groundwater at Olkiluoto. Posiva 2007-4, Posiva Oy, Finland.

Pitkänen P, Luukkonen A, Ruotsalainen P, Leino-Forsman H, Vuorinen U, 1999. Geochemical modelling of groundwater evolution and residence time at the Olkiluoto site. Posiva 98-10, Posiva Oy, Finland.

Pitkänen P, Partamies S, Luukkonen A, 2004. Hydrogeochemical interpretation of baseline groundwater conditions at the Olkiluoto site. Posiva 2003-7, Posiva Oy, Finland.

Pitkänen P, Ahokas H, Ylä-Mella M, Partamies S, Snellman M, Hellä P, 2007. Quality review of hydrochemical baseline data from the Olkiluoto site. Posiva 2007-5, Posiva Oy, Finland.

Pitkänen P, Partamies S, Lahdenperä A-M, Lehtinen A, Pedersen K, Ahokas T, Penttinen T, Lamminmäki T, Hatanpää E, 2008. Results of monitoring at Olkiluoto in 2007: Hydrogeochemistry. Posiva Working Report 2008-24, Posiva Oy, Finland.

Pitzer K S, 1991. Ion interaction approach- theory and data correlation. In: Pitzer K S (ed). Activity coefficients in electrolyte solutions. 2nd ed. Boca Raton, FL: CRC Press.

Pitzer K S, 1995. Thermodynamics. 3rd ed. New York: McGraw-Hill.

Plyasunova N V, Wang M, Zhang Y, Muhammed M, 1997. Critical evaluation of thermodynamics of complex formation of metal ions in aqueous solutions II. Hydrolysis and hydroxo-complexes of Cu^{2+} at 298.15 K. Hydrometallurgy, 45, pp 37–51.

Posiva, 2005. Olkiluoto site description 2004. Vol 1–3. Posiva 2005-3, Posiva Oy, Olkiluoto.

Posiva, 2009. Olkiluoto site description 2008. Posiva 2009-1, Posiva Oy, Finland.

Pourbaix M, Pourbaix A, 1992. Potential-pH diagrams for the system SH_2O from 25 to 150°C: Influence of access of oxygen in sulphide solutions. Geochimica et Cosmochimica Acta, 56, pp 3157–3178.

Power G P, Ritchie I M, 1981. Mixed potential measurements in the elucidation of corrosion mechanisms – 1. Introductory theory. Electrochimica Acta, 26, pp 1073–1078.

Prommer H, Barry D A, Davis G B, 1999. A one-dimensional reactive multi-component transport model for biodegradation of petroleum hydrocarbons in groundwater. Environmental Modelling & Software, 14, pp 213–223.

Prommer H, Barry D A, Davis G B, 2000. Numerical modelling for design and evaluation of groundwater remediation schemes. Ecological Modelling, 128, pp 181–195.

Pugh E N, 1979. The stress-corrosion cracking of copper alloys. In: Arup H, Parkins R N (eds). Stress corrosion research. Alphen aan den Rijn: Sijthoff and Noordhoff, pp 177–208.

Pugh E N, Montague W G, Westwood A R C, 1966. Stress-corrosion cracking of copper. Corrosion Science, 6, pp 345–346.

Pugh E N, Craig J V, Sedriks A J, 1969. The stress-corrosion cracking of copper, silver and gold alloys. In: Staehle R W, Fory A J, van Rooyen D (eds). Fundamental aspects of stress corrosion cracking: proceedings of conference, 11–15 September 1967, the Ohio State University. National Association of Corrosion Engineers, Houston, Texas, pp 118–158.

Puigdomenech I, Taxén C, 2000. Thermodynamic data for copper. Implications for the corrosion of copper under repository conditions. SKB TR-00-13, Svensk Kärnbränslehantering AB.

Puigdomenech I, Taxén C, 2001. Thermodynamic data for copper from SKB TR-00-13, Svensk Kärnbränslehantering AB. Appendix I in this chapter.

Puigdomenech I, Rard J A, Plyasunov A V, Grenthe I, 1997. Temperature corrections to thermodynamic data and enthalpy calculations. In: Grenthe I, Puigdomenech I (eds). Modelling in aquatic chemistry. Paris: OECD Nuclear Energy Agency, pp 427–493.

Puigdomenech I, Ambrosi J-P, Eisenlohr L, Lartigue J-E, Banwart S A, Bateman K, Milodowski A E, West J M, Griffault L, Gustafsson E, Hama K, Yoshida H, Kotelnikova S, Pedersen K, Michaud V, Trotignon L, Rivas Perez J, Tullborg E-L, 2001. O_2 depletion in granitic media. The REX project. SKB TR-01-05, Svensk Kärnbränslehantering AB.

Pusch R, 2008. Geological storage of highly radioactive waste. Berlin: Springer.

Qafsaoui W, Mankowski G, Dabosi F, 1993. The pitting corrosion of pure and low alloyed copper in chloridecontaining borate buffered solutions. Corrosion Science, 34, pp 17–25.

Raiko H, 1996. Thermal optimisation of the final disposal of spent nuclear fuel. Posiva 96-03, Posiva Oy, Finland.

Raiko H, Salo J-P, 1999. Design report of the disposal canister for twelve fuel assemblies. Posiva 99-18, Posiva Oy, Finland.

Raiko H, Sandström R, Rydén H, Johansson M, 2010. Design analysis report for the canister. SKB TR-10-28, Svensk Kärnbränslehantering AB.

Rard J A, Staggs K J, Day S D, Carroll S A, 2005. Boiling temperature and reversed deliquescence relative humidity measurements for mineral assemblages in the NaCl + $NaNO_3$ + KNO_3 + $Ca(NO_3)_2$ + H_2O system. Report UCRL-JRNL-217704, Lawrence Livermore National Laboratory, California.

Reed D T, Van Konynenburg R A, 1991. Effect of ionizing radiation on moist air systems. In: Abrajano T A, Johnson L H (eds). Scientific basis for nuclear waste management XIV: symposium held in Boston, Massachusetts, USA, 26–29 November 1990. Pittsburgh PA: Materials Research Society. (Materials Research Society Symposium Proceedings 212), pp 317–325.

Reed D T, Swayambunathan V, Tani B S, Van Konynenburg R A, 1990. Corrosion product identification and relative rates of corrosion of candidate metals in an irradiated air-steam environment. In: Oversby V M, Brown P W (eds). Scientific basis for nuclear waste management XIII: symposium held in Boston, Massachusetts, USA, 27–30 November 1989. Pittsburgh, PA: Materials Research Society. (Materials Research Society Symposium Proceedings 176), pp 517–524.

Reitner J, Schumann G A, Pedersen K, 2005. Fungi in subterranean environments. In: Gadd G J (ed). Fungi in biogeochemical cycles. Cambridge: Cambridge University Press, pp 788–1002.

Rice D W, Peterson P, Rigby E B, Phipps P B P, Cappel R J, Tremoureux R, 1981. Atmospheric corrosion of copper and silver. Journal of the Electrochemical Society, 128, pp 275–284.

Robie R A, Hemingway B S, 1995. Thermodynamic properties of minerals and related substances at 298.15 K and 1 bar (10^5 Pascals) pressure and at higher temperatures. Washington, D.C.: U.S. Government Printing Office. (U.S. Geological Survey Bulletin 2131)

Robinson R A, Stokes R H, 1959. Electrolyte solutions. 2nd ed. London: Butterworths.

Romanoff M, 1989. Underground Corrosion. Houston, TX: NACE.

Rosborg B, 1998. The resistance of the copper canister to stress corrosion cracking. Report STUDSVIK/M98/100, Studsvik Material AB.

Rosborg B, Svensson B-M, 1994. Stress corrosion testing of copper in synthetic groundwater. Report STUDSVIK/M94/73, Studsvik Material AB.

Rosborg B, Werme L, 2001. The resistance of pure copper to stress corrosion cracking in repository environments. Presentation at 2001 MRS Spring Meeting, San Francisco, May 2001. In: Nuclear waste containment materials. Papers related to the SKB waste disposal programme presented at the Materials Research Society Spring Meeting, April 19, 2001. SKB TR-01-25, Svensk Kärnbränslehantering AB, pp 17–24.

Rosborg B, Karnland O, Quirk G, Werme L, 2003. Measurements of copper corrosion in the LOT project at the Äspö hard rock laboratory. In: Féron D, Macdonald D D (eds). Prediction of long term corrosion behaviour in nuclear waste systems: proceedings of an international workshop, November, Cadarache, France. London: Maney Pub. (European Federation of Corrosion Publications 36), pp 412–423.

Rosborg B, Eden D, Karnland O, Pan J, Werme L, 2004a. Real-time monitoring of copper corrosion at the Äspö HRL. In: Proceedings of the 2nd International Workshop On Prediction Of Long Term Corrosion Behaviour In Nuclear Waste Systems, Nice, France, September 2004. European Federation of Corrosion.

Rosborg B, Eden D, Karnland O, Pan J, Werme L, 2004b. The corrosion rate of copper in a test parcel at the Äspö Hard Rock Laboratory. In: Oversby V M, Werme L O (eds). Scientific basis for nuclear waste management XXVII: symposium held in Kalmar, Sweden, 15–19 June 2003. Warrendale, PA: Materials Research Society. (Materials Research Society Symposium Proceedings 807), pp. 489–494.

Rosborg B, Pan J, Eden D, Karnland O, Werme L, 2004c. Real-time monitoring of copper corrosion at the Äspö Hard Rock Laboratory. Corrosion/2004, NACE International, Houston, Texas, Paper 04687.

Rosborg B, Pan J, Leygraf C, 2005. Tafel slopes used in monitoring of copper corrosion in a bentonite/groundwater environment. Corrosion Science, 47, pp 3267–3279.

Roy S K, Sircar S C, 1981. A critical appraisal of the logarithmic rate law in the thin film formation during oxidation of copper and its alloys, Oxidation of Metals, 15, pp 9–20.

Ryan S R, King F, 1994. The adsorption of Cu(II) on sodium bentonite in a synthetic saline groundwater. AECL11062, COGI94125, Atomic Energy of Canada Limited.

Ryan S R, Clarke C F, Ikeda B M, King F, Litke C D, McKay P, Mitton D B, 1994. An investigation of the long-term corrosion behaviour of selected nuclear fuel waste container materials under possible disposal vault conditions. Technical Record TR489, COG9455, Atomic Energy of Canada Limited.

Saario T, Betova I, Heinonen J, Kinnunen P, Lilja C, 2004. Effect of the degree of compaction of bentonite on the general corrosion rate of copper. In: Proceedings of the 2nd International Workshop on Prediction Of Long Term Corrosion Behaviour in Nuclear Waste Systems, Nice, France, September 2004. European Federation of Corrosion.

Saario T, Laitinen T, Mäkelä K, Bojinov M, 1999. Literature survey on stress corrosion cracking of Cu in presence of nitrites, ammonia, carbonates and acetates. Posiva Working Report 9957, Posiva Oy, Finland.

Sato, S, Nagata K, 1978. Stress corrosion cracking of phosphorus deoxidised copper. Journal of the Japan Copper and Brass Research Association, 17, pp 202–214.

Schüssler A, Exner H E, 1993. The corrosion of nickel-aluminium bronzes in seawater – I. Protective layer formation and the passivation mechanism. Corrosion Science, 34, pp 1793–1802.

Schwentenwein S, Mori G, Zitter H, 2002. Stress corrosion cracking of semi-hard DHP-copper tubes in potassium nitrite solution. Corrosion/2002, NACE International, Houston, Texas, Paper 02432.

Shalaby H M, Al-Kharafi F M, Gouda V K, 1989. A morphological study of pitting corrosion of copper in soft tap water. Corrosion, 45, pp 536–547.

Sharma V K, Millero F J, 1988. The oxidation of Cu(I) in electrolyte solutions. Journal Solution of Chemistry, 17, pp 581–599.

Shoesmith D W, King F, 1999. The effects of gamma radiation on the corrosion of candidate materials for the fabrication of nuclear waste packages. AECL-11999, Atomic Energy of Canada Limited.

Shoesmith D W, Lee W, 1977. The dissolution of cupric hydroxide films from copper surfaces. Electrochimica Acta, 22, pp 1411–1417.

Shreir L L, Jarman R A, Burstein G T, 1994. Corrosion. Vol 1. Metal/environment reactions. 3rd ed. Oxford: Butterworth-Heinemann.

Sieradzki K, Kim J S, 1992. Etch pitting and stress-corrosion cracking of copper. Acta Metallurgical et Materialia, 40, pp 625–635.

Sieradzki K, Sabatini R L, Newman R C, 1984. Stress-corrosion cracking of copper single crystals. Metallurgical and Materials Transactions A, 15A, pp 1941–1946.

Simpson J P, 1984. Experiments on container materials for Swiss high-level waste disposal projects. Part II. Nagra Technical Report 84-01, National Cooperative for the Disposal of Radioactive Waste, Switzerland.

Sirkiä P, Saario T, Mäkelä K, Laitinen T, Bojinov M, 1999. Electric and electrochemical properties of surface films formed on copper in the presence of bicarbonate anions. STUKYTOTR 157, Radiation and Nuclear Safety Authority (STUK), Finland.

SITE-94, 1996. SKI SITE-94, deep repository performance assessment project. SKI Report 96:36, Statens kärnkraftinspektion (Swedish Nuclear Power Inspectorate).

Sjöland K A, Bockgård N, 2006. Present status of the Äspö Hard Rock Laboratory. In: Proceedings of the 11th International High Level Radioactive Waste Management 2006, Las Vegas, NV, 30 April – 4 May 2006. American Nuclear Society, La Grange Park, IL, pp 515–525.

SKBF/KBS, 1983. Final storage of spent nuclear fuel – KBS3. Volumes IIV. Svensk Kärnbränsleförsörjning AB.

SKB, 1992. Background report to RD&D-programme 92. Treatment and final disposal of nuclear waste. Detailed R&D-programme 1993–1998. Svensk Kärnbränslehantering AB.

SKB, 1995. SR 95. Template for safety reports with descriptive example. SKB TR-92-05, Svensk Kärnbränslehantering AB.

SKB, 1999a. Deep repository for spent nuclear fuel. SR 97 – Post-closure safety. Main report, Vol I. SKB TR-99-06, Svensk Kärnbränslehantering AB.

SKB, 1999b. Deep repository for spent nuclear fuel. SR 97 – Post-closure safety. Main report, Summary. SKB TR-99-06, Svensk Kärnbränslehantering AB.

SKB, 2006a. Long-term safety for KBS-3 repositories at Forsmark and Laxemar – a first evaluation. Main report of the SR-Can project. SKB TR-06-09, Svensk Kärnbränslehantering AB.

SKB, 2006b. Fuel and canister process report for the safety assessment of SR-Can. SKB TR 06-22, Svensk Kärnbränslehantering AB.

SKB, 2006c. Climate and climate-related issues for the safety assessment SRCan. SKB TR 06-23, Svensk Kärnbränslehantering AB.

SKB, 2010. Design, production and initial state of the canister. SKB TR-10-14, Svensk Kärnbränslehantering AB.

Smart N R, Rance A P, Fennell P, Werme L, 2003. Expansion due to anaerobic corrosion of steel and cast iron: experimental and natural analogue studies. In: Férom D, Macdonald D D (eds). Proceedings of the international Workshop Prediction of Long Term Corrosion Behaviour in Nuclear Waste Systems, November, Cadarache, France. London: Maney Pub. (European Federation of Corrosion Publications 36), paper 19, pp 280–294.

Smart N R, Fennell P A H, Rance A P, Werme L, 2004. Galvanic corrosion of copper-cast iron couples in relation to the Swedish radioactive waste canister concept. In: Proceedings of the 2nd International Workshop on Prediction Of Long Term Corrosion Behaviour in Nuclear Waste Systems, Nice, France, September 2004. European Federation of Corrosion, pp 52–60.

Smart N R, Rance A P, Fennell P A H, 2005. Galvanic corrosion of copper-cast iron couples. SKB TR-05-06, Svensk Kärnbränslehantering AB.

Smith J M, 2007. The corrosion and electrochemistry of copper in aqueous, anoxic sulphide solutions. Ph.D. thesis, University of Western Ontario.

Smith R M, Martell A E, 1989. Critical stability constants. Vol 6: Second supplement. New York: Plenum Press.

Smith R M, Martell A E, Motekaitis R J, 1998. NIST Critically selected stability constants of metal complexes database. Version 5. National Institute of Standards and Technology (NIST). Standard Reference Data Program, Gaithersburg. [Online]. Available at: http://www.nist.gov/srd.

Smith J, Qin Z, Shoesmith D W, King F, Werme L, 2004. Corrosion of copper nuclear waste containers in aqueous sulphide solutions. In: Hanchar J M, Stroes-Gascoyne S, Browning L (eds). Scientific Basis for Nuclear Waste Management XXVIII: symposium held in San Francisco, California, USA, 13–16 April 2004. Warrendale, PA: Materials Research Society. (Materials Research Society Symposium Proceedings 824), pp 45–50.

Smith J, Qin Z, King F, Werme L, Shoesmith D W, 2006. The electrochemistry of copper in aqueous sulphide solutions. In: Van Iseghem P (ed). Scientific Basis for Nuclear Waste Management XXIX: proceedings of a meeting held in Ghent, Belgium, 12–16 September 2005. Warrendale, PA: Materials Research Society. (Materials Research Society Symposium Proceedings 932), pp 869–875.

Smith J, Qin Z, King F, Werme L, Shoesmith D W, 2007a. Sulphide film formation on copper under electrochemical and natural corrosion conditions. Corrosion, 63, pp 135–144.

Smith J M, Wren J C, Odziemkowski M, Shoesmith D W, 2007b. The electrochemical response of preoxidized copper in aqueous sulphide solutions. Journal of the Electrochemical Society, 154, pp C431–C438.

Smith J M, Qin Z, Shoesmith D W, 2008. Electrochemical impedance studies of the growth of sulphide films on copper. In: Proceedings of the 17th International Corrosion Congress, Las Vegas, 6–10 October 2008. Houston, TX: NACE International.

Smith J M, Qin Z, King F, Shoesmith D W, 2009. The influence of chloride on the corrosion of copper in aqueous sulphide solutions. In: Proceedings of the SACNUC (Sulphur-Assisted Corrosion in Nuclear Waste Disposal Systems) Workshop, Brussels, 21–23 October 2008. European Federation of Corrosion, to be published.

Snellman M, Uotila H, Rantanen J, 1987. Laboratory and modelling studies of sodium bentonite groundwater interaction. In: Bates J K, Seefeldt W B (eds). Scientific basis for nuclear waste management X: symposium held in Boston, Massachusetts, USA, 1–4 December 1986. Pittsburgh, PA: Materials Research Society. (Materials Research Society Symposium Proceedings 84), pp 781–790.

Sridhar N, Cragnolino G A, 1993. Effects of environment on localized corrosion of copperbased, highlevel waste container materials. Corrosion, 49, pp 967–976.

SSM, 2009. A review of evidence for corrosion of copper by water. SSM 2009:30, Strålsäkerhetsmyndigheten (Swedish Radiation Safety Authority).

Stroes-Gascoyne S, Pedersen K, Haveman S A, Dekeyser K, Arlinger J, 1997. Occurrence and identification of microorganisms in compacted clay-based buffer material designed for use in a nuclear fuel waste disposal vault. Canadian Journal of Microbiology, 43, pp 1133–1146.

Stroes-Gascoyne S, Hamon C J, Kohle C, Dixon D A, 2006. The effects of dry density and porewater salinity on the physical and microbiological characteristics of highly compacted bentonite. Report 06819REP0120010016, Ontario Power Generation, Nuclear Waste Management Division, Canada.

Stroes-Gascoyne S, Hamon C J, Dixon D A, Kohle C, Maak P, 2007a. The effects of dry density and porewater salinity on the physical and microbiological characteristics of highly compacted bentonite. In: Dunn D, Poinssot C, Begg B (eds). Scientific basis for nuclear waste management XXX: symposium held in Boston, Massachusetts, USA, 27 November– 1 December 2006. Warrendale, PA: Materials Research Society. (Materials Research Society Symposium Proceedings 985).

Stroes-Gascoyne S, Maak P, Hamon C J, Kohle C, 2007b. Potential implications of microbes and salinity on the design of repository sealing system components. NWMO TR200710, Nuclear Waste Management Organization, Canada.

Stumm W, Morgan J J, 1996. Aquatic chemistry: chemical equilibria and rates in natural waters. 3rd ed. New York: Wiley.

Sunder S, Christensen H, 1993. Gamma radiolysis of water solutions relevant to the nuclear fuel waste management program Nuclear Technology, 104, pp 403–417.

Suzuki Y, Hisamatsu Y, 1981. Stress corrosion cracking of pure copper in dilute ammoniacal solution. Corrosion Science, 21, pp 353–368.

Suzuki I, Ishikawa Y, Hisamatsu Y, 1983. The pitting corrosion of copper tubes in hot water. Corrosion Science, 23, pp 1095–1106.

Swedish Corrosion Institute, 1978. Copper as a canister material for unreprocessed nuclear waste – evaluation with respect to corrosion. KBS TR 90, Svensk Kärnbränsleförsörjning AB.

Swedish Corrosion Institute, 1983. The corrosion resistance of a copper canister for spent nuclear fuel – follow up. SKBF/KBS TR 83-24, Svensk Kärnbränsleförsörjning AB.

Syrett B C, 1981. The mechanism of accelerated corrosion of copper-nickel alloys in sulphide-polluted seawater. Corrosion Science, 21, pp 187–209.

Szakálos P, Hultquist G, Wikmark G, 2007. Corrosion of copper by water. Electrochemical and Solid-State Letters, 10, pp C63–C67.

Taniguchi N, Kawasaki M, 2008. Influence of sulfide concentration on the corrosion behaviour of pure copper in synthetic seawater. Journal of Nuclear Materials, 379, pp 154–161.

Taxén C, 1991. Pitting corrosion of copper with sulphide as the reaction of determining reactant. Report 53 698/3, Swedish Corrosion Institute.

Taxén C, 1996. Pitting corrosion of copper. Equilibrium-mass transport study. In: Proceedings of the 13th International Corrosion Conference, Melbourne, Australia, 25–29 November 1996, Paper 141.

Taxén C, 2000. Pitting corrosion of copper. Equilibrium-mass transport limitations. In: Smith R W, Shoesmith D W (eds). Scientific basis for nuclear waste management XXIII: symposium held in Boston, Massachusetts, USA, 29 November –2 December 1999. Warrendale, PA: Materials Research Society. (Materials Research Society Symposium Proceedings 608), pp 103–108.

Taxén C, 2002a. Pitting corrosion of copper. An equilibrium-mass transport study. SKB TR-02-22, Svensk Kärnbränslehantering AB.

Taxén C, 2002b. Pitting corrosion of copper. Further model studies. SKB TR-02-23, Svensk Kärnbränslehantering AB.

Taxén C, 2004. Atmospheric corrosion of copper 450 metres underground. Results from three years exposure in the Äspö HRL. In: Oversby V M, Werme L O (eds). Scientific basis for nuclear waste management XXVII: symposium held in Kalmar, Sweden, 15–19 June 2003. Warrendale, PA: Materials Research Society. (Materials Research Society Symposium Proceedings 807), pp. 423–428.

Taxén C, Puigdomenech I, 2001. Simplified treatment of conditions for pitting corrosion of copper in chloride containing media. In: Nuclear waste containment materials. Papers related to the SKB waste disposal programme presented at the Materials Research Society Spring Meeting, April 19, 2001. SKB TR-01-25, Svensk Kärnbränslehantering AB, pp 11–16.

Thomas J G N, Tiller A K, 1972a. Formation and breakdown of surface films on copper in sodium hydrogen carbonate and sodium chloride solutions. I. Effects of anion concentrations. British Corrosion Journal, 7, pp 256–262.

Thomas J G N, Tiller A K, 1972b. Formation and breakdown of surface films on copper in sodium hydrogen carbonate and sodium chloride solutions. II. Effects of temperature and pH. British Corrosion Journal, 7, pp 263–267.

Thompson, D H, Tracy A W, 1949. Influence of composition on the stress-corrosion cracking of some copper-base alloys. Metallurgical Transactions 1949, pp 100–109.

Tromans D, 1997. Copper and zinc equilibria in concentrated ammonia solutions: relevance to stress corrosion cracking of alpha-brass. Corrosion Science, 39, pp 1307–1319.

Uchida H, Inoue S, Koyama M, Morii M, Koterazawa K, 1991. Susceptibility to stress corrosion cracking of pure copper in $NaNO_2$ solutions. Society of Material Science Japan, 40, pp 1073–1078.

Var'yash L N, 1989. Equilibria in the Cu - Cu_2O - H_2O system at 150 - 450 °C. Geochemistry International, 26, pp 80–90.

Vazquez Moll D, de Chialvo MRG, Salvarezza R C, Arvia A J, 1985. Corrosion and passivity of copper in solutions containing sodium sulphide. Analysis of potentiostatic current transients. Electrochim. Acta 30, 1011–1016.

Vazquez M V, de Sanchez S R, Calvo E J, Schiffrin D J, 1994a. The electrochemical reduction of oxygen on polycrystalline copper in borax buffer. Journal of Electroanalytical Chemistry, 374, pp 189–197.

Vazquez M V, de Sanchez S R, Calvo E J, Schiffrin D J, 1994b. The electrochemical reduction of hydrogen peroxide on polycrystalline copper in borax buffer. Journal of Electroanalytical Chemistry, 374, pp 179–187.

Wagman D D, Evans W H, Parker V B, Schumm R H, Halow I, Bailey S M, Churney K L, Nuttall R L, 1982. The NBS tables of chemical thermodynamic properties. Selected values for inorganic and C1 and C2 organic substances in SI units. Journal of Physical and Chemical Reference Data, 11, Supplement 2.

Walter R J, Matejczyk D E, Gunderloy F C, Morinishi R, 1989. Methane-fuel corrosion in regeneratively cooled rocket-engine combustors. Corrosion, 45, pp 685–688.

Wang M, Zhang Y, Muhammed M, 1997. Critical evaluation of thermodynamics of complex formation of metal ions in aqueous solutions III. The system Cu(I,II) – Cl^- – e at 298.15 K. Hydrometallurgy, 45, pp 53–72.

Wanner H, Östhols E, 2000. Guidelines for the assignment of uncertainties. OECD/NEA Thermochemical Data Base Project, TDB-3. Le Seine-St. Germain: OECD/NEA. [Online]. Available at: http://www.oecd-nea.org/dbtdb/guidelines/tdb3new.pdf.

Wanner H, Wersin P, Sierro N, 1992. Thermodynamic modelling of bentonite-groundwater interaction and implications for near field chemistry in a repository for spent fuel. SKB TR 92-37, Svensk Kärnbränslehantering AB.

Wehrli B, 1990. Redox reactions of metal ions at mineral surfaces. In: Stumm W (ed). Aquatic chemical kinetics. New York: Wiley, Chapter 11.

Werme L, 1992. Copper canisters for nuclear high level waste disposal: corrosion aspects. In: Corrosion problems related to nuclear waste disposal. London: Institute of Materials. (European Federation of Corrosion Publications 7), pp 32–42.

Werme L, 2001. Copper canisters for nuclear high-level waste disposal: corrosion aspects. In: Proceedings of the International Workshop on Prediction of Long Term Corrosion Behaviour in Nuclear Waste Systems, EFC Event N° 256, Cadarache, France, 26–29 November 2001.

Werme L, Sellin P, Kjellbert N, 1992. Copper canisters for nuclear high level waste disposal. Corrosion aspects. SKB TR 92-26, Svensk Kärnbränslehantering AB.

Werme L, King F, Ahonen L, Taxén C, Vuorinen U, 2004. KBS-TR-90 twenty-five years on – progress in the understanding of the long-term corrosion behavior of copper canisters. In: Oversby V M, Werme L O (eds). Scientific basis for nuclear waste management XXVII: symposium held in Kalmar, Sweden, 15–19 June 2003. Warrendale, PA: Materials Research Society. (Materials Research Society Symposium Proceedings 807), pp 417–422.

Wersin P, 2002. Geochemical modelling of bentonite porewater in high-level waste repositories. Journal of Contaminant Hydrology, 61, pp 405–422.

Wersin P, Spahiu K, Bruno J, 1994a. Kinetic modelling of bentonite-canister interaction. Long-term predictions of copper canister corrosion under oxic and anoxic conditions. SKB TR 94-25, Svensk Kärnbränslehantering AB.

Wersin P, Spahiu K, Bruno J, 1994b. Time evolution of dissolved oxygen and redox conditions in a HLW repository. SKB TR 94-02, Svensk Kärnbränslehantering AB.

Wersin P, Johnson L H, McKinley I G, 2007. Performance of the bentonite barrier beyond 100°C: a critical review. Physics and Chemistry of the Earth, 32, pp 780–788.

Wieland E, Wanner H, Albinsson Y, Wersin P, Karnland O, 1994. A surface chemical model of the bentonite water-interface and its implications for modelling the near field chemistry in a repository for spent fuel. SKB TR 94-26, Svensk Kärnbränslehantering AB.

Xiao Z, Gammons C H, Williams-Jones A E, 1998. Experimental study of copper(I) chloride complexing in hydrothermal solutions at 40 to 300° C and saturated water vapor pressure. Geochimica et Cosmochimica Acta, 62, pp 2949–2964.

Yang C, Samper J, Molinero J, Bonilla M, 2007. Modelling geochemical and microbial consumption of dissolved oxygen after backfilling a high level radioactive waste repository. Journal of Contaminant Hydrology, 93, doi:10.1016/j.jconhyd.2007.01.008.

Yu J, Parkins R N, 1987. Stress corrosion crack propagation in αbrass and copper exposed to sodium nitrite solutions. Corrosion Science 27, 159–182.

Yu J, Parkins R N, Xu Y, Thompson G, Wood G C, 1987. Stress corrosion crack initiation in αbrass exposed to sodium nitrite solutions. Corrosion Science, 27, pp 141–157.

Yunker W H, 1990. Corrosion behavior of copper-base materials in a gamma-irradiated environment. Final report. Report WHCEP0188, Westinghouse Hanford Company, Richland, Washington.

Yunker W H, Glass R S, 1986. Long-term corrosion behavior of copper-base materials in a gamma-irradiated environment. In: Bates J K, Seefeldt W B (eds). Scientific basis for nuclear waste management X: symposium held in Boston, Massachusetts, USA, 1–4 December 1986. Pittsburgh, PA: Materials Research Society. (Materials Research Society Symposium Proceedings 84), pp 579–590.

Zhang J, Wang J, Wang Y, 2005. Micro-droplets formation during the deliquescence of salt particles in atmosphere. Corrosion, 61, pp 1167–1172.

Appendix I

Thermodynamic data from SKB TR-00-13

Table AI-1. Thermodynamic data at 25°C for copper, copper compounds and aqueous species.

Species	$\Delta G_f°$	$S°$	$C_p°(T)/(J·K^{-1}·mol^{-1}) = a + bT + cT^{-2}$		
	(kJ/mol)	$(J·K^{-1}·mol^{-1})$	$a^\dagger$	$b·10^3$	$c·10^{-6}$
Cu(cr)	0	33.15	20.531	8.611	0.155
Cu^+	48.87	40.6	57.3		
CuOH(aq)	–122.32	226	–280		
$Cu(OH)_2^-$	–333.05	–135	562		
Cu_2O(cr)	–147.90	92.36	58.199	23.974	–0.159
Cu^{2+}	65.04	–98.0	–23.8		
$CuOH^+$	–126.66	–61	382		
$Cu(OH)_2$(aq)	–316.54	26	214		
$Cu(OH)_3^-$	–493.98	–14	105		
$Cu(OH)_4^{2-}$	–657.48	–175	800		
$Cu_2(OH)_2^{2+}$	–285.1	–4	190		
$Cu_3(OH)_4^{2+}$	–633.0	–59	404		
CuO(cr)	–128.29	42.6	48.597	7.427	–0.761
$Cu(OH)_2$(cr)	–359.92	87.0	86.99	23.26	–0.54
CuF(cr)	–192.22	65.26	47.9		
CuF^+	–225.5	–38	99		
CuF_2(cr)	–501.5	73.0	72.01	19.96	–1.138
$CuF_2·2H_2O$(cr)	–998.21	152.75	152.3		
CuCl(aq)	–101.2	173	–215		
$CuCl_2^-$	–245.6	202	–20		
$CuCl_3^{2-}$	–372.48	217	98		
$Cu_2Cl_4^{2-}$	–487.42	325	80		
$Cu_3Cl_6^{3-}$	–731.99	349	70		
CuCl(cr)	–120	87	38.28	34.98	
$CuCl^+$	–69.81	–3.25	88		
$CuCl_2$(aq)	–198.75	73.4	158		
$CuCl_3^-$	–321.25	121.6	187		
$CuCl_4^{2-}$	–437.05	145.9	174		
$CuCl_2$(cr)	–176.07	116.7	67.03	17.57	
$CuCl_2·3Cu(OH)_2$(cr)	–1,339.9	335.57	312.621	134.86	–3.10959
$Cu_{37}Cl_8(SO_4)_2(OH)_{62}·8H_2O$(cr)	–15,635.12	3,409	3,525.3		
$CuClO_3^+$	55.14	36.3	161		
CuHS(aq)	–13.2	206	–209		
$Cu(HS)_2^-$	–22.98	239	32		
$Cu_2S(HS)_2^{2-}$	–32.59	80	–270		
Cu_2S(cr)	–84.11	116.2	52.84	78.74	
$Cu_{1.934}S$(cr)	–82.4	109.6	73.0		

Species	$\Delta G_f°$	$S°$	$C_p°(T)/(J·K^{-1}·mol^{-1}) = a + bT + cT^{-2}$		
	(kJ/mol)	($J·K^{-1}·mol^{-1}$)	a†	$b·10^3$	$c·10^{-6}$
$Cu_{1.75}S$(cr)	–76.4	98.3	68.4		
CuS(cr)	–48.65	64.4	44.35	11.05	
$CuS_2O_3^-$	–531.36	130	–35		
Cu_2SO_4(cr)	–657.4	201	126.8		
$CuSO_4$(aq)	–692.154	–18.15	–96		
$CuSO_4$(cr)	–662.2	109.2	152.84	–12.30	–7.159
$CuSO_4·5H_2O$(cr)	–1,880.0	301.2	70.88	–18.58	
$Cu_4SO_4(OH)_6$(cr)	–1,818.0	339.7	258.57	387.23	–4.4649
$Cu_4SO_4(OH)_6·H_2O$(cr)	–2,044.0	335	403.5		
$Cu_3SO_4(OH)_4$(cr)	–1,446.6	266.4	362.7		
$CuO·CuSO_4$(cr)	–792.26	157.3	170.83	45.355	–3.925
$Cu(NH_3)_2^+$	–64.5	272	207		
$CuNH_3^{2+}$	15.0	12.1	51		
$Cu(NH_3)_2^{2+}$	–31.2	112	126		
$Cu(NH_3)_3^{2+}$	–73.9	197	201		
$Cu(NH_3)_4^{2+}$	–112.1	272	276		
$CuNH_3OH^+$	–183.4	68	126		
$Cu(NH_3)_2(OH)_2$(aq)	–399.8	191	276		
$Cu(NH_3)_3OH^+$	–257.9	210	275		
$CuNO_2^+$	21.64	43.5	115		
$Cu(NO_2)_2$(aq)	–14.01	166	170		
$CuNO_3^+$	–48.61	34	130		
$Cu(NO_3)_2$(aq)	–154.26	185	–160		
$Cu(NO_3)_2·3Cu(OH)_2$(cr)	–1,278.67	399.2	415.0		
CuH_2PO_4(aq)	–1,093.25	150	0		
$Cu(H_2PO_4)_2^-$	–2,235.71	230	0		
$Cu(HPO_4)(H_2PO_4)^{2-}$	–2,208.31	170	0		
$CuHPO_4$(aq)	–1,054.35	–20	–70		
$Cu(HPO_4)_2^{2-}$	–2,168.94	–170	–200		
$Cu(HPO_4)(H_2PO_4)^-$	–2,198.64	–40	–200		
$CuH_2PO_4^+$	–1,078.62	0	200		
$Cu(H_2PO_4)_2$(aq)	–2,220.34	100	0		
$Cu_3(PO_4)_2$(cr)	–2,066.20	370	229		
$Cu_3(PO_4)_2·3H_2O$(cr)	–2,767.75	504	351		
$CuCO_3$(aq)	–501.50	–19	–117		
$Cu(CO_3)_2^{2-}$	–1,048.98	122	–410		
$CuHCO_3^+$	–532.08	65.4	170		
$CuCO_3$(cr)	–528.20	87.9	92.05	38.91	–1.799
$Cu_2CO_3(OH)_2$(cr)	–902.35	166.3	49.57	328.36	–0.616
$Cu_3(CO_3)_2(OH)_2$(cr)	–1,431.43	254.4	137.89	387.46	–2.205

† For aqueous ions and complexes "*a*" corresponds to the standard partial molar heat capacity at 25°C, and its temperature dependence has been calculated with the revised Helgeson-Kirkham-Flowers model as described in the text.

Table AI-2. Thermodynamic data at 25°C for auxiliary species.

Species	$\Delta G_f°$	$S°$	$C_p°$
	(J·K^{-1}·mol^{-1})	(J·K^{-1}·mol^{-1})	(J·K^{-1}·mol^{-1})
H_2(g)	0	130.68	‡
H^+	0	0	0
OH^-	–157.22	–10.9	–125
F^-	–281.5	–13.8	–113.9
HF(g)	–275.4	173.78	29.14
HF(aq)	–299.675	88	–58.6
HF_2^-	–583.709	92.68	–138.9
Cl^-	–131.20	56.6	–123.2
ClO_3^-	–7.903	162.3	–51.5
S(cr)	0	32.05	‡
H_2S(g)	–33.4	205.81	‡
H_2S(aq)	–27.648	126.0	178.7
HS^-	12.243	67.0	–93
S^{2-}	120.7	–14.6	–300
S_5^{2-}	66.96	187	–180
HS_5^-	32.14	269	27
H_2S_5(aq)	9.88	328	297
S_4^{2-}	66.22	165	–210
HS_4^-	27.98	247	267
H_2S_4(aq)	4.0	306	273
S_3^{2-}	78.2	95	–240
S_2^{2-}	97.17	5	–210
S_2^-	58.18	144	–105
$S_2O_3^{2-}$	–522.58	66.94	–240
$HS_2O_3^-$	–532.21	127.6	14.6
$H_2S_2O_3$(aq)	–535.55	188.3	115.1
SO_3^{2-}	–487.47	–29	–318
HSO_3^-	–528.69	139.7	–6
H_2SO_3(aq)	–539.19	231.9	270
SO_4^{2-}	–744.00	18.5	–269
HSO_4^-	–755.32	131.7	–18
H_2SO_4(aq)	–748.47	83.5	250
NO_3^-	–110.79	146.7	–69
NO_2^-	–32.22	123.0	–97.5
HNO_2(aq)	–50.63	135.56	28
NH_3(g)	–16.41	192.77	‡ ‡
NH_3(aq)	–26.67	109.04	74.9
NH_4^+	–79.40	111.17	65.9
PH_3(g)	13.4	210.23	‡ ‡
PH_3(aq)	25.36	120.1	188
H_3PO_4(aq)	–1,149.367	161.91	98.7
$H_2PO_4^-$	–1,137.15	92.5	–29.3
HPO_4^{2-}	–1,095.99	–33.5	–243.9
PO_4^{3-}	–1,025.49	–220.97	–480.7
CO_2(g)	–394.37	213.79	‡ ‡
"CO_2(aq)"	–385.97	119.36	243.1
HCO_3^-	–586.845	98.4	–35.4
CO_3^{2-}	–527.899	–50.0	–290.8

Species	$\Delta G_f°$	$S°$	$C_p°$
	(J·K^{-1}·mol^{-1})	(J·K^{-1}·mol^{-1})	(J·K^{-1}·mol^{-1})
C(cr)	0	5.74	‡ ‡
CH_4(g)	–50.7	186.26	‡ ‡
CH_4(aq)	–34.451	87.82	277.4
Na^+	–262.00	58.45	37.9
NaOH(aq)	–417.98	44.8	–13.4
NaF(aq)	–537.94	50.2	46.9
NaCl(aq)	–388.74	117.2	35.6
$NaSO_4^-$	–1,010.12	95	–16.1
$NaCO_3^-$	–792.99	–43.9	–37.9
$NaHCO_3$(aq)	–847.89	120.9	89.5
$NaPO_4^{2-}$	–1,295.61	–100.5	–192.8
$NaHPO_4^-$	–1,360.79	–27.4	9.0
Ca^{2+}	–552.8	–56.2	–31.5
$CaOH^+$	–716.72	28.0	5.9
$Ca(OH)_2$(cr)	–898.0	83.4	‡ ‡ ‡
CaF^+	–838.43	–37.7	125.9
CaF_2(cr)	–1,175.3	68.9	‡ ‡ ‡
$CaCl^+$	–682.41	18.8	73.1
$CaCl_2$(aq)	–811.70	25.1	129.5
$CaSO_4$(aq)	–1,309.3	20.9	–104.6
$CaSO_4$(cr)	–1,321.8	107.4	‡ ‡ ‡
$CaSO_4·2H_2O$(cr)	–1,797.0	193.8	183
$CaCO_3$(aq)	–1,099.76	10.5	–123.9
$CaHCO_3^+$	–1,145.99	101.1	163.1
$CaCO_3$(cr)	–1,129.10	91.71	‡ ‡ ‡
$CaPO_4^-$	–1,615.17	–110.0	–212.2
$CaHPO_4$(aq)	–1,664.43	9.1	–78.4
$CaH_2PO_4^+$	–1,698.01	111.02	89.2
$Ca_5(PO_4)_3OH$(cr)	–6,337.1	390.4	‡ ‡ ‡
$Ca_5(PO_4)_3F$(cr)	–6,489.7	387.9	‡ ‡ ‡

‡ **Heat capacity functions:**

H_2(g) $C_p°(T)/(J·K^{-1}·mol^{-1}) = 7.442 + 0.011707\ T - 1.3899·10^{-6}\ T^2 - 5.1041·10^5\ T^{-2} + 410.17\ T^{-0.5}$

S(cr) $C_p°(T)/(J·K^{-1}·mol^{-1}) = 14.795 + 0.024075\ T + 7.1·10^4\ T^{-2}$

H_2S(g) $C_p°(T)/(J·K^{-1}·mol^{-1}) = 26.356 + 0.026497\ T - 6.0244·10^{-6}\ T^2 + 2.6599·10^5\ T^{-2} - 43.559\ T^{-0.5}$

‡ ‡ **Heat capacity functions:**

NH_3(g) $C_p°(T)/(J·K^{-1}·mol^{-1}) = 51.39 + 0.0266\ T - 4.90·10^{-6}\ T^2 + 7.584·10^5\ T^{-2} - 548.0\ T^{-0.5}$

PH_3(g) $C_p°(T)/(J·K^{-1}·mol^{-1}) = 26.3 + 0.04048\ T - 1.14·10^5\ T^{-2}$

CO_2(g) $C_p°(T)/(J·K^{-1}·mol^{-1}) = 87.82 - 0.0026442\ T + 7.064·10^5\ T^{-2} - 99.886\ T^{-0.5}$

C(cr) $C_p°(T)/(J·K^{-1}·mol^{-1}) = 60.86 - 0.01024\ T + 1.669·10^{-6}\ T^2 + 7.139·10^5\ T^{-2} - 99.22\ T^{-0.5}$

CH_4(g) $C_p°(T)/(J·K^{-1}·mol^{-1}) = 119.4 + 0.02055\ T - 5.0·10^{-6}\ T^2 + 2.814·10^6\ T^{-2} - 2090\ T^{-0.5}$

‡ ‡ ‡ **Heat capacity functions:**

$Ca(OH)_2$(cr) $C_p°(T)/(J·K^{-1}·mol^{-1}) = 186.7 - 0.02191\ T - 1600\ T^{-0.5}$

CaF_2(cr) $C_p°(T)/(J·K^{-1}·mol^{-1}) = 2033 - 1.436\ T + 5.04·10^{-4}\ T^2 + 2.988·10^7\ T^{-2} - 33120\ T^{-0.5}$

$CaSO_4$(cr) $C_p°(T)/(J·K^{-1}·mol^{-1}) = 372.8 - 0.1574\ T + 7.99·10^{-5}\ T^2 + 1.695·10^6\ T^{-2} - 4330.8\ T^{-0.5}$

$CaCO_3$(cr) $C_p°(T)/(J·K^{-}1·mol^{-}1) = 99.546 + 0.027137\ T - 2.1481·10^6\ T^{-2}$

$Ca_5(PO_4)_3OH$(cr) $C_p°(T)/(J·K^{-}1·mol^{-}1) = 387.8 + 0.1186\ T - 1.27·10^7\ T^{-2} + 1811\ T^{-0.5}$

$Ca_5(PO_4)_3F$(cr) $C_p°(T)/(J·K^{-}1·mol^{-}1) = 754.3 - 0.03026\ T - 9.084·10^5\ T^{-2} - 6201\ T^{-0.5}$

Appendix II

Discussion and selection of thermodynamic data (L. Ahonen)

Cu^{+} – Cu^{2+} equilibrium

A revised, internally consistent thermodynamic data set for different oxidation states of copper is given in Table AII-1. Compared to the corresponding data set of Ahonen (1995), certain changes have been made, and are explained below.

Wang et al. (1997) re-interpreted the data of several earlier studies on copper disproportionation (equation 1 in Table AII-1). Their results indicated that the stability constant for this reaction, obtained by the extrapolation of data from several experiments to an ionic strength of I = 0, fall 0.2–0.3 units below 6.0 (Figure AII-1). The final values given were $\log K^{o} = -5.76 \pm 0.06$, $\Delta H^{o} = 87.8 \pm 5.0$).

Using the CODATA key values for Cu^{2+}, Wang et al. (1997) calculated a ΔG^{o}-value of 48.99±0.24 kJ/mol for aqueous Cu^{+}, compared with the value of 50.0 kJ/mol given by Robie and Hemingway (1995). Due to the discrepancy between these values, as well as the need to maintain internal consistency of the database, the logK-value for copper disproportionation was rounded to 5.8. Consequently, the value of the standard free energy of formation of Cu^{+}(aq) increases to 49.1, which is clearly within the given range of uncertainty.

Table AII-1. Thermodynamic data for the system Cu^{o}(cr)–Cu^{+}(aq)–Cu^{2+}(aq). CODATA key values are indicated by bold text.

	ΔG^{o} kJ/mol	ΔH^{o} kJ/mol	C_p^{o} J/K·mol	$\log K_{25}$	$\log K_{100}$	Eqn. #
$2Cu^{+} = Cu^{2+} + Cu^{o}$	–33.1	–87.8	–118	5.8	2.6	1
$Cu^{o} = Cu^{2+} + 2e–$	**65.1**	**64.9**	–44	–11.4	–9.2	2
$Cu^{o} = Cu^{+} + e–$	49.1	76.35	+37	–8.6	–5.9	3
$Cu^{+} = Cu^{2+} + e–$	16.0	–11.45	–81	–2.8	–3.3	4

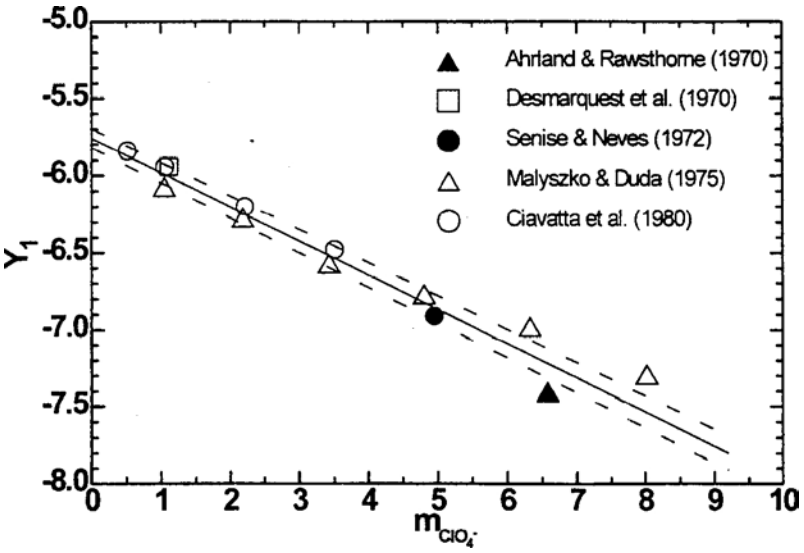

Figure AII-1. *Extrapolation to infinite dilution of the stability constant for the copper disproportionation reaction to I=0 (from Wang et al. 1997).*

Copper-chloride complexes

Since 1995 (Ahonen 1995), new research papers on the thermodynamics of the system Cu-Cl have been published: Wang et al. (1997) re-extrapolated the data of several previous studies to infinite dilution (I=0) using the specific interaction theory (SIT), and Xiao et al. (1998) reported an experimental study of the copper(I)-chloride complexes for the temperature range 40°–300°C. Generally, the new information is in accordance with the earlier data on the thermodynamics of this system. However, certain relationships between Cu-Cl complexes are now defined more precisely. The revised thermodynamic data are presented in Table AII-2.

Stability-constant determinations of copper(I) chloride complexes are mainly based on solubility measurements of solid cuprous chloride (nantokite, CuCl(cr)). At different chloride concentrations, different complexes prevail:

$$CuCl(cr) + (x-1)Cl^- = CuCl_x^{(1-x)} \quad (x = 1 \text{ or higher}) \qquad \text{AII-1}$$

Data on the stability constant of the uncharged complex ($CuCl^o$) are scarce in low-temperature studies, probably because of the predominance of the higher complexes. However, formation of this complex has been frequently reported in experiments carried out at higher temperatures, and the data can be reliably extrapolated to 25°C (e.g. Xiao et al. 1998).

The most important copper(I)-chloride complexes are $CuCl_2^-$ and $CuCl_3^{2-}$. With respect to these complexes, the results of Wang et al. (1997) and Xiao et al. (1998) are in agreement; at chloride concentrations from 10 mM to 5 M, $CuCl_2^-$ is the predominant form.

Copper(II)-chloride complexes are much less stable than those of Cu(I). In numerous studies, the stability constant values are reported to be around zero. Data presented in Table AII-2 are taken from Wang et al. (1997), whenever possible, in order to maintain consistency. Some values for the standard free energy and logK's are not exactly the same as in the original paper, but are always within the given limits of uncertainty. Consistency with CODATA recommended key values were also checked.

Data for the two solid cupric chloride phases in Table AII-2 are taken from Wagman et al. (1982) and Barton and Bethke (1960). Different polynuclear copper(I) chloride complexes may exist in concentrated chloride solutions (> 3–5 M) and high copper concentrations (> 1 M) (Wang et al. 1997). Due to the large uncertainties involved and their negligible role for chloride concentrations below 1 M, the complexes $CuCl_4^{2-}$, $Cu_2Cl_4^{2-}$ and $Cu_3Cl_6^{3-}$ are not included in the present database. A mixed hydroxide-chloride complex, CuClOH was included in the database of Ahonen (1995). The existence of this complex may be considered questionable, because of the scarcity of data. However, because this complex may be important in basic conditions (pH ~8 and higher) in warm (80–100°C) water (Ahonen 1995), it is also included in the present database.

Table AII-2. Thermodynamic data for the aqueous system Cu^+ – Cu^{2+} – Cl^-.

	ΔG^o kJ/mol	ΔH^o kJ/mol	ΔC_r^o J/K·mol	$logK_{25}$	$logK_{100}$	Eqn.#
$CuCl(cr) = Cu^+ + Cl^-$	39.1	47.35	–104	–6.9	–5.4	5
$Cu^+ + Cl^- = CuCl(aq)$	–18.8	+2	–149	3.3	+3.2	6
$Cu^+ + 2Cl^- = CuCl_2^-$	–32.6	–20	+169	5.7	+5.2	7
$Cu^+ + 3Cl^- = CuCl_3^{2-}$	–28.5	–33	+410	5.0	+4.3	8
$Cu^{2+} + Cl^- = CuCl^+$	–3.7	8.7	+235	0.64	+1.2	9
$Cu^{2+} + 2Cl^- = CuCl_2^o$	–3.5	23	+428	0.6	+1.9	10
$Cu^{2+} + 3Cl^- = CuCl_3^-$	5.7	20	+580	–1	+0.4	11
$CuCl_2(cr) = Cu^{2+} + 2Cl^-$	21.6	37	–337	–3.8	–2.9	12
$CuCl_2{\cdot}3Cu(OH)_2(cr) + 6H^+ = 4Cu^{2+} + 2Cl^- + 6H_2O$	–85	–130	–202	14.9	+10.1	13
$Cu^+ + Cl^- + H_2O = CuClOH^- + H^+$	24.5	+13	0	–4.3	–3.8	14

Hydrolysis of copper

Formation of hydroxo-complexes are important reactions for copper(II) in natural waters. The thermodynamic properties of the copper-hydroxide complexes have been extensively studied (a list of references up to 1995 was given by Ahonen 1995). Plyasunova et al. (1997) published a critical evaluation of several recent publications, and re-extrapolated the data to infinite dilution using the SIT method. The data are summarized in Table AII-3.

Copper(I) is far less hydrolyzable than Cu(II). There are very few experimental data on the stability constants of Cu(I) hydroxide complexes. Beverskog and Puigdomenech (1998) reported the standard free energies of formation of complexes $Cu(OH)^o$ and $Cu(OH)_2^-$, based on the data of Var'yash (1989). Standard enthalpy values for reactions 23 and 24 (Table AII-3) are estimated to match the temperature dependence of the free energy change between 25°C and 200°C reported by Var'yash (1989).

Table AII-3. Thermodynamic data for the system Cu^+–Cu^{2+} – H_2O.

	ΔG^o kJ/mol	ΔH^o kJ/mol	ΔC_r^o J/K·mol	$\log K_{25}$	$\log K_{100}$	Eqn.#
$CuO(cr) + 2H^+ = Cu^{2+} + H_2O$	–43.6	–64.9	3	7.64	5.4	15
$Cu^{2+} + H_2O = Cu(OH)^+ + H^+$	45.5	36	331	–7.97	–6.3	16
$Cu^{2+} + 2H_2O = Cu(OH)_2^o + 2H^+$	92.7	92.8	87	–16.2	–12.8	17
$Cu^{2+} + 3H_2O = Cu(OH)_3^- + 3H^+$	152	–	–97	26.6	+26.4	18
$Cu^{2+} + 4H_2O = Cu(OH)_4^{2-} + 4H^+$	227	178	+523	39.7	+46.6	19
$2Cu^{2+} + 2H_2O = Cu_2(OH)_2^{2+} + 2H^+$	60.2	75	+87	–10.5	–7.8	20
$3Cu^{2+} + 4H_2O = Cu_3(OH)_4^{2+} + 4H^+$	120	110	+174	–21.0	–16.9	21
$Cu_2O(cr) + 2H^+ = 2Cu^+ + H_2O$	8.86	37.5	+131	–1.55	–0.1	22
$Cu^+ + H_2O = Cu(OH)^o + H^+$	66	75	–413	–11.6	–9.5	23
$Cu^+ + 2H_2O = Cu(OH)_2^- + 2H^+$	92	15	+354	–16.1	–15.1	24

Complexes of Cu with N-compounds

Copper(II)-ammonia complexes have been extensively studied over the last few decades and stability constants reported in recent studies agree well with each other. The data listed in Table AII-4 are derived from Puigdomenech and Taxen (2000), being in accordance with the most recent compilations of thermodynamic properties of these complexes. The main uncertainty is in the enthalpy values of the mixed hydroxo-ammonia complexes, which have been estimated as the sum of enthalpies for the single-ligand complex reactions.

The existence and stability of Cu(I)-ammonia complexes is far less well-established than that of the corresponding Cu(II) complexes. There are only a few studies in the literature reporting the existence of $CuNH_3^+$ or $Cu(NH_3)_2^+$. However, in strong reducing conditions, Cu(I) and N(-III) (NH_4^+) are expected to be the predominant oxidation states of copper and nitrogen, respectively. Consequently, the possible existence of these complexes should be taken into consideration.

Nitrite is not a thermodynamically stable oxidation state of nitrogen, but it may exist in small amounts in natural groundwaters and in residues from explosives used during blasting. Only Cu(II) complexes with NO_2^- have been reported. Stability constants reported in Table AII-4 for these complexes are those given by Puigdomenech and Taxen (2000), being in accordance with other sources. Enthalpy data for the formation of these complexes are not available. Formation of the corresponding complexes of silver ($AgNO_2^o$ and $Ag(NO_2)_2^-$) and cadmium have negative enthalpies (Smith and Martell 1989), indicating that the stability of the complexes decreases with increasing temperature. In order to get qualitative information on the temperature dependence of the copper-nitrite complexes, enthalpy data for the silver complexes was used for copper in Table AII-4.

Table AII-4. Thermodynamic data for the copper-nitrogen complexes.

	ΔG° kJ/mol	ΔH° kJ/mol	ΔC_r° J/K·mol	$\log K_{25}$	$\log K_{100}$	Eqn. #
$NH_4^+ = NH_3(aq) + H^+$	52.7	52.1	–2	–9.2	–7.4	25
$Cu^{2+} + NH_4^+ = CuNH_3^{2+} + H^+$	29.9	28.1	–36	–5.2	–4.3	26
$Cu^{2+} + 2NH_4^+ = Cu(NH_3)_2^{2+} + 2H^+$	62.5	59.2	–76	–11	–9.0	27
$Cu^{2+} + 3NH_4^+ = Cu(NH_3)_3^{2+} + 3H^+$	99.2	88	–109	–17.4	–14.4	28
$Cu^{2+} + 4NH_4^+ = Cu(NH_3)_4^{2+} + 3H^+$	140	118	–145	–24.6	–20.6	29
$Cu^{2+} + NH_4^+ + H_2O = CuNH_3OH^+ + 2H^+$	68	64	–37	–11.9	–9.7	30
$Cu^{2+} + 2NH_4^+ + 2H_2O = Cu(NH_3)_2(OH)_2 + 4H^+$	170	145	–73	–30	–25	31
$Cu^{2+} + 3NH_4^+ + H_2O = Cu(NH_3)_3OH^+ + 4H^+$	154	120	–110	–27	–22.9	32
$Cu^+ + 2NH_4^+ = Cu(NH_3)_2^+ + 2H^+$	46	48	–73	–8	–6.4	33
$Cu^{2+} + NO_2^- = CuNO_2^+$	–11	–30	236	2	+1.2	34
$Cu^{2+} + 2NO_2^- = Cu(NO_2)_2$	–15	–45	389	2.6	+1.5	35
$Cu^{2+} + NO_3^- = CuNO_3^+$	–3	0	223	0.5	+0.8	36
$Cu^{2+} + 2NO_3^- = Cu(NO_3)_2$	2	0	2	–0.4	–0.4	37

Copper(II) forms two weak complexes with nitrate (NO_3^-), their stability constants listed in Smith et al. (1998) are given in Table AII-4. No data on the temperature-dependence of the formation of these complexes are available, but the temperature dependence is assumed to be negligible between 25° and 100°C (Puigdomenech and Taxen 2000), and the enthalpy value was set to zero in Table AII-4.

Copper-carbonate complexes

Bicarbonate is a common constituent of natural waters, and copper (II) has a strong tendency to form complexes with CO_3^{2-} and HCO_3^-. Puigdomenech and Taxen (2000) reviewed the recent literature, and recommended the data set presented in Table AII-5. Compared to Ahonen (1995), the main difference is in the stability constant of the bicarbonate complex; the value of log K = 1.8 (equation 41) has been used instead of the earlier value 4.27 of Ahonen (1995). The main implication of this correction is that the predominance field of the Cu(II)-bicarbonate complex vanishes at pH values below 6.

Table AII-5. Thermodynamic data for the copper-carbonate complexes and solids.

	ΔG° kJ/mol	ΔH° kJ/mol	ΔC_r° J/K·mol	$\log K_{25}$	$\log K_{100}$	Eqn. #
$CuCO_3(s) = Cu^{2+} + CO_3^{2-}$	+65.4		–407	–11.5	–12.0	38
$Cu^{2+} + HCO_3^- = CuCO_3(aq) + H^+$	+20.2	+25	–58	–3.5	–2.7	39
$Cu^{2+} + 2HCO_3^- = Cu(CO_3)_2^{2-} + 2H^+$	+59.6	?	–15	–10.4	–10.4	40
$Cu^{2+} + HCO_3^- = CuHCO_3^+$	–10.2	?	+229	+1.8	+2.1	41
$Cu_2CO_3(OH)_2(s) + 3H^+ = 2Cu^{2+} + HCO_3^- + 2H_2O$	–28.3	?		+5		42
$Cu_3(CO_3)_2(OH)_2(s) + 4H^+ = 3Cu^{2+} + 2HCO_3^- + 2H_2O$						43